

ANION CONDUCTING STATES OF EXCITATORY AMINO ACID TRANSPORTERS

By

Christopher Brad Divito

B.A. Shippensburg University 2005

Submitted to the Graduate Faculty of

The School of Medicine in partial fulfillment

Of the requirements for the degree of Doctor of Philosophy

University of Pittsburgh 2013

UNIVERSITY OF PITTSBURGH

SCHOOL OF MEDICINE

This thesis was presented

By

Christopher Brad Divito

It was defended on

November 18th, 2013

and approved by

Dissertation Director: Jon W. Johnson, Ph.D., Professor, Department of Neuroscience

Michael Cascio, Ph.D., Associate Professor, Department of Chemistry and Biochemistry,
Duquesne University; Adjunct Professor, Department of Microbiology and Molecular Genetics

Aurelio Galli, Ph.D., Professor, Department of Molecular Physiology and Biophysics, Vanderbilt
University

Steven D. Meriney, Ph.D., Professor Department of Neuroscience

Rebecca P. Seal, Ph.D., Assistant Professor, Department of Neurobiology

Thesis Advisor: Susan G. Amara, Detre Professor and Chair, Department of Neurobiology;
Scientific Director, National Institute of Mental Health, National Institute of Health

Copyright © by Christopher Brad Divito

2013

ANION CONDUCTING STATES OF EXCITATORY AMINO ACID TRANSPORTERS

Christopher Brad Divito, Ph.D.

University of Pittsburgh, 2013

Excitatory amino acid transporters (EAATs) are secondary active, electrogenic transporters which translocate L-glutamate (glu) against its concentration gradient using the co-transport of 3 Na^+ , 1 H^+ , and the counter-transport of 1 K^+ ion. In addition, these carriers possess a thermodynamically uncoupled anion channel that fluxes Cl^- but is promiscuous with several permeant anionic species. The roles of EAATs are to shape the spatio-temporal profile of released glu in both the synaptic cleft and extra-synaptic regions as well as maintaining a low ambient extracellular concentration of glu. This transport activity regulates activation of glu receptors and thus regulates excitatory neurotransmission.

Using a combination of techniques, we were successful in identifying inward oriented transporter conformations which allow transitions to open channels states. This observation was enabled by our development of a novel method to isolate EAAT1 in the inward facing conformation. While constrained to these conformations, currents with the same macroscopic amplitudes as conducting states mediated by the outward facing, Na^+ bound states were observed. The persistence of currents is indicative of a channel gating mechanism that is insensitive to transporter orientation and that the anion channel is open during the majority of the transport cycle. Additional conducting states allows for a larger contribution of the anion channel function of EAATs to shape cellular function than previously assumed.

Next we investigated the gating mechanism of the anion channel. We assayed for the ability of Na^+ to gate the anion channel in both glial (EAAT1 and EAAT2) and neuronal (EAAT3 and EAAT4) isoforms. We discovered that the glial isoforms are not gated by Na^+ but are leak

channels with an open probability and single channel conductance that is insensitive to Na^+ concentrations. In contrast, neuronal EAAT isoforms EAAT3 and EAAT4 both display Na^+ dependent channel activity. This is the first example of a significant functional difference between glial and neuronal transporter isoforms of the solute carrier 1 (SLC1) family. The research presented here allows for a greater understanding of low open probability channel states and the possible contributions of the EAAT anion channel to the functioning of the nervous system.

TABLE OF CONTENTS

PREFACE.....	XV
1. INTRODUCTION.....	1
1.1.1. Isoforms and Localization.....	1
1.2. MECHANISM OF TRANSPORT.....	3
1.2.1. Characterization of Glu Transport.....	3
1.2.2. Physiological Regulation of Transport.....	6
1.3. LIGAND-GATED ANION CHANNELS.....	9
1.3.1. Characterization of Channel Activity.....	9
1.3.2. Role of the Chloride Channel in Regulating Synaptic Transmission.....	10
1.4. STRUCTURE OF THE SLC1 FAMILY.....	11
1.4.1. EAAT Topology.....	11
1.4.2. The Crystal Structure of an Archeal Homolog of Mammalian EAATs.....	13
1.4.3. Structural Influences of the Trimeric Organization of EAATs on Glu Uptake.....	14
1.5. THE ROLE OF EAATS IN SYNAPTIC TRANSMISSION.....	14
1.5.1. The Roles of EAATs in Glutamatergic Neurotransmission in the Hippocampus.....	14
1.5.2. The Role of EAATs in the Cerebellum.....	17
1.5.3. EAATs Influence Activation of Metabotropic Glu Receptors and Synaptic Plasticity.....	18
1.6. CONCLUSION.....	19

2. INWARD FACING STATES OF EXCITATORY AMINO ACID TRANSPORTERS	
MEDIATE OPEN CHANNEL STATES.....	21
2.1. INTRODUCTION.....	21
2.2. EXPERIMENTAL PROCEDURES.....	23
2.2.1. Generation of Mutant EAAT Constructs and Cell Transfections.....	23
2.2.2. Radiolabeled Glu Transport Assays.....	23
2.2.3. Cell Surface and Cysteine Targeted Biotinylations.....	24
2.2.4. Electrophysiology.....	24
2.2.5. Homology and Kinetic Models.....	25
2.2.6. Data Analysis and Statistics.....	25
2.3. RESULTS.....	28
2.3.1. NEM Modification of L376C Captures the Inward Facing Conformations of the Transport Cycle.....	28
2.3.2. Modification of HP1 to Restrict Conformation is Time and Concentration Dependent.....	32
2.3.3. Inward Facing States Possess Anion Channel Activity.....	27
2.3.4. Modification of HP1a Residue A355C Also Captures Inward Facing States.....	34
2.3.5. HP1 Accommodates Alternative Modification Reagents.....	40
2.3.6. EAAT1 Possesses Open Channel States During the Cytoplasmic Facing Conformations of the Transport Cycle.....	41
2.4. DISCUSSION.....	41
3. DIFFERENCE IN THE Na^+ DEPENDENCE OF ANION CHANNEL GATING BETWEEN NEURONAL AND GLIAL ISOFORMS OF GLUTAMATE TRANSPORTERS.....	49
3.1. INTRODUCTION.....	49

3.2. EXPERIMENTAL PROCEDURES.....	51
3.2.1. Transfections in Mammalian Cell Lines and cRNA Injections in <i>Xenopus</i> Oocytes.....	51
3.2.2. Radiolabeled Glu Transport Assays.....	51
3.2.3. Two-Electrode Voltage Clamp Recordings.....	52
3.2.4. Whole-Cell Patch Clamp Recordings.....	52
3.2.5. Data Analysis and Statistics.....	53
3.3. RESULTS.....	53
3.3.1. Neuronal and Glial EAATs Diverge by Their Na ⁺ Dependence of Anion Channel Activity.....	53
3.3.2. Choline Buffers do not Support Transporter Activity.....	59
3.3.3. Na ⁺ Mediated Channel Gating in EAAT3 and EAAT4 is Concentration- dependent.....	62
3.3.4. The Channel Activity Mediated by the Inward Facings States of EAAT1 and EAAT4 Display a Disparate Na ⁺ Dependence.....	65
3.3.5. Glial and Neuronal EAATs have a Different Number of Open Channel States.....	68
3.4. DISCUSSION.....	68
4. CONCLUSION.....	72
4.1. EXCITATORY AMINO ACID TRANSPORTERS AND ANION CONDUCTION.....	72
4.2. SUBSTRATE-MEDIATED CHANNEL GATING.....	73
4.3. THE ROLE OF THE ANION CONDUCTANCE IN CELLULAR FUNCTION.....	75
4.4. LEAK CONDUCTING STATES IN EAATS.....	76
4.5. SUMMARY.....	79
5. REFERENCES.....	80

APPENDIX A. THE LOCATION OF THE ANION PORE IN EXCITATORY AMINO ACID TRANSPORTERS.....	A1
A.1. INTRODUCTION.....	A1
A.2. EXPERIMENTAL PRECEDURES.....	A4
A.2.1. Generation and Subcloning of EAAT1 Cysteine Mutations.....	A4
A.2.2. Transient Transfection of COS-7 cells and cRNA injections into <i>Xenopus</i> Oocytes.....	A4
A.2.3. Radiolabeled Transport Assays.....	A4
A.2.4. Electrophysiology.....	A5
A.3. RESULTS.....	A5
A.3.1. Transport Kinetics of Cysteine Point Mutations in EAAT1.....	A5
A.3.2. Transport Kinetics of Non-cysteine Point Mutations in EAAT1.....	A7
A.4. DISCUSSION.....	A7
A.5. REFERENCES.....	A10
APPENDIX B. CLOSE ENCOUNTERS OF THE OILY KIND: LIPID REGULATION OF NEUROTRANSMITTER TRANSPORTERS.....	B1
APPENDIX C. THE MECHANISM OF CYSTEINE TRANSPORT IN EXCITATORY AMINO ACID TRANSPORTERS.....	C1
C.1. SUMMARY OF CONTRIBUTIONS.....	C1
C.2. INTRODUCTION.....	C1
C.3. EXPERIMENTAL PROCEDURES.....	C3
C.3.1. Generation of Constructs.....	C3
C.3.2. Transfection of HEK293 and cRNA Injection in <i>Xenopus</i> oocytes.....	C3
C.3.2. Radiolabeled Transport Assays.....	C4
C.3.3. Electrophysiology.....	C4
C.3.4. Cell Imaging Experiments.....	C4

C.4. RESULTS.....	C5
C.4.1. EAATs Readily Transport the Deprotonated Cysteine Analog Selenocysteine.....	C5
C.4.2. Selenocysteine Binding Competes for Glutamate Interaction in EAATs.....	C7
C.4.3 Optical Observation of Proton Coupled EAAT Transport Processes.....	C7
C.4.4. Cysteine is Transported as a Thiolate Anion Through EAAT3.....	C11
C.4.5. pH Dependence of Cysteine Interactions in EAAT3.....	C14
C.5. DISCUSSION.....	C14
C.6. REFERENCES.....	C18
APPENDIX D. COUPLING BETWEEN SUBSTRATE TRANSPORT AND ANION CHANNEL GATING IN EXCITATORY AMINO ACID TRANSPORTERS.....	
D.1. SUMMARY OF CONTRIBUTIONS.....	D1
D.2. ABSTRACT.....	D1
D.3. INTRODUCTION.....	D2
D.4. EXPERIMENTAL PROCEDURE.....	D4
D.4.1. Heterologous Expression of hEAAT1.....	D4
D.4.2. Electrophysiology.....	D4
D.4.3. Radiolabeled Transport Assays.....	D5
D.4.4. Data Analysis.....	D5
D.5. RESULTS.....	D5
D.5.1. Mutating Arginine 388 Affected Substrate Transport.....	D5
D.5.2. Arginine 388 Plays a Crucial Role in Anion Channel Gating.....	D9
D.5.3. Mutating Arginine 388 to an Acidic Amino acid, Shifts the Conformational Equilibrium of the Channel to the Leak Conducting States.....	D9

D.5.4. R388E/D Alters Accessibility of HP1 Residues in the Outward-facing Conformations.....	D14
D.6. DISCUSSION.....	D19
D.7. REFERENCES.....	D22
APPENDIX E. STRUCTURE OF THE PENTAMERIC LIGAND-GATED ION CHANNEL GLIC BOUND WITH ANESTHETIC KETAMINE.....	
	E1

LIST OF TABLES

Table 1. Kinetic Data of EAAT1 Cysteine Point Mutations in COS-7 Cells.....	A6
Table 2. Kinetic Data of Non-cysteine EAAT1 Point Mutations in COS-7 Cells.....	A8
Table 3. Eight Lipid Categories and Subclassification According to LIPID MAPS.....	B4
Table 4. Transporter Regulation by Polyunsaturated Fatty Acids.....	B8
Table 5. Data Collection and Refinement Statistics.....	2E

LIST OF FIGURES

Figure 1: Localization of EAATs in the synapse.....	2
Figure 2: EAATs are secondary, electrogenic transporters.....	5
Figure 3: EAATs mediate anion channel flux through multiple open states.....	8
Figure 4: General structure of the SLC1 family of transporters.....	12
Figure 5: Modification of L376C restricts the transporter to inward facing states.....	26
Figure 6: Modification of L376C is time and concentration dependent.....	30
Figure 7: The inward facing conformations of EAAT1 have open channel states.....	33
Figure 8: Modifications of HP1 residue A335C.....	36
Figure 9: HP1 is readily accessible by the bulky modification reagent NPEM.....	39
Figure 10: Model of hEAAT1 structures and proposed state diagram of general EAAT transport cycle including novel anion conducting states.....	42
Figure 11: Replacement of external Na^+ with Ch^+ abolishes anion flux in EAAT4 but not EAAT1.....	54
Figure 12: Replacement of external Na^+ affects EAAT3 but not EAAT2.....	57
Figure 13: NMDG ⁺ replacement of Na^+ mimics Ch^+ substitution on EAATs 1-4.....	60
Figure 14: Na^+ gating of anion channel activity is concentration dependent in neuronal EAATs.....	63
Figure 15: Replacement of internal Na^+ causes a loss of inward facing anion channel gating in neuronal isoforms only.....	64
Figure 16: State diagrams for neuronal and glial EAATs differ in number of open channel states.....	66

Figure A1. EAAT1 Homology Model Depicting Point Mutations.....	A3
Figure B1. The dynamic lipid bilayer and membrane phases.....	B5
Figure B2. Lipid moieties found within high-resolution structures of integral membrane proteins.....	B6
Figure C1. Selenocysteine is transported by EAATs 1-3 in oocytes.....	C6
Figure C2. Comparison of [³ H]-L-Glutamate transport inhibition by L-Selenocysteine and L-Cysteine for EAAT2 and EAAT3.....	C8
Figure C3. mEGFPpH detects intracellular pH changes induced by glutamate transport.....	C9
Figure C4 Transport of substrates in cells expressing hEAAT2 and hEAAT3 differentially affects intracellular pH.....	C12
Figure C5. Effect of pH on L-cysteine transport properties of hEAAT3.....	C13
Figure D1. R388 has a significant role in substrate transport.....	D6
Figure D2. R388 has a crucial role in activating the substrate gated anion conductance.....	D10
Figure D3. Relative anion conductance in R388D EAAT1 is not affected by glutamate.....	D12
Figure D4 Relative anion permeability and relative anion conductance in R410E EAAT4 mimic the leak conducting state of WT transporters.....	D15
Figure D5. R388D mediates an altered accessibility of HP1 residues to modifying reagents.....	D17
Figure E1. Ketamine Inhibition of GLIC at EC20.....	E2
Figure E2. The Crystal Structure of GLIC Bound with Five Ketamine Molecules.....	E3
Figure E3. Stereo View of Atomic Details of the Ketamine Binding Pocket.....	E4
Figure E4. Functional Relevance of the Ketamine-Binding Site.....	E4

PREFACE

I would to thank my thesis committee. Many of you have been mentors in many ways from the start of graduate school and have served on several of my committees over the years. Jon and Mike have been there from the start and never minded my endless questions wither stupid or not. Steve served on my comprehensive exam and has been a valued mentor since. I know who I can count on for sage advice. Becky is my scientific big sister and has shown me the road map for my career. Us former EAATologist have to stick together. I truly have the thesis Dream Team and for that, I thank you all.

To members of the Amara lab; you have all been either sources of knowledge, advice, or laughs; many laughs. Everyone in 6068 knows when we are joking around on our end. Jie was a model for what a quality graduate student looks like. Spencer was my first lab mentor and an all-around great guy. Anytime you want to trade a desk cleaning for some cookies, I am in. Delany was a great influence who helped me refine my skills and expertise. Suzanne was like a sister to me and I will never forget our pubs at the pub and how we could throw hypothesis and experimental ideas around for hours a day. Thanks for all those last minute revisions. Lastly, I would like to thank Megan, Mads, Ole, Andrea, Conrad, and Ethan for working alongside me and always willing to lend a hand or provide some input. Thank you all for making my time in the Amara lab both fun and productive. I would like to especially thank my mentor Susan G. Amara for teaching me so many things. She has led with a grace and wisdom that is both exceptionally rare and exceptionally inspiring. Thank you for everything.

I would like to thank my friends who I have known for coming up on two decades. Without our Friday night dice throwing, I would have gone insane. Sean has been like a brother

to me and I am glad we get to work alongside each other in the near future. So this is to Noah, Fabus, Caralee, Candace, JD, and all the others who kept me human or at least humanoid.

Thank you to the kind souls who work at Fredo's Deli and Uptown Coffee for tolerating the endless days of me writing this document sucking up space in their fine establishments, and the occasional free cup of coffee.

I would like to thank my family. My sister was an inspiration and a model of success, my brother for boxing, beers, and supplies. My father for keeping 70 hour work weeks in perspective ("that's nothing"), and my mother for always letting me know my future was in my hands.

Lastly and definitely most importantly, I would like to thank my wife Erin Blaine Divito for being my best friend, my cheerleader, and my bug slayer. You are amazing and I am forever proud of you my dear. I cannot wait to see what the future brings us. Whatever it is, we will conquer it together.

1. INTRODUCTION

L-glutamate (glu) is the primary excitatory amino acid in the central nervous system. Dysfunction of glutamatergic signaling is related to many debilitating diseases (1), and therefore proper coordination and fidelity of release, activation, and reuptake of this neurotransmitter is paramount for total system homeostasis. Excitatory amino acid transporters (EAATs) are secondary active, electrogenic transport systems that couple the accumulation of glu into the cytoplasm to downhill movement of co-transported ions along their concentration gradient. Alteration of these ion gradients, such as during anoxic depolarization, halts or even reverses glu transport and can contribute to excitotoxic conditions (2-5). The roles of the EAATs have been studied intensely for the last 30 years and much insight has been gathered into their structure, function, localization, and how they regulate neurotransmission. EAATs regulate glutamatergic neurotransmission but the mechanism by which they accomplish this process is by a dynamic coupling of bioenergetics of the transport process and the localization of the transporters themselves. The consequence of this coupling is the creation of complex spatio-temporal profiles for extracellular glu. Here we will review background information on the SLC1 family of transporters including their function and structure and how these transporters regulate neurotransmission.

1.1.1. Isoforms and Localization

The solute carrier 1 (SLC1) family of neurotransmitter transporters is comprised of several solute carriers including the excitatory amino acid transporter (EAATs). The initial cloning of a glu carrier in the SLC1 family was performed in 1992 with the isolation of a 60 kDa protein from rat brain termed the glutamate/aspartate transporter (GLAST) (6). One month later, glutamate

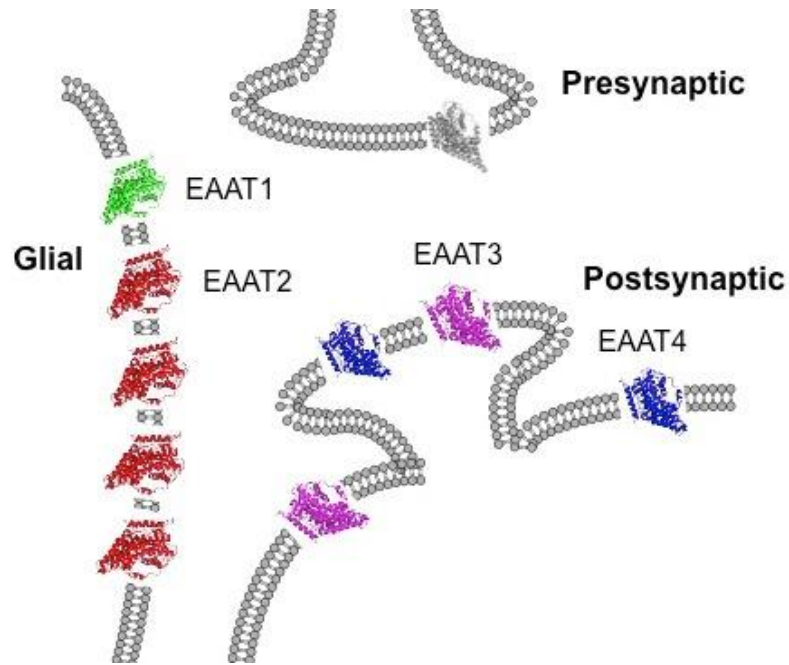


Figure 1: Localization of EAATs in the synapse: Model of a basic synapse illustrating the localization of EAATs 1-4. EAAT1 (green) and EAAT2 (red) are localized to glial membranes. EAAT3 (blue) and EAAT4 (magenta) are localized to post-synaptic membranes. Expression and function of a presynaptic carrier (grey) is unclear, but EAAT2 and EAAT3 isoforms have both been implicated. Structures are modeled as monomers of an archeal homolog of a glu transporter from *Pyrococcus horikoshii* (Glt_{ph}) and were modified from (7). The Glt_{ph} pdb file 1FXH was modified using pymol vs 1.3.

transporter 1 (GLT-1) from rat, and excitatory amino acid carrier 1 (EAAC1) from rabbit were both cloned (8,9). All of these carriers were described as Na⁺ and K⁺ dependent, SLC1 family members that accumulate glu and L- or D-aspartate (asp). Subsequently two novel human isoforms were cloned from the cerebellum and retina, excitatory amino acid transporter 4 (EAAT4) and EAAT5, respectively (10,11). Human isoforms of GLAST, GLT-1, and EAAC1 were also cloned and renamed EAAT1-3 to denote their human species of origin (12). EAAT1-5 share an approximate 65% primary sequences homology between them. The transporters can roughly be divided into two classes – astrocytic or neuronal (Figure 1). EAATs 1 and 2 are found predominantly in astrocytes while EAAT3, EAAT4, and EAAT5 are neuronal. EAAT1 is enriched in cerebellar astrocytes but also found in astrocytes throughout the brain (6,13). EAAT2 is the most abundant glu transporter found in the brain and, by some estimates, accounts for ~90% of the total glu uptake in the brain (14,15). EAAT3 is most often described as a postsynaptic neuronal carrier with expressing ranging throughout the brain. EAAT4, like EAAT3, is also a neuronal transporter (16). While the Purkinje cell localization of EAAT4 is dramatic, this carrier is also found in other neurons at low levels (16,17). Expression of EAAT5 is exclusively in the retina (11). Throughout this paper will refer to general properties of the carriers using their EAAT nomenclature unless specifically in reference to the non-human isoforms. Although basic properties of the various isoforms are largely similar, minor differences in their kinetics, localization, and regulation dramatically affect glutamatergic neurotransmission.

1.2. MECHANISM OF TRANSPORT

1.2.1. Characterization of Glu Transport

Initial functional studies of glu translocation were done in rat brain synaptosomes and the translocation were described as Na⁺ and K⁺ dependent processes (18). Experiments controlling the transmembrane potential in synaptosomes demonstrated that accumulation of glu was also an electrogenic process. Initial electrophysiological recordings of glu carriers described the

electrogenic nature of the transport cycle and supported the basic findings of earlier biochemical studies. A large, rectifying inward current, between -160 and +80 mV, in response to extracellular glu addition was generated in whole cell patch recording of Müller glial cells (19). These currents were voltage and Na^+ dependent and only responded to applications of D- and L-aspartate and L-glutamate but not D-glutamate, congruent with the initial characterizations of glu transport performed by Kanner's group. Early electrophysiological reports also corroborated conclusions from biochemical data when the dependence of transport on intracellular K^+ was investigated by whole cell patch recordings from glia (20).

The translocation of glu is a reversible cycle, and homoexchange of glu was characterized before the molecular identity of the EAATs were known (21,22). All experiments pointed to a relatively high affinity carrier which could translocate substrates in the low micromolar range. Work done on a bacterial homolog glu transporter from *Bacillus stearothermophilus*, GLT_{BS}, demonstrated that electrogenic glu uptake was accompanied by a proton as well as a sodium ion (23), although confirmation of this proton co-transport was contentious and the possibility of OH^- counter transport as the source of pH change associated with glu transport arose (24,25). The most accurate estimation of stoichiometry was demonstrated using a series of experiments controlling ion concentrations and measuring reversal potentials of transport as well as pre-steady state kinetic measurements using substrate concentration jumps (26-28). From data presented in these studies, it can be concluded that EAATs likely function by transporting 1 glu with 3 Na^+ , 1 H^+ , and the counter transport of 1 K^+ (Figure 2).

Initial investigations into the transport kinetics revealed that hyperpolarization of the membrane stimulated transport in a manner that was dependent on glu concentration. This led authors to propose that glu translocation was the rate limiting step of the transport cycle (29,30). It wasn't until pre-steady state kinetics were investigated using a photo-releasable glu analog that a detailed study of initial glu binding and translocations steps were possible (27). Glu

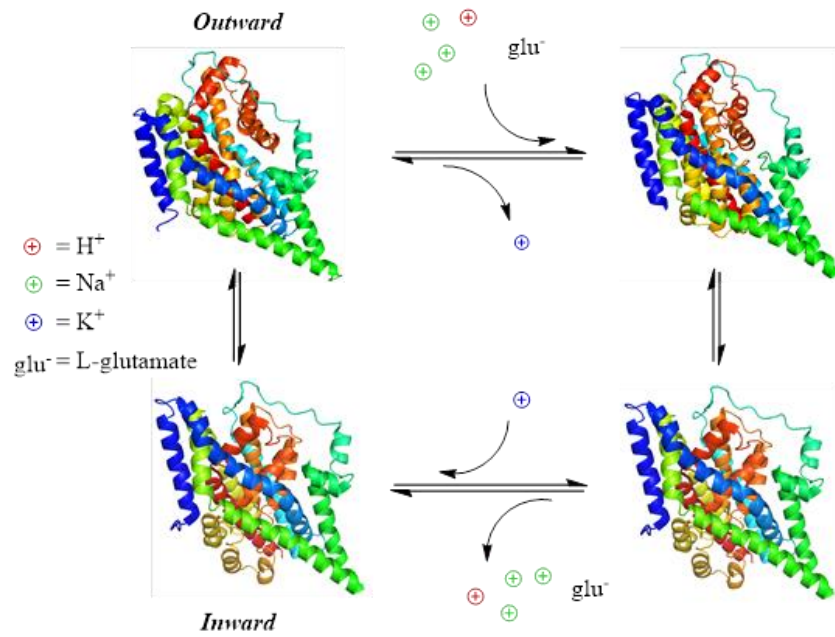


Figure 2: EAATs are secondary, electrogenic transporters. 4-state transport diagram depicting coupled stoichiometry of glu transport and ion movement. Transporters are displayed to represent the outward facing, HP2 open state (upper left), the outward facing, glu-bound, HP2 occluded state (upper right), the inward facing, HP1 occluded state (lower right), and the inward facing, HP1 open state (lower left). The structures used are adapted from the pdb files 2NWW, 1FXH, and 3KBC of Glt_{Ph} (7,31,32).

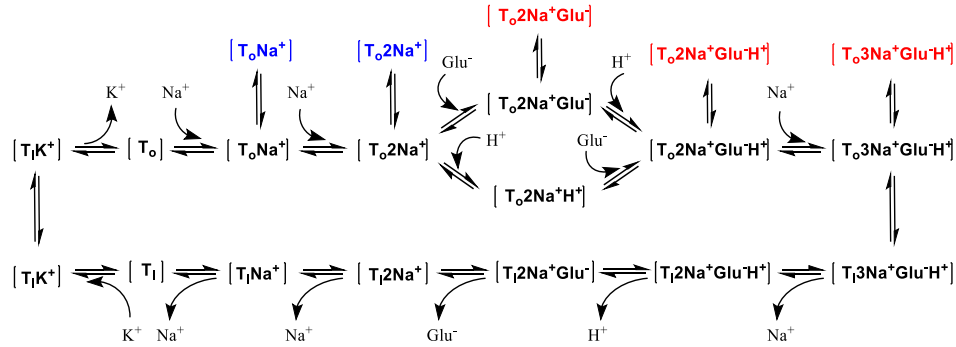
release on a sub-millisecond time scale revealed an initial transient electrogenic component which rapidly decayed down to a steady state level. This voltage and concentration dependent decay process is associated with the initial translocation of glu. Furthermore, these data can only be reconciled with a transport cycle with a rate limiting step not related to glu translocation but to the K^+ mediated reorientation process. A rate limiting glu translocation would not produce the same transient components (33). Additionally, replacement of internal K^+ with Cs^+ dramatically affected cycling times, support that K^+ interaction and reorientation are the late limiting steps of the transport cycle (34). The translocation of glu is dependent on the binding and co-transport of several cationic species. Na^+ binding to the empty transporter has been shown to be a voltage dependent process, generating measureable capacitive currents (35,36). Since the steady state affinity of EAATs for glu is voltage independent although glu translocation generates net inward charge movements, then another voltage dependent process has to produce an equal and opposite charge movement. K^+ reorientation has, therefore, been hypothesized to neutralize more than -1 elementary charge (33). To further test the hypothesis that co-transported cations are used to neutralize the endogenous charges present in the empty transporter (37), a combination of pre-steady state concentration and voltage jump experiments with computational modeling were used. These data led to the conclusion that the negative charge generated by the movement of the empty transport is, indeed, in part compensated by the binding and translocation of Na^+ , H^+ , and K^+ ions (38). The compensation of endogenous transporter charges by ion binding, in addition to a defocused electric field and distribution of electrogenic steps, allows for a tightly regulated and energetically reasonable transport mechanism (Figure 2).

1.2.2. Physiological Regulation of Transport

The transport of glu against its concentration gradient is coupled to the downhill movement of co-transported ions with their gradient. Alterations of the ion gradients for Na^+ , H^+ , and K^+ would, therefore, impact the ability for the EAATs to transport substrates. Evidence for reverse

transport came early when Kanner and Marva used vesicles from rat brain which were loaded with high internal Na^+ and high extracellular K^+ to efflux radiolabeled glu which had been loaded into the vesicle (22). In whole cell patch recording of Müller glial cells of the salamander retina, dialysis of the internal solution using a pipette solution containing Na^+ and glu drove glu transporters in the reverse direction with the addition of extracellular K^+ (39). The reversal of the transport cycle, or glutamate mediated efflux, has been demonstrated in a variety of glu transporters isoforms such as EAAT1 or EAAC1 (rat EAAT3), suggesting that reverse transport capability is intrinsic to the SLC1 family (40,41). During normal physiological conditions, it is unlikely that reverse transport occurs frequently enough to have a physiological consequence (42), yet during anoxic depolarization it has been suggested that glu efflux mediated by reversal of the EAAT transport cycle can mediate excitotoxic conditions (4). So how do the bioenergetics of transport influence glutamatergic neurotransmission? First, the coupled movement of three sodium ion indicates that glu can be concentrated inside a neuron or astrocyte with a 10^6 fold glu concentration difference or keep extracellular glu levels down to the low nanomolar concentration (26). Additionally, under ambient conditions, the low affinity for Na^+ and glu at the intracellular face of the transporter means that reverse transport would occur with a negligible frequency (36). During ischemic conditions, however, in which the Na^+ and K^+ concentrations and transmembrane voltage are disturbed, a significant amount of glu has been demonstrated to be released through an EAAT mediated reverse transport process (4). Thus, the bioenergetics of glu transport tightly controls the rates and amount of neurotransmitter removal from the synaptic space. Because cessation of excitatory neurotransmission is dependent on the efficient removal of extracellular glu, the bioenergetics of EAAT transport contributes to the termination of glutamatergic neurotransmission in an essential manner.

A



B

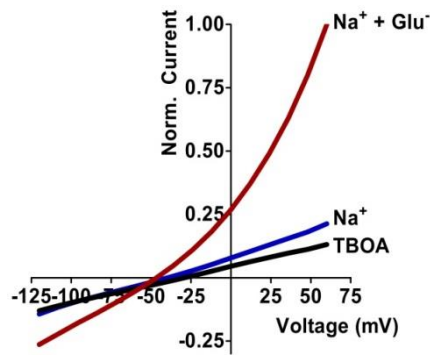


Figure 3: EAATs mediate anion flux through multiple open states. A) 20 step state diagram depicting stable conformations of glu transport (black) and open channel states gated by either Na⁺ interaction (blue) or Na⁺ and glu interaction (red) associated with the outward facing conformations of the transport cycle. Inward facing open channel states have been removed for clarity. **B)** Demonstrative current-voltage relationship for an EAAT in response to extracellular application of Na⁺ + DL-threo-β-benzyloxyaspartate (DL-TBOA; black), Na⁺ alone (blue), or Na⁺ + 500 μM glu (red). Currents are representative of NO₃ flux through EAAT4.

1.3. LIGAND-GATED ANION CHANNELS

1.3.1. Characterization of Channel Activity

In 1994, electrophysiological characterization of a novel EAAT cloned from cerebellar mRNA of humans, revealed a remarkable property of glu transporters (10). An EAAT-mediated Cl^- flux which was Na^+ and glu dependent but thermodynamically independent of the transport process was demonstrated (Figure 3). These data was the first to unambiguously reveal anion channel activity in the EAATs. Initial voltage clamp studies of the EAAT anion channel revealed several basic properties. First, the anion channel is promiscuous, with a permeability sequence generally following $\text{SCN}^- > \text{ClO}_4^- > \text{NO}_3^- > \text{I}^- > \text{Br}^- > \text{Cl}^- > \text{F}^-$ (43-45). Second, the interaction of substrates with EAATs elicits a robust anion current, but this anion flux occurs, with diminished amplitude, in the absence of substrates as well. This “leak” current was originally revealed by the loss of a tonic cellular conductance in the presence of inhibitors (46). Anion conductances in the absence of extracellular glu were substantiated by several groups (40,47,48). It was demonstrated that the leak current is actually dependent on extracellular Na^+ (49) and indeed gated by Na^+ interaction with the EAATs in the absence of glu (34,50). Stationary and non-stationary noise analyses have been used to characterize channel properties mediated by Na^+ and glu interaction (40,51-53). These data revealed that Na^+ interaction with the EAATs mediates a low open probability and the open probability of the channel is increased upon glu binding subsequent to Na^+ , without a significant change in low (0.5-500 fS) single channel conductance. The physiological role or impact of these tonic anion fluxes in the absence of active transmission has yet to be examined in detail.

The mechanism by which substrate interaction with the EAATs gates the channel is still under investigation. Initial work by Vandenberg's group using a series of point mutations between residues R90 and K114 of EAAT1 demonstrated that the D112A mutation significantly reduced glu gated anion current amplitudes yet strongly enhanced Na^+ gated currents (54). These data suggest that D112 is involved in the ability of substrate to gate that the anion

channel. Similarly, when R388 in transmembrane domain 8 (TM8) is mutated to an acidic amino acid residue, substrate gated anion channel activity is completely abolished while current amplitudes in the presence of Na⁺ alone are enhanced several fold (Appendix D). Other residues have been implicated in the gating mechanism in addition to D112 and R388. Mutations of D272 (TM5), K384, and R385 (TM7) in hEAAT1 have all been demonstrated to increase channel activity after mutation to alanine (55). Only a handful of mutations have been demonstrated to alter channel activity, however non-mutational data have also contributed to our understanding of the mechanism of channel gating. Pre-steady state kinetics has been a powerful technique to study the initial steps in substrate interaction and channel activity. Laser pulse photolysis of caged glu was employed for a series of investigations to measure the initial kinetics of substrate binding, translocation, and substrate gating. These elegant experiments have lent great insight in the mechanism of transport and channel activity and have been thoroughly reviewed elsewhere (56,57).

1.3.2. Role of the Chloride Channel in Regulating Synaptic Transmission

The physiological role of a low conductance anion channel present in a family of neurotransmitter transporters remains elusive. One possible role for this ligand-gated channel is the stabilization of the membrane potential to offset the positive ion influx associated with electrogenic transport of substrates during neurotransmission (44). Veruki et al. (2006) used whole cell and paired recordings from rod bipolar cells and AII amacrine cells to demonstrate that glutamatergic activation of EAAT5 causes a membrane hyperpolarization which reduces subsequent transmitter release (58). These data demonstrate that anion flux through the EAATs is capable of regulating cellular excitability. Additional work demonstrated that EAAT5 mediated a large inhibitory current in response to bipolar cell depolarization, confirming a role for the EAAT mediated anion conductance in shaping neurotransmission (59).

1.4. STRUCTURE OF THE SLC1 FAMILY

1.4.1. EAAT Topology

Upon cloning of the first members of the SLC1 family, hydropathy plots gave initial insight into the secondary structure of these carriers. A bacterial SLC1 family member, the glutamate-proton co-transporter (GltP) from *E. coli*, displayed 12 putative transmembrane domains (TM) with a cytoplasmic C-terminus (60). Topology models of GLT-1 and EAAC1 displayed 8 and 10 transmembrane domains respectively, but both models contained a large glycosylated loop between TM3 and 4, an intracellular N-terminus, and a long, intracellular C-terminal tail (8,9). Structural experiments were used extensively by several groups in order to further refine the topology of the transporter during different conformational states. Rat membrane vesicles containing GLT-1 were probed for their sensitivity to trypsin digestion in the presence and absence of the GLT-1 inhibitor dihydrokainate (DHK) as well as the substrate glu. The difference in trypsin induced fragments with bound substrates and antagonist indicated at least two conformational states representing inhibitor stabilized, outward facing states and substrate induced, transporting states of GLT-1 (61). Additional topology models were proposed over the next few years including a refined 4 TM domain C-terminal region (62) and a possible β -sheet structure in the C-terminal transmembrane domains (63).

In order to increase the resolution of the structural topology data, a method originally used to screen pore lining domains using modification of single cysteine residues was employed (64-66). Initial experiments employing cysteine mutagenesis based methods revealed a topology for GLT-1 with 8 TM domains and a reentrant loop (HP2) between TM 7 and 8 (67). Additional data using substituted cysteine accessibility method (SCAM) supported the presence of two reentrant loops, although disagreeing on their location in the c-terminal half of the transporter (68-70). The first accurate report of EAAT membrane topology came when Grunewald et al. (2000) performed SCAM experiments across residues 347 to 393 (71). The

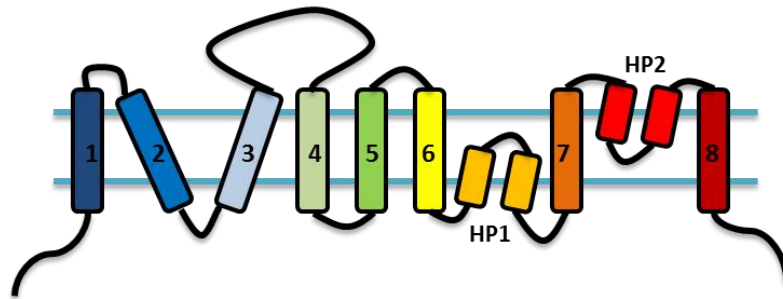
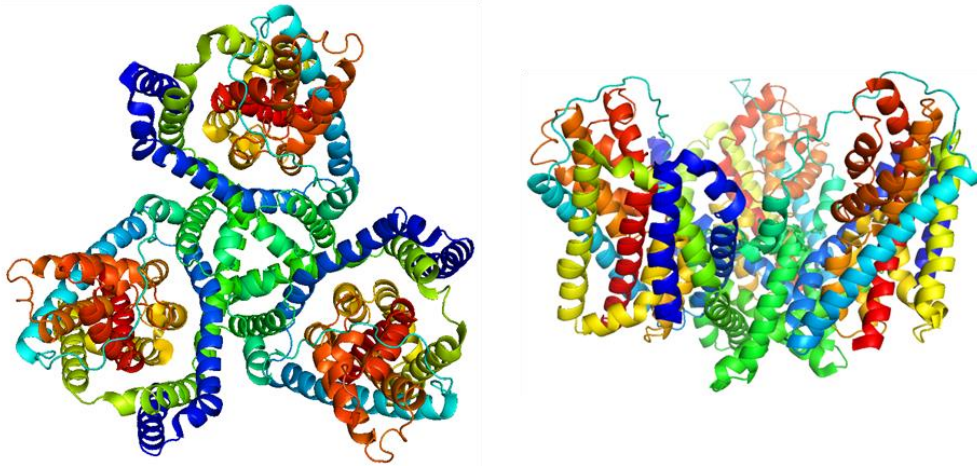
A**B**

Figure 4: General structure of the SLC1 family of transporters. A. Two-dimensional representation of the topology of the Glt_{Ph} monomer colored with a rainbow pattern. **B.** (*Left*) Top-down view of the homotrimeric Glt_{Ph} crystal from pdb file # 1FXH. Each monomer was colored with the same rainbow pattern as in A) using Pymol version 1.3. (*Right*) View of the same trimeric representation of the Glt_{Ph} crystal structure from a horizontal or membrane view.

ability for only residues A364C and G365C (GLT-1) to be labeled by the extracellular application of the non-permeable MTSET, depicted another reentrant loop (HP1) located upstream of TM7. Currently the model for EAAT topology is 8 TM domains and 2 hairpin loops (HP1 and HP2); HP1 located between TM 6 and 7, and HP2 located between TM7 and 8 (Figure 4A).

1.4.2. The Crystal Structure of an Archeal Homolog of Mammalian EAATs

Work investigating the oligomerization of EAATs was incipient with exposing liposomes reconstituted from rat forebrain and cerebellum with chemical crosslinking reagents (72). These experiments, along with similar data from assays using heterologous expression of EAATs, support a homotrimeric organization of EAATs (73). However, the homotrimeric, quaternary structure of EAATs was disputed by freeze-fracture electron microscopy data which suggested a pentameric assembly (74). The first definitive picture of tertiary and quaternary structure came in 2004 when the crystal structure of an archeal homolog to the EAATs, Glt_{ph} was solved (7). The crystal architecture displayed 8 transmembrane domains and two hairpin loops located between TM6-7 and TM7-8, as previously described (71). The organization of the transporter in the membrane was that of a homotrimer with the subunit interface comprised of TM 2, 4, and 5 regions (Figure 4B). The trimer shape of the Glt_{ph} crystal formed a bowl or extracellular solvent-accessible basin and the co-crystallization of bound substrates confirmed the location of the hypothesized binding site. The binding site is adjacent to TM7, at the tips of HP2 and HP1 and the substrate was coordinated by several residues previously demonstrated to have a role in substrate interactions (28,75-78). The conformational state that seemed to be displayed by this snapshot was the outward conformation with the binding site occluded by HP2. Although the mutated archeal transporter used for crystallized was inactive, the resulting crystal structure was in strong congruence with structure-function data and served well to refine lingering questions in the field. To date, three more crystal structures have been solved using the archeal asp carrier Glt_{ph}. The location of the substrate-binding site was confirmed with investigations demonstrating that D394 in TM8 coordinates the amino group of asp or glu and R397 interacts with the side

chain carboxyl group. Additional structures demonstrated DL-TBOA bound states with slight differences in the location of HP2 suggested possible outward open states (31) (see also Figure 2). One of the next structural developments depicted a possible inward-facing state. Through crosslinking of distal residues in HP2 and TM2, crystals were obtained and a transport mechanism was proposed to explain the transition of the previously described outward facing structures to the HP2/TM2 cross-linked structure. The model includes a substantial inward shift of TM3, TM6, HP1, TM7, HP2, and TM8, which was termed the translocation domain as it contained the HP2 and HP1 occluded, substrate binding site. This piston-like movement leaves both the translocation domain and TM1, TM2, TM4, and TM5, termed the scaffold domain, largely similar in conformation, when considered individually, albeit over an 18 Å inward shift of the substrate binding site (32).

1.4.3. Structural Influences of the Trimeric Organization of EAATs in Glu Uptake

Although many of the functional and structural features of the EAATs have been resolved, there may be other aspects of the structure which can influence carrier activity in unforeseen ways. Indeed it has been proposed that the bowl-like shape of the trimer may play a role in restricting glu diffusion after initial binding, thus helping to reduce effective glu release after initial binding events during synaptic transmission (79). Future work may further reveal aspect of how the quaternary structure of EAATs support their function roles in regulating excitatory neurotransmission.

1.5. THE ROLE OF EAATS IN SYNAPTIC TRANSMISSION

1.5.1. The Roles of EAATs in Glutamatergic Neurotransmission in the Hippocampus

The role of EAATs is to control extracellular glu levels, both ambient and in response to exocytosis of neurotransmitter due to neuronal activity. Levels of ambient glu have been estimated as low as 25 nM and blocking the carriers with a specific antagonist causes a non-linear rise in ambient levels, supporting the classic role of EAATs in maintaining low

extracellular glu concentrations (80). Synaptic concentrations of glu, after vesicular release from dissociated hippocampal neurons, were initially estimated to be in the millimolar range, approximately 1.0 - 1.5 mM (81). Early studies looked at the effect of EAAT blockade, or competition at the carrier binding site, on activation of post-synaptic ionotropic glu receptors (iGluRs) and indicated that loss of active transporters could increase the concentration of neurotransmitter in the synapse, observed as a slight, transient increase in mEPSC amplitudes (82) or as a decrease in decay rates of EPSCs (83). Through the delicate manipulation of α -amino-3-hydroxy-5-methyl-4-isoxazolepropionic acid receptor (AMPA) kinetics with various pharmacology, it was demonstrated that in the first 100 μ sec of glu release from the presynaptic terminal, EAATs act to reduce mEPSC amplitude and shorten rise times of the transient post synaptic currents (84). Since the transport cycle is significantly slower than this timing, approximately 15 - 90 s^{-1} (33,35), it was proposed that glu transporters act to buffer synaptic glu with a relatively high affinity binding interaction, yet the slow kinetics of transport allows for some unbinding of substrate before a substantial amount of glu can be transported (33). To support the hypothesis of rapid buffering, EAAT expression near the synapse would need to be at remarkably high levels. Indeed estimates for EAAT2 concentrations in hippocampal astrocytes are as high as 12,000/ μm^3 and EAAC1 neuronal levels were estimated to be 130 / μm^3 (14,85). Thus, EAATs can modulate the concentration of synaptic glu to some degree but also act to control the temporal profile of postsynaptic receptor activation and diffusion to perisynaptic regions as glu binds and unbinds rapidly to a high number of carriers.

Diffusion accounts for much of the rapid decrease in synaptic levels of the neurotransmitter and elevated perisynaptic concentrations of glu can be detected for a sustained period of time (>10 msec). This sustained activation of peri-synaptic transporters has been demonstrated for EAAT expressing astrocytes in the CA1 region of the hippocampus with stimulation of Schaffer collaterals synapsing on CA1 pyramidal cells (48). These data

demonstrate that rapid clearance of synaptic glu is accomplished mainly through diffusion but a significant level of glu persists at the perisynaptic regions. This persistence of neurotransmitter is not due to heteroexchange functions of the EAATs (glu in - glu out) since application of the competitive transportable substrate threo-hydroxyaspartate (THA; a substrate which could induce heteroexchange for cytoplasmic glu) results in the same activation of iGluRs as does application of the non-transportable competitive inhibitor DL-threo- β -hydroxybenzoylaspartate (DL-TBOA; 86). The influence of EAAT-mediated glu buffering and transport capacity on hippocampal circuitry during high frequency stimulation was investigated (87). Synaptically evoked transporter currents (STCs) from CA1 region astrocytic carriers (EAAT1 and EAAT2) were not significantly altered after a series of stimulations at near-physiological temperatures arguing for a very capacious glu uptake system in the hippocampus. To further clarify the mechanism of glu removal surrounding the synapse (perisynaptic regions), Schaffer collaterals-CA1 pyramidal cells synapses were exposed to a low affinity N-methyl-D-aspartate receptor (NMDAR) antagonist and the effects of TBOA blockade on NMDAR mediated EPSCs were measured (88). Results indicated that TBOA inhibition of the perisynaptic EAATs resulted in an increase in non-synaptically located, or distal, NMDAR activation. Additionally, replacement of internal cations in a post-synaptic neuron for NMDG⁺, effectively blocking transport, also significantly altered the activation of NMDARs suggesting a role for post-synaptic neuronal EAATs in limiting spillover activation from adjacent synapses, a role which was previously attributed predominately to the glial EAAT isoforms. Investigations using EAAC1 (mouse EAAT3) knock-out transgenic models refined the role of post-synaptic EAAC1 by speeding the decay constant of NMDAR activation in the presence of a low affinity antagonist, supporting the role these carrier play in modulating NDMAR activation, especially NR2B containing receptors, in perisynaptic spaces (89). This study, however, did not support the role of EAAC1 in limiting glu spillover to adjacent synapses. From these data, it is clear that EAATs not only modulate post-synaptic receptor activation but can regulate activation of ionotropic receptors located at

sites beyond the synaptic cleft. The distance that synaptically released glu can influence activity supports the need for a diverse and widely localized family of carriers.

1.5.2. The Role of EAATs in the Cerebellum

The role of glu transporters is similar for many brain regions although differences in expression pattern, synaptic architecture, and general features of circuitry all can influence glutamatergic neurotransmission. Due to the high concentration of EAAT4 (a higher affinity yet lower turnover rate isoform) expressed in the cerebellum, Otis et al. (1997) (90) investigated buffering of released glu from climbing fiber-Purkinje cell synapses (CF-PC). Results indicated some synaptic glu transporters as well as perisynaptic EAATs could rapidly buffer upwards of 22% of glu released from a single vesicle. In the cerebellar cortex, EAAT4 mimics the actions of EAAT3 in the hippocampus by rapidly buffering synaptic glu. Although both EAAT3 and EAAT4 are expressed in CF synapses, investigations using EAAT3 and EAAT4 transgenic knockouts into the relative contribution of these two carriers in the CF synapse revealed a dominate role for EAAT4 as compared to EAAT3 in this system (91). To investigate the role of glial carriers (predominately EAAT1) in cerebellar excitatory neurotransmission, climbing fibers were stimulated and caused a rapid onset of EAAT transport currents in Bergmann glial cells which persisted for a prolonged period of time, supporting the notion of rapid escape of glu from the synapse and slow re-uptake once diffused to extrasynaptic regions (92).

One of the most striking features of the CF-PC synapse is the concentrations of glu that are released following CF stimulation. CF-PC synapses have been thoroughly demonstrated to mediate multivesicular release and moderate firing rates induce a significant glu spillover (93). Spillover of glu causes activation of molecular layer interneurons (MLIs) and was observed in the cerebellum during activation of CF-PC synapses (94). This spillover mechanism is so profound that excitation of MLIs can mediate feed-forward inhibition and alter activity patterns in neighboring interneurons and Purkinje cells (95). Thus at the synaptic cleft, perisynaptic space,

and even at adjacent synapses glu transporters play vital roles in regulating the concentration of extracellular glu.

1.5.3. EAATs Influence Activation of Metabotropic Glu Receptors and Synaptic Plasticity

It is clear that glu transporters in conjunction with diffusion regulate the temporal and spatial pattern of glu after various modes of release. How does this spatial-temporal profile effect perisynaptic receptor activation and downstream processes such as synaptic plasticity? It has been observed that EAAC1 activity regulates NMDAR activation in the hippocampus but the consequences of ionotropic activation go beyond basic excitatory transmission. It is well demonstrated that activation of NMDAR (and some Ca^{2+} permeable AMPARs) can lead to several forms of synaptic plasticity (96-98). NMDAR activation is a key component to many alterations of synaptic strength. This alteration has been demonstrated to take various forms such as presynaptic alteration, typically reported as a difference in quanta, as well as postsynaptic alterations such as changes in AMPAR surface expression (99-101). The extent to which EAAT3 limits activation of perisynaptic NMDARs is great enough to influence both LTP and LTD in the CA1 region of the hippocampus (89). Metabotropic GluRs (mGluRs) have a significant role in changes in synaptic strength in the CA1 region of the hippocampus (98,102). As we have described here, it is clear that EAATs mediate the ability for glu to activate perisynaptic receptors and as the affinity of many of the mGluRs for glu is lower as compared to iGluRs, the role of EAATs in regulating mGluR activation is pronounced. Indeed, inhibition of EAATs in the CA1 region of the hippocampus caused an enhancement of mGluR1 α mediated currents in O-LM interneurons in that region (103). Likewise, application of TBOA to rat hippocampal slices altered the activation of mGluR5 and group III mGluRs supporting a general mechanism of EAATs regulating glu accessibility to any perisynaptically localized glu receptor (104). Thus, in the hippocampus, EAAT mediated regulation of receptor activation is a critical process that modulates not only fast excitatory neurotransmission but ionotropic and metabotropic regulation of synaptic function and strength.

The role of EAATs in modulating synaptic plasticity is not constrained to the hippocampus as demonstrated by investigations into the cerebellum. EAAT4 expression in the cerebellum is localized adjacent to the post-synaptic density (PSD) which overlaps with that of metabotropic glutamate receptors (mGluRs). Inhibition of post-synaptic EAAT4 (and EAAT3 to some extent) causes a significant enhancement of long-term depression (LTD) in PF-PC synapses through an mGluR dependent process (105,106). Additionally, in CF-PC synapses the presence of a group 1 mGluR component is only observed when EAATs are inhibited (106,107). This mGluR activation has profound roles in CF associated LTD but also in synaptic pruning of multiple climbing fiber inputs to the PC early in development, and in general provides a CF-PF homosynaptic form of regulation tightly mediated by glu release and EAAT activity. Thus, one of the many roles of EAATs is to influence activation of mGluRs and subsequent synaptic functioning. Regional differences in the ability of Purkinje cells to be regulated through mGluR dependent activity are strongly controlled by the expression pattern of EAAT4 in the cerebellum (108). Another study demonstrated that LTD of PCs synapses results in a decrease in postsynaptic AMPAR expression and a concomitant persistent increase of post-synaptic EAAT4 currents (109). Thus, as synaptic strength is decreased by AMPAR trafficking, EAAT4 levels likely increase to compensate for the decreased number of receptors by enhanced rapid buffering of glu and regulation of perisynaptic glu concentrations. Overall, these data presented here, and elsewhere, strongly support the role of glu carriers in shaping several aspects of neuronal functioning.

1.6. CONCLUSION

Glu transporters or EAATs regulate extracellular glu dynamics throughout the nervous system. The role of neuronal isoforms has expanded to include such processes as cysteine transport for glutathione synthesis (110,111) and glu uptake for GABA synthesis (112), but the prevailing hypothesis is that glial isoforms mediate the bulk of glu transport and have the greatest degree

of influence on extrasynaptic receptor activation. Excess glutamatergic signaling can lead to excitotoxic cell death and during ischemic conditions the transporters themselves become potent releasers of glu. The activities of EAATs are indicated in almost every process of neurotransmission and we are still trying to understand the roles of the chloride channel activity these transporters mediate. It is likely that the channel function of the EAATs can indeed regulate cellular activity either through offsetting inward positive charge movement associated with a high capacity transport mechanism or through acting as a classic ionotropic Cl^- receptor. Indeed it is an exciting time to study this fascinating family of carriers and their roles in shaping glutamatergic neurotransmission.

2. INWARD FACING STATES OF EXCITATORY AMINO ACID TRANSPORTERS MEDIATE OPEN CHANNEL STATES

2.1. INTRODUCTION

L-glutamate (glu) is the major excitatory neurotransmitter in the brain. Synaptically released glu is rapidly buffered by binding to neuronal transporters although the majority of neurotransmitter diffuses and is cleared by glial and perisynaptic neuronal carriers (81,82,84). Dysfunction of excitatory amino acid transporters (EAATs) has been hypothesized to be pathogenic in Alzheimer's disease, amyotrophic lateral sclerosis (ALS), Parkinson's disease, and ischemia (1,113). In humans, a family of five glu transporters are responsible for the clearance of glu (114). EAATs are organized as homotrimers within the membrane and possess 8 transmembrane domains (TM1-8) and 2 re-entrant or hairpin loops (HP1 and HP2), (7). These secondary active, electrogenic carriers co-transport substrates with 2-3 Na⁺ and 1 H⁺ (26). After intracellular release of substrates, a K⁺ ion binds to the cytoplasmic facing transporter and allows for reorientation of the carrier in a rate-limiting process (27,33). Glu binds to a transporter already bound with at least 1 Na⁺ ion, followed by H⁺ and the last Na⁺ ion(s) (27,35,50). The initial translocation of substrate generates approximately 2 inward charge movements and happens on a rapid time scale of 3-5 milliseconds (33). This leaves the transporter in the inward facing states for the majority of the transport cycle, ~ 15-30 msec.

EAATs also possess a thermodynamically uncoupled anion conductance that is activated by ligand interactions (10,43,45). Modifying single cysteine mutants in HP2, a hairpin loop that serves as the external gate for substrate binding, locks the gate in the open position. This significantly disrupts glu transport capacity yet still allows for substrate binding and full

channel activity, thus supporting the hypothesis that distinct domains influence channel and transport function in the EAATs (115-117). These data demonstrate that gate modifications can restrict transporter conformation and can be used to study intact channel functionality.

The EAAT associated anion channel is gated by initial Na^+ interactions and the channel open probability is increased upon subsequent glu binding (46,50,52,53). Although, the channel activity during these first steps of the transport cycle has been thoroughly examined, a detailed investigation of channel activity mediated during other steps of the transport cycle, including steps where Na^+ and/or glu ions remain bound to inward facing conformations, has not yet been performed in EAAT1. Experiments investigating the ability for glu to induce channel activity when applied to the intracellular face of the other EAAT isoforms using inside-out patch clamp recordings revealed that glu can induce significant anion flux (40,41,45). Recent results from combined experiments and modeling using EAAT4 indicate the possibility that all states in the transport cycle have an associated open channel state (118). To date, similar experiments have not been performed in EAAT1, thus it remains unclear if EAAT1 shares the same conducting states as the other isoforms.

In the present study we developed an approach to restrict the transporter to inward facing states of the cycle by modifying the intracellular gate HP1 and then assaying for channel activity. Incubation of EAATs with high external K^+ has been demonstrated to drive the carriers to the inward facing states where the transporter would need to rebind K^+ or both Na^+ and glu to reorient back to the outward facing states (20,22,39,119). Chemical modification of single cysteine mutants in the region of HP1 occur within the cytoplasm only when the carrier is inwardly oriented (120). After incubations with K^+ conditions to drive the transporter to the inward facing state, modification of the exposed HP1 region restricts subsequent conformational changes, thus effectively trapping the carriers in an inward facing conformation. By chemically modifying L376C, a point mutation within HP1, we were able to use two electrode voltage clamp (TEVC) to observe an anion flux with similar properties to the outward, Na^+ bound conducting

states. These novel data reveal anion conducting states during the glu transport cycle. Because the transporter spends the majority of the time in inward facing states, these findings highlight the potential of anion flux to contribute to neuronal function through prolonged channel activity.

2.2. EXPERIMENTAL PROCEDURES

2.2.1. Generation of Mutant EAAT Constructs and Cell Transfections

Site directed mutagenesis was performed as previously described (116). Briefly, human CSLS EAAT1 constructs, in which all endogenous cysteine residues were mutated to serine, were used as a background for subsequent Quikchange (Stratagene) reactions to generate all cysteine point mutations used. All mutations were performed with the EAAT1 construct in the oocyte expression vector pOTV and were subsequently subcloned into pCDNA3.1 (rEAAT4) or pCMV5 (hEAAT1) using Kpn1 and Xba1 (New England Biolabs) restriction sites for mammalian expression. COS7 cells were transiently transfected using Lipofectamine 2000 (Invitrogen) two days prior to use for experiments. For oocyte experiments, stage VI oocytes were injected with 10 ng of cRNA generated from EAAT1 pOTV constructs using mMessage mMachine T7 kit (Ambion) (10).

2.2.2. Radiolabeled Glu Transport Assays

Radiolabeled uptake assays were performed two days after transient transfection. 500 μ M of either Na⁺ glu or K⁺ glu salts were mixed with 200 nM 3,4-³H-L-glu (Perkin Elmer) and applied to EAAT expressing COS-7 cells or *Xenopus* oocytes for 10 min. Cells were washed with phosphate buffered saline containing 1 mM MgCl₂ and 0.1 mM CaCl₂ (PBSCM) before and after glu incubations in COS-7 experiments. Oocytes were washed with ND96 buffer containing 96 mM NaCl, 2 mM KCl, 1.8 mM MgCl₂, 1 mM CaCl₂, and 10 mM HEPES, pH 7.4. Various concentrations of N-ethylmaleimide (NEM) (Sigma-Aldrich) or (R)-(+)-N-(1-Phenylethyl)maleimide (NPEM) (Sigma-Aldrich) were applied for various time points and then removed by washing immediately before addition of radiolabeled glu. Cells were lysed with 0.1

N NaOH and 1% SDS and liquid scintillation counting was used to record radiolabel accumulation in the cells.

2.2.3. Cell Surface and Cysteine Targeted Biotinylations

COS-7 were transiently transfected two days prior to experimentation. Cells were washed 3x with PBS before incubation with 80 μ M maleimide-long arm-biotin (Vector Labs) or BCCM-Biotin (Pierce) for 40 min at 4°C. Reactions were quenched by addition of 100 mM L-glycine for 20 min and cells were lysed before addition of EZ-link neutravidin agarose beads (Thermo Scientific). Western blots were run on a 8-16% tris-glycine gel (Invitrogen) and the transferred blot was probed using a lab-generated rabbit α hEAAT1 C-terminus antibody at a 1:1000 dilution (68). Secondary antibodies, goat α rabbit conjugated to HRP, were used at a 1:5000 dilution.

2.2.4. Electrophysiology

Two electrode voltage clamp recordings were performed using a Geneclamp 500 (Molecular Devices). Holding potential was set to -60 mV and 500 msec command ramps were performed from -120 mV to +60 mV. Current amplitudes used for data analysis were taken from the last 100 msec of the ramp to ensure measurement of steady state conditions. Standard extracellular recording buffers used consisted of 96 mM NaNO₃, 2 mM KCl, 1.8 mM MgCl₂, 1 mM CaCl₂, and 10 mM HEPES, pH 7.4 (NaNO₃ or high extracellular Na⁺ buffer). Incubations with modification reagents were done with either 96 mM NaCl, 2 mM KCl, 1.8 mM MgCl₂, 1 mM CaCl₂, and 10 mM HEPES, pH 7.4 (ND96), or 98 mM KCl, 1.8 mM MgCl₂, 1 mM CaCl₂, and 10 mM HEPES, pH 7.4 (K98 or high extracellular K⁺ buffer). Standard electrodes were pulled to a resistance of 0.5 – 2 M Ω and were filled with 3 M KCl. A 3 M KCl salt bridge was used for all experiments and signals were filtered at 1 kHz with a low-pass Bessel filter and sampled at 50 kHz. All currents were recorded using pClamp10 software and digitized with a Digidata 1440A A/D converter (Molecular Devices). Modification of cys point mutations with permeable reagents used a 4 min perfusion of various concentrations of N-ethylmaleimide (NEM) or N-phenylethylmaleimide

(NPEM) in K98 or ND96 buffers with a gravity fed flow rate of ~ 5-10 ml/min unless otherwise noted. Post-modification washes consisted of ND96 for at least 2 min to ensure complete removal of reagents before recording.

2.2.5. Homology and Kinetic Models

Tertiary structural models of EAAT1 were generated using the software package Modeller version 9.11 (121). First, the sequence for EAAT1 was aligned with the protein sequence of Gl_{Tph} extracted from the coordinate files of the open (3KBC.pdb) or the closed (1XFH.pdb) structures obtained from the pdb repository (RCSB.org). The alignments were accomplished using a combination of a Clustal algorithm and manual optimization in the MacVector software suite. These alignments were then used by Modeller to thread the EAAT1 sequence on the published structures followed by optimization to satisfy spatial restraints. The PyMOL Molecular Graphics System, Version 1.5.0.4 (Schrödinger, LLC) was used to modify color and orient structures. ChembiDraw Version 13 (Perkin Elmer) was used to construct the state diagram.

2.2.6. Data Analysis and Statistics

Electrophysiology data were analyzed using Clampfit version 10.2 (Molecular Devices) and Prism version 5 (Graphpad). All other data were analyzed using Prism. To control for expression variability in the oocytes, TEVC data were normalized within each oocyte as indicated in the figures. Time course data was fit with a single exponential decay of

$$Activity = (Activity_{Initial} - Plateau) \times \exp^{-t/\tau} + Plateau$$

and was used to generate a time constant τ . Kinetic curves of steady state current amplitudes at +60 mV in response to various concentrations of glu were fit with a Michaelis-Menten equation of

$$Channel\ Activity = \frac{(V_{MAX} \times [glu])}{(K_M + [glu])}$$

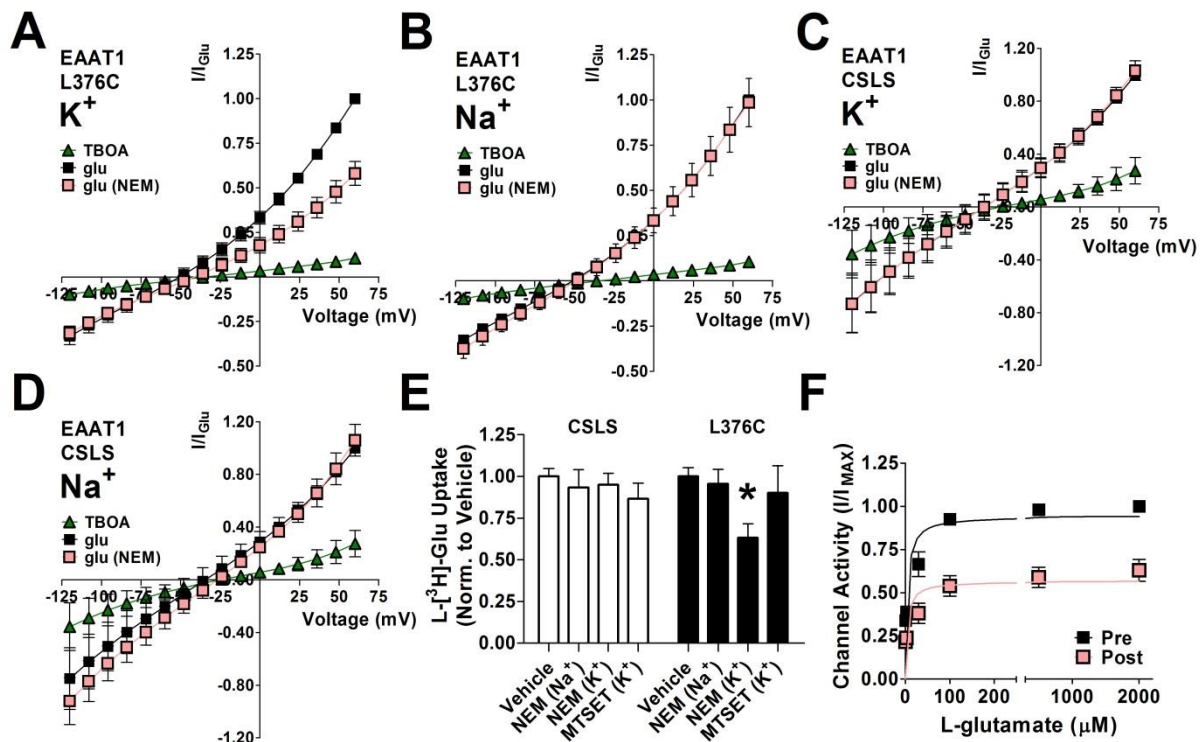


Figure 5: Modification of L376C restricts the transporter to inward facing states. (A-D)

Current-voltage relationships obtained from oocytes expressing EAAT1 L376C (**A, B**) or EAAT1 CSLS (**C, D**) in response to a series of voltage ramps ranging from -120 mV to +60 mV. Each experimental group was perfused with $NaNO_3$ + 500 μM L-glu (black squares), and $NaNO_3$ + 100 μM DL-TBOA (green triangles). 250 μM NEM was perfused for 4 min in the presence of high extracellular K^+ buffer (A, C), or a high extracellular Na^+ buffer (B, D). $NaNO_3$ + 500 μM L-glu applications were then repeated following NEM incubation (pink). Data are displayed as the mean and std dev. and was normalized to currents at + 60 mV for the unmodified L-glu response. (A-D) Data are an average of 20 individual cells for each condition from at least 3 separate frogs. (**E**) Radiolabeled uptake assay of CSLS EAAT1 (white) and L376C (black) expressed in *Xenopus* oocytes. Conditions are a 4 min pre-incubation of either vehicle control, 250 μM NEM in either high extracellular K^+ buffer (K^+) or high extracellular Na^+ buffer (Na^+), or 1 mM MTSET in high extracellular K^+ buffer (K^+). Counts per min were normalized to vehicle

conditions. **(F)** Current amplitudes from varying concentrations of L-glu in L376C, pre- (black squares) and post- (pink squares) modification using a 250 μ M NEM perfusion for 4 min. The currents were fit to a Michaelis-Menton equation as described in the experimental procedure. (E-F) Data are displayed as the mean and S.E.M. with an N of 8 for all conditions from 3 separate frogs. Stars indicate statistical significant difference with a Bonferroni post-analysis after a significant 2-way ANOVA comparing isoform and condition.

All statistical analysis was done using a 2-way ANOVA comparing isoform/construct versus condition with an $\alpha = 0.05$ (unless otherwise noted) and comparisons between conditions were made using a Bonferroni post-test analysis.

2.3. RESULTS

2.3.1. NEM Modification of L376C Captures the Inward Facing Conformations of the Transport Cycle

To examine whether the inward facing states of EAAT1 can mediate anion channel activity, we used a cysteine modification strategy to trap or restrain transporters in the inward facing conformations. To capture carriers in these states, we modified a single cysteine point mutation, L376C, located in HP1. Modification consisted of a 4 min incubation of 250 μM NEM in conjunction with high external K^+ to stabilize the inward facing conformations of the transport cycle or high extracellular Na^+ buffers to stabilize the outward facing conformations. After modification, we tested whether extracellularly applied substrates could still bind and gate the channel. We hypothesized that modification of the inward oriented transporter with an exposed HP1 could sterically hinder further conformational changes or the ability to reenter outward facing conformations of the transport cycle. Therefore, we would expect to see a decrease in glu induced current amplitudes subsequent to modification of HP1. Incubation of *Xenopus* oocytes expressing L376C EAAT1, with a high K^+ extracellular solution (K^+) containing 250 μM of the sulfhydryl-modifying reagent NEM, caused a $41.9 \pm 2.3\%$ reduction ($p < 0.001$) in the amplitude of NO_3 currents activated by 500 μM L-glu (Fig 5A). This modification was selective for the inward facing state of the transporter because incubation of NEM in high Na^+ -containing buffer ND96 (Na^+), which stabilized the outward facing states in the absence of glu, did not alter glu-induced NO_3 current amplitudes at positive membrane potentials after modification (Fig 5B). We chose to highlight potentials at +60 mV because there are no significant contributions of currents generated by electrogenic glu transport to the macroscopic currents observed at this

potential. In addition, parallel incubations of CSLS EAAT1 controls with NEM in either K^+ or Na^+ based solutions did not alter glu-induced channel activity after exposure to NEM (Fig 5C, D). These results indicate that L376C undergoes partial modification when the carrier is inwardly oriented, due to K^+ mediated reversal of the transport cycle, but this residue remains inaccessible when the carrier is in the outward facing- Na^+ bound orientations. As hypothesized, there was a dramatic loss of extracellular substrate mediated channel activity after successful modification of L376C. Moreover, these results also suggest that the modification of HP1 maintains the carrier in the inward conformation as there was a dramatic loss of current amplitudes mediated by extracellularly applied substrates. These results are consistent with a decreased number of transporters in the outward conformation necessary for interaction with extracellular substrates.

Changes in glu induced current amplitudes after modification of L376C with NEM while the transporter is the inward conformation could be due to an unknown alteration to the anion pore. To test for a specific loss of anion flux or a loss in the number of transporter available for interaction with extracellular substrates, we assayed for a change in transport activity in L376C. Modification of L376C by NEM in high extracellular K^+ buffers alters transport capacity as radiolabeled glu accumulation inside the cell was disrupted by $36.8 \% \pm 8.5 \%$ ($p < 0.05$) (Fig 5E), indicating an effect beyond simple alteration of anion flux. Additionally, as a control for an unforeseen effect of mutation and/or modification of L376C on the structure of the transporter, we also tested whether a membrane impermeant sulfhydryl modification reagent applied to the L376C EAAT1 while the transporter is driven to the inward facing states using high extracellular K^+ buffers could label the L376C residue. Oocytes preincubated with 1 mM MTSET in high K^+ buffer displayed no significant effect on uptake, consistent with L376C only able to be labeled from the cytoplasmic face. We next examined whether the reduction in the glu induced current amplitudes after modification (Fig 5A) was due to a loss of glu mediated gating of the anion channel caused by changes to substrate recognition and binding. To address a possible change

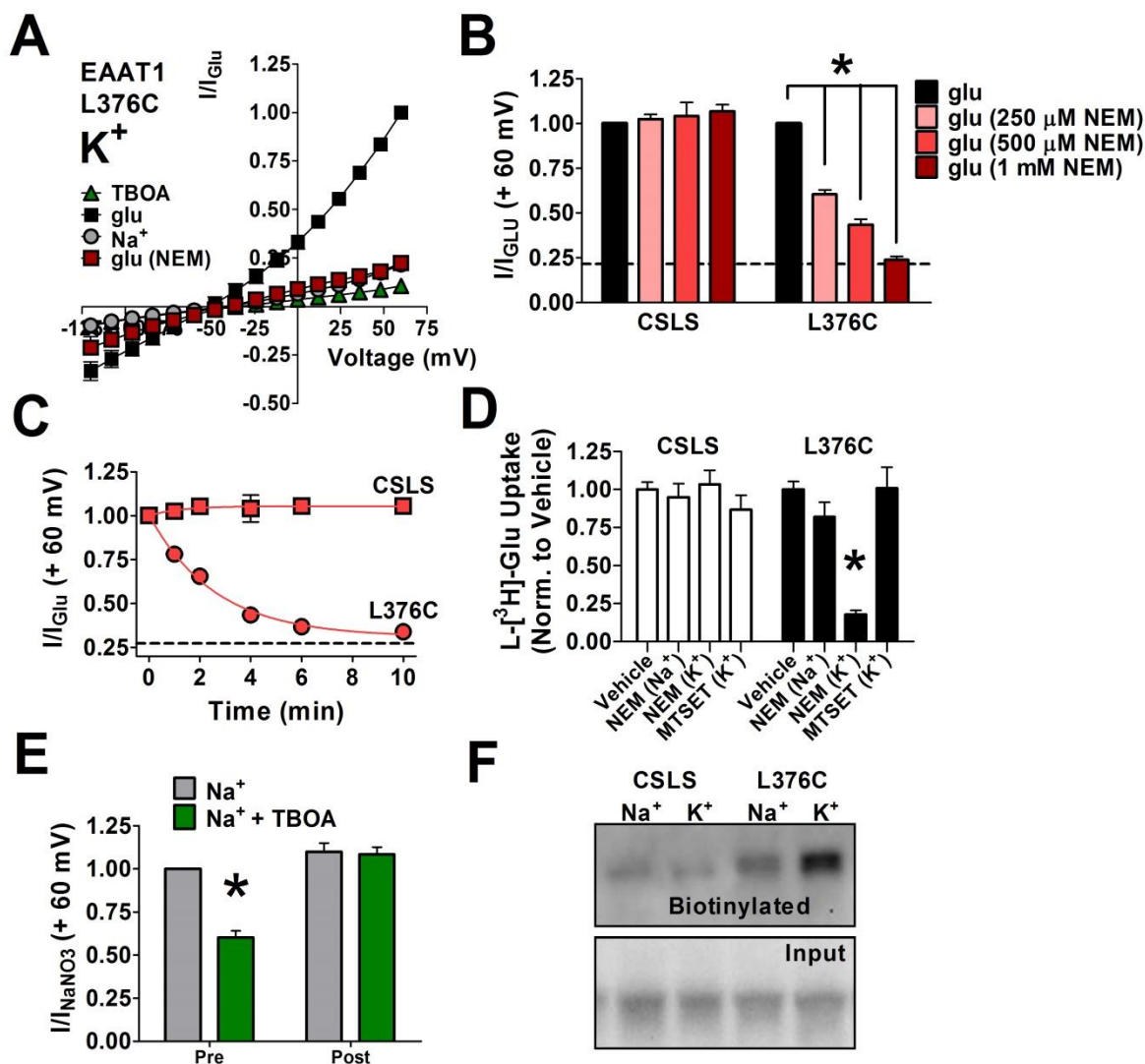


Figure 6: Modification of L376C is time and concentration dependent (A) Current-voltage relationship of L376C pre and post exposure to 1 mM NEM for 4 min. Shown are $NaNO_3$ induced currents (grey circles), 500 μM L-glu induced currents (black squares), current in the presence of 100 μM DL-TBOA (green triangles), and glu induced current amplitudes post-NEM incubation (maroon squares). Data are presented as the mean and Std. dev. between 6 and 15 oocytes from at least 3 distinct experiments. **(B)** CSLS or L376C EAAT1 current amplitudes from +60 mV quantitated in bar graph form. Conditions are $NaNO_3$ + 500 μM L-glu (black), $NaNO_3$ + 500 μM L-glu after a 4 min perfusion of 250 μM NEM (pink), after 500 μM NEM (red), or after 1 mM NEM (maroon). Data are normalized to the response elicited by unmodified

transporters exposed to glu (black). The dashed line indicated cellular current amplitudes elicited by NaNO_3 application alone. Data are displayed as the mean and S.E.M. from between 8 and 15 oocytes from 3 frogs **(C)** Time course of the loss of glu-gated anion current amplitudes at + 60 mV in CSLS (red squares) or L376C (red circles) transporters with exposure to 500 μM NEM for various times in high extracellular K^+ buffer. Currents were normalized to the amplitude elicited by saturating glu concentrations before exposure to NEM. Data are represented by the mean and S.E.M. for an N of 6 and was fit with a single exponential decay according to the experimental procedures. The dashed line indicated cellular current amplitudes elicited by NaNO_3 application alone. **(D)** Uptake of radiolabeled glu in CSLS (white) or L376C (black), with a 4 min preincubation of either high extracellular Na^+ buffer alone (Vehicle), 1 mM NEM in high extracellular Na^+ buffer (NEM (Na^+)), 1 mM NEM in high extracellular K^+ buffer (NEM (K^+)), or 1 mM MTSET in high extracellular K^+ buffer (MTSET (K^+)). Data are the mean and S.E.M. of between 8 -30 oocytes from ≥ 3 frogs. **(E)** Current amplitudes of NaNO_3 induced anion channel activity (grey) and in the presence of 100 μM DL-TBOA (green) pre (left) and post (right) exposure of L376C to 500 μM NEM for 6 min in high extracellular K^+ buffer. Data are reported as the mean and S.E.M. of an N of 8 from at least three individual frogs. Stars indicate statistical significant difference with a Bonferroni post-analysis after a significant 2-way ANOVA comparing isoform and condition. **(F)** Representative western blot of COS-7 cells expressing either CSLS E1 or L376C proteins exposed to maleimide-biotin as described in the experimental procedure. Immunoreactivity was between 62 and 84 kDa as per previously described for EAAT1 (116).

in glu recognition, we assayed for the apparent affinity of glu for L376C EAAT1 before and after modification by NEM. Furthermore, the affinity for glu to gate the anion channel was not significantly altered by NEM modification of L376C. The K_M of glu for gating of the anion channel, pre and post NEM modified L376C were $4.29 \pm 0.93 \mu\text{M}$ and $4.25 \pm 1.60 \mu\text{M}$ respectively, with a 37.7 % decrease in activity post-modification (Fig 5F), results congruent with loss of the number of transporters available for interaction with extracellular substrates.

2.3.2. Modification of HP1 to Restrict Conformation is Time and Concentration Dependent

The modification of HP1 using a 4 min perfusion of 250 μM NEM resulted in only a partial loss of subsequent glu induced currents (Fig 5A). If modification of L376C is indeed restricting the carrier to the inward facing state, then a complete loss of glu interaction after full modification of the transporter population would be observed, if the modification of L376C restricts further conformational changes of the transporters. Consistent with this hypothesis, the reduction of glu current amplitudes should be dependent on the concentration and time of NEM exposure. A representative I-V plot of the mean of responses to extracellular glu, pre- and post- modification using 1 mM NEM for 4 min, displays the complete loss of substrate interactions after complete modification of L376C in high extracellular K^+ conditions (Fig 6A). When oocytes were exposed to either 500 μM or 1 mM NEM for 4 min, total cellular currents at +60 mV in the presence of glu were reduced by $56.5 \pm 3.1\%$ and $75.9 \pm 2.4\%$ respectively, as compared to the 30.4% reduction seen with a 4 min perfusion of 250 μM NEM in these experiments ($p < 0.001$; Fig 6B) . Modifications using 1 mM NEM for 4 min reduces glu induced currents to amplitudes observed for Na^+ gated or leak currents (dashed line) suggesting a complete modification (Fig 6A and 6B). To further characterize the modification reaction, 500 μM NEM was perfused onto oocytes for several time points in either ND96 or K98 extracellular solutions. The time course of NEM-dependent reduction of glu induced currents in L376C followed a single exponential decay with

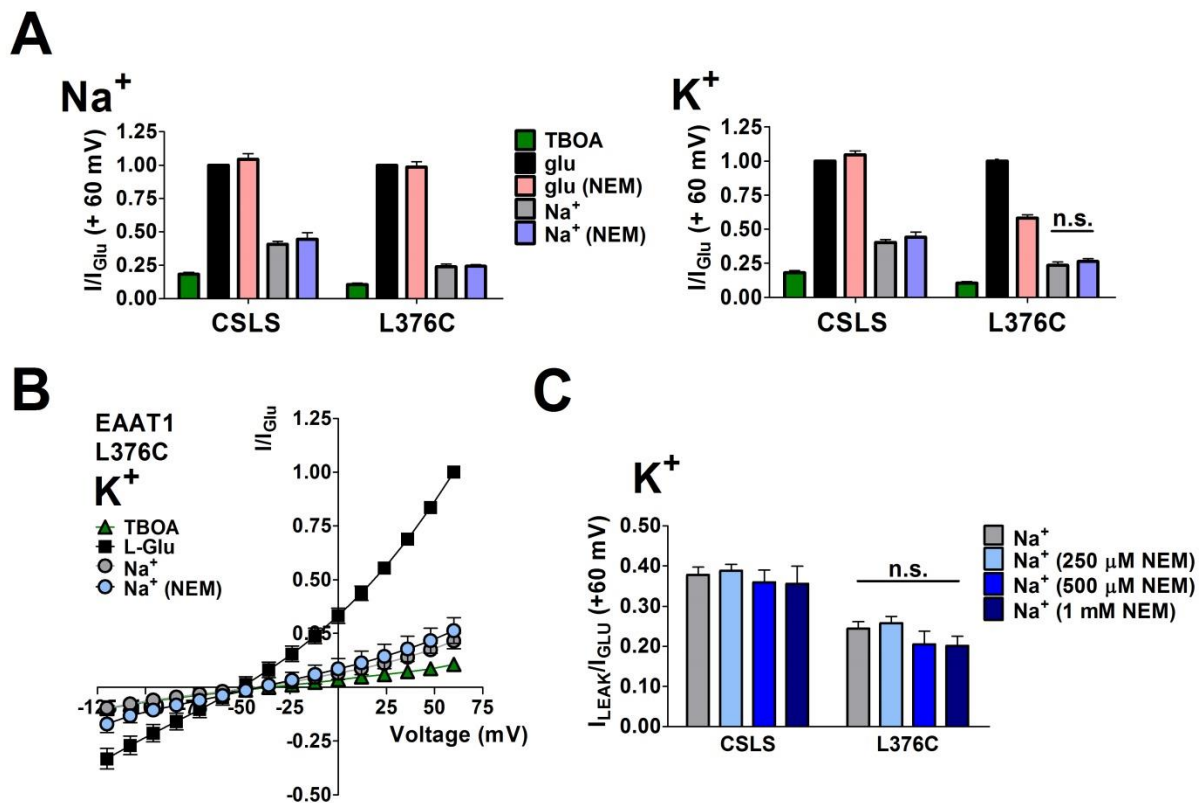


Figure 7: The inward facing conformations of EAAT1 have open channel states. (A) (left) Current amplitudes from +60 mV, displayed in bar graph form, of CSLS and L376C responses from perfusion of $\text{NaNO}_3 + 500 \mu\text{M}$ L-glu (black), $100 \mu\text{M}$ DL-TBOA (green), and NaNO_3 (grey). A 4min incubation of $250 \mu\text{M}$ NEM in high extracellular K^+ buffer (K^+) buffer was performed and then conditions retested, $\text{NaNO}_3 + 500 \mu\text{M}$ L-glu post NEM (pink) and NaNO_3 post NEM (light blue). (right) Conditions are the same as in (left) except the 4 min perfusion of NEM was done in high extracellular Na^+ buffer (Na^+). Bar graphs are presented as the mean and S.E.M. of between 6 and 20 oocytes from ≥ 3 frogs. **(C)** Current-voltage relationship from cellular responses between -150 mV to +60 mV to the application of $100 \mu\text{M}$ DL-TBOA (green triangles), NaNO_3 (grey circles), $\text{NaNO}_3 + 500 \mu\text{M}$ L-glu (black squares), and NaNO_3 post modification (light blue circles). Modification was a 4 min perfusion of $250 \mu\text{M}$ NEM in high extracellular K^+ buffer (K^+) buffer. I-V curve presented is the mean and std. dev. for an N of 15

from ≥ 3 frogs. **(D)** Mean cellular current amplitudes of CSLS and L376C expressing oocytes (N of 8-15 oocytes from ≥ 3 frogs) at +60 mV in the presence of NaNO_3 alone after exposure to either vehicle controls (grey), 250 μM NEM (light blue), 500 μM NEM (blue), or 1 mM NEM (dark blue) for 4 min. (A-D) Stars indicate statistical significant difference with a Bonferroni post-analysis after a significant 2-way ANOVA comparing isoform and condition.

a time constant of 2.41 ± 0.57 min, consistent with a simple bimolecular reaction (Fig 6C). These simple reaction kinetics also support the idea that L376C is readily accessible in the K^+ induced conformation and does not require more additional conformational changes in order to be modified as additional conformational changes would significantly alter the kinetics of the labeling reaction. Radiolabeled glu uptake was also impaired after modification with 1 mM NEM for 4 min in high K^+ buffer, with $17.8 \% \pm 2.7 \%$ of transport activity remaining ($p < 0.001$). Additionally, Oocytes preincubated with 1 mM MTSET in high K^+ buffer for 4 min displayed no significant effect on uptake, consistent with accessibility of L376C only from the cytoplasmic face (Fig 6D). To provide additional support for the total loss of substrate interaction observed after complete modification, saturating concentrations (100 μ M) of the competitive antagonist DL-TBOA were applied before and after modification with 500 μ M NEM in high extracellular K^+ buffer for 4 min. Total cellular current amplitudes were reduced by $39.8 \% \pm 3.8 \%$ ($p < 0.001$) with antagonist application before modification, and no change in current amplitude was seen with TBOA exposure after modification, consistent with a loss of inhibitor interaction (Fig 6E). To further support the modification strategy, we attempted to selectively pull down inward facing conformational states of the transporter using biotin labeling of L376C under high extracellular K^+ buffers. Western blot analysis of protein demonstrate our ability to selectively pull down inward facing L376C EAAT1 molecules using either BCCM-biotin or maleimide (long arm) biotin labeling of L376C under the high extracellular K^+ conditions (Fig 6F). Incubation of cells with the same cysteine specific biotinylation reagents in high Na^+ buffer did not enrich for biotinylated proteins. Thus the labeling of the mutant HP1 residue L376C allows for a continuous exposure of the biotin moiety to avidin conjugated beads. This supports the idea that HP1 persist in an exposed state after modification as we can capture inward facing transported with a biotin labeled HP1. All these data support that after modification of L376C, HP1 is constrained in an exposed state/s and limits subsequent conformational changes to the outward facing states, eliminating extracellular substrate or inhibitor interactions.

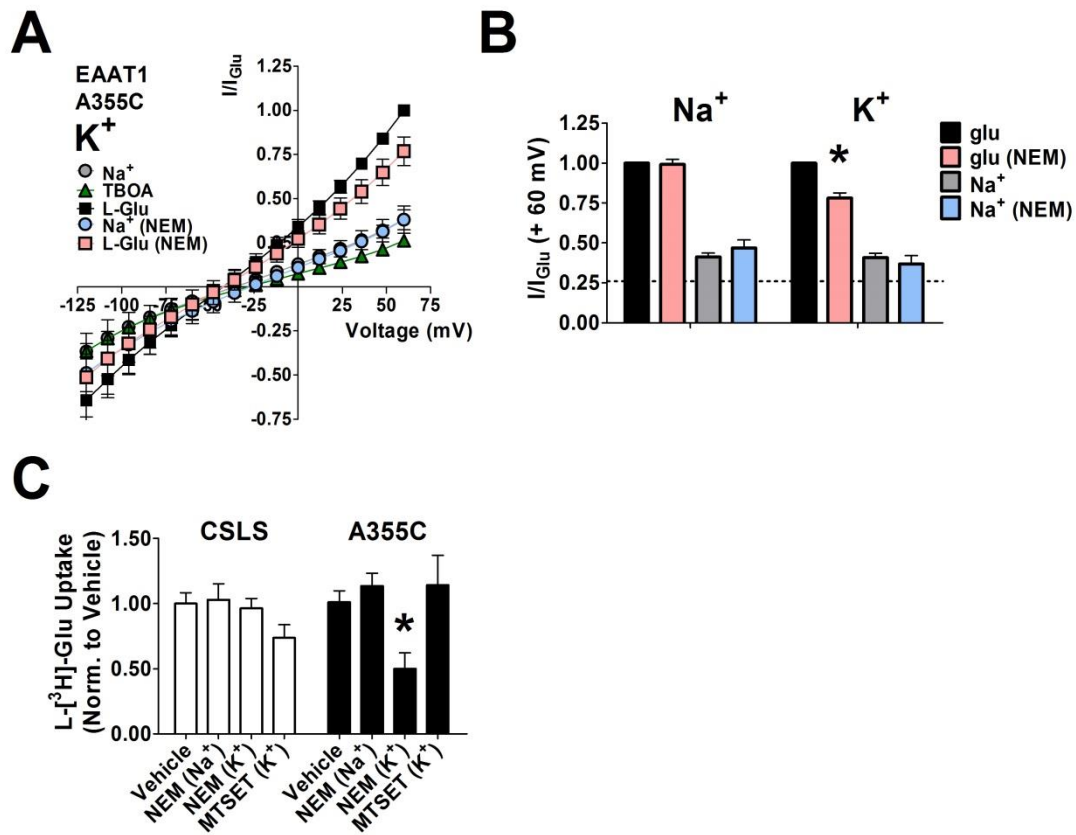


Figure 8: Modifications of HP1 residue A355C. **(A)** Current-voltage relationship of HP1 mutant A355C perfused with NaNO₃ + 500 μM L-glu (black squares), NaNO₃ alone (grey circles), and NaNO₃ + 100 μM DL-TBOA (green triangles). 250 μM NEM was perfused for 4 min in the presence of high extracellular K⁺ buffer. NaNO₃ alone (light blue circles) and NaNO₃ + 500 μM L-glu (pink squares) applications were then repeated following NEM incubation. Data were normalized to currents at +60 mV for the unmodified L-glu response. Data are shown as the mean and std. dev. of current amplitudes from 5 to 12 oocytes from ≥ 3 experiments. **(B)** Current amplitudes at +60 mV quantitated in bar graph form for A355C exposed to NEM incubations in either high extracellular Na⁺ buffer (**Na⁺**) or high extracellular K⁺ buffer (**K⁺**). Conditions displayed are NaNO₃ + 500 μM L-glu pre- (black) and post- (pink) application of 250 μM NEM for 4 min. The current response in the presence of NaNO₃ alone pre- (grey) and post- (light blue) NEM application is also displayed. Dashed line indicated background oocytes

currents as revealed by application of 100 μ M DL-TBOA. **(C)** Radiolabeled glu uptake assay of CSLS (white) and A355C (black) expressed in *Xenopus* oocytes. Conditions are a 4 min pre-incubation of either vehicle control (ND96), 250 μ M NEM in either ND96 (Na^+) or K98 (K^+), and 1 mM MTSET in K98 (K^+) followed by a 10 min incubation with 500 μ M glu + 200 nM radiolabeled glu. Counts per minute were normalized to control conditions. (B) and (C) are depicted as the means and S.E.M. Data are an average of at least 20 individual oocytes for each condition from at least 3 separate frogs. Stars indicate statistical significant difference with a Bonferroni post-analysis after a significant 2-way ANOVA comparing salt and condition.

2.3.3. Inward Facing States Possess Anion Channel Activity

The modification of HP1 after the carrier is in the inward facing states results in the capture of one or more inward states. We next used two electrode voltage clamp recordings (TEVC) to examine channel activity after HP1 modification. Application of 250 μ M NEM for 4 min in high extracellular K^+ buffer results in a significant reduction in extracellular glu interaction yet current amplitudes in $NaNO_3$ alone were not altered with the carriers trapped in the inward facing state (Fig 7A, C). While the modification of HP1 is dependent on NEM in the presence of external K^+ , there is no significant difference in currents in the presence of $NaNO_3$ alone in either L376C or CSLS when exposed to 250 μ M NEM for 4 min in either high Na^+ or high K^+ buffers (Fig 7B). As complete modification of L376C requires higher concentrations of NEM or longer incubation times of the reagent (Fig 6A and 6C), $NaNO_3$ induced current amplitudes were measured after exposing either L376C or CSLS expressing oocytes to 250 μ M, 500 μ M, or 1 mM NEM (Fig 7D). No significant change in EAAT1 currents in the absence of glu was observed indicating that the inward facing states of EAAT1 can mediate transitions to open channel states with macroscopic properties which mimics the outward facing, open states in the presence of $NaNO_3$ alone. This is the first evidence for open channel states mediated by EAATs while biochemically restricted to the cytoplasmic facing conformations.

2.3.4. Modification of HP1a Residue A355C Also Captures Inward Facing States

In order to control for non-specific effects of L376C modification affecting channel properties through long range distortions, we repeated the basic phenomenon using another HP1 cysteine substitution mutant, A355C. This residue has also been previously demonstrated to be conformationally sensitive, with intracellular accessibility to reagents only during incubations in high extracellular K^+ buffers (71,120). Modification of A355C expressing oocytes with 250 μ M NEM for 4 min caused a $21.9\% \pm 3.4\%$ decrease in subsequent glu induced current amplitudes ($p < 0.0001$) (Fig 8A, B). Likewise, radiolabeled glu uptake was reduced by $50.1\% \pm 12.4\%$ ($p < 0.01$) under the same experimental conditions (Fig 8C). As seen with L376C, application of

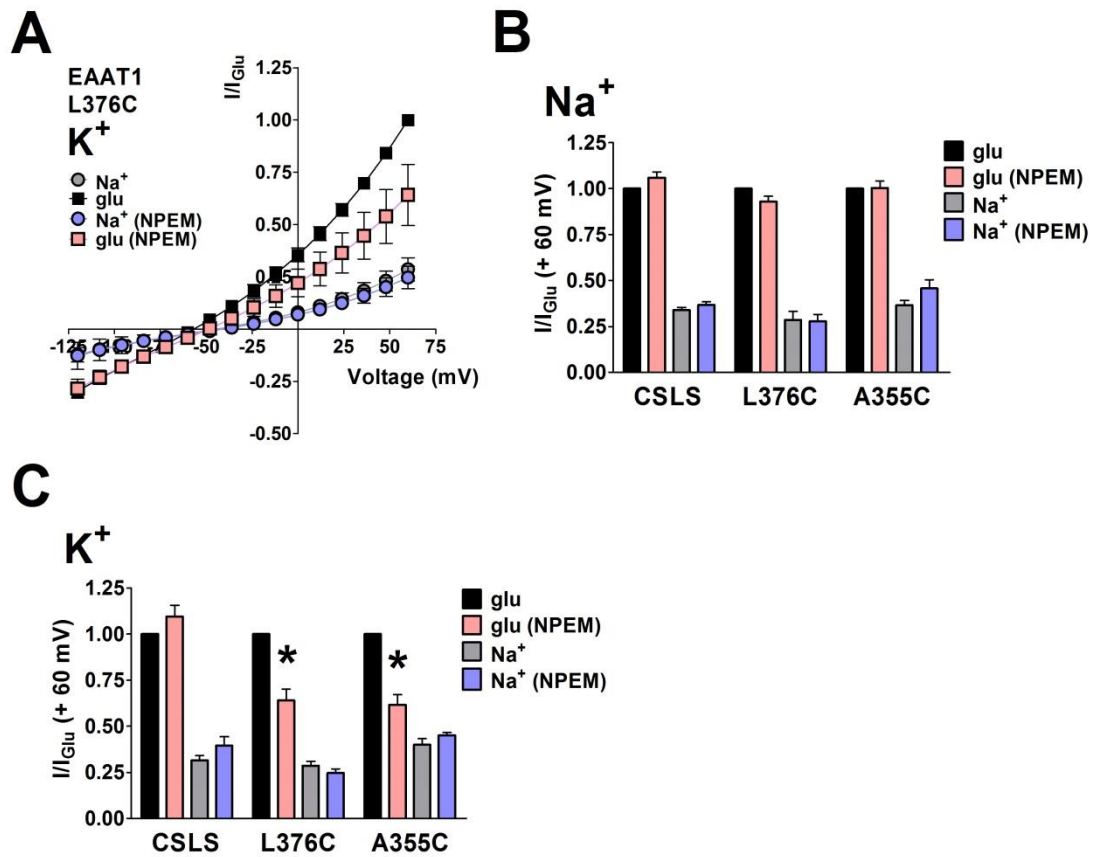


Figure 9: HP1 is readily accessible by the bulky modification reagent NPEM. (A) I-V plot of TEVC recordings of L376C exposed to a $NaNO_3$ (grey circles) or $NaNO_3 + 500 \mu M$ L-glu (black squares) and after a 4 min incubation of $250 \mu M$ NPEM in high extracellular K^+ buffers (K^+), (light blue circles and pink squares, respectively). Data are shown as the mean and Std. dev. of an N of 6 oocytes from 3 frogs. **(B, C)** Bar graph of CSLS, L376C, and A355C current amplitudes at + 60 mV exposed to either $NaNO_3 + 500 \mu M$ L-glu (black), $NaNO_3 + 500 \mu M$ L-glu post NPEM exposure (pink), $NaNO_3$ (grey), and $NaNO_3$ post NPEM exposure (light blue). NPEM was perfused in high extracellular K^+ buffers (B) or high extracellular Na^+ buffers (C). (B) and (C) are reported as the mean and S.E.M. of 6 to 10 oocytes from at ≥ 3 frogs. Stars indicate statistical significant difference with a Bonferroni post-analysis after a significant 2-way ANOVA comparing isoform and condition.

1mM MTSET in high external K^+ buffers had no significant effects of transport activity suggesting that A355C is not modifiable from the extracellular milieu. These data are consistent with the hypothesis that HP1 dynamics are important for conformational changes subsequent to the inward facing states. Additionally, the effects of NEM on A355C support the interpretation that modification of HP1 limits subsequent conformational changes of the transporter and the effects of modification on accessibility to extracellular substrates is not due to other non-specific alteration in transporter structure since it would be highly improbable that modification of two distant residues would both lead to the same structural and functional aberrations.

2.3.5. HP1 Accommodates Alternative Modification Reagents

We next examined whether different modifying reagents might have distinct effects on the function of HP1 mutants after modification. We hypothesized that a larger modifying reagent may have less accessibility to HP1 and thus display a decreased change to glu induced current amplitudes after modification on HP1a (A355C) versus HP1b (L376C). (R)-(+)-N-(1-Phenylethyl)maleimide (NPEM) is another sulfhydryl-reactive, membrane permeable reagent that when applied to either L376C or A355C caused an identical phenotype to that observed with NEM (Fig 9A). A 4 min exposure of 250 μ M NPEM under high extracellular K^+ buffers caused a $39.1\% \pm 6.0\%$ and a $38.4\% \pm 5.6\%$ decrease ($p < 0.001$) in saturating glu induced current amplitudes at +60 mV for L376C and A355C respectively (Fig 9B). As demonstrated with NEM modifications, labeling of HP1 residues with NPEM is dependent on extracellular K^+ driving the transporter to the inward facing states because incubations conducted in high Na^+ have no significant effect on transporter currents at +60 mV (Fig 9C). As both NEM and NPEM have similar effects on HP1 residues, these residues are readily accessed by both large and small reagents, consistent with the idea that the carrier resides in the inward conformation with HP1 possibly locked open after modification (32,122).

2.3.6. The EAAT1 Transport Cycle Depicting Open Channel States

Our data presented here demonstrate that EAAT-associated anion conductances persist when the transporter is restricted to the inward facing states. The first crystal structure from *Pyrococcus horikoshii* (Glt_{ph}) likely depicts an outward-occluded state and illustrates a HP1 domain embedded within transmembrane helices associated with transport function. Although residues of the HP1a/b loop can be modified by impermeant reagents in the outward conformations (122), residues buried lower in either HP1a or HP1b appear occluded in this structure. Interestingly, another crystal structure which was captured using HP2/TM2 crosslinking depicts a cytoplasmically exposed HP1 where modifications of this structure would be predicted to occur readily. Human EAAT1 (hEAAT1) homology models based on the Glt_{ph} archeal asp transporter also illustrate these two distinct orientations of HP1 and support the changes in accessibility of this region in the outward and inward-oriented states (Fig 10A and B, respectively).

Current models for open channel states occupied during the glu transport cycle rarely consider channel activity while in the inward facing state. Our model includes two new open states mediated by Na⁺ interaction in the cytoplasmic facing carrier (Fig 10C). These open channel states are likely identical to the open channel states seen in the outward, Na⁺-bound conformations. Additionally, these new open states are presumed to have the same unitary conductance and open probabilities because compensatory alterations in both parameters that generate the same net current amplitudes would be possible, although improbable.

2.4. DISCUSSION

Here we describe a simple approach to conformationally restrain glu transporters into the inward facing states through modifying HP1 residues under high external K⁺ conditions. Under these conditions we readily observe a conductance state in the absence of glu that allows for currents similar in amplitude to the open channel states mediated by the outward facing conformations in

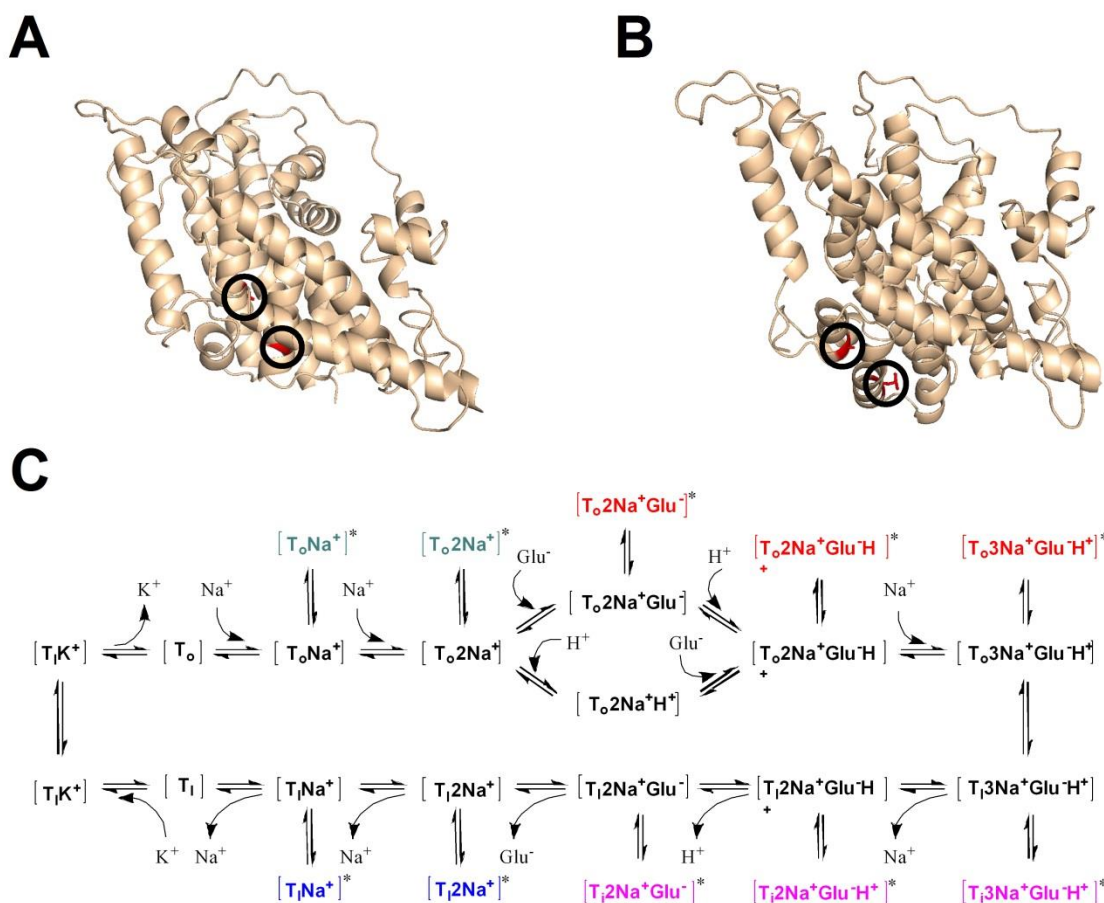


Figure 10: Model of hEAAT1 structures and proposed state diagram of general EAAT transport cycle including novel anion conducting states. (A) Homology model of hEAAT in the outward facing state based on the Glt_{Ph} crystal structure from (7) (pdb file 3FXH). Helices are depicted in ribbon form (wheat) with a stick model of A355C and L376C (red) circled for easy of identification. **(B)** Homology model of hEAAT1 crystal structure in a proposed inward-facing state adapted from (32) (pdb file 3KBC) color scheme is the same as in (A). **(C)** Kinetic diagram depicting substrate interactions and conformational states. Depicted are open channel states (*) in outward facing conformations in the absence of glu (grey), inward-facing open channel states in the absence of glu (blue), glu induced open channel states in outward facing

conformations (black), and inward facing open channel states mediated by glu interaction (fuchsia). Substrate binding order was adapted from (34).

the absence of glu. To our knowledge this is the first direct evidence for a conductance or open probability of the channel states mediated by the inward facing conformations seen during the transport cycle in the absence of glu. Since there are at least several inward facing states which are known to exist, it is not possible to ascertain which specific state or sub-states our modification restricts the transporter in. Nonetheless, these data supports that after modification of the carriers in the presence of high extracellular K^+ , the carriers are indeed inward facing for at least three reasons. First, it has been demonstrated by multiple groups that a high extracellular concentration of K^+ will drive the reverse transport of glu but only in conditions where the intracellular composition of the cell has been altered to allow for reverse transport, i.e. high intracellular Na^+ and glu concentrations (4,20,22,36). This is not the case for oocytes where reverse transport would be minimal due to the low intracellular concentrations of Na^+ and the low affinity of the inward facing conformations of the transporters for glu (39,123). Therefore, a high extracellular concentration of K^+ will allow the accumulation of carriers into the inward facing states, presumably in equilibrium between the inward open, K^+ bound, Na^+ bound, and Na^+ /glu bound states. It is under these states that modifications explored in the current study occur and thus it is likely that we have captured one or more of these states.

Second, the lack of extracellular glu interactions is what functionally defines the occluded and inward facing states. As we have demonstrated here, after complete modification of HP1 residues, we no longer have extracellular accessibility of substrates to the transporter. Again, it is presumed that the transporters are mediating channel activity through interactions with substrates with the intracellular facing binding site or are alternatively observing novel gating mechanisms of the channel. Although these data presented here does not demonstrate the existence of inward facing, glu-induced conductances, these data do not preclude their existence. Indeed, it has been demonstrated using inside-out patches that intracellular glu can gate the anion conductance of transporters thus supporting the existence of inward-facing, glu-gated anion conductance (41,45). Since intracellular concentrations of Na^+ are low in the

oocyte, and the inward facing carrier's affinity for glu is significantly reduced (27), it is likely that the fraction of glu-bound, inward oriented transporters is very low. This state may be such a low probability in our system that it would not significantly alter macroscopic current amplitudes over current amplitudes in the presence of Na⁺ alone. Thus, our model (Fig 10C), does depict glu induced open channel states in the cytoplasmic facing carriers (T_i) as they have been demonstrated previously (36,41,45) although these glu induced, inward facing states are not observed in our experiments.

Lastly, modification of EAAT reentrant loops and their relationship to channel activity has been previously examined. Modification of a cysteine point mutation V449C in HP2 has been reported to lock the transporter into the outward open conformation. Glu and TBOA binding from the extracellular space was not significantly altered nor was there any inhibition of channel function by the modification alone (115). These results have been demonstrated for several HP2 point mutations as well suggesting that modifying the external gate in several residue positions in HP2 is sufficient to restrict the transporter into the outward open state (117,124). It is generally thought that HP1 functions in a manner analogous to HP2 (for a cogent argument, see (57)). Therefore, it is likely that an open, inward conformation is a low energy, stable state and that HP1 modification locks the transporter into the inward open state. Additionally, our rate of modification closely models a simple bimolecular reaction. These data would not have been observed if the transporter was undergoing additional conformational changes as a prerequisite for modification to occur. Additional conformational changes would have altered the order and the kinetics of the reactions and therefore would be observed in the experiments. Although these data do not rule out a possible unimolecular rearrangement of the transporter conformation after modification has occurred, we were able to isolate exposed, biotin modified L376C EAATs using an avidin capture as demonstrated in Fig 6F. These data all support the interpretation that we have likely captured inward-facing conformations of the transport cycle

through modification of HP1 while in the inward facing states, mediated by K^+ induced reorientation of the EAATs.

Bergles et al. (34) first described a kinetic model comprised of 15 individual states in the transport cycle. This diagram is a combination of data and modeling and 8 of those 15 states were described to have associated open channel states in which anions could permeate. The “leak” or Na^+ gated channel state was attributed to the outward, 2 Na^+ and H^+ bound state. The only inward states described in this model to permit anion flux were the 2 Na^+ bound state (T_i2Na), and the K^+ bound state (T_iK). As many of these states, such as the T_iK open channel state, were never directly examined, it is unclear which channel states exists for all EAAT isoforms (47). Recently, work from Kovermann et al. (2010) (125) and Machtens et al. (2001) (118) supports additional anion conducting states accessible during multiple conformations of the glu transport cycle. For rEAAT4, independent or mutually exclusive channel and transport states were assigned for all outward Na^+ bound states as well as the T_iNa and T_iK states (125) (see Fig 10C). Additionally, experiments as well as simulations were combined in order to describe conducting states associated with other steps in the transport cycle. Our data support many of the interpretations of these groups, that multiple anion conducting states are mediated by inward-facing conformations.

We have performed several assays in order to better describe the nature of this modification and its effects on function. L376C exposure to a low concentration of NEM in conjunction with high extracellular K^+ buffers results in a loss of available carriers for extracellular substrate binding (reduced V_{max}) with an unaltered binding mechanism (similar K_M) (Fig 6B). These data are typical of reduced availability of extracellularly exposed transporters, but the available transporters still maintain an intact binding mechanism. If the modification of L376C was reducing surface transporter levels, then there would be a reduction in current amplitudes in the absence of glu, to a similar degree as observed for glu gated conductance post-modification. As displayed by Fig 7D, increasing the number of transporters

modified by increasing the concentration of NEM used in the experiment, never alters current amplitudes in the presence of NaNO_3 alone.

Mutations and modifications can yield effects through unforeseen alterations or long range effects and so we examined a different residue to test that our strategy for mediating inward facing states is valid. A355C is an HP1a residue and shows a conformation-dependent accessibility similar to L376C, which is located in HP1b. If L376C was perturbing the structure of EAAT1 through unusual means, then we might expect to see disparate results with other residues which are separated by even a moderate distance. This is not the case as A355C modifications using high external K^+ buffers results in near identical channel phenotypes, supporting our interpretation of how HP1 modifications can affect transporter functionality. Our procedure is also robust in that it can accommodate at least 3 different modification reagents as well. NPEM has similar properties to NEM but possesses a large phenyl group. This could, in theory, have different accessibility to either L376 or A355 but our data shows identical results when compared to NEM-based modifications. A comparison of these data from NEM, NPEM, and maleimide-biotin modifications suggest that even modification of HP1 residues by NEM is sufficient to restrict further conformational change in EAAT1. This accommodating yet sensitive behavior of HP1 might suggest that an inward structure contains a more constricted environment surrounding HP1 than initially indicated from structural data depicting a dramatic cytoplasmic exposure of HP1 (Fig 10B), or possibly it could indicate a more dynamic role for HP1, then has previously been hypothesized (7,126,127). It is always a significant challenge is made structural interpretations based on functional data. Although we cannot definitively identify exactly what conformation of the transporter a modified L376C is in, our data all support the interpretation that a modified L376C is likely trapped in inward facing conformations of the transport cycle.

Little is known about the how anion channel activity regulates neuronal functioning. Although strong evidence supports a role for EAAT5 regulating neuronal activity in the retina

(44,58,59), EAAT5 has some distinct properties compared to the other isoforms (128). Additional data will be required to establish the significance of EAAT mediated channel activity for the other isoforms. Here we describe a simple method to isolate inward facing conformations of the EAAT transport cycle, and using this approach we identified novel open channel states. An understanding of the contributions of these novel states to EAAT function should aid in efforts to establish the role of the anion channel in regulating neuronal or glial excitability and glu clearance.

3. THE DIFFERENCE IN THE Na⁺ DEPENDENCE OF ANION CHANNEL GATING BETWEEN NEURONAL AND GLIAL ISOFORMS OF GLUTAMATE TRANSPORTERS

3.1. INTRODUCTION

Excitatory amino acid transporters (EAATs) are a family of five carriers in the central nervous system (1). EAAT1 and 2 are located in glial, although there are some reports of neuronal expression of EAAT2 (6,8). EAAT3 is ubiquitously expressed in neurons and EAAT4 neuronal expression is extensive but most notable for its robust expression in the cerebellum (9,10,12). EAAT5 is exclusively expressed in neurons of the retina (11). Glial EAATs have been demonstrated to mediate the majority of L-glutamate (glu) transport and EAAT2 (GLT-1 in rodents) specifically is responsible for upwards of 90% of glu removal after synaptic release due to its high levels of expression in the glial membrane (14,85). Strong evidence supports the hypotheses that neuronal transporters such as EAAT3 and EAAT4 limit activation of peri- or extra- synaptic receptors through rapid buffering of synaptically released glutamate (82,84,88,89). This buffering activity has been demonstrated to affect processes such as synaptic plasticity through activation of N-methyl-D-aspartate receptors (NMDARs) or metabotropic glutamate receptors (mGluRs) (89,103,105,106,129).

All members of the EAAT family function as secondary active, electrogenic transporters with the translocation of 1 glu molecule coupled to the co-transport of 3 Na⁺, 1 H⁺, and the counter-transport of 1 K⁺ ion (26,27). This coupling allows the net inward movement of 2 positive charges with each glu molecular translocated into the cytoplasm. EAATs have a turnover rate of approximately 15-90 cycles per second across the isoforms (33,35). EAATs also possess a thermodynamically uncoupled anion conductance. This anion channel is

promiscuous with a permeability sequence generally following $\text{SCN}^- > \text{ClO}_4^- > \text{NO}_3^- > \text{I}^- > \text{Br}^- > \text{Cl}^-$. Contemporary data support that the anion channel is gated by the initial binding of Na^+ and the open probability of the channel is subsequently increased upon glu interaction (49,50,53,130). Although a physiological role for the EAAT-mediated anion conductance has yet to be demonstrated in all isoforms, there are data which describe the significance of the EAAT5 anion channel in regulating cellular activity in the retina (44). One elegant study has demonstrated that Cl^- flux through EAAT5 regulates bipolar cell membrane potentials and modulates synaptic release rates (58). Additional data have substantiated the role of EAAT5 as a ligand gated ionotropic receptor (11,59,128) and together these data support the need for additional research in order to better address the roles of these channel activities.

To date, only minor differences have been found between the 5 mammalian isoforms such as the affinity for glu (2.5 μM for EAAT4 to 97 μM for EAAT2) and the kinetics of transport (12,53,131,132). Any difference in the basic stoichiometry or number of open channel states has not been readily observed in previous studies (34,47,48,133). However, It has been suggested that EAAT2 may possess some additional conducting states compared to EAAT4 (or EAAT3) (34,47). These minor differences have not been attributed to any particular residues or structural disparities and are not known to mediate any significant difference in the regulation of glutamate in the synapse and beyond. Interestingly, no differences in function discovered thus far can be attributed to the difference in cell-type expression *in vivo*. Here we report that glial isoforms of glutamate transporters, EAAT1 and EAAT2, mediate Na^+ independent open channel states or “leak” conductance states as compared to the classically Na^+ dependent, neuronal isoforms EAAT3 and EAAT4. This is the first report to correlate a difference in anion channel gating mechanism by cell-type expression and ushers in a new avenue to study the relative roles of the various EAAT isoforms in shaping synaptic activity.

3.2. EXPERIMENTAL PROCEDURES

3.2.1. Transfections in Mammalian Cell lines and cRNA Injections in *Xenopus* Oocytes

Human EAAT1 (hEAAT1), hEAAT2, hEAAT3, or rat EAAT4 (rEAAT4) were subcloned into pcDNA3.1 (Invitrogen) using Kpn1 and Xba1 restriction sites. rEAAT4 was used over hEAAT4 due to significantly better expression in oocytes and only minor differences in primary sequence. tsA201 cells (European Collection of Cell Lines, ECACC) were transfected using Lipofectamine 2000 (Invitrogen) or Fugene 6 (Promega) and incubated in DMEM with 10% FBS and pen/strep. pEGFP was used as a co-transfection marker for electrophysiological recordings. 1 day before recording, cells were trypsinized and plated onto 12 mm coverslips for whole cell patch clamp experiments.

For expression in *Xenopus* oocytes hEAAT1, hEAAT2, hEAAT3, and rEAAT4 were subcloned into pOTV using Kpn1 and Xba1 restriction sites as previously described (36). Constructs were linearized with either Sma1 (EAAT1-3) or BamHI (EAAT4). cRNA was made using mMessage mMachine T7 kit (Ambion) (5). 50 μ l injection (10 ng total RNA) was delivered to each oocyte using a Nanoliter 2000 injection system (WPI). Oocytes were incubated at 18°C for 2 days after injection in 96 mM NaCl, 2 mM KCl, 1 mM CaCl₂, 1.8 mM MgCl₂, and 5 mM HEPES, pH 7.4 (ND96) containing 50 μ g/ml pen/strep, 50 μ g/ml of gentamycin, and 50 μ M Na⁺ pyruvate.

3.2.2. Radiolabeled Glu Transport Assays

Radiolabeled uptake assays were performed two to three days after injection of cRNA. Oocytes were pre-incubated for 4 hours in either 96 mM NaNO₃, 2 mM KNO₃, 1 mM CaCl₂, 1.8 mM MgCl₂, and 5 mM HEPES, pH 7.4 (NaNO₃), or 96 mM ChOH, 96 mM HNO₃, 2 mM KNO₃, 1 mM CaCl₂, 1.8 mM MgCl₂, and 5 mM HEPES, pH 7.4 (ChNO₃) prior to transport assays. Oocytes were washed with either NaNO₃ or ChNO₃ and incubated with 10 μ M glu with 200 nM 3,4-3H-L-glu (Perkin Elmer) for 10 min in the appropriate buffers. All oocytes were washed three times with NaNO₃ after glu incubations and were lysed with 0.1 N NaOH and 1% SDS before liquid

scintillation counting was used to record radiolabel accumulation of tritiated glu in individual cells.

3.2.3. Two-Electrode Voltage Clamp Recordings

Two electrode voltage clamp recordings (TEVC) were performed using a Geneclamp 500 (Molecular Devices) on stage V-VI oocytes two days after injection of cRNA constructs. Holding potential was set to -60 mV and 500 msec voltage command ramps were performed from -120 mV to +60 mV. Current amplitudes used for data analysis were taken from the last 100 msec of the ramp to ensure measurement of steady state conditions. Standard extracellular buffers used were either NaNO₃, ChNO₃, or 96 mM NMDG⁺, 96 mM HNO₃, 2 mM KNO₃, 1 mM CaCl₂, 1.8 mM MgCl₂, and 5 mM HEPES, pH 7.4 (NMDGNO₃). Electrodes were pulled to a resistance of 0.5 – 2 MΩ and were filled with 3 M KCl. A 3 M KCl salt bridge was used for all experiments. All currents were recorded using pClamp10 software with on-line filtering at 1 kHz using a Bessel filter and digitized with a Digidata 1440A A/D converter (Molecular Devices) at 50 Hz.

3.2.4. Whole-Cell Patch Clamp Recordings

Pipettes were pulled from borosilicate glass (Warner Instruments) and fire polished to a tip resistance of 2-5 MΩ. Pipette solutions contained 115 mM CholineCl, 2 mM MgCl₂, 5 mM EGTA, and 10 mM HEPES. pH was adjusted to 7.3 with 8.6 M CholineOH. Extracellular solutions contained 140 mM NaSCN, 4 mM KCl, 2 mM MgCl₂, 2 mM CaCl₂, and 10 mM HEPES, or 144 mM KSCN, 2 mM MgCl₂, 2 mM CaCl₂, and 10 mM HEPES, unless otherwise noted. pH was adjusted to 7.4 with 10 N NaOH. Whole-cell recordings were made from tsA201 cells 2-3 days after transfection with an Axopatch 200B amplifier (Molecular Devices) in voltage-clamp mode. Series resistance compensation was set to at least 85% in all experiments. Signals were low-pass filtered at 5 kHz (8-pole Bessel; Warner Instruments) and collected at a sampling frequency of 10 kHz. Recordings from cells where series resistance exceeded 20 MΩ or

currents exceeded -100 pA at -70 mV in the presence of 100 μ M DL-TBOA were excluded from analysis.

3.2.5. Data Analysis and Statistics

All data was analyzed with Prism v5 (Graphpad) and electrophysiological recordings were also analyzed using Clampfit v10 (Molecular Devices). 2-way ANOVAs comparing isoform vs condition, unless otherwise noted, with an $\alpha = 0.05$ were used for all experiments. Bonferroni post analysis test were used to compare between groups. Stars indicate a significant difference between groups as noted in the figure captions. EAAT mediated currents are defined here as the whole cell currents observed minus the currents observed in the presence of Na^+ and saturating concentrations (100 μ M) of the competitive EAAT channel and transporter antagonist DL-threo- β -benzoyloxyaspartate (DL-TBOA). Macroscopic currents are defined as the whole cell currents observed without any subtraction procedure.

3.3. RESULTS

3.3.1. Neuronal and Glial EAATs Diverge by Their Na^+ Dependence of Anion Channel Activity

Anion channel activity has been demonstrated to be gated by substrate interaction (10), however a comprehensive analysis of the ability of Na^+ interaction to gate the anion channel in all isoforms has not been performed. In EAAT1, replacement of total extracellular Na^+ with choline (Ch^+) does not affect EAAT mediated NO_3^- current amplitudes (Figure 11A, C). The same Na^+ replacement strategy reduces EAAT mediated current amplitudes in EAAT4 expressing oocytes by $95.8 \pm 4.6\%$ (equivalent to a $50.5 \pm 4.8\%$ reduction in macroscopic current amplitude; $p < 0.001$; Figure 11B, C). Interaction of either glu or DL-TBOA is dependent

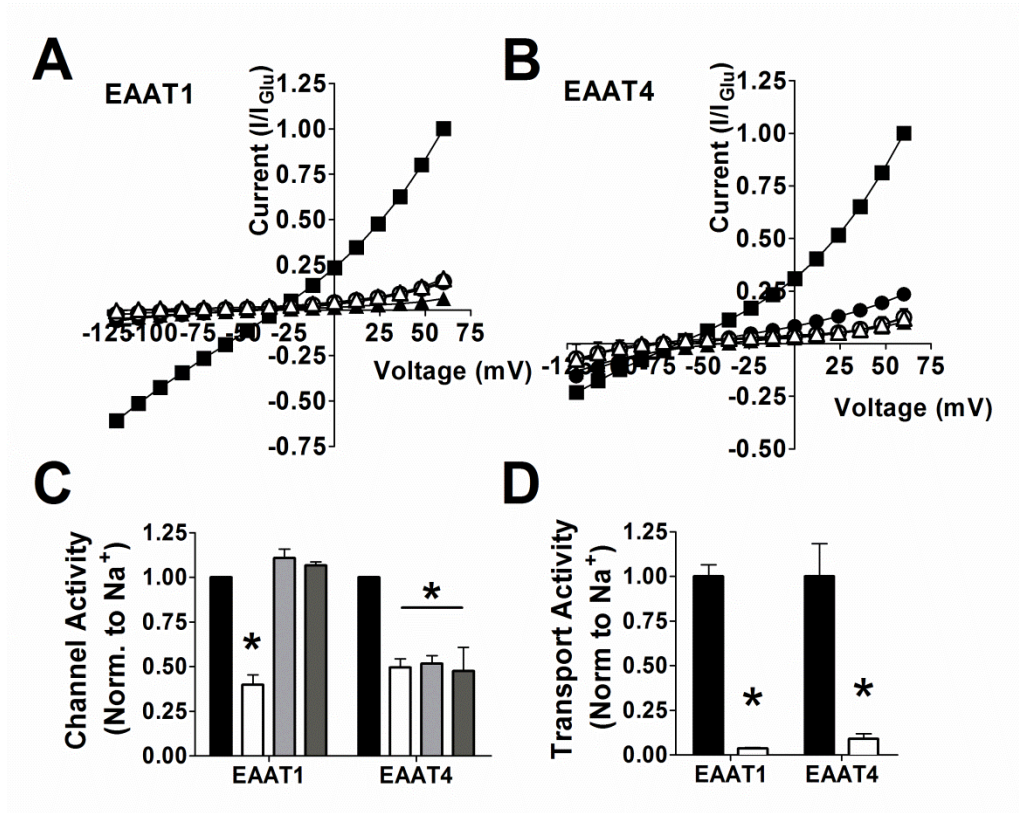


Figure 11: Replacement of external Na⁺ with Ch⁺ abolishes anion flux in EAAT4 but not EAAT1. A-B) Conditions displayed are NaNO₃ (closed circles), NaNO₃ + 500 μM glu (closed squares), NaNO₃ + 100 μM DL-TBOA (closed triangles), ChNO₃ (open circles), and ChNO₃ + 100 μM DL-TBOA (open triangles). Currents were normalized to the response to application of saturating glu application at +60 mV and are represented by the mean and S.E.M. of 8 individual oocytes from ≥ 3 frogs. **A)** Plot of the current-voltage relationship (I-V plot) of *Xenopus* oocytes expressing EAAT1. **B)** I-V plot of the responses to conditions described in A) from oocytes expressing EAAT4. **C)** Bar graph of the currents amplitudes at +60 mV in oocytes expressing EAAT1 and EAAT4 in response to applications of NaNO₃ (black), NaNO₃ + 100 μM TBOA (white), ChNO₃ (grey), and ChNO₃ + 100 μM TBOA (dark grey). Data are normalized to the cellular response to perfusion of NaNO₃ alone at +60 mV and is expressed as the mean and S.E.M. for 10-12 oocytes from ≥ 3 frogs. **D)** Radiolabeled accumulation of 200 nM 3,4-³H-L-glu and 10 μM glu in oocytes expressing EAAT1 or EAAT4 in the presence of NaNO₃ (black) or

ChNO₃ (white) buffers as described in the experimental procedures. Data in CPMs were normalized to transport activity for the NaNO₃ conditions and is displayed as the mean and S.E.M. for 8-12 oocytes from ≥ 3 frogs. Stars indicate statistical significant difference with a Bonferroni post-analysis after a significant 2-way ANOVA comparing isoform and condition.

on the ordered binding of 1 or 2 Na^+ ions and replacement of extracellular Na^+ with Ch^+ abolishes all substrate or inhibitor interactions. This is demonstrated by the loss of inhibition of EAAT1 mediated current amplitudes in the presence of saturating DL-TBOA when co-applied with a ChNO_3 buffer (Figure 11A). Current amplitudes mediated by EAAT4 were already reduced by over 95% with the removal of Na^+ and therefore DL-TBOA co-application did not significantly alter the loss of these currents (Figure 11B). Also, co-application of glu in ChNO_3 buffers does not significantly alter current amplitudes above application of ChNO_3 alone (Figure 1C; $p < 0.001$). Consistent with the loss of glutamate mediated channel activity in the absence of Na^+ , radiolabeled transport in EAAT1 is reduced after Ch^+ substitutions by $96.4 \pm 0.7\%$ ($p < 0.001$) and uptake is abolished after removal of Na^+ in EAAT4 by $90.9 \pm 2.8\%$ (Figure 11D; $p < 0.001$). These data all suggest that substrate interactions are disrupted by Na^+ replacement. Taken together, these data support the hypothesis that EAAT4 anion channel activity is dependent on the presence of Na^+ ions but EAAT1 demonstrates Na^+ independent conducting states.

One of the apparent differences between EAAT1 and EAAT4 is their cell type expression in tissue. EAAT1 is exclusively glial while EAAT4 is restricted to neurons (13,134,135). Therefore to test if the functional difference in Na^+ gating activity is related to this divergence in expression in the nervous system, we examined EAAT2, a glial isoform, and EAAT3, another neuronal isoform. As demonstrated for EAAT1, the replacement of extracellular Na^+ for Ch^+ resulted in no significant alteration in NO_3 current amplitudes for EAAT2 expressing oocytes (Figure 12A, C). A $59.7 \pm 4.6\%$ decrease in macroscopic amplitudes ($p < 0.001$) was observed in EAAT3 expressing oocytes in Ch^+ buffer as compared to the $72.6 \pm 1.8\%$ decrease in macroscopic current amplitudes in the presence of $100 \mu\text{M}$ DL-TBOA. Therefore the removal of extracellular Na^+ results in an 82.2% decrease in EAAT3 mediated current amplitudes, with 17.8 % of channel activity remaining (Figure 12B, C). These results are consistent with the data

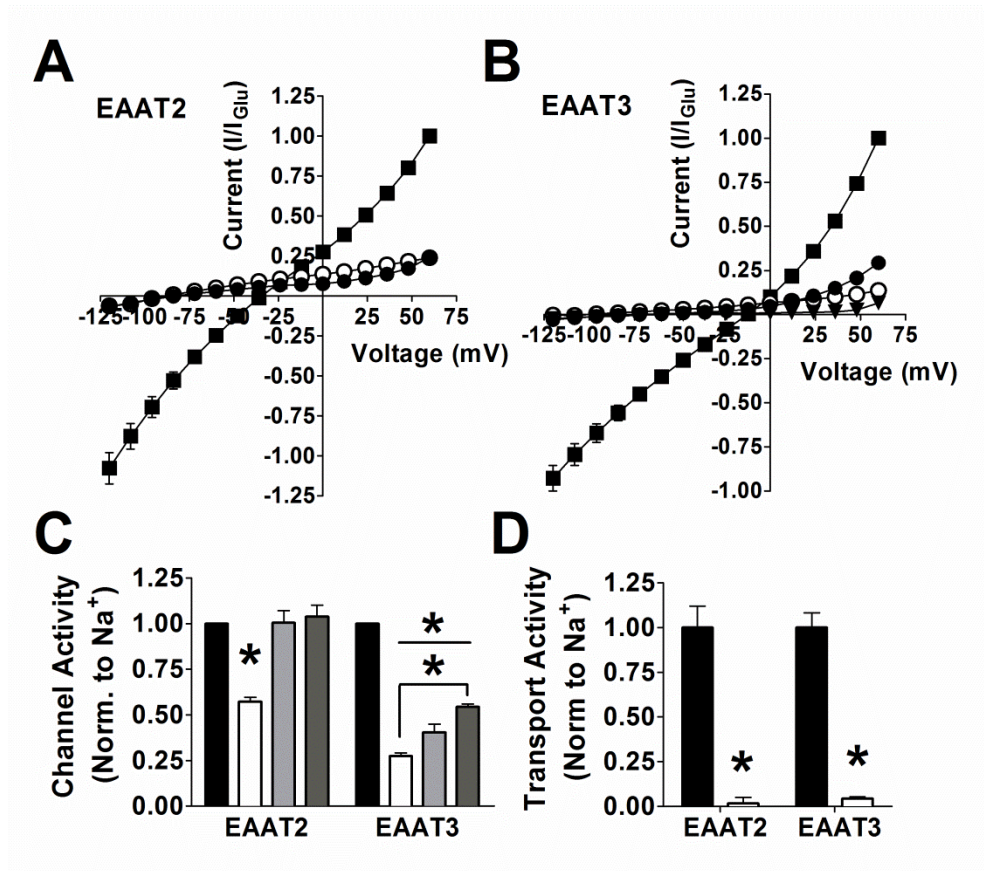


Figure 12: Replacement of external Na⁺ affects EAAT3 but not EAAT2. A-B) Conditions displayed are NaNO₃ (closed circles), NaNO₃ + 500 μM glu (closed squares), NaNO₃ + 100 μM DL-TBOA (closed triangles), and ChNO₃ (open circles). Currents were normalized to the response to application of saturating glu application at +60 mV and are represented by the mean and S.E.M. of 9-17 individual oocytes from ≥ 3 frogs. **A)** Plot of the current-voltage relationship (I-V plot) of *Xenopus* oocytes expressing EAAT2. **B)** I-V plot of the responses to conditions described in A) from oocytes expressing EAAT3. **C)** Bar graph of the currents amplitudes from +60 mV in oocytes expressing EAAT2 and EAAT3 in response to applications of NaNO₃ (black), NaNO₃ + 100 μM DL-TBOA (white), ChNO₃ (grey), and ChNO₃ + 500 μM glu (dark grey). Data are normalized to the cellular response to perfusion of NaNO₃ alone at +60 mV and is expressed as the mean and S.E.M. for 6-20 oocytes from ≥ 3 frogs. **D)** Radiolabeled accumulation of 200 nM 3,4-³H-L-glu and 10 μM glu in oocytes expressing EAAT1 or EAAT4 in

the presence of NaNO_3 (black) or ChNO_3 (white) buffers. Data in CPMs were normalized to transport activity for the NaNO_3 conditions and is displayed as the mean and S.E.M. for 15-25 oocytes from ≥ 3 frogs. Stars indicate statistical significant difference with a Bonferroni post-analysis after a significant 2-way ANOVA comparing isoform and condition.

observed with EAAT1 and EAAT4, radiolabeled glu uptake in the presence of Ch^+ buffers was significantly decreased by $98.3 \pm 3.3\%$ and $95.7 \pm 1.2\%$ ($p < 0.001$) for EAAT2 and EAAT3, respectively. Thus, glial isoforms EAAT1 and EAAT2 display Na^+ independent anion channel activity while neuronal isoforms display a strong Na^+ dependence of anion channel activity.

3.3.2. Choline Buffers do not Support Transporter Activity

Although glu addition to ChNO_3 didn't significantly increase current amplitudes at +60 mV, suggesting that Ch^+ is not binding to the Na^+ binding site (Fig 11C and 12C). It could be argued that Ch^+ may be binding allosterically to EAAT1 and EAAT2 and this could support channel activity in some manner. To control for this possibility, we repeated the previous Na^+ replacement experiments using N-methyl-D-glucamine (NMDG^+) instead of Ch^+ . As demonstrated for the Ch^+ substitution experiments, replacement of extracellular Na^+ with NMDG^+ caused a significant reduction in channel activity in oocytes expressing EAAT3 and EAAT4 but not EAAT1 or EAAT2 (Figure 13A-D). Interestingly, EAAT3 current amplitudes were not reduced to background levels as observed with application of 100 μM DL-TBOA. Indeed EAAT3 mediated currents were only reduced by $61.0 \pm 1.8\%$ in the presence of NMDG^+ . EAAT4 expressing oocytes displayed a $103 \pm 1.9\%$ decrease in EAAT mediated current amplitudes in response to Na^+ replacement with NMDG^+ . Interestingly, the incomplete loss of channel activity observed with EAAT3 in the presence of ChNO_3 as well as NMDG^+ (Figures 11C, 12B, C) might indicate the presence of both Na^+ gated and Na^+ independent open states. This is in contrast to the other isoforms which display either a complete retention (EAATs 1 and 2) or abolishment (EAAT4) of current amplitudes in the presence of either Ch^+ or NMDG^+ .

The application of saturating (500 μM) glu concentrations in the presence of NMDG^+ did not significantly alter current amplitudes in any of the EAAT isoforms tested (Figure 13D) as opposed to Na^+ and glu co-applications (Figure 13E). In addition to NMDG^+ not supporting the gating mechanism induced by glu binding, NMDG^+ substitution also does not support glu

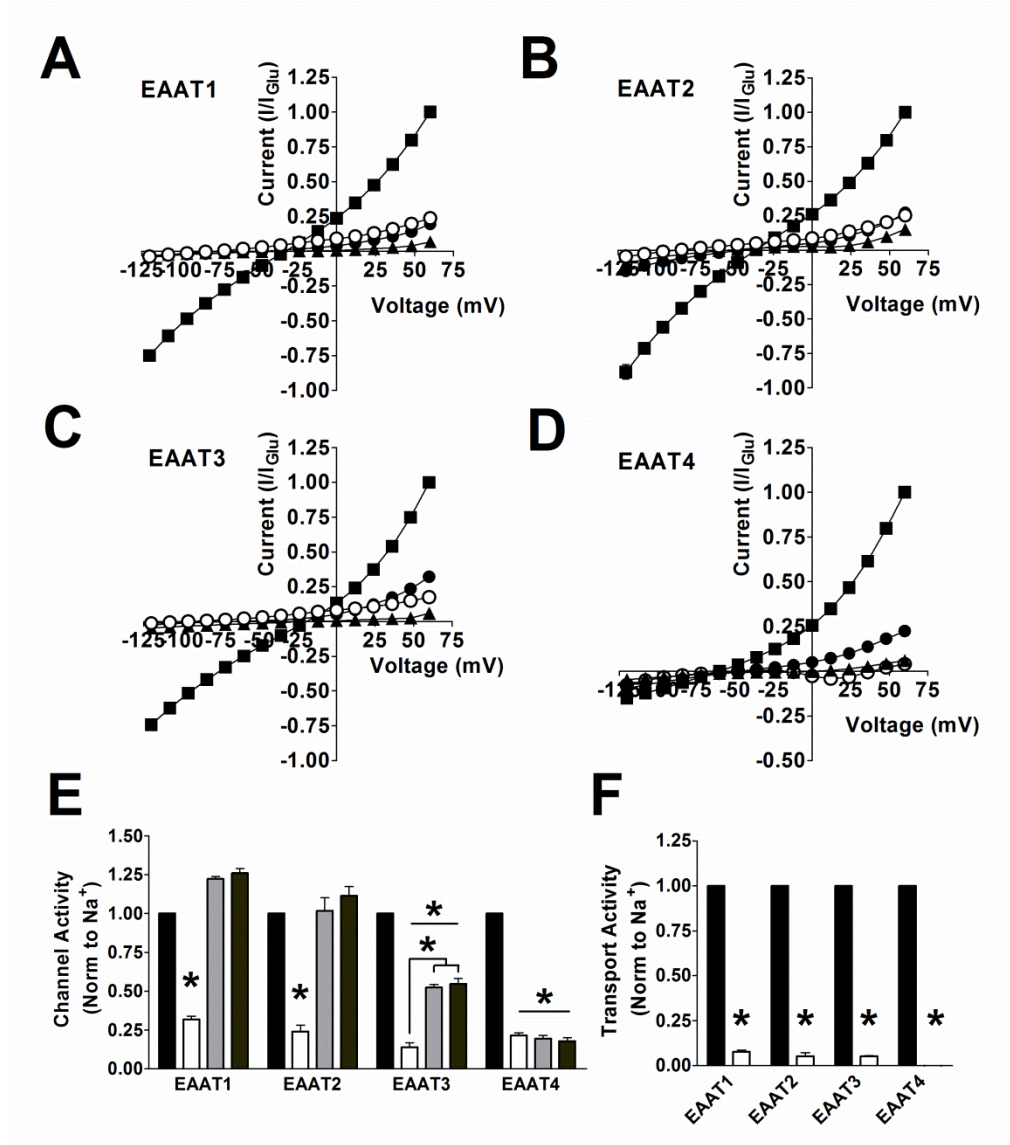


Figure 13: NMDG⁺ replacement of Na⁺ mimics Choline substation on EAATs 1-4. A-D) Conditions displayed are NaNO₃ (closed circles), NaNO₃ + 500 μM glu (closed squares), NaNO₃ + 100 μM DL-TBOA (closed triangles), NMDGNO₃ (open circles). Currents were normalized to the response to application of saturating L-glu application at +60 mV and are represented by the mean and S.E.M. of 6-14 individual oocytes from ≥ 3 frogs. **A)** Plot of the current-voltage relationship (I-V plot) of *Xenopus* oocytes expressing EAAT1. **B)** I-V plot of the responses to conditions described from oocytes expressing EAAT2. **C)** I-V plot of the responses to conditions described from oocytes expressing EAAT3. **D)** I-V plot of the responses to

conditions described from oocytes expressing EAAT4. **E)** Bar graph of the currents amplitudes from +60 mV in oocytes expressing EAAT1, EAAT2, EAAT3, and EAAT4 in response to applications of NaNO_3 (black), $\text{NaNO}_3 + 100 \mu\text{M DL-TBOA}$ (white), NMDGNO_3 (grey), and $\text{NMDGNO}_3 + 500 \mu\text{M glu}$ (dark grey). Data are normalized to the cellular response to perfusion of NaNO_3 alone at +60 mV and is expressed as the mean and S.E.M. for 5-12 oocytes from ≥ 3 experiments. **F)** Radiolabeled accumulation of 200 nM 3,4- $^3\text{H-L-glu}$ and 10 $\mu\text{M L-glu}$ in oocytes expressing EAATs 1-4 in the presence of NaNO_3 (black) or NMDGNO_3 (white) buffers. Data in CPMs were normalized to transport activity for the NaNO_3 conditions and is displayed as the mean and S.E.M. for 6-20 oocytes from ≥ 3 experiments.

transport activity. Radiolabeled transport is significantly reduced in EAATs 1-4 with EAAT1 demonstrating a $92.2 \pm 0.9\%$ decrease in transport capabilities, EAAT2 a $94.6 \pm 2.0\%$ reduction, EAAT3 a $94.6 \pm 0.4\%$ reduction, and EAAT4 a $103 \pm 14.9\%$ reduction (Figure 13F; $p < 0.001$ for all conditions). Therefore, the loss of anion channel activity in neuronal EAAT isoforms 3 and 4 is due to the loss of Na^+ interactions when we replace all external Na^+ with either Ch^+ or NMDG^+ . Likewise, the persistence of currents in EAAT1 and EAAT2 are due to Na^+ independent conducting states. Since the macroscopic amplitudes of the leak states are similar or the same as the channel states in the presence of Na^+ , these EAAT1 and EAAT2 leak open channels states are possibly of the same single channel conductance and open probability as the channel states in the presence of Na^+ . Alternatively these properties would have to be altered in the opposite but equal manner to mediate an unaltered macroscopic current.

3.3.3. Na^+ Mediated Channel Gating in EAAT3 and EAAT4 is Concentration-dependent

We next examined the nature of Na^+ mediated channel gating in both glial and neuronal isoforms by assaying the relationship between Na^+ concentration and channel activity. By systematically replacing increasing amounts of Na^+ with equal molar concentrations of Ch^+ , we observed a significant dependence of EAAT4 channel activity on extracellular Na^+ concentration (Figure 14A). EAAT4 demonstrated a concentration-dependent decrease in whole cell currents with a $73.5 \pm 8.9\%$ reduction of macroscopic current amplitudes in 0 mM Na^+ as compared to 98 mM $[\text{Na}^+]$ ($p < 0.001$). Channel activity in EAAT1 was not significantly altered at any concentration of Na^+ (Figure 14A). Comparing EAAT2 and EAAT3 demonstrates the same patterns of responses. Macroscopic current amplitudes in EAAT3 expressing oocytes, in the absence of glu, are significantly reduced with systematic Na^+ removal yet EAAT2 macroscopic current amplitudes do not significantly change at any concentration of Na^+ (Figure 4B). EAAT3 macroscopic currents were reduced by $68.6 \pm 5.3\%$ in 0 mM Na^+ ($p < 0.001$). Typically an estimation of Na^+ affinity would be possible with the datum generated by this type of assay, however, without a saturation of currents with increasing Na^+ concentrations, a curve fit would

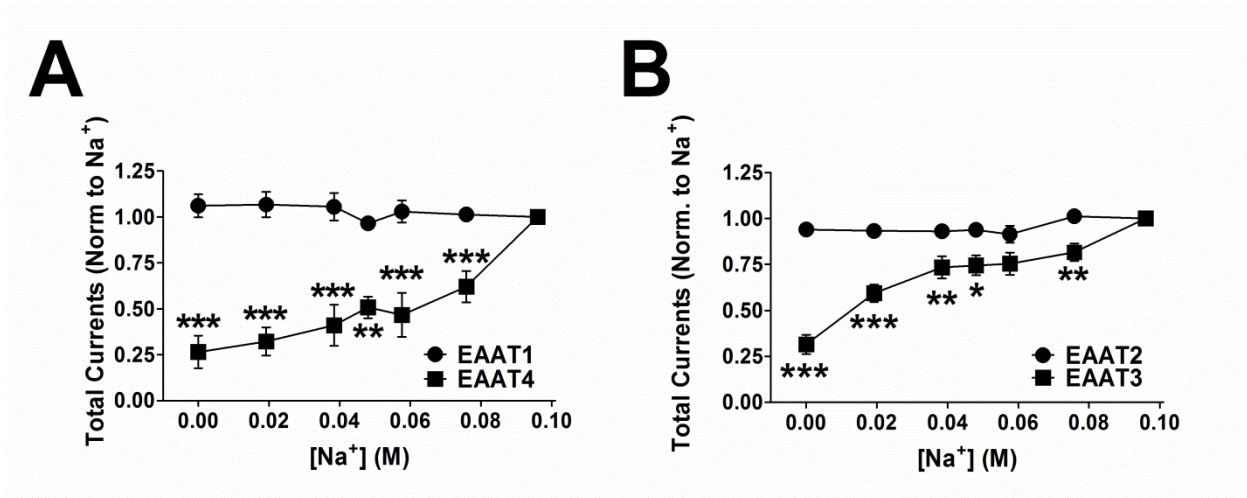


Figure 14: Na^+ gating of anion channel activity is concentration dependent in neuronal EAATs. **A)** Total cellular currents from oocytes expressing either EAAT1 (circles) or EAAT4 (squares) in response to perfusions of varying concentrations of Na^+ . Na^+ was replaced with equal molar concentrations of Ch^+ . **B)** Currents recorded from oocytes expressing EAAT2 (circles) or EAAT3 (squares) in response to application of varying concentrations of Na^+ as described in A). A-B) Currents were normalized to the response of application of NaNO_3 at +60 mV and represent the mean and S.E.M. from 5-12 oocytes for each condition and ≥ 3 experiments. (*) indicates a probability that the two isoforms are significantly different at each Na^+ concentration point with a of $p < 0.05$, (**) indicates a $p < 0.01$, and (***) indicates a $p < 0.001$ from a 2-way ANOVA with a Bonferroni post-analysis comparison as described under the experimental procedures.

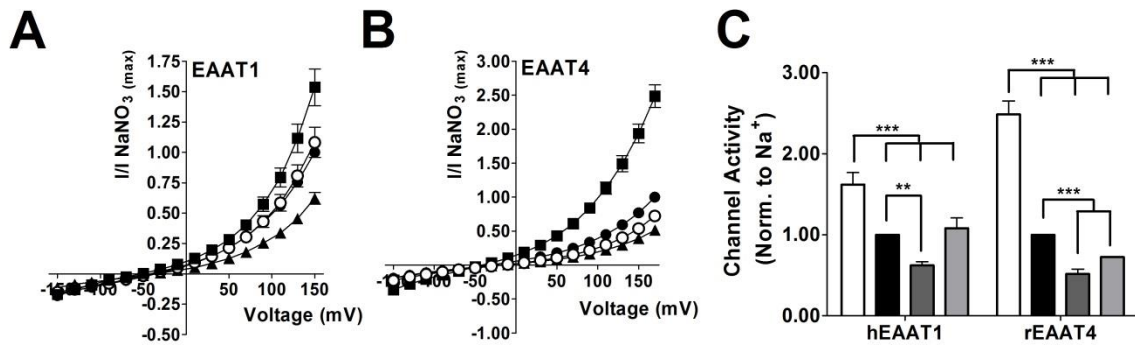


Figure 15: Replacement of internal Na^+ causes a loss of inward facing anion channel currents in neuronal isoforms only. **A)** Whole cell patch clamp recordings of I-V curves from tsA201 cells transiently expressing EAAT1. Cells were dialyzed with a ChCl pipette solution as described in the experimental procedures. Extracellular solutions used were NaSCN (closed circles), NaSCN + 500 μ M L-glu (closed squares), NaSCN + 100 μ M DL-TBOA (closed triangles), and KSCN buffer (open circles). Currents were normalized the response elicited by application of NaSCN alone at +150 mV and represent the mean and S.E.M. of 7 cells. **B)** Whole cell patch clamp recordings of I-V curves from tsA201 cells transiently expressing EAAT4. Conditions are the same as described for A) and are displayed as the mean and S.E.M. from 3 cells from 2 experiments. **C)** Bar graph displaying the quantitation of current amplitudes at +150 mV from cells as described in A) and B). Conditions displayed are NaSCN + 500 μ M glu (white), NaSCN (black), NaSCN + 100 μ M DL-TBOA (dark grey), and KSCN buffer (light grey).

not be accurate and therefore we did not attempt to estimate an affinity for Na^+ . Previous estimations place the effective concentration of Na^+ which yields half maximal channel activity (EC_{50}) for the empty, outward facing transporters at 98 mM for EAAT2 (35), 80 mM for EAAC1 (EAAT3) (50), and 42 mM for EAAT4 (132), consistent with our partial data.

3.3.4. The Channel Activity Mediated by the Inward Facing States of EAAT1 and EAAT4 Display a Disparate Na^+ Dependence

EAATs operate through a reversible transport cycle. Therefore, exposure of EAATs to high extracellular K^+ concentrations drives the carriers to the inward facing states during the reverse transport cycle (20,22,39,119). Inward facing transporters need to bind either intracellular K^+ to complete the forward transport cycle or Na^+ and glu to mediate reverse transport or an exchange cycle. Thus, without these intracellular conditions, the carriers will be locked in the inward facing states in the presence of high extracellular K^+ solutions. Using whole-cell patch configurations of EAAT expressing tsA201 cells, we dialyzed the endogenous cytoplasmic K^+ and Na^+ and replaced these cations with Ch^+ . This allows for the persistence of the inward facing states and the determination of the Na^+ dependence of the inward facing conducting states. Under these conditions we see no significant difference in current amplitudes from inward oriented open channels states, mediated by the KSCN extracellular solutions and the outward facing conformation-mediated open channel states observed in NaSCN extracellular solutions, in EAAT1 (Figure 15A, 15C). However, in the same experimental paradigm, EAAT4 macroscopic currents, under high extracellular K^+ buffers (KSCN), were significantly reduced in amplitude by $27.6 \pm 0.8 \%$ ($p < 0.001$, student's t-test; Figure 15B, 15C). Thus, the conducting states mediated by inward facing conformations show a similar Na^+ dependence as the outward facing conducting states (Fig 11). The glial carrier EAAT1 mediates a Na^+ independent anion “leak” conductance while the neuronal carrier EAAT4 displays Na^+ dependent channel activity in both the outward and inward facing conformations of the transport cycle.

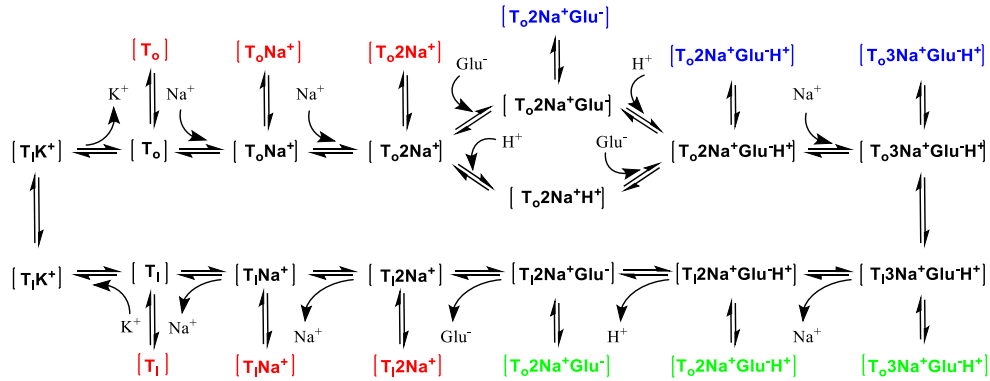
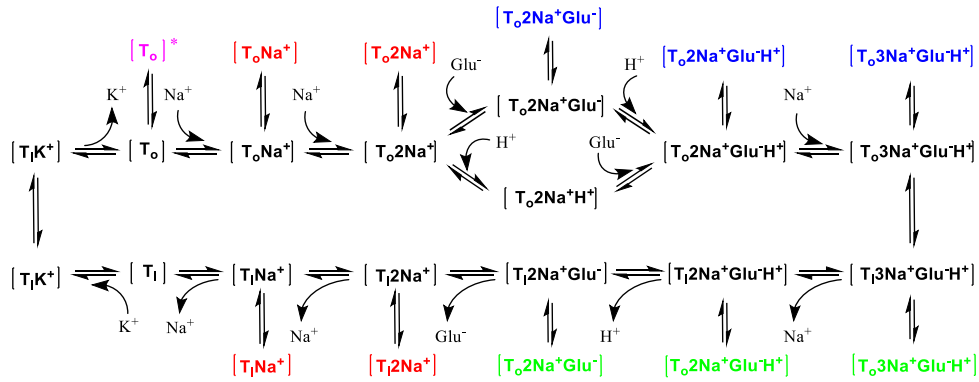
A**EAAT1 and EAAT2****B****EAAT3* and EAAT4**

Figure 16: State diagrams for neuronal and glial EAATs differ in number of open channel states. A) State diagram representing the transport cycle and open channel states of glial glutamate carriers EAATs 1 and 2. Conformations of the transport cycle are colored black. Open channel states are depicted in various colors; Leak conducting states (red), glutamate gated open states (blue), glutamate gated states mediated by the inward facing transporter conformations (green). **B)** State diagram representing the transport cycle and open channel states of neuronal EAATs 3 and 4. Open channel states displayed are low conductance or open probability leak states (fuchsia, EAAT3 only), Na^+ gated open states (red), glutamate gated open states (blue), glutamate gated states mediated by the inward facing transporter

conformations (green). Substrate binding order was adapted from (34). Inward facing open channel states were interpreted from (41,45). The $[T_o2Na^+H^+]$ conducting state was omitted for clarity of the diagram and would be a low open probability conducting state colored red. State diagrams were made using ChemBioDraw v13 (Perkin-Elmer).

3.3.1. Glial and Neuronal EAATs have a Different Number of Open Channel States

These data presented here allows us to refine the EAAT state diagram to include novel open channel states and to separate glial and neuronal carriers. Our models are adapted from the 15 state transport cycle originally proposed by Bergles et al. (34). Depicted for the glial carriers EAAT1 and EAAT2 are 12 open channel states of at least two different open probabilities or single channel amplitudes (Figure 16A). The “leak” or low open probability channel states are depicted in red and the glu gated open channel states are shown as blue (outward facing conformations) and green (inward facing conformations). As demonstrated by our model, the empty, outward facing carrier ($[T_o]$) mediates the same macroscopic currents as the Na^+ bound conformations ($[T_oNa^+] - [T_o2Na^+]$) and thus are both colored red. Figure 16B depicts the open channel states for neuronal carriers EAAT3 and EAAT4. EAAT4 is diagramed with 10 open channel states in the presence of bound Na^+ (red) and $Na + glu$ (blue/green) (Figure 16B). EAAT3 is depicted to possess an additional open channel state mediated by the empty transporter that is a lower open probability and/or single channel conductance (fuchsia) than in the presence of extracellular Na^+ . The glu gated anion conducting states modeled in green for both glial and neuronal transport diagrams represent conducting states reported in previous publications (41,45).

3.4. DISCUSSION

Here we demonstrate a difference in the gating mechanism between neuronal and glial EAAT isoforms. The ability of EAATs to mediate an anion flux in the absence of glutamate binding, classically term the “leak” conductance, has been accepted for many years. Our data indicate that Na^+ binding to EAAT3 and EAAT4 is necessary for channel opening but EAATs 1 and 2 mediate a “leak” anion flux through the empty, unbound transporters. Initial studies into the EAAT mediated anion conductance displayed the loss of a tonic current in Muller glial cells when extracellular Na^+ was replaced by Ch^+ (49) Alternatively, the presence of the tonic or leak

currents in the presence of Na^+ alone (glu free) were revealed when inhibitors such as DL-TBOA were used to inhibit the tonic anion flux (46). The presence of currents in extracellular Na^+ buffers (glu free) was subsequently demonstrated for all EAAT isoforms (11,33,40,48). Studies which described the Na^+ dependence of these anion conducting states were, however, limited to neuronal EAAT3 and EAAT4 isoforms (50,130,132) or Müller glial cells from salamander (49), the latter of which displays some disparate properties from the mammalian EAATs (136). Therefore, attributes of neuronal carriers were assumed to apply to all isoforms which our data presented here refutes.

One of the early kinetic models of the glutamate transport cycle described a 15 state transport cycle with 8 conducting states in GLT-1 (rat EAAT2). These conducting states were limited to Na^+ bound and Na^+ and glu bound states, in the outward facing conformations. The only inward facing conformations that the model displayed with an associated conducting state was the 2Na^+ bound state and the K^+ bound conformations (34). The presence of the inward facing 2Na^+ bound conducting state was not directly experimentally determined (47). Recently, experimental data were combined with simulations to further refine our knowledge of the relationship between conducting states and transporter conformations in EAAT4 (118). These data support the hypothesis that there are additional conducting states which are associated with conformations not previously believed to mediate channel activity. Our data here partially support this hypothesis because we demonstrate that EAATs 1 and 2 mediate open channel states in the unbound transporters. We also demonstrate a partial or total loss of all channel activity with EAAT3 and EAAT4 with the removal of extracellular Na^+ . One possible reason for the difference in our interpretation of the number of conducting states in EAAT4 compared with the results in Machtens et al. (2011) (118) is that our background is defined by currents in the presence of DL-TBOA. There is could be some residual open probability that exists even in the presence of saturating concentrations of this antagonist. Thus it is possible that our removal of Na^+ from EAAT4, for example, may leave us with a small residual EAAT mediated current that

we do not recognize because it is equal to currents in the presence of saturating DL-TBOA. Despite these factors, we can now develop or refine individual state diagrams for glial and neuronal transporters.

It is intriguing that complete removal of extracellular Na^+ from EAAT3 only causes a partial loss of channel currents in *Xenopus* oocytes. We interpret these data to indicate that EAAT3 is unique in that it has an open probability associated with both the unbound and Na^+ bound states and that the open probability or single channel conductance is lower in the unbound state. Watzke et al. (2001) (50) assayed for channel activity in the presence or absence of extracellular Na^+ similar to the experiment shown in Figure 14B. However, in their experiments, DL-TBOA was added in conjunction with the removal of Na^+ and this might have blocked the residual currents which we observed with a similar Na^+ replacement. Nonetheless, the Na^+ independent channel activity seen with EAAT3, in addition to the Na^+ dependent channel activity, will need further examination in the future.

It is unclear what role the neuronal or glial EAAT-mediated, channel activity plays in glutamatergic neurotransmission. The role of the anion channel in regulating cellular activity has been supported by EAAT5-mediated regulation of rod bipolar cells in the retina. However, similar experiments have not been performed examining the role of the anion channel with other EAAT isoforms. Additionally, experiments testing the ability for EAAT5 anion currents to effect cellular activity were always performed in the presence of glu and no data exist which support a role for the EAAT-mediated regulation of cellular activity in the absence of glu. Thus it is challenging to speculate on the impact of these low open probability conducting states in the presence of Na^+ alone (EAAT3 and EAAT4) or in the unbound transporter (EAATs 1, 2, and 3).

The difference in gating mechanism between glial and neuronal isoforms allows us to form better hypotheses surrounding the question of the role of the anion channel in regulating cellular activity in the absence of extracellular glu. For example, anoxic depolarization would significantly disrupt anion currents mediated by neuronal EAATs as the Na^+ gradient would be

dissipated (4,39,57,137). This could lead to a loss of a neuroprotective hyperpolarization in EAAT3 and EAAT4 expressing neurons, which has been hypothesized to be caused by EAAT anion channel activity (44). Conversely, astrocytes would still mediate a steady Cl^- flux through either EAAT1 or EAAT2 their channel activity is independent of extracellular Na^+ concentrations (10,35). Although this hypothesis of glial regulation in the presence of an altered ion gradient is currently just speculative, the additional knowledge provided in this study will assist in generating more meaningful hypotheses for future studies.

4. CONCLUSIONS

4.1. EXCITATORY AMINO ACID TRANSPORTERS AND ANION CONDUCTION

EAATs are secondary active, electrogenic transporters which also possess a thermodynamically uncoupled anion channel. This anion channel functionality is ubiquitous in the EAAT containing, SLC1 family of transporters yet a significant role for this channel function has yet to be established in many of the EAAT isoforms. The anion channel function has been described since the early 90s (49) and was further elucidated in 1994 when the human EAAT4 isoform was cloned. In EAAT4, and subsequently all EAAT isoforms, it was demonstrated that channel function was integral to the EAAT4 protein (10). To characterize the anion flux, the temperature dependence of anion and substrate flux through EAAT2 was measured (40). Macroscopic currents at negative potentials, predominately transport processes, were highly temperature sensitive with a thermal coefficient (Q_{10}) of > 3 , while currents measured at various temperatures at positive potentials displayed a Q_{10} of ~ 1 , indicating a passive diffusion mechanism for anions through an open pore. These types of experiments have been repeated for other EAAT isoforms with similar results (138). Additional data which support that this channel like activity is mediated by a pore came from noise analysis data which displays power spectra which can be fitted to a lorentzian function, indicative of a stochastic gating transition or channel mediated anion flux (40,51-53,139,140). The permeability of anions through this pore is akin to many promiscuous Cl^- channels and generally follows a sequence of $\text{SCN}^- > \text{ClO}_4^- > \text{NO}_3^- > \text{I}^- > \text{Br}^- > \text{Cl}^-$ (10,44,45). The channel behaves in a manner consistent with a multi-ion pore for SCN^- flux through EAAT4, although, a lack of anomalous mole fraction behavior, characteristic of single-file, multi-ion pores, has been described for the EAATs as well (43,52). Thus, it is

unclear if the EAATs possess a classical pore design which is similar in nature to many other anion channels. A notable difference between the EAAT anion channels and those of classical chloride channels, such as GABA_A receptors or CLC channels, is that the EAAT channels have a particularly low conductance. Both stationary and non-stationary noise analysis has been performed on various EAAT isoforms and these data indicate a low conductance permeation pathway of between 0.3 fS to 700 fS (51-53). Many of these studies agree that the single channel conductance is not altered upon substrate interaction and that an increase of the open probability underlies the change in macroscopic currents in the presence of substrates. Melzer et al. (2003) reported that dissociation rate of the highly permeant anion SCN⁻ to the channel was increased by increasing concentrations of substrates, although they concluded that this likely related by an increase in the unitary conductance of the channel (52).

4.2. SUBSTRATE-MEDIATED CHANNEL GATING

Since the discovery of the anion channel in the EAATs, the interaction of substrate translocation and the anion channel gating function has been thoroughly investigated. It is clear that substrate interaction mediates the increased macroscopic current above basal channel activity, but not all substrates act on the channel in the same way. The application of D-aspartate caused macroscopic reversal potential (E_{rev}) to move close to the Cl⁻ reversal potential (E_{Cl}) then application of glutamate (43). The current/flux ratio (Φ Cl⁻ / Φ substrate) was different between the two substrates. In contrast, pre-steady state kinetic data have suggested that D-aspartate transport is less efficient in gating the anion flux than glutamate and that D-aspartate transport alters the rate limiting step of the transport cycle in EAAT3 from K⁺ mediated reorientation to a step earlier in the transport cycle (141). The decrease in transport rate could decrease the relative contribution of the stoichiometric transport current, thus shifting E_{Rev} closer to E_{Cl} . However, similar experiments in EAAT2 have yielded opposite results where application of D-aspartate led to an ~ 2 fold increase in steady state current amplitudes as compared to glutamate. Concentration jumps of D-aspartate elicited a

decay in current amplitudes with a significantly slower time course than those observed with application of glu (40). The binding of substrates and the relationship of binding to the gating function of the anion channel has been investigated using pre-steady state kinetics as well. Using photo-release of caged glu molecules, Grewer et al. (2000) demonstrated a rapid voltage independent binding of glu and a subsequent, voltage-dependent slow process, likely glu translocation. In addition, the formation of the anion conducting state is slightly delayed in comparison to the formation of glu bound states but does occur before glu translocation across the membrane (33). These data indicate that binding of the transporter is not sufficient to gate the anion channel and a secondary process after the binding comprises the gating mechanism. Consistent with these observations, mutation of R388 to acidic residues glu or asp eliminates substrate induced open channel states yet allows for the binding and translocation of those substrates (Appendix D). These data support the hypothesis that channel gating is not induced by substrate binding alone but is dependent on subsequent conformational changes that occur before the translocation of substrates.

Two additional sets of data are worth considering when contemplating the gating mechanism in the EAATs. First, binding of DL-TBOA, a competitive and non-transportable inhibitor of the EAATs, has been demonstrated to block not only glutamate interactions and transport, but also anion channel activity, including the leak conducting states (142). The mechanism by which TBOA blocks all channel activity is unknown. Recent data have indicated that binding of TBOA locks HP2 into an open or intermediate-open state (31), but conversely modification of HP2, locking it into the open state, leads to heightened channel activity (115-117). Thus it is not unreasonable to hypothesize that HP2 dynamics are involved in anion channel gating but at this point a concise mechanism has yet to emerge. Additional data supporting the role of HP2 in channel gating comes from double site-directed spin labeling electron paramagnetic resonance spectroscopy (DSDSL-EPR) demonstrated that Na⁺ binding to the empty transporter induced and stabilized an open conformation of spin labeled HP2

(143). Thus, gating of the anion channel may involve HP2 dynamics, possibly part of the occlusion mechanism that must occur between substrate binding and translocation. It is clear that lingering questions remain about the mechanism of substrate interactions and how these relate to the gating of the anion channel.

4.3. THE ROLE OF THE ANION CONDUCTANCE IN CELLULAR FUNCTION

The role of the EAAT anion channel in cellular function has yet to be clarified. However, the anion channel activity of EAAT5 has been demonstrated to influence cellular activity in rod bipolar cells in the retina. Veruki et al. (2006) demonstrated that the Cl^- flux through EAAT5 was capable of modulating firing rates of the bipolar cell as well as influence the release probability of glu containing vesicles (58). EAAT5 was also able mediate a substantial Cl^- flux from activation by adjacent bipolar cells through spillover of glu. Other work has substantiated the role of EAAT5 as a ligand gated receptor in the retina (59). Unfortunately, analogous data have not been demonstrated to date for the other EAAT isoforms. Like EAAT5, EAAT4 has a lower transport rate and thus has a prominent anion conductance in comparison to its transport capacity. Thus, many have speculated that EAAT4, which is ubiquitously expressed throughout the CNS in low levels, may be playing a similar role to a ligand gated receptor because it likely does not transport a significant amount of synaptically release glu. Indeed the majority of glu that is released to the synapse diffuses and is transported by the glial EAAT2 isoform (14,85). In addition to rapidly buffering released glu, roles for the neuronal isoform EAAT3 include providing avenues for GABA synthesis with the small amount of glu transport it mediates (112). Data from EAAT3 knock-out mice strongly suggest a role for EAAT3 mediating cysteine transport and influencing glutathione synthesis (111) (Appendix C). Because the majority of released glu is transported by glial EAAT isoforms, it is possible that anion channel activity is the predominate role for neuronal isoforms (84). Surprisingly, the enhanced expression of EAAT4 in the cerebellum has provided little insight into its role beyond that typical of glutamate carriers (144).

Experiments have described a significant role for neuronal EAATs in the cerebellum in regulating perisynaptic activation of ionotropic and metabotropic receptors but few studies have isolated the contributions of EAAT4 in these processes (105,106).

The anion channel activity of glial isoforms EAATs 1 and 2 have not been thoroughly investigated for their role in regulating glial activity. The single channel properties of EAAT3 and EAAT4 measured by noise analysis indicated that the difference in macroscopic currents are due solely to differences in transport kinetics, more specifically time spent transporter conformations that can mediate open channel states (53,132). Since EAAT3 and EAAT4 possess similar single channel properties, it is possible that glial isoforms do not differ in channel properties either. One difference in channel activity between glial and neuronal EAATs is the gating of the anion channel where we have demonstrated that glial isoforms have a basal open probability in the absence of Na^+ in contrast to neuronal isoforms which are strongly Na^+ dependent (Figure 11 and Figure 13).

4.4. LEAK CONDUCTING STATES IN EAATS

The anion conductance in the family of EAATs has been demonstrated to be gated by Na^+ interaction and the anion channel activity increased upon subsequent glu binding (40,46,48). The Na^+ gated channel activity has been classically referred to as the “leak” conductance because the mechanism of channel gating in the absence of glu was unresolved at that time. Initial estimations of the number of anion conducting states were limited to those readily observed; the outward Na^+ -bound conformations and the outward Na^+ and glu-bound conformations. Additional conducting states were proposed based on minimal evidence. These included the inward 2Na^+ -bound conformation and the inward K^+ -bound conformation (34). The glutamate transport cycle last from approximately 8 – 66 msec. the majority of this time is spent during the inward facing steps because K^+ reorientation is the rate limiting process. Thus, if the inward facing steps of the transport cycle had transitions to open channel states, the relative

contribution of the Na⁺ gated or leak anion conductance would be significantly greater than previously assumed. Indeed, our data demonstrate that when EAAT1 is restricted to the inward facing conformations through modification of HP1 while in the inward, HP1-open conformation, we readily observe anion conductances that mimic the outward Na⁺ bound states (Figure 7). This work was significant for two reasons. First, we developed a novel method for capturing the inward facing states. Initial strategies for accomplishing this goal were based on those used by Reyes et al (2009) involving crosslinking of HP2 to TM2 (32). Crosslinking of these two regions, however, did not yield results indicative of the inward facing state. If the inward facing state was captured, then the carriers would be insensitive to extracellular substrate application. Application of saturating concentrations of glu to the extracellular face of the 1,10-Cu²⁺-Phenanthroline (CuPh) treated V454C-Q93C double mutant yielded ~125% of the channel activity as dithreoretinal (DTT) treated double mutant. Our current strategy was based on another set of observations. Modification of the external gate HP2 using cysteine point mutations and cysteine specific modifying reagents results in a transport state that is locked outward and open. Substrate transport is eliminated yet binding and channel activity are intact after this modification. Experiments which used inside-out patch clamp recording of EAATs demonstrated that substrates applied to the intracellular face of the transporters could readily bind and gate the substrate induced anion channel activity. It is likely that a significant fraction of the transporter population was in the inward, HP1-open conformation under conditions that drive carriers to inward facing states, i.e. high extracellular K⁺. Combining these data, we hypothesized that driving the transporter into the inward facing states, then modifying the proposed internal gate HP1, would likely restrict the transporter into the inward open state. Although we cannot say precisely which state was captured by our modification strategy, our modified transporters exhibit a complete loss of transport activity and have no response to extracellularly applied substrates or inhibitors. If the open (binding site accessible) and closing (occluded) transition of the internal gate is similar to the external gate, then a modified open

HP1 would be prevented from closing by steric hindrance, and thus prevent further conformational changes. With this strategy of hindering conformational changes after stabilizing one or more inward facing states, we observed a significant anion conductance. These data support our hypothesis that the inward facing conformations visited during the transport cycle can mediate transitions to open, conducting states (Figure 7).

We were curious why these inward facing open channel states mediated the same macroscopic current amplitudes as those observed with the outward facing conformations of the EAAT transport cycle. One possibility is that the channel can only exist with two different open probabilities, leak and substrate gated, which are accessible from multiple conformations in the transport cycle. Another explanation is that there are additional substrates present which could be binding and mediating this channel activity. To test the gating requirement of the EAAT anion channel in the absence of substrates, we used an ion replacement strategy where all the extracellular Na^+ was replaced by choline (Ch^+). For EAATs 1 and 2, the persistence of anion conducting states of the same macroscopic amplitudes in the absence of Na^+ as in the presence of Na^+ is indicative of leak conducting states (Figures 11 and 12). In contrast, the reduction in current amplitudes in the absence of external Na^+ in EAAT3 and EAAT4 are consistent with previously published data indicating that the open channel states in the absence of substrates are Na^+ mediated (50,130,132). Thus, we now possess a more accurate state diagram where glial EAAT isoforms have a basal open probability in the unbound and Na^+ bound states, and this increases upon glutamate interaction. Once glutamate is translocated and released to the intracellular space, the channel returns to its lower open probability states. The only states which have not been investigated to date are the K^+ interacting states. It is unclear if these states mediate an anion flux. Data recorded in EAAT4 demonstrated a current “overshoot” effect when fast application of glu caused a coordinated movement of the transporter population through the initial steps of the transport cycle involving Na^+ and glu translocation across the membrane. Entry of the population of transporters into non-conducting states caused a transient

reduction or “overshoot” of anion channel mediated currents below background (Na^+ alone) (47). This effect was absent in the EAAT2 isoform (34). The absence of anion conducting steps in the glu unbound conformational states in EAAT4 compared to the additional conducting states in the glu unbound EAAT2 could explain the presence of the current overshoot effect in EAAT4 alone. Although these data do not resolve the question of whether K^+ interaction mediates anion channel activity, it is likely that such an overshoot effect would need additional non-conducting states visited during the transport cycle to mediate this phenomenon. Thus we speculate that the K^+ interacting steps do not mediate channel activity in at least the neuronal isoforms, if not in all EAATs.

4.5. SUMMARY

The anion channel found in EAATs could be an important regulator of cellular activity. Its proposed roles have ranged from offsetting the depolarizing effect electrogenic transport mediates to regulating cellular excitability and neurotransmission as an ionotropic receptor. The work presented here pushes forward our understanding of not only the link between substrate transport and open channel states but also the gating mechanism of the anion channel. Although much of this work has elucidated low open probability conductance states classical termed “leak” states, the transport spends the majority of the duration of the transport cycle in conformations that are associated with such states. These data presented here will assist in resolving the role of EAAT associated anion channel and pave the way for future studies investigating dual transport-channel systems.

5. REFERENCES

1. Danbolt, N. C. (2001) Glutamate uptake. *Prog Neurobiol* **65**, 1-105
2. Djali, S., and Dawson, L. A. (2001) Characterization of endogenous amino acid efflux from hippocampal slices during chemically-induced ischemia. *Neurochemical research* **26**, 135-143
3. Phillis, J. W., Smith-Barbour, M., Perkins, L. M., and O'Regan, M. H. (1994) Characterization of glutamate, aspartate, and GABA release from ischemic rat cerebral cortex. *Brain research bulletin* **34**, 457-466
4. Rossi, D. J., Oshima, T., and Attwell, D. (2000) Glutamate release in severe brain ischaemia is mainly by reversed uptake. *Nature* **403**, 316-321
5. Seki, Y., Feustel, P. J., Keller, R. W., Jr., Tranmer, B. I., and Kimelberg, H. K. (1999) Inhibition of ischemia-induced glutamate release in rat striatum by dihydrokinate and an anion channel blocker. *Stroke; a journal of cerebral circulation* **30**, 433-440
6. Storck, T., Schulte, S., Hofmann, K., and Stoffel, W. (1992) Structure, expression, and functional analysis of a Na(+)-dependent glutamate/aspartate transporter from rat brain. *Proc Natl Acad Sci U S A* **89**, 10955-10959
7. Yernool, D., Boudker, O., Jin, Y., and Gouaux, E. (2004) Structure of a glutamate transporter homologue from *Pyrococcus horikoshii*. *Nature* **431**, 811-818
8. Pines, G., Danbolt, N. C., Bjoras, M., Zhang, Y., Bendahan, A., Eide, L., Koepsell, H., Storm-Mathisen, J., Seeberg, E., and Kanner, B. I. (1992) Cloning and expression of a rat brain L-glutamate transporter. *Nature* **360**, 464-467
9. Kanai, Y., and Hediger, M. A. (1992) Primary structure and functional characterization of a high-affinity glutamate transporter. *Nature* **360**, 467-471

10. Fairman, W. A., Vandenberg, R. J., Arriza, J. L., Kavanaugh, M. P., and Amara, S. G. (1995) An excitatory amino-acid transporter with properties of a ligand-gated chloride channel *Nature* **375**, 599-603
11. Arriza, J. L., Eliasof, S., Kavanaugh, M. P., and Amara, S. G. (1997) Excitatory amino acid transporter 5, a retinal glutamate transporter coupled to a chloride conductance *Proc Natl Acad Sci U S A* **94**, 4155-4160
12. Arriza, J. L., Fairman, W. A., Wadiche, J. I., Murdoch, G. H., Kavanaugh, M. P., and Amara, S. G. (1994) Functional comparisons of three glutamate transporter subtypes cloned from human motor cortex. *J Neurosci* **14**, 5559-5569
13. Lehre, K. P., Levy, L. M., Ottersen, O. P., Storm-Mathisen, J., and Danbolt, N. C. (1995) Differential expression of two glial glutamate transporters in the rat brain: quantitative and immunocytochemical observations. *J Neurosci* **15**, 1835-1853
14. Holmseth, S., Dehnes, Y., Huang, Y. H., Follin-Arbelet, V. V., Grutle, N. J., Mylonakou, M. N., Plachez, C., Zhou, Y., Furness, D. N., Bergles, D. E., Lehre, K. P., and Danbolt, N. C. (2012) The Density of EAAC1 (EAAT3) Glutamate Transporters Expressed by Neurons in the Mammalian CNS. *The Journal of neuroscience : the official journal of the Society for Neuroscience* **32**, 6000-6013
15. Tanaka, K., Watase, K., Manabe, T., Yamada, K., Watanabe, M., Takahashi, K., Iwama, H., Nishikawa, T., Ichihara, N., Kikuchi, T., Okuyama, S., Kawashima, N., Hori, S., Takimoto, M., and Wada, K. (1997) Epilepsy and exacerbation of brain injury in mice lacking the glutamate transporter GLT-1. *Science* **276**, 1699-1702
16. Fairman, W. A., Sonders, M. S., Murdoch, G. H., and Amara, S. G. (1998) Arachidonic acid elicits a substrate-gated proton current associated with the glutamate transporter EAAT4. *Nat Neurosci* **1**, 105-113
17. Massie, A., Cnops, L., Smolders, I., McCullumsmith, R., Kooijman, R., Kwak, S., Arckens, L., and Michotte, Y. (2008) High-affinity Na⁺/K⁺-dependent glutamate

- transporter EAAT4 is expressed throughout the rat fore- and midbrain. *The Journal of comparative neurology* **511**, 155-172
18. Kanner, B. I., and Sharon, I. (1978) Active transport of L-glutamate by membrane vesicles isolated from rat brain. *Biochemistry* **17**, 3949-3953
 19. Brew, H., and Attwell, D. (1987) Electrogenic glutamate uptake is a major current carrier in the membrane of axolotl retinal glial cells. *Nature* **327**, 707-709
 20. Barbour, B., Brew, H., and Attwell, D. (1988) Electrogenic glutamate uptake in glial cells is activated by intracellular potassium. *Nature* **335**, 433-435
 21. Kanner, B. I., and Bendahan, A. (1982) Binding order of substrates to the sodium and potassium ion coupled L-glutamic acid transporter from rat brain. *Biochemistry* **21**, 6327-6330
 22. Kanner, B. I., and Marva, E. (1982) Efflux of L-glutamate by synaptic plasma membrane vesicles isolated from rat brain. *Biochemistry* **21**, 3143-3147
 23. de Vrij, W., Bulthuis, R. A., van Iwaarden, P. R., and Konings, W. N. (1989) Mechanism of L-glutamate transport in membrane vesicles from *Bacillus stearothermophilus*. *J Bacteriol* **171**, 1118-1125
 24. Bouvier, M., Szatkowski, M., Amato, A., and Attwell, D. (1992) The glial cell glutamate uptake carrier countertransports pH-changing anions. *Nature* **360**, 471-474
 25. Amato, A., Ballerini, L., and Attwell, D. (1994) Intracellular pH changes produced by glutamate uptake in rat hippocampal slices. *J Neurophysiol* **72**, 1686-1696
 26. Zerangue, N., and Kavanaugh, M. P. (1996) Flux coupling in a neuronal glutamate transporter. *Nature* **383**, 634-637
 27. Watzke, N., Rauen, T., Bamberg, E., and Grever, C. (2000) On the mechanism of proton transport by the neuronal excitatory amino acid carrier 1. *J Gen Physiol* **116**, 609-622

28. Grewer, C., Watzke, N., Rauen, T., and Bicho, A. (2003) Is the glutamate residue Glu-373 the proton acceptor of the excitatory amino acid carrier 1? *J Biol Chem* **278**, 2585-2592
29. Kanai, Y., Stelzner, M., Nussberger, S., Khawaja, S., Hebert, S. C., Smith, C. P., and Hediger, M. A. (1994) The neuronal and epithelial human high affinity glutamate transporter. Insights into structure and mechanism of transport. *J Biol Chem* **269**, 20599-20606
30. Kanai, Y., Nussberger, S., Romero, M. F., Boron, W. F., Hebert, S. C., and Hediger, M. A. (1995) Electrogenic properties of the epithelial and neuronal high affinity glutamate transporter. *J Biol Chem* **270**, 16561-16568
31. Boudker, O., Ryan, R. M., Yernool, D., Shimamoto, K., and Gouaux, E. (2007) Coupling substrate and ion binding to extracellular gate of a sodium-dependent aspartate transporter. *Nature* **445**, 387-393
32. Reyes, N., Ginter, C., and Boudker, O. (2009) Transport mechanism of a bacterial homologue of glutamate transporters. *Nature* **462**, 880-885
33. Grewer, C., Watzke, N., Wiessner, M., and Rauen, T. (2000) Glutamate translocation of the neuronal glutamate transporter EAAC1 occurs within milliseconds. *Proc Natl Acad Sci U S A* **97**, 9706-9711
34. Bergles, D. E., Tzingounis, A. V., and Jahr, C. E. (2002) Comparison of coupled and uncoupled currents during glutamate uptake by GLT-1 transporters. *J Neurosci* **22**, 10153-10162
35. Wadiche, J. I., Arriza, J. L., Amara, S. G., and Kavanaugh, M. P. (1995) Kinetics of a human glutamate transporter *Neuron* **14**, 1019-1027
36. Zhang, Z., Tao, Z., Gameiro, A., Barcelona, S., Braams, S., Rauen, T., and Grewer, C. (2007) Transport direction determines the kinetics of substrate transport by the glutamate transporter EAAC1 *Proc Natl Acad Sci U S A* **104**, 18025-18030

37. Larsson, H. P., Tzingounis, A. V., Koch, H. P., and Kavanaugh, M. P. (2004) Fluorometric measurements of conformational changes in glutamate transporters. *Proc Natl Acad Sci U S A* **101**, 3951-3956
38. Grewer, C., Zhang, Z., Mwaura, J., Albers, T., Schwartz, A., and Gameiro, A. (2012) Charge compensation mechanism of a Na⁺-coupled, secondary-active glutamate transporter. *The Journal of biological chemistry*
39. Szatkowski, M., Barbour, B., and Attwell, D. (1990) Non-vesicular release of glutamate from glial cells by reversed electrogenic glutamate uptake. *Nature* **348**, 443-446
40. Wadiche, J. I., and Kavanaugh, M. P. (1998) Macroscopic and microscopic properties of a cloned glutamate transporter/chloride channel *J Neurosci* **18**, 7650-7661
41. Watzke, N., and Grewer, C. (2001) The anion conductance of the glutamate transporter EAAC1 depends on the direction of glutamate transport *FEBS Lett* **503**, 121-125
42. Attwell, D., Barbour, B., and Szatkowski, M. (1993) Nonvesicular release of neurotransmitter. *Neuron* **11**, 401-407
43. Wadiche, J. I., Amara, S. G., and Kavanaugh, M. P. (1995) Ion fluxes associated with excitatory amino acid transport *Neuron* **15**, 721-728
44. Eliasof, S., and Jahr, C. E. (1996) Retinal glial cell glutamate transporter is coupled to an anionic conductance. *Proc Natl Acad Sci U S A* **93**, 4153-4158
45. Billups, B., Rossi, D., and Attwell, D. (1996) Anion conductance behavior of the glutamate uptake carrier in salamander retinal glial cells. *J Neurosci* **16**, 6722-6731
46. Vandenberg, R. J., Arriza, J. L., Amara, S. G., and Kavanaugh, M. P. (1995) Constitutive ion fluxes and substrate binding domains of human glutamate transporters *J Biol Chem* **270**, 17668-17671
47. Otis, T. S., and Jahr, C. E. (1998) Anion currents and predicted glutamate flux through a neuronal glutamate transporter. *J Neurosci* **18**, 7099-7110

48. Bergles, D. E., and Jahr, C. E. (1997) Synaptic activation of glutamate transporters in hippocampal astrocytes. *Neuron* **19**, 1297-1308
49. Schwartz, E. A., and Tachibana, M. (1990) Electrophysiology of glutamate and sodium co-transport in a glial cell of the salamander retina. *J Physiol* **426**, 43-80
50. Watzke, N., Bamberg, E., and Grewer, C. (2001) Early intermediates in the transport cycle of the neuronal excitatory amino acid carrier EAAC1 *J Gen Physiol* **117**, 547-562
51. Larsson, H. P., Picaud, S. A., Werblin, F. S., and Lecar, H. (1996) Noise analysis of the glutamate-activated current in photoreceptors. *Biophys J* **70**, 733-742
52. Melzer, N., Biela, A., and Fahlke, C. (2003) Glutamate modifies ion conduction and voltage-dependent gating of excitatory amino acid transporter-associated anion channels *J Biol Chem* **278**, 50112-50119
53. Torres-Salazar, D., and Fahlke, C. (2007) Neuronal Glutamate Transporters Vary in Substrate Transport Rate but Not in Unitary Anion Channel Conductance in *The Journal of Biological Chemistry*
54. Ryan, R. M., Mitrovic, A. D., and Vandenberg, R. J. (2004) The chloride permeation pathway of a glutamate transporter and its proximity to the glutamate translocation pathway *J Biol Chem* **279**, 20742-20751
55. Huang, S., and Vandenberg, R. J. (2007) Mutations in transmembrane domains 5 and 7 of the human excitatory amino acid transporter 1 affect the substrate-activated anion channel *Biochemistry* **46**, 9685-9692
56. Grewer, C., and Rauen, T. (2005) Electrogenic glutamate transporters in the CNS: molecular mechanism, pre-steady-state kinetics, and their impact on synaptic signaling *J Membr Biol* **203**, 1-20
57. Grewer, C., Gameiro, A., Zhang, Z., Tao, Z., Braams, S., and Rauen, T. (2008) Glutamate forward and reverse transport: from molecular mechanism to transporter-mediated release after ischemia *IUBMB Life* **60**, 609-619

58. Veruki, M. L., Morkve, S. H., and Hartveit, E. (2006) Activation of a presynaptic glutamate transporter regulates synaptic transmission through electrical signaling. *Nature neuroscience* **9**, 1388-1396
59. Wersinger, E., Schwab, Y., Sahel, J. A., Rendon, A., Pow, D. V., Picaud, S., and Roux, M. J. (2006) The glutamate transporter EAAT5 works as a presynaptic receptor in mouse rod bipolar cells. *The Journal of physiology* **577**, 221-234
60. Tolner, B., Poolman, B., Wallace, B., and Konings, W. N. (1992) Revised nucleotide sequence of the gltP gene, which encodes the proton-glutamate-aspartate transport protein of Escherichia coli K-12. *J Bacteriol* **174**, 2391-2393
61. Grunewald, M., and Kanner, B. (1995) Conformational changes monitored on the glutamate transporter GLT-1 indicate the existence of two neurotransmitter-bound states. *J Biol Chem* **270**, 17017-17024
62. Slotboom, D. J., Lolkema, J. S., and Konings, W. N. (1996) Membrane topology of the C-terminal half of the neuronal, glial, and bacterial glutamate transporter family. *J Biol Chem* **271**, 31317-31321
63. Wahle, S., and Stoffel, W. (1996) Membrane topology of the high-affinity L-glutamate transporter (GLAST-1) of the central nervous system. *J Cell Biol* **135**, 1867-1877
64. Akabas, M. H., and Karlin, A. (1995) Identification of acetylcholine receptor channel-lining residues in the M1 segment of the alpha-subunit. *Biochemistry* **34**, 12496-12500
65. Javitch, J. A., Fu, D., Chen, J., and Karlin, A. (1995) Mapping the binding-site crevice of the dopamine D2 receptor by the substituted-cysteine accessibility method. *Neuron* **14**, 825-831
66. Wilson, G., and Karlin, A. (2001) Acetylcholine receptor channel structure in the resting, open, and desensitized states probed with the substituted-cysteine-accessibility method. *Proc Natl Acad Sci U S A* **98**, 1241-1248

67. Grunewald, M., Bendahan, A., and Kanner, B. I. (1998) Biotinylation of single cysteine mutants of the glutamate transporter GLT-1 from rat brain reveals its unusual topology. *Neuron* **21**, 623-632
68. Seal, R. P., and Amara, S. G. (1998) A reentrant loop domain in the glutamate carrier EAAT1 participates in substrate binding and translocation. *Neuron* **21**, 1487-1498
69. Zarbiv, R., Grunewald, M., Kavanaugh, M. P., and Kanner, B. I. (1998) Cysteine scanning of the surroundings of an alkali-ion binding site of the glutamate transporter GLT-1 reveals a conformationally sensitive residue. *The Journal of biological chemistry* **273**, 14231-14237
70. Seal, R. P., Leighton, B. H., and Amara, S. G. (2000) A model for the topology of excitatory amino acid transporters determined by the extracellular accessibility of substituted cysteines. *Neuron* **25**, 695-706
71. Grunewald, M., and Kanner, B. I. (2000) The accessibility of a novel reentrant loop of the glutamate transporter GLT-1 is restricted by its substrate. *J Biol Chem* **275**, 9684-9689
72. Haugeto, O., Ullensvang, K., Levy, L. M., Chaudhry, F. A., Honore, T., Nielsen, M., Lehre, K. P., and Danbolt, N. C. (1996) Brain glutamate transporter proteins form homomultimers. *J Biol Chem* **271**, 27715-27722
73. Yernool, D., Boudker, O., Folta-Stogniew, E., and Gouaux, E. (2003) Trimeric subunit stoichiometry of the glutamate transporters from *Bacillus caldotenax* and *Bacillus stearothermophilus*. *Biochemistry* **42**, 12981-12988
74. Eskandari, S., Kreman, M., Kavanaugh, M. P., Wright, E. M., and Zampighi, G. A. (2000) Pentameric assembly of a neuronal glutamate transporter. *Proceedings of the National Academy of Sciences of the United States of America* **97**, 8641-8646
75. Tao, Z., and Grewer, C. (2007) Cooperation of the conserved aspartate 439 and bound amino acid substrate is important for high-affinity Na⁺ binding to the glutamate transporter EAAC1. *J Gen Physiol* **129**, 331-344

76. Teichman, S., Qu, S., and Kanner, B. I. (2012) Conserved asparagine residue located in binding pocket controls cation selectivity and substrate interactions in neuronal glutamate transporter. *J Biol Chem* **287**, 17198-17205
77. Rosental, N., Gameiro, A., Grewer, C., and Kanner, B. I. (2011) A conserved aspartate residue located at the extracellular end of the binding pocket controls cation interactions in brain glutamate transporters. *The Journal of biological chemistry* **286**, 41381-41390
78. Teichman, S., and Kanner, B. I. (2007) Aspartate-444 is essential for productive substrate interactions in a neuronal glutamate transporter. *J Gen Physiol* **129**, 527-539
79. Leary, G. P., Holley, D. C., Stone, E. F., Lyda, B. R., Kalachev, L. V., and Kavanaugh, M. P. (2011) The central cavity in trimeric glutamate transporters restricts ligand diffusion. *Proceedings of the National Academy of Sciences of the United States of America* **108**, 14980-14985
80. Herman, M. A., and Jahr, C. E. (2007) Extracellular glutamate concentration in hippocampal slice. *J Neurosci* **27**, 9736-9741
81. Clements, J. D., Lester, R. A., Tong, G., Jahr, C. E., and Westbrook, G. L. (1992) The time course of glutamate in the synaptic cleft. *Science* **258**, 1498-1501
82. Tong, G., and Jahr, C. E. (1994) Block of glutamate transporters potentiates postsynaptic excitation. *Neuron* **13**, 1195-1203
83. Barbour, B., Keller, B. U., Llano, I., and Marty, A. (1994) Prolonged presence of glutamate during excitatory synaptic transmission to cerebellar Purkinje cells. *Neuron* **12**, 1331-1343
84. Diamond, J. S., and Jahr, C. E. (1997) Transporters buffer synaptically released glutamate on a submillisecond time scale. *J Neurosci* **17**, 4672-4687
85. Lehre, K. P., and Danbolt, N. C. (1998) The number of glutamate transporter subtype molecules at glutamatergic synapses: chemical and stereological quantification in young adult rat brain. *J Neurosci* **18**, 8751-8757

86. Mennerick, S., Shen, W., Xu, W., Benz, A., Tanaka, K., Shimamoto, K., Isenberg, K. E., Krause, J. E., and Zorumski, C. F. (1999) Substrate turnover by transporters curtails synaptic glutamate transients. *J Neurosci* **19**, 9242-9251
87. Diamond, J. S., and Jahr, C. E. (2000) Synaptically released glutamate does not overwhelm transporters on hippocampal astrocytes during high-frequency stimulation. *J Neurophysiol* **83**, 2835-2843
88. Diamond, J. S. (2001) Neuronal glutamate transporters limit activation of NMDA receptors by neurotransmitter spillover on CA1 pyramidal cells. *The Journal of neuroscience : the official journal of the Society for Neuroscience* **21**, 8328-8338
89. Scimemi, A., Tian, H., and Diamond, J. S. (2009) Neuronal transporters regulate glutamate clearance, NMDA receptor activation, and synaptic plasticity in the hippocampus. *The Journal of neuroscience : the official journal of the Society for Neuroscience* **29**, 14581-14595
90. Otis, T. S., Kavanaugh, M. P., and Jahr, C. E. (1997) Postsynaptic glutamate transport at the climbing fiber-Purkinje cell synapse. *Science* **277**, 1515-1518
91. Huang, Y. H., Dykes-Hoberg, M., Tanaka, K., Rothstein, J. D., and Bergles, D. E. (2004) Climbing fiber activation of EAAT4 transporters and kainate receptors in cerebellar Purkinje cells. *J Neurosci* **24**, 103-111
92. Bergles, D. E., Dzubay, J. A., and Jahr, C. E. (1997) Glutamate transporter currents in bergmann glial cells follow the time course of extrasynaptic glutamate. *Proceedings of the National Academy of Sciences of the United States of America* **94**, 14821-14825
93. Wadiche, J. I., and Jahr, C. E. (2001) Multivesicular release at climbing fiber-Purkinje cell synapses. *Neuron* **32**, 301-313
94. Szapiro, G., and Barbour, B. (2007) Multiple climbing fibers signal to molecular layer interneurons exclusively via glutamate spillover. *Nat Neurosci* **10**, 735-742

95. Coddington, L. T., Rudolph, S., Vande Lune, P., Overstreet-Wadiche, L., and Wadiche, J. I. (2013) Spillover-mediated feedforward inhibition functionally segregates interneuron activity. *Neuron* **78**, 1050-1062
96. Kauer, J. A., Malenka, R. C., and Nicoll, R. A. (1988) NMDA application potentiates synaptic transmission in the hippocampus. *Nature* **334**, 250-252
97. Malenka, R. C., and Nicoll, R. A. (1993) NMDA-receptor-dependent synaptic plasticity: multiple forms and mechanisms. *Trends Neurosci* **16**, 521-527
98. Nicoll, R. A., Oliet, S. H., and Malenka, R. C. (1998) NMDA receptor-dependent and metabotropic glutamate receptor-dependent forms of long-term depression coexist in CA1 hippocampal pyramidal cells. *Neurobiol Learn Mem* **70**, 62-72
99. Manabe, T., Renner, P., and Nicoll, R. A. (1992) Postsynaptic contribution to long-term potentiation revealed by the analysis of miniature synaptic currents. *Nature* **355**, 50-55
100. Kauer, J. A., Malenka, R. C., and Nicoll, R. A. (1988) A persistent postsynaptic modification mediates long-term potentiation in the hippocampus. *Neuron* **1**, 911-917
101. Madison, D. V., Malenka, R. C., and Nicoll, R. A. (1991) Mechanisms underlying long-term potentiation of synaptic transmission. *Annu Rev Neurosci* **14**, 379-397
102. Xiao, M. Y., Zhou, Q., and Nicoll, R. A. (2001) Metabotropic glutamate receptor activation causes a rapid redistribution of AMPA receptors. *Neuropharmacology* **41**, 664-671
103. Huang, Y. H., Sinha, S. R., Tanaka, K., Rothstein, J. D., and Bergles, D. E. (2004) Astrocyte glutamate transporters regulate metabotropic glutamate receptor-mediated excitation of hippocampal interneurons. *J Neurosci* **24**, 4551-4559
104. Selkirk, J. V., Naeve, G. S., and Foster, A. C. (2003) Blockade of excitatory amino acid transporters in the rat hippocampus results in enhanced activation of group I and group III metabotropic glutamate receptors. *Neuropharmacology* **45**, 885-894

105. Brasnjo, G., and Otis, T. S. (2001) Neuronal glutamate transporters control activation of postsynaptic metabotropic glutamate receptors and influence cerebellar long-term depression. *Neuron* **31**, 607-616
106. Otis, T. S., Brasnjo, G., Dzubay, J. A., and Pratap, M. (2004) Interactions between glutamate transporters and metabotropic glutamate receptors at excitatory synapses in the cerebellar cortex. *Neurochemistry international* **45**, 537-544
107. Dzubay, J. A., and Otis, T. S. (2002) Climbing fiber activation of metabotropic glutamate receptors on cerebellar purkinje neurons. *Neuron* **36**, 1159-1167
108. Wadiche, J. I., and Jahr, C. E. (2005) Patterned expression of Purkinje cell glutamate transporters controls synaptic plasticity. *Nat Neurosci* **8**, 1329-1334
109. Shen, Y., and Linden, D. J. (2005) Long-term potentiation of neuronal glutamate transporters. *Neuron* **46**, 715-722
110. Zerangue, N., and Kavanaugh, M. P. (1996) Interaction of L-cysteine with a human excitatory amino acid transporter. *J Physiol* **493 (Pt 2)**, 419-423
111. Aoyama, K., Suh, S. W., Hamby, A. M., Liu, J., Chan, W. Y., Chen, Y., and Swanson, R. A. (2006) Neuronal glutathione deficiency and age-dependent neurodegeneration in the EAAC1 deficient mouse. *Nat Neurosci* **9**, 119-126
112. Mathews, G. C., and Diamond, J. S. (2003) Neuronal glutamate uptake Contributes to GABA synthesis and inhibitory synaptic strength. *The Journal of neuroscience : the official journal of the Society for Neuroscience* **23**, 2040-2048
113. Beart, P. M., and O'Shea, R. D. (2007) Transporters for L-glutamate: an update on their molecular pharmacology and pathological involvement. *Br J Pharmacol* **150**, 5-17
114. Jiang, J., and Amara, S. G. (2010) New views of glutamate transporter structure and function: Advances and challenges *Neuropharmacology*
115. Seal, R. P., Shigeri, Y., Eliasof, S., Leighton, B. H., and Amara, S. G. (2001) Sulfhydryl modification of V449C in the glutamate transporter EAAT1 abolishes substrate transport

- but not the substrate-gated anion conductance *Proc Natl Acad Sci U S A* **98**, 15324-15329
116. Jiang, J., Shrivastava, I. H., Watts, S. D., Bahar, I., and Amara, S. G. (2011) Large collective motions regulate the functional properties of glutamate transporter trimers. *Proceedings of the National Academy of Sciences of the United States of America* **108**, 15141-15146
 117. Ryan, R. M., and Vandenberg, R. J. (2002) Distinct conformational states mediate the transport and anion channel properties of the glutamate transporter EAAT-1 *J Biol Chem* **277**, 13494-13500
 118. Machtens, J. P., Kovermann, P., and Fahlke, C. (2011) Substrate-dependent Gating of Anion Channels Associated with Excitatory Amino Acid Transporter 4. *The Journal of biological chemistry* **286**, 23780-23788
 119. Amato, A., Barbour, B., Szatkowski, M., and Attwell, D. (1994) Counter-transport of potassium by the glutamate uptake carrier in glial cells isolated from the tiger salamander retina. *J Physiol* **479 (Pt 3)**, 371-380
 120. Shlaifer, I., and Kanner, B. I. (2007) Conformationally Sensitive Reactivity to Permeant Sulfhydryl Reagents of Cysteine Residues Engineered into Helical Hairpin 1 of the Glutamate Transporter GLT-1. *Molecular Pharmacology* **71**, 1341-1348
 121. Sali, A., and Blundell, T. L. (1993) Comparative protein modelling by satisfaction of spatial restraints. *J Mol Biol* **234**, 779-815
 122. Slotboom, D. J., Sobczak, I., Konings, W. N., and Lolkema, J. S. (1999) A conserved serine-rich stretch in the glutamate transporter family forms a substrate-sensitive reentrant loop. *Proc Natl Acad Sci U S A* **96**, 14282-14287
 123. Costa, P. F., Emilio, M. G., Fernandes, P. L., Ferreira, H. G., and Ferreira, K. G. (1989) Determination of ionic permeability coefficients of the plasma membrane of *Xenopus laevis* oocytes under voltage clamp. *J Physiol* **413**, 199-211

124. Grunewald, M., Menaker, D., and Kanner, B. I. (2002) Cysteine-scanning mutagenesis reveals a conformationally sensitive reentrant pore-loop in the glutamate transporter GLT-1. *J Biol Chem* **277**, 26074-26080
125. Kovermann, P., Machtens, J. P., Ewers, D., and Fahlke, C. (2010) A conserved aspartate determines pore properties of anion channels associated with excitatory amino acid transporter 4 (EAAT4). *The Journal of biological chemistry* **285**, 23676-23686
126. Brocke, L., Bendahan, A., Grunewald, M., and Kanner, B. I. (2002) Proximity of two oppositely oriented reentrant loops in the glutamate transporter GLT-1 identified by paired cysteine mutagenesis. *J Biol Chem* **277**, 3985-3992
127. Leighton, B. H., Seal, R. P., Watts, S. D., Skyba, M. O., and Amara, S. G. (2006) Structural rearrangements at the translocation pore of the human glutamate transporter, EAAT1. *J Biol Chem* **281**, 29788-29796
128. Gameiro, A., Braams, S., Rauen, T., and Grever, C. (2011) The discovery of slowness: low-capacity transport and slow anion channel gating by the glutamate transporter EAAT5. *Biophysical journal* **100**, 2623-2632
129. Diamond, J. S., Bergles, D. E., and Jahr, C. E. (1998) Glutamate release monitored with astrocyte transporter currents during LTP. *Neuron* **21**, 425-433
130. Torres-Salazar, D., and Fahlke, C. (2006) Intersubunit interactions in EAAT4 glutamate transporters *J Neurosci* **26**, 7513-7522
131. Seal, R. P., and Amara, S. G. (1999) Excitatory amino acid transporters: a family in flux. *Annu Rev Pharmacol Toxicol* **39**, 431-456
132. Mim, C., Balani, P., Rauen, T., and Grever, C. (2005) The glutamate transporter subtypes EAAT4 and EAATs 1-3 transport glutamate with dramatically different kinetics and voltage dependence but share a common uptake mechanism *J Gen Physiol* **126**, 571-589

133. Otis, T. S., and Kavanaugh, M. P. (2000) Isolation of current components and partial reaction cycles in the glial glutamate transporter EAAT2 *J Neurosci* **20**, 2749-2757
134. Danbolt, N. C., Lehre, K. P., Dehnes, Y., Chaudhry, F. A., and Levy, L. M. (1998) Localization of transporters using transporter-specific antibodies. *Methods Enzymol* **296**, 388-407
135. Dehnes, Y., Chaudhry, F. A., Ullensvang, K., Lehre, K. P., Storm-Mathisen, J., and Danbolt, N. C. (1998) The glutamate transporter EAAT4 in rat cerebellar Purkinje cells: a glutamate-gated chloride channel concentrated near the synapse in parts of the dendritic membrane facing astroglia. *J Neurosci* **18**, 3606-3619
136. Eliasof, S., Arriza, J. L., Leighton, B. H., Kavanaugh, M. P., and Amara, S. G. (1998) Excitatory amino acid transporters of the salamander retina: identification, localization, and function. *J Neurosci* **18**, 698-712
137. Nicholls, D., and Attwell, D. (1990) The release and uptake of excitatory amino acids. *Trends Pharmacol Sci* **11**, 462-468
138. Mim, C., Tao, Z., and Grever, C. (2007) Two Conformational Changes Are Associated with Glutamate Translocation by the Glutamate Transporter EAAC1 *Biochemistry* **46**, 9007-9018
139. Picaud, S. A., Larsson, H. P., Grant, G. B., Lecar, H., and Werblin, F. S. (1995) Glutamate-gated chloride channel with glutamate-transporter-like properties in cone photoreceptors of the tiger salamander. *Journal of neurophysiology* **74**, 1760-1771
140. Picaud, S., Larsson, H. P., Wellis, D. P., Lecar, H., and Werblin, F. (1995) Cone photoreceptors respond to their own glutamate release in the tiger salamander. *Proceedings of the National Academy of Sciences of the United States of America* **92**, 9417-9421

141. Grewer, C., Madani Mobarekeh, S. A., Watzke, N., Rauen, T., and Schaper, K. (2001) Substrate translocation kinetics of excitatory amino acid carrier 1 probed with laser-pulse photolysis of a new photolabile precursor of D-aspartic acid *Biochemistry* **40**, 232-240
142. Shimamoto, K., Sakai, R., Takaoka, K., Yumoto, N., Nakajima, T., Amara, S. G., and Shigeri, Y. (2004) Characterization of novel L-threo-beta-benzyloxyaspartate derivatives, potent blockers of the glutamate transporters. *Mol Pharmacol* **65**, 1008-1015
143. Focke, P. J., Moenne-Loccoz, P., and Larsson, H. P. (2011) Opposite movement of the external gate of a glutamate transporter homolog upon binding cotransported sodium compared with substrate. *The Journal of neuroscience : the official journal of the Society for Neuroscience* **31**, 6255-6262
144. Wadiche, J. I., Tzingounis, A. V., and Jahr, C. E. (2006) Intrinsic kinetics determine the time course of neuronal synaptic transporter currents. *Proc Natl Acad Sci U S A* **103**, 1083-1087

APPENDIX A: THE LOCATION OF THE ANION PORE OF EXCITATORY AMINO ACID TRANSPORTERS

A.1 INTRODUCTION

Glutamate is the major excitatory neurotransmitter in the central nervous system. The spatio-temporal profile of synaptically released glutamate is regulated by a family of five excitatory amino acid transporters or EAATs. EAATs 1 and 2 are expressed in glia while EAATs 3-5 are expressed exclusively in neurons (1-5). Dysregulation of glutamate transport has been hypothesized to be involved in many diseases or disorders such as Alzheimer's, Parkinson's, Amyotrophic lateral sclerosis (ALS), and ischemic conditions mediating excitotoxicity (6). EAATs are secondary active, electrogenic transporters which couple the energetically uphill movement of anionic glutamate (glu) into the cell with co-transport of 3 Na⁺, 1 H⁺, and the counter transport of 1 K⁺ ion (7-9). Therefore, each transport cycle mediates the net inward movement of 2 positive charges. In addition, EAATs possess a thermodynamically uncoupled anion channel which is either a leak conductance in glial isoforms or is gated by Na⁺ interaction in neuronal carriers (4,10). The channel open probability is increased by subsequent glu binding to the binding site (11) located at the intersection of transmembrane domains 7 and 8 (TM7 and TM8) and the hairpin, re-entrant loops HP1 and HP2 (12,13).

Initial investigations into the coupling of substrate interactions and channel activity demonstrated that modification of residues such as V449 or V452 in the outer hairpin loop, HP2, with methanesthiosulfonate (MTS) allowed for full or even enhanced anion channel activity while completely abolishing substrate transport (14,15). Thus, glutamate mediated gating of the

channel was dependent on substrate binding but not transport. This data also supported the hypothesis that the pore domain was in a location distinct from the substrate binding site. Further support for this hypothesis was reported by Vandenberg's group which used site directed mutagenesis in the regions of transmembrane domain 2 and 5 (TM2 and TM5). Mutations of residues S102 (TM2), D112 (TM2), or D272 (TM5) were demonstrated to significantly alter channel properties while not affecting transport functionality (16,17). In 2004, the crystal structure of an archeal homolog of glutamate transporters, Glt_{Ph}, revealed many properties of the carriers including residues which participate in substrate coordination in the ligand binding site (12). Unfortunately, the location or presence of a pore domain was not observable in the crystal structure and only limited evidence exist to support the presence of an uncouple chloride flux in Glt_{Ph} (18). Beyond these initial studies no significant progress has been made to determine the exact location of the pore domain.

Efforts to determine the location of pore regions in other channels or transporters have been developed with similar strategies. Substituted cysteine accessibility methods or SCAM has been used to determine residues which display accessibility to extracellular or intracellular reagents, indicative of an aqueous pore region, as well as residues which influence channel function and ion flux after modification. These strategies have been used successfully to identify residues lining the pore of acetylcholine receptors (AChRs) (19,20), γ -aminobutyric acid (GABA_A) receptors (21,22), as well as the palytoxin-modified pore of the Na⁺-K⁺ ATPase (23,24). Here we used as similar strategy in human EAAT1 to determine if the location of the pore region lies in the area of TM2. We used site directed mutagenesis to create cysteine point mutations at every position of TM2 as well as several other regions of EAAT1. We will determine which residues in these regions display accessibility to intracellular and extracellularly applied MTS reagents as well as the permeable non-reversible cysteine modifying reagent N-ethylmaleimide (NEM). After modification, two-electrode voltage clamp recordings will determine

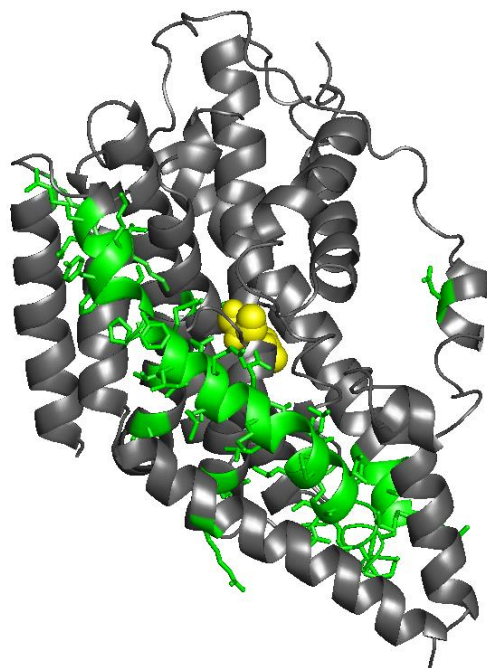


Figure A1. EAAT1 Homology Model Depicting Point Mutations.

Homology model of hEAAT in the outward facing state based on the Glt_{Ph} crystal structure from (12) (pdb file 3FXH). Helices are depicted in ribbon form (grey) with a stick model of mutated residues (green). L-aspartate is depicted by a space filling model placed over the electron density pattern of bound L-cysteine sulfinic acid (yellow).

which residues are important for anion flux through EAAT1. With this strategy, we will unambiguously determine if the pore regions lies in the region of surrounding TM2 as previously proposed (16).

A.2. EXPERIMENTAL PROCEDURES

A.2.1. Generation and Subcloning of EAAT1 Cysteine Mutations

hEAAT1 was as previously described (25) and was subcloned into pOTV and pcDNA3.1 (Invitrogen) using Kpn1 and Xba1 restriction sites. Quikchange site-directed mutagenesis (Stratagene) was used to create half of the cysteine point mutations and the other half was purchased from Genewiz Inc custom mutagenesis services. All mutations were confirmed by sequencing before use.

A.2.2. Transient Transfection of COS-7 cells and cRNA injections into *Xenopus* Oocytes

COS-7 cells were transiently transfected using Lipofectamine 2000 (Invitrogen) two days prior to use in assays. hDAT-GFP-pCDNA3.1 was transfected in parallel to estimate transfection efficiency and serve as a negative control for COS-7 experiments. cRNA was synthesized from linearized capped DNA using T7 mMessage mMachine kit (Ambion) from pOTV constructs. 50 ng of cRNA was injected into store bought stage VI oocytes (Ecocyte). Oocytes were incubated for 2-3 days in ND96 buffer containing penicillin, streptomycin, gentamycin, and Na⁺ pyruvate at 18°C.

A.2.3. Radiolabeled Transport Assays

COS-7 cells transiently transfected with hEAAT1 WT, hEAAT1 CSLS, and hEAAT1 mutations were washed 3 times with phosphate buffered saline containing 1.0 mM MgCl₂ and 0.1 mM CaCl₂ (PBSCM). 1 mM L-glutamate + 200 nM 3,4-³H-L-glutamate was serially diluted to create the concentrations described. Glu was applied for 10 min and then washed out using ice cold

PBSCM. Cells were washed a total of 3 times before being lysed using 0.1 N NaOH and 1% SDS. The accumulated radiolabeled substrate was counted using liquid scintillation counting.

A.2.4. Electrophysiology

Two-electrode voltage clamp recordings were performed on hEAAT1 constructs expressed in stage VI *Xenopus* oocytes as previously described (4). 500 msec voltage pulses were applied every 15 mV ranging from -150 mV to +60 mV. Isochronal current amplitudes were taken from the last 100 msec of the sweep. All currents were recorded using a Geneclamp 500 (Molecular Devices) and pClamp10 software (Molecular Devices). Data was digitized using a Digidata 1440A and was filtered using a Bessel filter at 1 kHz and sampled at 50 kHz. Solutions were applied using a gravity fed perfusion system and for basic experiments were 96 mM NaNO₃, 2 mM KCl, 1.8 mM MgCl₂, 1 mM CaCl₂, and 10 mM HEPES, pH 7.4 (NDNO₃). For permeability studies, the 96 mM NaNO₃ was replaced with 96 mM NaX (where X is Cl, I, Br, or SCN). MTS reagents, dithioreitol (DTT), and NEM are applied for 5 min and then washed out with ND96 for 2 min before recordings.

A.3. RESULTS

A.3.1. Transport Kinetics of Cysteine Point Mutations in EAAT1

TM2 contains residues which, when altered through mutagenesis can affect anion flux. In order to fully characterize the role of TM2 in the flux of anions, we designed a series of point mutations to comprehensively map out amino acid positions which affect anion flux in order to determine which residues line the pore of the anion channel (Figure 1). In order to determine the basic transport functions of mutant EAATs, radiolabeled glutamate dose-response curves were performed on EAAT residues altered to cysteine side chains. The apparent affinity (K_M) and maximal velocity (V_{max}) of residues altered to cysteine in comparison to CSLS EAAT1 controls are presented in Table 1. None of the 11 residues tested thus far demonstrate a significantly

Table 1. Kinetic Data of EAAT1 Cysteine Point Mutations in COS-7 Cells

Mutant	K _m μ M (CI95)	% Activity*	Number of Samples (N)	Location
WT				-
CSLS	53.4 (0 – 108.0)	100	6	-
R76C	94.6 (48.0 - 141.3)	55.2	6	TM1-2 loop
E77C	71.5 (46.3 - 96.7)	66.3	6	TM2
V78C	76.2 (45.2 - 107.2)	N.D.	6	TM2
K79C	110.1 (0 – 361.3)	N.D.	6	TM2
Y80C	5.64 (0 – 18.1)	N.D.	6	TM2
F81C				TM2
S82C	34.0 (0 - 80.0)	N.D.	6	TM2
F83C				TM2
P84C				TM2
G85C				TM2
E86C				TM2
L87C				TM2
L88C				TM2
M89C				TM2
R90C	70.6 (53.4 – 87.8)	60.1	9	TM2
M91C				TM2
L92C				TM2
Q93C	78.6 (0-177.6)	104.7	6	TM2
M94C				TM2
L95C				TM2
V96C				TM2
L97C				TM2
P98C				TM2
L99C				TM2
I100C				TM2
I101C				TM2
S102C				TM2
S103C				TM2
L104C				TM2
V105C				TM2
T106C				TM2
G107C				TM2
M108C				TM2-3 loop
R342C	120.7 (98.3 – 143.1)	54.6	5	TM6-HP1 loop
K343C	130.4 (56.5 – 204.4)	60.2	5	TM6-HP1 loop
N344C	105.0 (39.7 – 170.3)	31.3	5	TM6-HP1 loop

Normalized to WT uptake but not controlled for expression levels;

** N.D. describes active mutants whose kinetics parameters couldn't be accurately determined;*

*** N.E. describes mutants whose activity was < 10% of WT; Blank spaces indicate residues not yet assayed.*

different K_M from EAAT constructs lacking any cysteine residues (CSLS). Maximal transport rates, however, were significantly lower for all mutants tested except for Q93C which showed normal V_{max} compared to CSLS. This data does not take into consideration changes to membrane expression and therefore could be any combination of a loss of transport velocity or surface expression. Semi-quantitative membrane biotinylation experiments will be needed in order to estimate the change in surface expression.

A.3.2. Transport Kinetics of Non-cysteine Point Mutations in EAAT1

Modification of cysteine point mutations by specific cysteine modification reagents will assist in determining which residues line the pore domain. However, at locations in the pore region which might restrict accessibility to even the smallest of the cysteine modifying reagents, further mutational analysis is needed. Therefore, we also mutated a series of residues to glu side chains so that anion flux could be disrupted without the need for accessibility of exogenous modifying reagents to the residues. Table 2 depicts the K_M and V_{max} of residues altered to non-cysteine residues in comparison to CSLS EAAT1 controls. Of the mutants tested, only D172R (TM4), R342E (TM6-HP1 loop), K343E (TM6-HP1a loop), and T358E (HP1a) showed a significantly lower apparent affinity, K_M , than WT EAAT1 controls. However, almost all point mutations displayed a V_{max} below 80% except for R76E, K188E, and R122E. This loss of transport capacity could either be due to loss of transport velocity or surface expression as is the case for the cysteine point mutations.

A.4. DISCUSSION

The location of the anion pore is one of the most significant questions left in the field of EAAT biology and also one of the most elusive questions. Channel-like functionality has been demonstrated for not only the EAATs but also many other isoforms and families of neurotransmitter transporters such as the ASCTs (26-30) and the monoamine carriers (31-34).

Table 2. Kinetic Data for Non-cysteine EAAT1 Point Mutations in COS-7 Cells

Mutant	Km μ M (CI95)	% Activity*	Number of Samples (N)	Location
WT	26.9 (14.8 – 39.1)	100	12	-
CSLS	47.1 (0.79- 93.1)	82.8	5	-
R76E	29.9 (16.1 – 43.7)	98.2	6	TM1-TM2 loop
R79E				TM2
Y80E				TM2
F81E				TM2
S82E				TM2
E86R				TM2
R90E	81.1 (32.8 – 129.3)	42.7	12	TM2
P98A	85.1 (0 - 176.0)	20.3	12	TM2
G107A				TM2
K118E	26.5 (3.85-49.2)	109.8	6	TM2-TM3 loop
R122E	37.5 (0-80.9)	112.1	6	TM3
D172R	358.2 (99.7 – 616.8)	25.9	6	TM4a
E276K	19.2 (12.1 – 26.4)	30.3	6	TM5
M279A	N.E.	N.E.	N.E.	TM5
R280E	21.7 (12.6 – 30.7)	33.2	11	TM5
K300E	118.3 (10.8-225.8)	52.2	4	TM5
E303R	N.E.	N.E.	N.E.	TM5
H328E	36.7 (32.0 - 41.4)	31.5	5	TM6
R342E	90.4 (76.1 - 106.6)	62.4	5	TM6-HP1 loop
K343E	256.1 (N.D.)	41.6	4	TM6-HP1 loop
T358E	61.1 (45.8 - 76.4)	25.6	10	HP1a
K374E	29.5 (15.5 - 43.5)	45.6	5	TM7a
R385E	30.8 (25.4 - 36.2)	20	5	TM7a

Normalized to WT uptake but not controlled for expression levels;

* N.D. describes active mutants whose kinetics parameters couldn't be accurately determined;

** N.E. describes mutants whose activity was < 10% of WT; Blank spaces indicate not yet assayed.

To date, the exact location of the pores which are thought to mediate such conductances has not been resolved. Therefore, it is likely that extraordinary efforts are needed to define the pore region in these systems. Site-directed mutagenesis is a valuable tool to determine the location of channel lining residues and has been used as a successful strategy in the past (19,23,24). Here we developed a series of point mutations in the TM2 region of the transporter which has been demonstrated to alter anion channel function after mutation (16,17).

Through initial screening of transport activity in each of these mutants, we will be able to clearly exclude residues which demonstrate a loss of all transport functionality when mutated. These residues will be excluded from electrophysiological analysis since we would not be able to determine if changes to anion flux were due to large structural perturbations and/or loss of all surface expression. Second, kinetic analysis of transport will allow us to identify mutations which may have altered affinity for glutamate and allow for appropriate adjustments since we will apply saturating concentrations of glu during subsequent experiments.

Two-electrode voltage clamp recordings will be divided into three phases. First, the maximal current amplitudes from non-cysteine point mutations (Table 2) will be recorded in the presence of Cl^- , I^- , NO_3^- , and SCN^- buffers in order to determine if any point mutation has altered the permeability sequence or maximal anion flux of the EAAT-mediated anion channel. Next, cysteine point mutations will be assayed using the same experimental paradigm. Additionally, various anion containing buffers will be applied to cysteine point mutations before and after a 5 min perfusion of 1 mM 2-(trimethylammonium)ethylmethanethiosulfonate (MTSET), 10 mM 2-aminoethylmethanethiosulfonate (MTSEA), 10 mM 2-sulfonatoethylmethanethiosulfonate (MTSES), or 1 mM NEM. Experiments with modification of residues can be combined using 5 mM DTT perfusions to reverse modifications by MTS reagents. These data will be used to examine the role of each residue position in affecting the permeability of various anions through EAAT1. Together these data should allow for a comprehensive mapping of residues which show

a significant alteration to anion flux to form a contiguous pore region in the EAAT1 structural model (Figure 1). This approach has the strength of non-biasing positions or side chains and should be comprehensive enough to capture a structural trend in anion flux even with regions or inaccessibility to modifying reagents such as the selectivity filter.

EAATs are not the only neurotransmitter transports which possess dual transport and channel-like functionality. The SLC16 family or neurotransmitter Na⁺ symporters (NSS) have shown channel like activity and although its exact role in cellular function for many of the NSS members is unclear, evidence supports the flux of anions through the dopamine transporter can influence cellular excitability (32-35). These preliminary data presented here are the first steps into a comprehensive screen designed to delineate the pore lining residues of EAAT1. The location of the pore in EAATs is a major question in the field and elucidation of this question will allow for a new era of investigations resolving the role of channel like states in transporters.

A.5. REFERENCES

1. Kanai, Y., and Hediger, M. A. (1992) Primary structure and functional characterization of a high-affinity glutamate transporter. *Nature* **360**, 467-471
2. Pines, G., Danbolt, N. C., Bjoras, M., Zhang, Y., Bendahan, A., Eide, L., Koepsell, H., Storm-Mathisen, J., Seeberg, E., and Kanner, B. I. (1992) Cloning and expression of a rat brain L-glutamate transporter. *Nature* **360**, 464-467
3. Storck, T., Schulte, S., Hofmann, K., and Stoffel, W. (1992) Structure, expression, and functional analysis of a Na(+)-dependent glutamate/aspartate transporter from rat brain. *Proc Natl Acad Sci U S A* **89**, 10955-10959
4. Fairman, W. A., Vandenberg, R. J., Arriza, J. L., Kavanaugh, M. P., and Amara, S. G. (1995) An excitatory amino-acid transporter with properties of a ligand-gated chloride channel *Nature* **375**, 599-603

5. Arriza, J. L., Eliasof, S., Kavanaugh, M. P., and Amara, S. G. (1997) Excitatory amino acid transporter 5, a retinal glutamate transporter coupled to a chloride conductance *Proc Natl Acad Sci U S A* **94**, 4155-4160
6. Danbolt, N. C. (2001) Glutamate uptake. *Prog Neurobiol* **65**, 1-105
7. Zerangue, N., and Kavanaugh, M. P. (1996) Flux coupling in a neuronal glutamate transporter. *Nature* **383**, 634-637
8. Kanner, B. I., and Sharon, I. (1978) Active transport of L-glutamate by membrane vesicles isolated from rat brain. *Biochemistry* **17**, 3949-3953
9. Brew, H., and Attwell, D. (1987) Electrogenic glutamate uptake is a major current carrier in the membrane of axolotl retinal glial cells. *Nature* **327**, 707-709
10. Wadiche, J. I., Amara, S. G., and Kavanaugh, M. P. (1995) Ion fluxes associated with excitatory amino acid transport *Neuron* **15**, 721-728
11. Torres-Salazar, D., and Fahlke, C. (2007) Neuronal Glutamate Transporters Vary in Substrate Transport Rate but Not in Unitary Anion Channel Conductance in *The Journal of Biological Chemistry*
12. Yernool, D., Boudker, O., Jin, Y., and Gouaux, E. (2004) Structure of a glutamate transporter homologue from *Pyrococcus horikoshii*. *Nature* **431**, 811-818
13. Boudker, O., Ryan, R. M., Yernool, D., Shimamoto, K., and Gouaux, E. (2007) Coupling substrate and ion binding to extracellular gate of a sodium-dependent aspartate transporter. *Nature* **445**, 387-393
14. Seal, R. P., Shigeri, Y., Eliasof, S., Leighton, B. H., and Amara, S. G. (2001) Sulfhydryl modification of V449C in the glutamate transporter EAAT1 abolishes substrate transport but not the substrate-gated anion conductance *Proc Natl Acad Sci U S A* **98**, 15324-15329

15. Ryan, R. M., and Vandenberg, R. J. (2002) Distinct conformational states mediate the transport and anion channel properties of the glutamate transporter EAAT-1 *J Biol Chem* **277**, 13494-13500
16. Ryan, R. M., Mitrovic, A. D., and Vandenberg, R. J. (2004) The chloride permeation pathway of a glutamate transporter and its proximity to the glutamate translocation pathway *J Biol Chem* **279**, 20742-20751
17. Huang, S., and Vandenberg, R. J. (2007) Mutations in transmembrane domains 5 and 7 of the human excitatory amino acid transporter 1 affect the substrate-activated anion channel *Biochemistry* **46**, 9685-9692
18. Ryan, R. M., and Mindell, J. A. (2007) The uncoupled chloride conductance of a bacterial glutamate transporter homolog. *Nat Struct Mol Biol* **14**, 365-371
19. Akabas, M. H., and Karlin, A. (1995) Identification of acetylcholine receptor channel-lining residues in the M1 segment of the alpha-subunit. *Biochemistry* **34**, 12496-12500
20. Parikh, R., Bali, M., and Akabas, M. H. (2011) Structure of M2 transmembrane segment of GLIC, a prokaryotic Cys-loop receptor homologue from *Gloeobacter violaceus*, probed by substituted cysteine accessibility. *J Biol Chem*
21. Filippova, N., Wotring, V. E., and Weiss, D. S. (2004) Evidence that the TM1-TM2 loop contributes to the rho1 GABA receptor pore. *J Biol Chem* **279**, 20906-20914
22. Horenstein, J., Wagner, D. A., Czajkowski, C., and Akabas, M. H. (2001) Protein mobility and GABA-induced conformational changes in GABA(A) receptor pore-lining M2 segment. *Nat Neurosci* **4**, 477-485
23. Takeuchi, A., Reyes, N., Artigas, P., and Gadsby, D. C. (2008) The ion pathway through the opened Na(+),K(+)-ATPase pump. *Nature*
24. Reyes, N., and Gadsby, D. C. (2006) Ion permeation through the Na⁺,K⁺-ATPase. *Nature* **443**, 470-474

25. Arriza, J. L., Fairman, W. A., Wadiche, J. I., Murdoch, G. H., Kavanaugh, M. P., and Amara, S. G. (1994) Functional comparisons of three glutamate transporter subtypes cloned from human motor cortex. *J Neurosci* **14**, 5559-5569
26. Arriza, J. L., Kavanaugh, M. P., Fairman, W. A., Wu, Y. N., Murdoch, G. H., North, R. A., and Amara, S. G. (1993) Cloning and expression of a human neutral amino acid transporter with structural similarity to the glutamate transporter gene family. *J Biol Chem* **268**, 15329-15332
27. Zerangue, N., and Kavanaugh, M. P. (1996) ASCT-1 is a neutral amino acid exchanger with chloride channel activity *J Biol Chem* **271**, 27991-27994
28. Broer, A., Wagner, C., Lang, F., and Broer, S. (2000) Neutral amino acid transporter ASCT2 displays substrate-induced Na⁺ exchange and a substrate-gated anion conductance. *Biochem J* **346 Pt 3**, 705-710
29. Grewer, C., and Grabsch, E. (2004) New inhibitors for the neutral amino acid transporter ASCT2 reveal its Na⁺-dependent anion leak. *J Physiol* **557**, 747-759
30. Scopelliti, A. J., Ryan, R. M., and Vandenberg, R. J. (2013) Molecular determinants for functional differences between alanine-serine-cysteine transporter 1 and other glutamate transporter family members. *J Biol Chem* **288**, 8250-8257
31. Galli, A., DeFelice, L. J., Duke, B. J., Moore, K. R., and Blakely, R. D. (1995) Sodium-dependent norepinephrine-induced currents in norepinephrine-transporter-transfected HEK-293 cells blocked by cocaine and antidepressants. *J Exp Biol* **198**, 2197-2212
32. Sonders, M. S., Zhu, S. J., Zahniser, N. R., Kavanaugh, M. P., and Amara, S. G. (1997) Multiple ionic conductances of the human dopamine transporter: the actions of dopamine and psychostimulants. *J Neurosci* **17**, 960-974

33. Galli, A., Blakely, R. D., and DeFelice, L. J. (1998) Patch-clamp and amperometric recordings from norepinephrine transporters: channel activity and voltage-dependent uptake. *Proc Natl Acad Sci U S A* **95**, 13260-13265
34. Ingram, S. L., Prasad, B. M., and Amara, S. G. (2002) Dopamine transporter-mediated conductances increase excitability of midbrain dopamine neurons. *Nat Neurosci* **5**, 971-978
35. Mager, S., Min, C., Henry, D. J., Chavkin, C., Hoffman, B. J., Davidson, N., and Lester, H. A. (1994) Conducting states of a mammalian serotonin transporter. *Neuron* **12**, 845-859

**APPENDIX B: CLOSE ENCOUNTERS OF THE OILY KIND: REGULATION OF
TRANSPORTERS BY LIPIDS**



CLOSE ENCOUNTERS OF THE OILY KIND

Regulation of Transporters by Lipids

Neurotransmitter transporters are membrane proteins that serve as key regulators of extracellular neurotransmitter concentrations and have been long viewed as important targets for drug development by the pharmaceutical industry. Although many cellular signaling systems are known to modulate transport activity, much less is known about how transporters communicate with and are regulated by the various components of the lipid sea in which they reside. Variations in lipid content clearly affect the activity of a variety of transport systems, and with advances in techniques for lipid analysis and a clearer vision of carrier structure, this area of research appears poised for major advances.

■ *Christopher B. Divito and Susan G. Amara*

University of Pittsburgh, Department of Neurobiology, Pittsburgh, PA 15260

INTRODUCTION

Neurotransmitter transporters are essential to the homeostatic regulation of synaptic signaling throughout the nervous system. The extensive amount of research that has been devoted over the past few decades to these integral membrane proteins is an apt reflection of this importance. Transport mechanisms have been a prime target of the pharmaceutical industry, prompting the investment of billions of dollars into the development of drugs, such as the selective reuptake inhibitors, several of which have achieved blockbuster status in the treatment of depression and anxiety. The functions of many carriers are influenced by a variety of factors such as temperature, membrane voltage, pH, ion gradients, ligands, and accessory proteins. One mechanism for regulating membrane protein function that has only started to make the list has been the impact of lipid environment. Over the last few decades, lipids, the unsung heroes of regulation, have begun to emerge as critical modulators of membrane protein function through their direct actions on proteins, through their influence on the lipid milieu, and through their roles in signaling pathways.

A variety of mechanisms have been identified through which transporters act to regulate the storage, subcellular localization, and synaptic availability of neurotransmitters. Physiological factors that influence transporter function include temperature, membrane voltage, pH, ion gradients, endogenous ligands, and accessory proteins. The degree to which any particular mechanism contributes to transporter function or might be exploited for improved drug development is not always clear. But the importance of transporters in basic neurobiology and translational medicine certainly mandates investigation from a variety of approaches. The advent of lipidomics in past years has enriched our understanding of signal transduction in many contexts, including neurotransmission. The versatility of lipids in signaling has proven remarkable, and one aspect of this signaling is the role of lipids as modulators of regulatory proteins in the cell membrane.

Lipids, once viewed simply as building blocks of the membrane, have for many years now been appreciated for their role in signal transduction at the cell surface. Receptor- and enzyme-mediated hydrolysis of PIP_2 , producing DAG and IP_3 , has become a canonical feature of signaling cascades. Fatty acid amides and arachidonate metabolic products, including a fascinating array of endocannabinoids, are involved in regulating physiological and basic behavioral states through the activation of specific cell surface receptors. [For an excellent review of the contributions of lipids to cellular signaling, see (1).] The direct binding and allosteric modulation of proteins by lipid molecules has been proposed in many systems, yet additional subtle effects of lipids on protein function can also occur through variations in the structure, rigidity, or lateral pressure of the lipid components affecting protein conformation or dynamics.

This review will emphasize the direct effects of membrane lipids on transport proteins relevant to the central nervous system. [For a review of the actions of lipids on ion channel properties, see (2–4)]. We will attempt to complement traditional concepts of the neural cell membrane with data focusing on the interaction of both cholesterol and fatty acids with plasma membrane carriers. We will provide common names to discuss particular lipids (see Table 1), but we will also rely on the LIPID MAPS initiative, with its more precise nomenclature and comprehensive systematization of lipids and their metabolism (5). In accordance with much of the literature, we occasionally refer to “simple” lipids as those that produce only one or two products upon hydrolysis, as opposed to “complex” lipids, which yield a larger number of hydrolysis products.

LIPID COMPOSITION OF CELLULAR MEMBRANES

Many initial efforts to characterize the “lipidome” of neural tissues were limited in resolution to only a few of the predominant membrane constituents. For example, lateral vestibular neurons were reported to contain cholesterol [ST01010001], phosphatidylethanolamine [GP02], phosphatidylserine [GP03], oleic acid [FA01030002], stearic acid [FA01010018], palmitic acid [FA01010001], as well as phosphoinositols [GP06] (6). Differences in lipid composition between axonal plasma membranes and the surrounding myelin were in a sense some of the earliest “lipidomics” data: axonal membrane was reported as 20.1 % cholesterol, 20.1 % galactolipid [SP06], 14.6% phosphatidylethanolamine, 18.3% phosphatidylcholine [GP01], 9.3% sphingomyelin [SP0301], 5.6% phosphatidylserine, and 3.4% phosphatidylinositol [GP06]). Ceramides [SP02] and sulfoglycosphingolipids [SP0602] predominated as the 24:1 unsaturated form. In myelin, the saturated version of sphingolipid (i.e., 24:0) predominated (7–9). From this early work, it became clear that the plasma membrane of neurons (and indeed of most mammalian cells) is comprised of a combination of cholesterol, phosphatidylethanolamine, phosphatidylserine, phosphatidylcholine, sphingomyelin, and glycolipids in an asymmetrical leaflet distribution. [For a comprehensive review of history of early neuronal lipidomics, see (10).]

To understand how the lipid environment influences protein function it is imperative to define not only the lipid components of the membrane, but their organization in the membrane. It was shown almost fifty years ago that artificial lipid monolayers can transition from a gel-like state to a liquid-crystalline state with increasing temperature (11). In the gel phase, acyl chains in a predominately all-*trans* configuration undergo orderly packing, whereas in the liquid crystalline state acyl chains with disordered or random orientations predominate (Figure 1). Lipid bilayers can also transition between these states, and the plasma membrane is best modeled as a liquid-disordered state (12). Although the study of lipid monolayers and pure or controlled lipid environments has

Table 1. Eight Lipid Categories and Subclassification According to LIPID MAPS^a

Category	Subclassification and identification in LIPID MAPS structure database	
Fatty Acyls	Fatty Acids and Conjugates [FA01] ^b	Fatty amides [FA08]
	Octadecanoids [FA02]	Fatty nitriles [FA09]
	Eicosanoids [FA03]	Fatty ethers [FA10]
	Docosanoids [FA04]	Hydrocarbons [FA11]
	Fatty alcohols [FA05]	Oxygenated hydrocarbons [FA12]
	Fatty aldehydes [FA06]	Fatty acyl glycosides [FA13]
	Fatty esters [FA07]	
Glycerolipids	Monoradylglycerols [GL01]	Triradylglycerols [GL03]
	Diradylglycerols [GL02]	Glycosylmonoradylglycerols [GL04]
	Glycosyldiradylglycerols [GL05]	
	Glycerophosphocholines [GP01]	Glycerophosphates [GP10]
	Glycerophosphoethanolamines [GP02]	Glyceropyrophosphates [GP11]
	Glycerophosphoserines [GP03]	Glycerophosphoglycerophosphoglycerols [GP12]
	Glycerophosphoglycerols [GP04]	CDP-Glycerols [GP13]
	Glycerophosphoglycerophosphates [GP05]	Glycosylglycerophospholipids [GP14]
	Glycerophosphoinositols [GP06]	Glycerophosphoinositolglycans [GP15]
	Glycerophosphoinositol monophosphates [GP07]	Glycerophosphonocholines [GP16]
	Glycerophosphoinositol bisphosphates [GP08]	Glycerophosphonoethanolamines [GP17]
	Glycerophosphoinositol trisphosphates [GP09]	Diglycerol tetraether phospholipids (cardarchaeols) [GP18]
Sphingolipids	Sphingoid bases [SP01]	Neutral glycosphingolipids [SP05]
	Ceramides [SP02]	Acidic glycosphingolipids [SP06]
	Phosphosphingolipids [SP03]	Basic glycosphingolipids [SP07]
	Phosphosphingolipids [SP04]	Amphoteric glycosphingolipids [SP08]
	Arsenosphingolipids [SP09]	
Sterol Lipids	Sterols [ST01]	Bile acids and derivatives [ST04]
	Steroids [ST02]	Steroid conjugates [ST05]
	Secosteroids [ST03]	
Prenol Lipids	Isoprenoids [PR01]	Polyprenols [PR03]
	Quinones and hydroquinones [PR02]	Hopanoids [PR04]
Saccharolipids	Acylaminosugars [SL01]	Acyltrehaloses [SL03]
	Acylaminosugar glycans [SL02]	Acyltrehalose glycans [SL04]
	Other acyl sugars [SL05]	
Polyketides	Linear polyketides [PK01]	Angucyclines [PK08]
	Halogenated acetogenins [PK02]	Polyether antibiotics [PK09]
	Annonaceae acetogenins [PK03]	Aflatoxins and related substances [PK10]
	Macrolides and lactone polyketides [PK04]	Cytochalasins [PK11]
	Ansamycins and related polyketides [PK05]	Flavonoids [PK12]
	Polynes [PK06]	Aromatic polyketides [PK13]
	Linear tetracyclines [PK07]	Non-ribosomal peptide/polyketide hybrids [PK14]

^a The LIPID Metabolites and Pathways Strategy (LIPID MAPS) classifies eight broad categories, developed through chemical characteristics, that are subdivided into classes and subclasses.

^b Subsequent organization of lipids into subclasses can be identified by the root number shown followed by additional numbering for subclass and specific molecule within that subclass. This system allowed for universal inclusion of new lipids compounds discovered through high-throughput lipidomics analysis. Adapted from Fahy et al. 2005 and <http://lipidmaps.org/>.

revealed much about dynamics of lipids in general, such studies cannot offer a comprehensive model of a biological membrane that contains integral membrane proteins. In 1972, Singer described a model of the plasma membrane as a two-dimensional dynamic viscous solution in which integral membrane proteins maximize their hydrophobic and hydrophilic interactions in accordance with the surrounding lipid matrix and aqueous environment (13). Singer's "fluid mosaic model" has been well supported for over thirty years (14), and an extensive literature reveals that variability in lipid composition affects viscosity, depth, curvature, and lateral pressure (15–19).

Singer also recognized, in certain membrane regions, the possibility of liquid-ordered phases, characterized by restriction in the lateral movement of lipids. The emergence of lipid rafts as a field of study, although not without its share of debate, has established that local lipid composition can have profound impacts on integral protein structure and activity. Lipid rafts, or detergent resistant microdomains (DRMs), are defined as cholesterol- and sphingomyelin-rich membrane regions that impose an ordered state to the surrounding lipid environment (20, 21). Although not considered in detail here, this area of research has brought an exciting new focus of research and discussion that will further our understanding of lipids and membrane dynamics and how they relate to biological function.

INFLUENCE OF FATTY ACIDS ON TRANSPORTER FUNCTION

Polyunsaturated fatty acids (PUFAs; [FA0103]), such as arachidonic acid [FA01030001], comprise twenty to thirty percent of free fatty acids in the human brain (22). Typically derived from diet, polyunsaturated fatty acids in the brain are either transported from plasma and esterified into complex lipids or are released from membrane glycerophospholipids (23). Levels of brain PUFAs can increase with neuronal activity (e.g. activation of NMDA-type glutamate receptors) and are subsequently metabolized by lipases, typically phospholipase A₂ (PLA₂) (24). Arachidonic acid (and other PUFAs) can modulate both the electrical and biochemical properties of a variety of membrane proteins involved in cellular signaling mechanisms, including ion channels, receptors, and transporters. A critical question in all these examples is whether arachidonic acid modulates protein activity through a direct interaction with the protein or whether it indirectly modulates the protein either by altering membrane fluidity or through the actions of metabolites (e.g., mediated by cyclooxygenase and lipoxygenase pathways).

The effects of arachidonic acid on brain transporter activity were initially examined in assays of glutamate uptake, γ -aminobutyric acid (GABA) uptake, and Na⁺/K⁺-ATPase activity (25). Incubation of rat cortical slices with arachidonic acid caused a dose-dependent reduction in the Na⁺-dependent transport of GABA and glutamate but did not affect transport

of α -aminoisobutyric acid. Na⁺/K⁺-ATPase activity was reduced not only by arachidonic acid but also by docosahexaenoic acid [FA01030185]; the basis for these responses did not appear to stem from any detergent-like actions, as the addition of sodium dodecylsulfate at low concentrations had no effect. Similarly, in rat primary neuronal cultures, uptake of both glutamate and GABA was significantly inhibited by the two PUFAs, whereas glutamate transport alone was altered in astrocytes (26). The saturated fatty acid palmitate had no effect on transport in either neurons or glial cells. Taken together, these studies suggested that PUFAs modulate transport systems in a cell-type specific manner, perhaps related to intrinsic differences in membrane composition.

Melittin, a phospholipase A₂ activator, has been used to increase cellular production of arachidonic acid from endogenous glycerophospholipid precursors. In one study, the addition of melittin together with an acyltransferase inhibitor to cultured astrocytes increased arachidonic acid levels in a dose-dependent manner and concomitantly inhibited glutamate uptake (27). This inhibition is insensitive to the cyclooxygenase inhibitor indomethacin but is abolished upon application of bovine serum albumin, which binds free fatty acids. These experiments were not able to determine whether arachidonic acid affects the glutamate transporter through a direct interaction with the protein or whether it inhibits glutamate transport through an indirect mechanism. The metabolism of arachidonic acid generates free radicals and reactive oxygen species (ROS), which are reported to inhibit glutamate transport in cells; thus, ROS were examined as potential indirect means for arachidonic acid-mediated inhibition of glutamate transport (28–31). In astrocyte cultures treated with an ROS-producing agent, saturating doses of arachidonic acid produced further inhibition of glutamate uptake. In addition, transport inhibition was fully prevented in cultures treated with both BSA (to sequester arachidonic acid) and superoxide dismutase/catalase (to prevent the accumulation of ROS). Application of either agent alone recovered only a portion of the inhibition, confirming that arachidonic acid mediates transport in an ROS-independent manner. These investigations elegantly demonstrated that PUFA modulation is a distinct mechanism and not dependent on oxidative stress or related processes.

In isolated salamander retinal glial cells, arachidonic acid can inhibit the glutamate-evoked currents that arise from electrogenic glutamate uptake. Whole cell patch recordings of salamander Muller cells reveal that arachidonic, docosahexaenoic, and oleic acids reduce maximal transport currents without dramatically affecting glutamate affinity (32). These inhibitory effects did not appear to depend on metabolic turnover of the PUFAs, as the inhibition was affected by neither nordihydroguaiaretic acid nor indomethacin, inhibitors of lipoxygenase and cyclooxygenase, respectively. Using a different model system, Trotti and colleagues investigated the effects of a series of fatty acids on the uptake of radiolabeled glutamate in reconstituted proteoliposomes enriched in the glutamate transporter isoforms Glt-1 (33). They showed

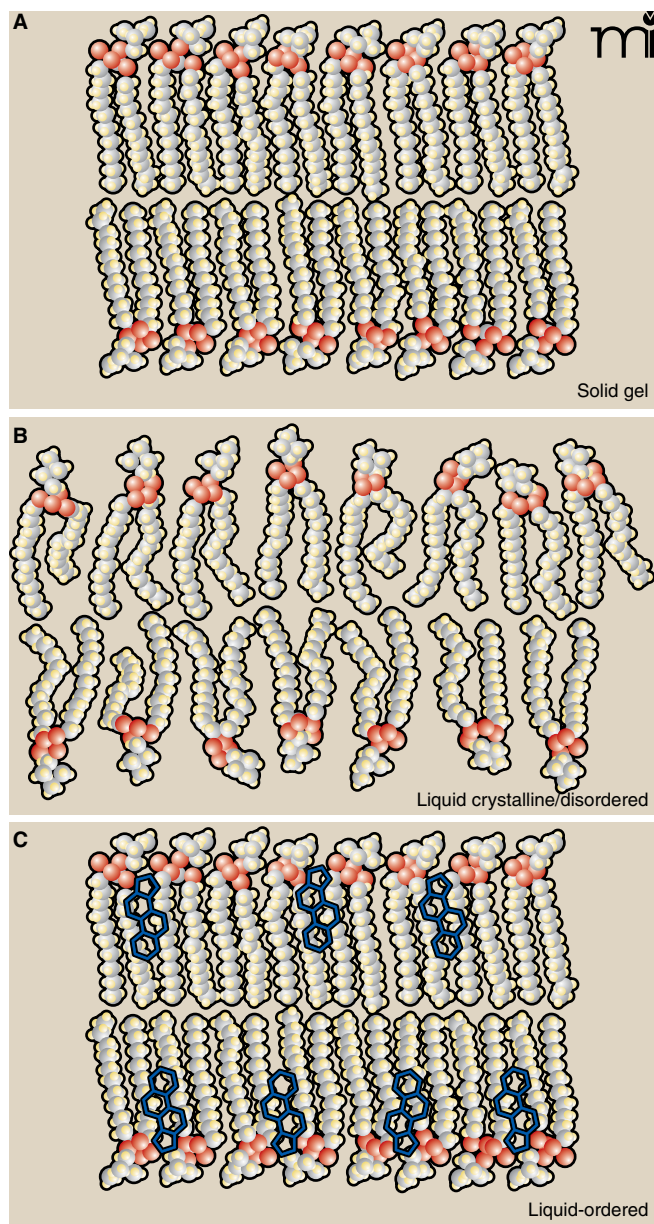


Figure 1. The dynamic lipid bilayer and membrane phases. Three different phases are generally described for membrane lipids. **A)** In the “solid gel state,” or “solid crystalline state,” hydrocarbon chains are typically found in the *trans* configuration and are highly ordered. Low temperatures can favor the solid gel phase. **B)** This “liquid crystalline state,” or “liquid disordered state,” is typical of high temperature and shows a disordered configuration of acyl chains. High lateral mobility is associated with the liquid disordered state; most pure fatty acid, detergent, or phospholipid liposomes are found in this state at room temperature. **C)** The “liquid ordered state” occurs in the presence of high levels of sphingolipids and cholesterol and results in mobility slightly under that of the pure liquid disorder state. Detergent-resistant microdomains or lipid rafts are endogenous liquid-ordered membrane patches. See text for details. Adapted from (63).

that oleic acid, methyl ester-arachidonic acid, α -linolenic acid [FA01030152], docosahexaenoic acid, and eicosapentaenoic acid [FA01030181] all inhibited glutamate transport, and interestingly, eicosapentaenoic acid inhibited uptake significantly more than did arachidonic acid. A major finding from this work was that arachidonic acid present in the aqueous but not the lipid phase was essential for the inhibitory effect. This observation supports the intriguing possibility that the inhibition of glutamate transport is the consequence of a direct interaction between arachidonic acid from the aqueous medium and the transporter protein. Remarkably, in 2004, the crystal structure of an archaeal ortholog of mammalian glutamate transporters revealed the presence of a lipid moiety bound within the solvent-filled basin. In this structure the lipid extends down into a hydrophobic crevice that is observed only in the substrate-bound carrier (34) (Figure 2A). This state-dependent lipid interaction at the aqueous interface of a glutamate transporter is intriguing and may provide a structural link to the lipid-mediated inhibition of carrier activity noted above.

The question of whether PUFAs act directly or indirectly to modulate transporter function was further addressed in investigations of the effects of arachidonic acid and other fatty acids on transport currents associated with human excitatory amino acid transporters (EAATs) (35). Because transport of glutamate by EAATs is coupled thermodynamically to the co-transport of one proton and two to three sodium ions, and to the counter-transport of one potassium ion, the process is electrogenic and can be studied using electrophysiological techniques in *Xenopus* oocytes. With all EAAT subtypes, most notably EAAT4 and EAAT5, substrates can additionally activate a thermodynamically uncoupled anion flux. Three glutamate transporter isoforms were expressed in *Xenopus* oocytes and tested for their sensitivity to arachidonic acid: EAAT1, a glial carrier; EAAT2, an abundant, predominantly astrocytic carrier; and EAAT3, a widely expressed neuronal carrier. The effects of PUFAs were distinct for each transporter subtype: maximal transport activity of EAAT 1 was decreased without alteration of glutamate affinity; the activity of EAAT2 was increased by decreasing its apparent K_m for glutamate; and little or no effect was observed on the activity of EAAT3. These results, together with synaptosomal studies reporting different arachidonic acid effects on glutamate transport in various regions of the rat central nervous system (36), first illustrated the subtype-selective actions of arachidonic acid on glutamate transporters. Proteoliposomal preparations further corroborate these observations, raising again the possibility that PUFAs such as arachidonic acid regulate transport through direct interactions with the carriers themselves, rather than through indirect effects on membrane organization or fluidity. Moreover, the rapid onset of modulation, along with its insensitivity to cyclooxygenase and lipoxygenase inhibitors, suggests that the effects on glutamate transport are mediated directly by arachidonic acid itself, rather than via a metabolite.

Further insight into the ability of arachidonic acid to differentially modulate the activity of glutamate transporters comes from investigation of human EAAT4, a carrier that possesses a prominent substrate-activated anion current (37). Although arachidonic acid does not significantly affect substrate transport, it causes a large increase in substrate-activated EAAT4-mediated currents. Ion substitution experiments have revealed that EAAT4 generates a distinctive substrate-gated proton-selective current that is PUFA-dependent. The proton conductance, activated at low, physiologically relevant, concentrations of arachidonic acid ($EC_{50} \approx 2 \mu M$), is not associated with changes in substrate flux, PUFA metabolism, ion coupling, or the well-established anion conductance. The phenomenon is characteristic of rat as well as human EAAT4 (38).

Thus, several lines of data indicate that arachidonic acid and other PUFAs alter the channel-like signaling properties of the EAAT4. [For reviews of EAAT modulation by PUFAs, see (39, 40)].

In addition to the excitatory amino acid family of carriers, which belong to solute carrier family 1 (SLC1), a second family of transporters, the biogenic amine carriers, are also regulated by PUFAs. These carriers are members of the neurotransmitter-sodium symporter family (SLC6). For example, arachidonic acid inhibits the uptake of L-dopamine into rat striatal synaptosomes in a dose-dependent manner (41). In contrast, C6 glioma cells stably expressing the dopamine transporter respond to arachidonic acid (20–160 μM) in a biphasic manner: dopamine transport is activated in the short term, but at later time points (incubations > 45 min), transport is inhibited relative to control (42). Thus, within a single cell line, arachidonic acid may have multiple modes of action on the dopamine transporter.

In addition to the electrogenic co-transport of Na^+ , Cl^- and dopamine, the dopamine transporter mediates a sodium-dependent cation leak conductance (43), which is relevant in determining the specific effects of PUFAs upon the transporter. Indeed, like the excitatory amino acid transporter discussed above (EAAT4), the dopamine transporter responds to arachidonic acid by display-

ing unique conductances. The application of arachidonic acid (1–100 μM) to *Xenopus* oocytes expressing the human dopamine transporter stimulates an inward current that is potentiated by dopamine and can be blocked by transport inhibitors such as cocaine (44). The current is qualitatively and quantitatively different from the currents typically associated with dopamine transport in several ways: it shows a distinctive selectivity for cations; its amplitude can be up to fiftyfold larger than current arising from electrogenic transport; and it is more pH-sensitive than transport. In voltage-clamped oocytes, arachidonic acid inhibits dopamine transport. Interestingly, dopamine, even in the absence of its co-substrate sodium, can potentiate the arachidonic acid-induced current. These effects appear to be produced by a direct action of arachidonic acid on the carrier, as they are not mimicked by non-metabolizable analogs and they are insensitive to a variety of inhibitors of fatty acid metabolism.

Because many studies have ruled out changes in fluidity or other membrane dynamics as contributors to the effect of PUFA actions on transporters, the observation that a range of these lipid molecules can mediate similar effects may well reflect a generally accommodating binding site. Nonselective binding is unlikely to be as energetically favorable as the binding of ligand to a more

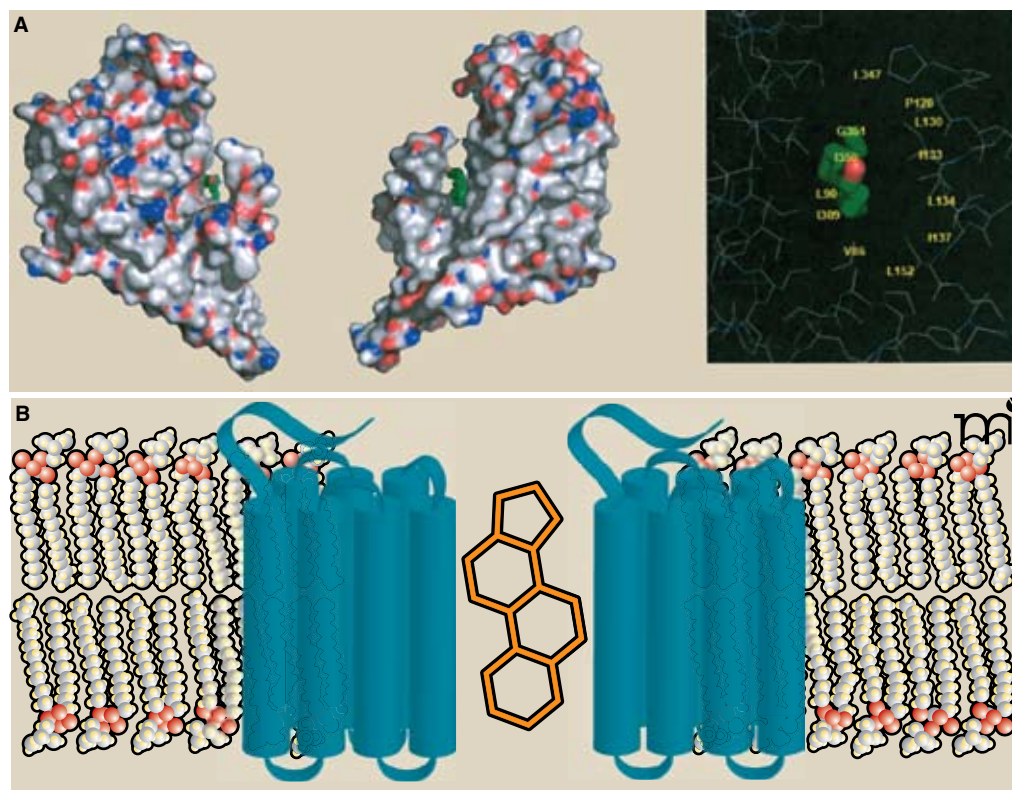


Figure 2. Lipid moieties found within high-resolution structures of integral membrane proteins. A) A high-affinity aspartate transporter (GltTph) from *Pyrococcus hirokoshii* resolved at 3.2 Å. Surface representation of a single GltTph monomer, colored by atom type, with the interacting palmitate molecule colored green. At right, the hydrophobic residues that are positioned to interact with the lipid molecule are shown. **B)** Membrane topology of the human $\beta 2$ -adrenergic receptor based on the crystal structure resolved at 2.4 Å. Intriguingly, association of the two receptor molecules (blue) appears to be mediated by cholesterol (orange). [Adapted from (34, 64).]

specific binding site. Nevertheless, the presence of lipid moieties within a number of high-resolution membrane protein structures lends additional credence to the possibility of allosteric lipid modulation (Figure 2).

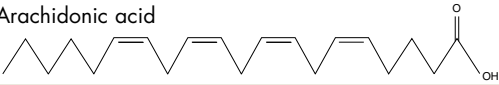
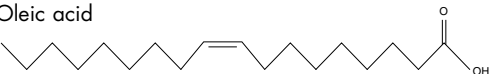

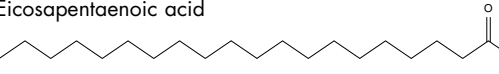
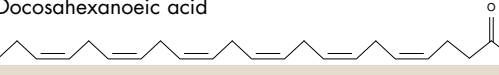
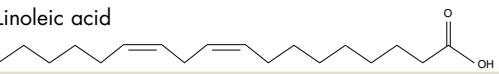
CHOLESTEROL AND TRANSPORTER FUNCTION

Cholesterol is another constituent of the membrane that has been shown to have a major effect on protein dynamics and function. Increases in membrane cholesterol content have been shown to affect lipid fluidity and to increase the viscosity of the membrane (45). The Na⁺/K⁺-ATPase is one of the most extensively studied carriers in biology, and early studies indicated that membrane cholesterol depletion increases pump activity. To establish whether cholesterol depletion alters maximal transport rates through a general change in membrane lipid fluidity or through a more direct mechanism, the effect of several additional amphiphilic molecules that enhance membrane fluidity were tested (46). Electronic spin resonance and fluorescence polarization measurements with these compounds revealed a membrane-disordering effect that mimicked cholesterol removal. All treatments decreased the apparent internal Na⁺ affinity but increased maximal transport velocity of the ATPase. In addition, the supplementation of bovine kidney membrane vesicles with phosphatidylcholine and sterols evoked a biphasic response in pump activity, in which low levels of cho-

lesterol stimulated activity, whereas high concentrations inhibited ATP hydrolysis (47).

Although initial studies consistently demonstrate a biphasic action of cholesterol on ATPase activity, the magnitude of inhibition observed varied widely among the various artificial membrane and tissue preparations studied. A comprehensive series of experi-

Table 2. Transporter Regulation by Polyunsaturated Fatty Acids^a

Transporter	Fatty acid (structure)	Regulation ^b	Ref.
Rat GAT	Arachidonic acid 	Transport inhibited	25, 26, 33
Rat GLT-1/ GLAST/EAAC1	Arachidonic acid	V _{max} decreased	25–31, 36
Rat GLT-1	Oleic acid 	V _{max} decreased	33
	A-Linolenic acid 		
	Eicosapentaenoic acid 		
	Docosahexaenoic acid 		
Rat EAAT4	Arachidonic acid	I increased, H ⁺ conductance	38
Human EAAT1	Arachidonic acid	I _{Transport} decreased	35
	A-Linolenic acid Linoleic acid 		
Human EAAT2	Arachidonic acid	I _{Transport} increased, K _m decreased	35
	A-Linolenic acid		
	Linoleic acid		
Human EAAT3	Arachidonic acid	I _{Transport} increased, K _m decreased	35
Human EAAT4	Arachidonic acid	I increased, H ⁺ conductance	37
	A-Linolenic acid		
	Linoleic acid		
	Docosahexaenoic acid		
	Oleic acid		
Salamander GLT1/GLAST	Arachidonic acid Oleic acid	V _{max} decreased	32
Rat DAT	Arachidonic acid	Transport inhibited	41
Human DAT	Arachidonic acid	V _{max} decrease, K _m decrease	42, 44
		I increased, Cation conductance	
Rat Na ⁺ /K ⁺ -ATPase	Arachidonic acid	Transport inhibited	25

^a Data reflect effects of fatty acids added to different membrane transport systems in different tissues and species as indicated.

^b Regulatory effects of the fatty acid addition.

Table 3. Transporter Responses to Alteration of Membrane Cholesterol Content^a

Transporter	Cholesterol treatment	Effect	Ref.
Na/K-ATPase (Human)	Removal ^b	Decreased Na affinity, Increased V _{max}	46
Na/K-ATPase (Bovine)	Minimal addition ^c Maximal addition	Increased ATPase Decreased ATPase	47
Na/K-ATPase (Shark)	Addition	Stimulated ATPase activity, Na transport, K release	48, 49, 52
GAT (Rat)	Removal	Decreased activity	54
GLT-1 (Rat)	Removal	Decreased activity	54
EAAT2 (Human)	Removal	Decreased activity	56
SERT (Rat)	Removal	Decreased V _{max} , Decreased K _m	57, 58
EAAC1 (EAAT3) (Rat)	Addition	Increased V _{max} , Increased expression	55
DAT (Human)	Removal	Decreased V _{max} , Decreased K _m , Increased lateral mobility	59
DAT (Rat)	Removal	Decreased activity	60
GLYT2 (Rat)	Removal	Decreased activity	61
GLYT1 (Human)	Removal	Decreased activity	62
GLYT2v (Human)	Removal	Increased activity	62

^a Data compiled from reviewed references demonstrate the effect of cholesterol manipulation on different transport systems across several species.

^b Removal is typically treatment with methyl- β -cyclodextran (M β CD) or incubation of the transporter-encompassed membrane with cholesterol-free liposomes.

^c Addition is either treatment with water-soluble cholesterol bound in M β CD as a carrier or incubation within high cholesterol concentrations in liposomes.

ments addressed the effects of cholesterol on the kinetic properties of the Na⁺/K⁺-ATPase isolated from the shark rectal gland; pump activity was reconstituted in liposomes consisting of phosphatidylcholine, phosphatidylinositol, and phosphatidylethanolamine. The addition of cholesterol to these liposomes caused a significant increase in steady-state rate of Na⁺/K⁺-exchange activity, Na⁺/Na⁺-exchange, and on Na⁺ uncoupled transport (48). Additionally, cholesterol increased the rates of ATPase phosphorylation and dephosphorylation by as much as forty percent. These data supported a model in which the incorporation of cholesterol into liposomes shifts the equilibrium of ATPase conformers, accounting for kinetic effects observed for the potassium deocclusion reaction as well as for the observed change in phosphoenzyme levels (49).

The fatty acid composition of the lipid bilayer can also affect Na⁺/K⁺-ATPase activity. Unsaturated fatty acids, which display fewer packing interactions and higher fluidity than saturated fatty acids, give rise to higher levels of ATPase activity in proteoliposome preparations (50). Additionally, acyl chain length is a variable that has been demonstrated to impact protein activity with optimal functioning of the ATPase in lipid vesicles containing between 16- and 20-carbon atom phosphatidylcholine acyl chains (51). When the Na⁺/K⁺-ATPase was assessed in a reconsti-

tuted liposome system in the absence of cholesterol, the optimal acyl chain length for a monounsaturated phospholipid was twenty-two carbons, whereas the optimal length in the presence of cholesterol was shifted to 18 carbons (52). No significant effect on pump activity was seen in response to temperature alteration supporting the notion that that bilayer thickness is a more critical variable for regulating activity than membrane fluidity. Subsequent work also revealed that interactions between cholesterol and the polyunsaturated acyl chains of lipids can significantly influence Na⁺/K⁺-ATPase activity. Specifically, the addition of phosphatidylcholine molecules containing docosahexaenoic acid acyl groups lowers pump activity and decreases Na⁺ binding (53), effects that vary inversely with the amount of chole-

sterol incorporated into the membrane. The docosahexaenoic acid moiety, with its six double bonds, induces a high degree of disorder within the membrane, whereas cholesterol favors a liquid-ordered state. Docosahexaenoic acid-containing phospholipids thus tend to segregate laterally away from cholesterol and establish liquid-disordered domains. These experiments demonstrate a fundamental effect of membrane properties on integral protein function, and also reveal more specific interactions of cholesterol and phospholipids with the ATPase.

Clearly, studies of Na⁺/K⁺-ATPase activity have established that the activity of an integral membrane protein can be regulated by membrane lipid composition, bilayer thickness, and general fluidity. Membrane cholesterol has also been shown to modulate the activity of neurotransmitter transporters. Transport by a rat brain GABA transporter reconstituted into liposomes was significantly impaired when the lipid bilayer consisted solely of asolectin (soybean phospholipids), but transport activity was restored upon addition of brain lipids containing cholesterol (54). This stimulation was specific in that it could not be replicated by cholesterol analogs. Brain glutamate transport in proteoliposomes is similarly cholesterol-dependent, and the stimulatory effect of cholesterol in this case could not be explained by any changes in ion coupling

or carrier surface expression. Remarkably, very modest amounts of cholesterol are required to restore GABA or glutamate transport activity, implying that a direct interaction of cholesterol with the carriers may mediate this effect. A more recent study has explored a distinct effect of cholesterol in primary neuronal cultures from rat cortex. The intrinsic glutamate transport activity of pure neuronal cultures is lower than that of neurons co-cultured with astrocytes (55). The transport deficiency manifested by pure neuronal cultures can be rescued by astrocyte-conditioned media, and cholesterol itself was identified as the molecule responsible for the observed increase in transport function. One additional study of the effect of cholesterol depletion on glutamate transport in rat cortical cultures showed that when the sterol chelator methyl- β -cyclodextrin (M β CD) was used to remove cholesterol, radiolabeled glutamate uptake was significantly reduced. Additional experiments showed that EAAT2 resides in detergent-resistant lipid microdomains and that M β CD treatment altered this localization (56).

Membrane cholesterol content can also regulate the activity of the serotonin transporter, which also belongs to the Neurotransmitter–Sodium Symporter family (NSS or SLC6 family). Treatment of HEK293 cells stably expressing the rat serotonin transporter with M β CD decreases maximal transport rate, lowers the apparent affinity for serotonin, and abolishes binding of the antagonist citalopram (57). These effects were specific for cholesterol and not due to alterations in membrane fluidity, because analogs of cholesterol that alter membrane fluidity had no effect on transport activity. In addition, disruption of lipid microdomains upon removal of cholesterol with M β CD has been linked to reduced SERT activity (58).

The human dopamine transporter is also regulated by its association with membrane lipid microdomains and by changes in cholesterol content (59). Based on fluorescence recovery after photobleaching (FRAP) experiments, an association of the dopamine transporter (tagged with yellow fluorescent protein) with lipid microdomains was reported in HEK293 cells. With the depletion of membrane cholesterol by M β CD treatment, the lateral mobility of the dopamine transporter was increased, and this effect was associated with a decline in the transporter V_{max} as well as its apparent affinity for dopamine. Interestingly, the disruption of the cytoskeleton by cytochalasin D also disrupted the localization of the dopamine transporter in this system, although it was unclear whether this effect alone was sufficient to alter transporter activity. Another study of the dopamine transporter, in which the effect of protein kinase C on dopamine transport was examined with respect for the distribution of the transporter at lipid microdomains (60), concluded that 1) the regulation of the dopamine transporter by cholesterol occurred within lipid rafts; and 2) that cholesterol-dependent regulation of dopamine transport was not mediated through alterations in cell surface expression of the transporter. In addition, studies examining the accessibility of cysteine residues introduced into the carrier sequence have demonstrated an increase in the number of cocaine binding sites when cells are pro-

vided with medium enriched with water-soluble cholesterol (Hong and Amara, unpublished data). These results support the notion that membrane cholesterol affects the conformational equilibrium of the transporter domains to favor an outward-facing state.

Two additional members of the SLC6 family, the glycine transporters GLYT1 and GLYT2, regulate glycine concentrations near central nervous system synapses. The neuronal carrier, GLYT2, localizes to detergent-resistant microdomains that are required to maintain full activity, and both cholesterol removal and sphingomyelinase treatment reduce GLYT activity (61). In contrast, a second study, using human GLYT1 and GLYT2 stably expressed in Chinese hamster ovary cells, reported that M β CD-mediated depletion of cholesterol reduced GLYT1 activity but actually increased GLYT2 activity (62). The same experiments, repeated in *Xenopus laevis* oocytes, revealed that although GLYT1 catalytic activity was reduced, GLYT2 activity was unaltered. Differences among these observations could arise from cell-specific differences in membrane thickness, fluidity, composition, or the presence of specific regulators.

CONCLUSIONS

The precise mechanisms for regulation of both primary and secondary carriers by lipids have remained elusive, in part reflecting the diversity of pathways and settings in which lipids can alter the structure and function of membrane proteins. Emerging data on the functional impact of lipids on membrane proteins, together with new high-resolution structures of protein–lipid complexes, support the idea that direct interactions of lipids and proteins will be found in many different transport systems. Nonetheless, the indirect effects of fatty acid composition, membrane fluidity, lateral segregation of membrane components, and bilayer dimensions in complex membrane environments will undoubtedly be part of the picture, too. Despite all the possibilities, the intimate association of membrane proteins with the lipid milieu guarantees that their functions will be shaped and regulated by a diverse, but essential cadre of oily characters. 📄 doi:10.1124/mi.9.5.8

References

1. Piomelli, D., Astarita, G., and Rapaka, R. A neuroscientist's guide to lipidomics. *Nat. Rev. Neurosci.* **8**, 743–754 (2007).
2. Hilgemann, D.W. Oily barbarians breach ion channel gates. *Science* **304**, 223–224 (2004).
3. Boland, L.M. and Drzewiecki, M.M. Polyunsaturated fatty acid modulation of voltage-gated ion channels. *Cell Biochem. Biophys.* **52**, 59–84 (2008).
4. Tillman, T.S. and Cascio, M. Effects of membrane lipids on ion channel structure and function. *Cell Biochem. Biophys.* **38**, 161–190 (2003).
5. Fahy, E., Subramaniam, S., Brown, H.A. et al. A comprehensive classification system for lipids. *J. Lipid Res.* **46**, 839–861 (2005).
6. Roots, B.I. and Johnston, P.V. Lipids of isolated neurons. *Biochem. J.* **94**, 61–3. (1965).
7. DeVries, G.H. and Norton, W.T. The fatty acid composition of sphingolipids from bovine CNS axons and myelin. *J. Neurochem.* **22**, 251–257 (1974).

8. DeVries, G.H. and Norton, W.T. The lipid composition of axons from bovine brain. *J. Neurochem.* **22**, 259–264 (1974).
9. DeVries, G.H., Zetuský, W.J., Zmachinski, C., and Calabrese, V.P. Lipid composition of axolemma-enriched fractions from human brains. *J. Lipid Res.* **22**, 208–216 (1981).
10. Roots, B.I. Locating lipids in the CNS: An historical perspective. *Neurochem. Res.* **20**, 1261–1268. (1995).
11. Yeagle, P. The Structure of biological membranes. Boca Raton, Fla., CRC Press. (2005).
12. Chapman, D. Liquid crystals and cell membranes. *Ann. N. Y. Acad. Sci.* **137**, 745–754. (1966).
13. Singer, S.J. and Nicolson, G.L. The fluid mosaic model of the structure of cell membranes. *Science* **175**, 720–731. (1972).
14. Reinert, J.C. and Steim J.M. Calorimetric detection of a membrane-lipid phase transition in living cells. *Science* **168**, 1580–1582 (1970).
15. Phillips, R., Ursell, T., Wiggins, P., and Sens, P. Emerging roles for lipids in shaping membrane-protein function. *Nature* **459**, 379–385 (2009). **This work highlights bilayer properties that can exert force onto integral membrane proteins. This article provides a strong emphasis on how alterations in membrane curvature, thickness, viscosity or several other factors affect channels properties in particular. The effect of membrane tensions on mechanosensitive gating is well described. Also provided is a quantitative theoretical framework which allows for distinctive insight into the manner in which lipids and proteins interact.**
16. Singer, S.J. A fluid lipid-globular protein mosaic model of membrane structure. *Ann. N.Y. Acad. Sci.* **195**, 16–23 (1972).
17. Engelman, D.M. The use of X-ray scattering in the study of lipid bilayer planar organization. *Biophys. J.* **15**, 940–944 (1975).
18. Hong-wei, S. and McConnell, H. Phase separations in phospholipid membranes. *Biochemistry* **14**, 847–854 (1975).
19. Jacobson, K. and Papahadjopoulos, D. Phase transitions and phase separations in phospholipid membranes induced by changes in temperature, pH, and concentration of bivalent cations. *Biochemistry* **14**, 152–161 (1975).
20. Pike, L.J. Lipid rafts: Heterogeneity on the high seas. *Biochem. J.* **378**, 281–292 (2004).
21. Jacobson, K., Mouritsen, O.G., Anderson, R.G. Lipid rafts: At a cross-road between cell biology and physics. *Nat. Cell Biol.* **9**, 7–14 (2007).
22. Spector, A.A. Plasma free fatty acid and lipoproteins as sources of polyunsaturated fatty acid for the brain. *J. Mol. Neurosci.* **16**, 159–65; discussion 215–221 (2001).
23. Irvine, R.F. How is the level of free arachidonic acid controlled in mammalian cells? *Biochem. J.* **204**, 3–16. (1982).
24. Rapoport, S.I. Arachidonic acid and the brain. *J. Nutr.* **138**, 2515–2520 (2008).
25. Chan, P.H., Kerlan, R., and Fishman, R.A. Reductions of gamma-aminobutyric acid and glutamate uptake and (Na⁺ + K⁺)-ATPase activity in brain slices and synaptosomes by arachidonic acid. *J. Neurochem.* **40**, 309–316 (1983).
26. Yu, A.C., Chan, P.H., and Fishman, R.A. Effects of arachidonic acid on glutamate and gamma-aminobutyric acid uptake in primary cultures of rat cerebral cortical astrocytes and neurons. *J. Neurochem.* **47**, 1181–1189 (1986).
27. Volterra, A., Trotti, D., Cassutti, P., Tromba, C., Salvaggio, A., Melcingi, R.C., and Racagni, G. High sensitivity of glutamate uptake to extracellular free arachidonic acid levels in rat cortical synaptosomes and astrocytes. *J. Neurochem.* **59**, 600–606 (1992).
28. Volterra, A., Trotti, D., Tromba, C., Floridi, S., and Racagni, G. Glutamate uptake inhibition by oxygen free radicals in rat cortical astrocytes. *J. Neurosci.* **14**, 2924–2932 (1994).
29. Volterra, A. Inhibition of high-affinity glutamate transport in neuronal and glial cells by arachidonic acid and oxygen-free radicals. Molecular mechanisms and neuropathological relevance. *Ren. Physiol. Biochem.* **17**, 165–167 (1994).
30. Volterra, A., Trotti, D., Floridi, S., and Racagni, G. Reactive oxygen species inhibit high-affinity glutamate uptake: Molecular mechanism and neuropathological implications. *Ann. N. Y. Acad. Sci.* **738**, 153–162 (1994).
31. Volterra, A., Trotti, D., and Racagni, G. Glutamate uptake is inhibited by arachidonic acid and oxygen radicals via two distinct and additive mechanisms. *Mol. Pharmacol.* **46**, 986–992 (1994).
32. Barbour, B., Szatkowski, M., Ingledew, N., and Attwell, D. Arachidonic acid induces a prolonged inhibition of glutamate uptake into glial cells. *Nature* **342**, 918–920 (1989).
33. Trotti, D., Volterra, A., Lehre, K.P., Rossi, D., Gjesdal, O., Racagni, G., and Danbolt, N.C. Arachidonic acid inhibits a purified and reconstituted glutamate transporter directly from the water phase and not via the phospholipid membrane. *J. Biol. Chem.* **270**, 9890–9895 (1995). **This series of investigations uses novel approaches to examine the effects of ten different lipids on transporter activity and kinetics. The most important observation is that arachidonic acid exerts its effect from the water phase and not through its initial partitioning into the membrane. This work foreshadows a recent observation of state-dependent lipid binding from within the aqueous basin of a high-resolution crystal structure of an archaeal glutamate transporter.**
34. Boudker, O., Ryan, R.M., Yernool, D., Shmimamot, K., and Gouaux, E. Coupling substrate and ion binding to extracellular gate of a sodium-dependent aspartate transporter. *Nature* **445**, 387–393 (2007). **This report presents the high-resolution structures of an archaeal glutamate/aspartate transporter with either inhibitor or substrate bound. The study reveals the transporter in an “open” conformation representing an early step in the transport cycle. The authors also provide strong support for the possibility that lipids can interact directly with glutamate transporters by showing a lipid moiety bound within the crystal in a crevice near the substrate binding site.**
35. Zerangue, N., Arriza, J.L., Amara, S.G., and Kavanaugh, M.P. Differential modulation of human glutamate transporter subtypes by arachidonic acid. *J. Biol. Chem.* **270**, 6433–6435 (1995).
36. Manzoni, C. and Mennini, T. Arachidonic acid inhibits 3H-glutamate uptake with different potencies in rodent central nervous system regions expressing different transporter subtypes. *Pharmacol. Res.* **35**, 149–151 (1997).
37. Fairman, W.A., Sonders, M.S., Murdoch, G.H., and Amara, S.G. Arachidonic acid elicits a substrate-gated proton current associated with the glutamate transporter EAAT4. *Nat. Neurosci.* **1**, 105–113 (1998).
38. Tzingounis, A.V., Lin, C.L., Rothstein, J.D., and Kavanaugh, M.P. Arachidonic acid activates a proton current in the rat glutamate transporter EAAT4. *J. Biol. Chem.* **273**, 17315–17317 (1998).
39. Fairman, W.A. and Amara, S.G. Functional diversity of excitatory amino acid transporters: Ion channel and transport modes. *Am. J. Physiol.* **277**, F481–486 (1999).
40. Amara, S.G. and Fontana, A.C. Excitatory amino acid transporters: Keeping up with glutamate. *Neurochem. Int.* **41**, 313–318 (2002).
41. L'Hirondel, M., Cheramy, A., Godeheu, G., and Glowinski, J. Effects of arachidonic acid on dopamine synthesis, spontaneous release, and uptake in striatal synaptosomes from the rat. *J. Neurochem.* **64**, 1406–1409 (1995).
42. Zhang, L. and Reith, M.E. Regulation of the functional activity of the human dopamine transporter by the arachidonic acid pathway. *Eur. J. Pharmacol.* **315**, 345–354 (1996).
43. Sonders, M.S., Zhu, S.J., Zahniser, N.R., Kavanaugh, M.P., and Amara, S.G. Multiple ionic conductances of the human dopamine transporter: The actions of dopamine and psychostimulants. *J. Neurosci.* **17**, 960–974 (1997).
44. Ingram, S. L. and Amara, S.G. Arachidonic acid stimulates a novel cocaine-sensitive cation conductance associated with the human dopamine transporter. *J. Neurosci.* **20**, 550–557 (2000). **This report describes a unique phenomenon observed following application arachidonic acid to the human dopamine transporter. The authors**

demonstrate that arachidonic acid activates a dopamine transporter-mediated non-selective cation conductance that is potentiated by dopamine and blocked by cocaine. The effects of arachidonic acid were mimicked by other fatty acids with a rank order of potency correlated with their degree of unsaturation, suggesting that arachidonic acid directly stimulates the novel cation current.

45. Kroes, J., Ostwald, R., and Keith, A. Erythrocyte membranes—compression of lipid phases by increased cholesterol content. *Biochim. Biophys. Acta* **274**, 71–74 (1972).
46. Giraud, F., Claret, M., Bruckdorfer, K.R., and Chailley, B. The effects of membrane lipid order and cholesterol on the internal and external cationic sites of the Na⁺-K⁺ pump in erythrocytes. *Biochim. Biophys. Acta* **647**, 249–258 (1981).
47. Yeagle, P.L., Young, J., and Rice, D. Effects of cholesterol on (Na⁺,K⁺)-ATPase ATP hydrolyzing activity in bovine kidney. *Biochemistry* **27**, 6449–6452 (1988).
48. Cornelius, F. Phosphorylation/dephosphorylation of reconstituted shark Na⁺,K⁺-ATPase: One phosphorylation site per alpha beta protomer. *Biochim. Biophys. Acta* **1235**, 197–204 (1995).
49. Cornelius, F., Turner, N., and Christensen, H.R. Modulation of Na,K-ATPase by phospholipids and cholesterol. II. Steady-state and pre-steady-state kinetics. *Biochemistry* **42**, 8541–8549 (2003).
50. Abeywardena, M.Y., Allen, T.M., and Charnock, J.S. Lipid-protein interactions of reconstituted membrane-associated adenosinetriphosphatases. Use of a gel-filtration procedure to examine phospholipid-activity relationships. *Biochim. Biophys. Acta* **729**, 62–74 (1983).
51. Johannsson, A., Smith, G.A., and Metcalfe, J.C. The effect of bilayer thickness on the activity of (Na⁺ + K⁺)-ATPase. *Biochim. Biophys. Acta* **64**, 416–421 (1981).
52. Cornelius, F. Modulation of Na,K-ATPase and Na-ATPase activity by phospholipids and cholesterol. I. Steady-state kinetics. *Biochemistry* **40**, 8842–8851 (2001).
53. Cornelius, F. Cholesterol-dependent interaction of polyunsaturated phospholipids with Na,K-ATPase. *Biochemistry* **47**, 1652–1658 (2008).
54. Shouffani, A. and Kanner, B.I. Cholesterol is required for the reconstruction of the sodium- and chloride-coupled, gamma-aminobutyric acid transporter from rat brain. *J. Biol. Chem.* **265**, 6002–6008 (1990).
A seminal report demonstrating that the rat GABA transporter displays a specific requirement for cholesterol to maintain transport activity during reconstitution. Because relatively small amounts of cholesterol are required and other sterols do not support transport, the data suggest that cholesterol directly modulates the function of the GABA transporter. This insightful work anticipates later reports confirming direct interactions of cholesterol with membrane proteins, as in the recent high-resolution structure of an adrenergic receptor with cholesterol bound at the dimeric interface.
55. Canolle, B., Masmejean, F., Melon, C., Nieoullon, A., Pisano, P., and Lortet, S. Glial soluble factors regulate the activity and expression of the neuronal glutamate transporter EAAC1: Implication of cholesterol. *J. Neurochem.* **88**, 1521–1532 (2004).
56. Butchbach, E.M., Tian, G., Guo, H., and Lin, C.L. Association of excitatory amino acid transporters, especially EAAT2, with cholesterol-rich lipid raft microdomains: Importance for excitatory amino acid transporter localization and function. *J. Biol. Chem.* **279**, 34388–34396 (2004).
57. Scanlon, S.M., Williams, D.C., and Schloss, P. Membrane cholesterol modulates serotonin transporter activity. *Biochemistry* **40**, 10507–10513 (2001).
58. Magnani, F., Tate, C.G., Wynne, S., Williams, C., and Haase, J. Partitioning of the serotonin transporter into lipid microdomains modulates transport of serotonin. *J. Biol. Chem.* **279**, 38770–38778 (2004).
59. Adkins, E.M., Samuvel, D.J., Fog, J.U., Eriksen, J., Jayanthi, L.D., Vaegter, C.B., Ramamoorthy, S., and Gether, U. Membrane mobility and microdomain association of the dopamine transporter studied with fluorescence correlation spectroscopy and fluorescence recovery after photobleaching. *Biochemistry* **46**, 10484–10497 (2007).
60. Foster, J.D., Adkins, S.D., Levers, J.R., and Vaughan, R.A. Phorbol ester induced trafficking-independent regulation and enhanced phosphorylation of the dopamine transporter associated with membrane rafts and cholesterol. *J. Neurochem.* **105**, 1683–1699 (2008).
61. Nunez, E., Alonso-Torres, P., Fornes, A., Aragon, C., and Lopez-Corcuera, B. The neuronal glycine transporter GLYT2 associates with membrane rafts: Functional modulation by lipid environment. *J. Neurochem.* Epub ahead of print (11 Mar 2008).
62. Liu, X., Mitrovic, A.D., and Vandenberg, R.J. Glycine transporter 1 associates with cholesterol-rich membrane raft microdomains. *Biochem. Biophys. Res. Commun.* **384**, 530–534 (2009).
63. van Meer, G., Voelker, D.R., and Feigenson, G.W. Membrane lipids: Where they are and how they behave. *Nat. Rev. Mol. Cell Biol.* **9**, 112–124 (2008).
64. Cherezov, V., Rosenbaum, D.M., Hanson, M.A. et al. High-resolution crystal structure of an engineered human beta2-adrenergic G protein-coupled receptor. *Science* **318**, 1258–1265 (2007).



Susan G. Amara, PhD, (right) is the Thomas Detre Professor and Chair of the Department of Neurobiology at the University of Pittsburgh School of Medicine and Co-director of the Center for Neuroscience at the University of Pittsburgh. Work in her laboratory focuses on neurotransmitter transporters and the plasma membrane proteins that limit the actions of neurotransmitters following their release from neurons. **Christopher B. Divito, BA, (left)** graduated from Shippensburg University of Pennsylvania with concentrations in psychology and biochemistry. He is currently a third-year graduate student, earning his PhD at the Center for Neuroscience of the University of Pittsburgh. Chris's research is focused on ligand binding mechanisms and lipid-protein interactions within the family of mammalian glutamate transporters.

APPENDIX C: MECHANISM OF CYSTEINE INTERACTION IN EXCITATORY AMINO ACID TRANSPORTERS

C.1. SUMMARY OF CONTRIBUTIONS

My contributions to this manuscript, which is in preparation, are significant in number. I developed the electrophysiological experiments and performed them in conjunction with Dr. Delany Torres-Salazar. I designed the use of L-selenocysteine as a cys congener and, along with Dr. Spencer Watts, interpreted all the data collected for the manuscript. I also attempted several challenging experiments looking at flux coupling ratios at various pHs and attempted to use deuterium containing buffers to modulate the mechanism of cysteine interaction with the EAATs. I also significantly assisted in the writing of this document.

C.2. INTRODUCTION

Excitatory amino acid transporters (EAATs) regulated the spatio-temporal profile of synaptically released glutamate (glu). Regulation of extracellular glu controls activation of synaptic and peri-synaptic ionotropic and metabotropic glutamate receptors (iGluRs and mGluRs) (1). EAATs are secondary active, electrogenic transporters of L-glu and L- and D-aspartate (asp) (2). This family of carriers is organized as homotrimers in the membrane and is comprised of 8 transmembrane domains (TM1-8) and two reentrant or hairpin loops (HP1 and HP2) (3-5). The translocation of 1 glu molecule is against its concentration gradient and therefore is co-transported with 3 Na⁺, 1 H⁺, and counter-transport of 1 K⁺ ion. This allows the net influx of ~2 positive charges per transported glu (6). In addition to this electrogenic activity, EAATs mediate a thermodynamically uncoupled anion conductance (7). This channel activity is open in the

empty transporter in glia (unpublished observation) and is gated by Na⁺ interaction in neuronal isoforms (8,9). The binding of substrates such as glu or asp occurs in an ordered manner after the initial binding of 1 or 2 Na⁺ and substrate interaction increases the open probability of the channel (10-12).

The mechanism of substrate interaction has been studied thoroughly for ligands such as glu or asp, yet many of the EAAT isoforms are capable of transporting a wide range of acidic species (2,13). One of the most atypical endogenous substrates for an EAAT family member is the transport of L-cysteine (cys) by EAAT3 (or EAAC1) (14). This carrier-substrate interaction was highlighted when EAAC1 KO mice showed a significant loss of neuronal viability, increased presence of reactive oxygen species, and a distinct decrease in glutathione levels (15). Thus, it is possible that EAAT3 influences glutathione levels through transport of cys, the rate limiting precursor to glutathione synthesis (16). The role of EAAT3 as a transporter of released glutamate is somewhat unclear. Although EAAT3 may influence the initial concentration of glutamate seen by post- and peri-synaptic receptors through rapid binding of released glu (17,18), the majority (> 90%) of glu transport is mediated by EAAT2 isoforms (19,20). Therefore, it has been proposed that EAAT3 uses the small amount of glu it transports as a precursor for γ -aminobutyric acid (GABA) synthesis (21). Thus, it is not surprising that EAAT3 has also been proposed to mediate the synthesis of glutathione (GSH) through transport of cys. This hypothesis is supported by a number of studies in addition to the initial EAAC1 knockout data. GSH levels are significantly affected by knockdown of GTRAP3-18, an interacting protein of EAAT3 (22,23). Also, application of N-acetylcysteine, a membrane permeable cysteine precursor, recovered GSH levels in EAAC1 ^{-/-} mice, suggesting that EAAT3 is the active transport protein for cysteine in the nervous system (24). These data together warrant the further investigation of cysteine interactions with this family of glutamate transporters.

Here we elucidate the mechanism of cys interaction with the family of EAATs. Through a combination of experimental techniques such as biochemistry, optical imaging, and

electrophysiology, we demonstrate that the transport of cysteine is dependent on a de-protonation mechanism mediated by EAAT3 alone among the EAATs. Our data support the potential neuronal transport of cys and aid in this field of investigation by providing critical insight into the mechanism of substrate interactions in the family of glutamate transporter.

C.3. EXPERIMENTAL PROCEDURES

C.3.1. Generation of Constructs

hEAAT1, hEAAT2, hEAAT3, and rEAAT4 were all subcloned into pOTV or pcDNA3.1 constructs using Kpn1 and Xba1 restriction sites (2). The EGFP-pH was constructed starting with pEGFP-N3 (Clontech) and using site directed mutagenesis to create the H148D substitution with primers (5' to 3') CTGGAGTACAACTACAACAGCGACAACGTCTATATCATGGCCGAC (sense) and GTCGGCCATGATATAGACGTTGTCGCTGTTGTAGTTGTACTCCAG (antisense) (C to G base change to create the CAC to GAC codon change) (25). Membrane targeting was accomplished by insertion of the coding sequence for the palmitoylation signal peptide from neuromodulin (GAP-43), MLCCMRRTKQVEKNDEDQKI, immediately 5' of the ATG start codon for EGFP-pH using the DNA sequence (ATGCTGTGCTGTATGAGAAGAACCAAACAGGTTGAAAAGAATGATGAGGACCAAAAGATC)(26).

C.3.1. Transfection of HEK293 and cRNA Injection into *Xenopus* oocytes

HEK293 cells were cultured at 37°C in a humidified 5% CO₂ incubator in DMEM (Lifetech, Gibco BRL, Invitrogen) supplemented with 10% FBS, penicillin (100 U/mL) and streptomycin (100 µg/mL). For imaging, 1 x 10⁵ cells/mL were batch transfected using 6 µL Lipofectamine 2000 (Invitrogen) and 1 µg DNA (0.5 µg EAAT and 0.5 µg mEGFPpH) with 2 x 10⁴ cells plated on poly-L-lysine coated 15mm coverslips. For radiolabeled transport experiments, cells were transfected as above with 1 µg EAAT DNA and plated at 5 x 10⁴ cells/well in 24 well Costar (Corning) plates. Following transfection and plating, cells were cultured 2-3 days prior to imaging or [³H]-L-glutamate transport experiments.

C.3.2. Radiolabeled Transport Assays

Radiolabeled transport assays were conducted using hEAAT1, hEAAT2, hEAAT3, or rEAAT4 transiently transfected into HEK293 cells or *Xenopus* oocytes. Briefly, 20 nM ^{35}S -L-cystiene (Perkin Elmer) was diluted with various concentrations of L-cysteine as described in the figure captions. 200 nM 3,4- ^3H -L-glu was combined with various concentrations of L-glutamate as described in the figure captions. All cells were washed 3 times before application of substrates with phosphate-buffered saline + 1 mM MgCl_2 and 0.1 mM CaCl_3 (PBSCM) for HEK293 cells or with ND96 buffer for oocytes. Cells were washed 3 times with their respective buffer after 10 min incubation with labeled substrates. Cells were lysed with 0.1 N NaOH + 1% SDS. HEK293 were counted by well using liquid scintillation counting (LSC) and oocytes were counted by individual cell by LSC.

C.3.3. Electrophysiology

Two-electrode voltage clamp recordings were performed on *Xenopus* oocytes 2-3 days after injection using a Geneclamp 500 (Molecular Devices) and were digitized using a 1440A Digidata (Molecular Devices). Various concentrations of substrates were perfused with a gravity fed perfusion system with a flow rate of 5-10 ml/min. Electrodes with a resistance between 0.5-2.0 were used to minimize voltage errors and were filled with 3 M KCl. A 3 M KCl agar bridge was used for all experiments. Samples were filtered at 1 kHz and were sampled at 50 kHz. Current-voltage (I-V) relationships were determined by applying voltage sweeps between -150 mV and +60 mV for 500 msec each. Isochronal current amplitudes were taken from the last 100 msec to ensure steady state conditions.

C.3.4. Cell Imaging Experiments

Cells were imaged with a Zeiss Axiovert 135T inverted microscope with a 40X NeoFluor oil immersion objective (NA1.3). A Lambda DG4 (Sutter Instrument Co.) equipped with a xenon arc lamp was used for high-speed excitation wavelength switching. Images were collected using either a Quantix (Roper Scientific, Tucson, AZ) or an Orca ER (Hamamatsu Co.) cooled

CCD. For pH imaging experiments, the fluorescence filters (Omega Optical) were: excitation 405 ± 20 and 485 ± 7.5 nm; dichroic 400-480-585 DLRP; emission 510 ± 11.5 nm. Software control and data acquisition were accomplished using Axon Imaging Workbench (INDEC Biosystems) or OpenLab acquisition software (Improvision, Perkin Elmer). Cells were incubated at room temperature with continuous perfusion using buffer containing (in mM): 146 NaCl, 5 KCl, 5 HEPES, 2.5 CaCl_2 and 1.2 MgCl_2 at pH 7.35 with additions (substrates etc.) as indicated in figure legends.

C.4. RESULTS

C.4.1. EAATs Readily Transport the Deprotonated Cysteine Analog Selenocysteine

It has been previously demonstrated that EAAT3 can mediate the transport of cys with an apparent affinity of approximately 200 μM . However, EAATs 1 and 2 made an affinity for cys ≥ 1 mM. This led us to the hypothesis that EAAT3 possessed a special mechanism for the transport of cysteine. We further hypothesized that this was due to the ability of EAAT3 to mediate the deprotonation of cys at physiological pH. To test if EAAT3 can readily mediate the deprotonation of cys, we used selenocysteine (Secys) as a model for deprotonated cysteine transport. With a pK_a of 5.5, Secys should be present in its negatively charged form at physiological pH. Application of various concentrations of Secys to *Xenopus* oocytes expressing EAAT1, 2, or 3 demonstrate that deprotonated Secys is readily transported by all EAAT isoforms. The apparent affinity of Secys for EAAT3 is 7.1 ± 2.0 μM (Figure C1A). The maximal current generated by transport of substrates is compared in oocytes expressing EAAT1, EAAT2, and EAAT3 (Figure C1B). Compared to saturating concentrations of glu, cysteine transport was significantly lower in both EAAT1 and EAAT2 ($p < 0.001$) while maximal transport currents in response to Secys were not significantly lower for EAATs 1, 2, or 3 ($p > 0.5$). Thus, selenocysteine is transported with a similar affinity and maximal velocity as glu. These data strongly suggest that any EAAT

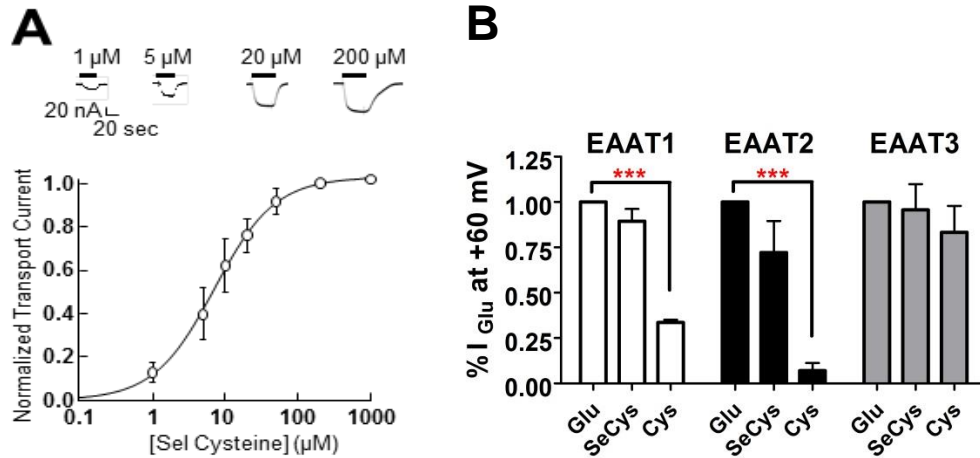


Figure C1. Selenocysteine is transported by EAATs 1-3 in oocytes. **A)** Perfusion of increasing concentrations of L-Selenocysteine (bars) induced increasing currents in voltage clamped oocytes expressing hEAAT3 (Upper panel). Normalized currents as a function of L-Selenocysteine concentration in hEAAT3 expressing oocytes (Lower panel). Data are presented as the mean and Std. dev. and were fit with a sigmoidal dose-response curve to estimate the K_M for transport. **B)** Comparison of the maximal transport currents for L-selenocysteine (Secys) and L-cysteine (Cys) by hEAAT1 (white), hEAAT2 (black), or hEAAT3 (grey) normalized to the maximal currents induced by L-glutamate (Glu) measured in the same oocytes.

isoform tested here is capable of transporting a deprotonated cys but only EAAT3 can readily accomplish this at physiological pH, suggesting a mechanism present for cys deprotonation in EAAT3 but not EAATs 1 or 2.

C.4.2. Selenocysteine Binding Competes for Glutamate Interaction in EAATs

The transport of Secys in the EAATs could be indicative of the mechanism of cys binding in EAAT3 but further characterization is needed. The presence of increasing concentrations of Secys caused a specific decrease in transport of radiolabeled glu in HEK293 cells expressing EAAT2 with an IC_{50} of $37.2 \pm 2.0 \mu M$ (Figure C2B), indicating that these substrates were competitive. In contrast, the IC_{50} of cys for glu transport in EAAT2 was $> 5 mM$ (Figure C2B). EAAT3 showed competitive inhibition of glu transport with both Secys ($IC_{50} = 68.3 \pm 10.7 \mu M$) and cys ($IC_{50} = 399 \pm 48.7 \mu M$). These data are consistent with both cys and Secys binding to the glu binding site in all of the EAAT isoforms tested and the affinity of the interaction is dependent on charged state for EAAT2 but not for EAAT3 as only the deprotonated Secys, and not cys, was readily transported by EAAT2.

C.4.3 Optical Observation of Proton Coupled EAAT Transport Processes.

One interpretation is that EAAT3 can mediate a binding mechanism that involves a deprotonation step of cys which the other EAAT isoforms cannot readily mediate. An alternative hypothesis is that EAAT3 can mediate the transport of the protonated form of cys as previously hypothesized (14). To differentiate between these two possibilities we developed an EGFP-pH sensor as a monitor for proton coupled substrate transport through the EAATs. To serve as a sensitive measure of proton influx mediated by EAAT transport processes, the EGFPpH sensor was membrane bound by adding a myristoylation sequence to anchor it after translation. Transient transfection of HEK293 cells with the mEGFPpH sensor resulted in fluorescent signals indicative of membrane expression and localization (Figure C3A). Application of NH_4Cl caused cells to significantly, transiently alkylate but then the cells rapidly acidified in response. The response of the mEGFPpH sensor demonstrates this behavior and, thus, would act as a

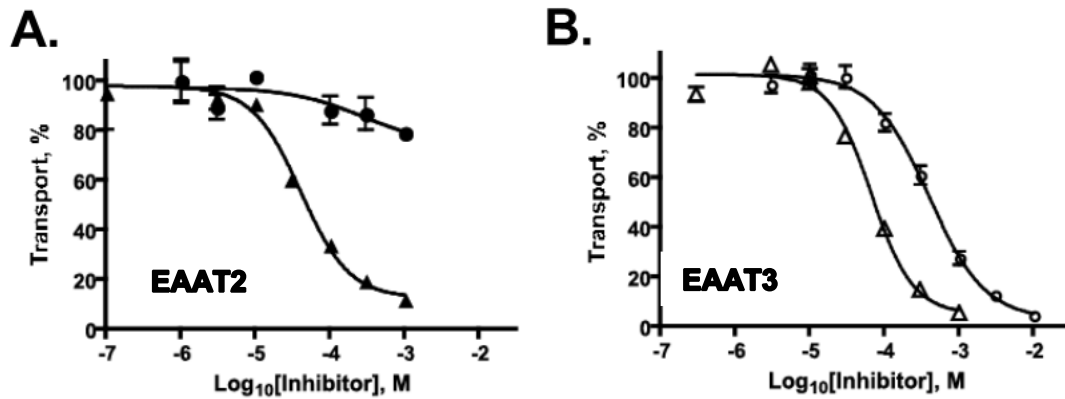


Figure C2. Comparison of [³H]-L-Glutamate transport inhibition by L-Selenocysteine and L-Cysteine for EAAT2 and EAAT3. Inhibition of 10 μ M [³H]-L-glutamate with increasing concentrations of L-cysteine (circles) or L-selenocysteine (triangles) in HEK293 cells expressing hEAAT2 (**A**) or hEAAT3 (**B**). Data are represented as the mean and S.E.M. with non-linear curve fit to calculate the IC₅₀.

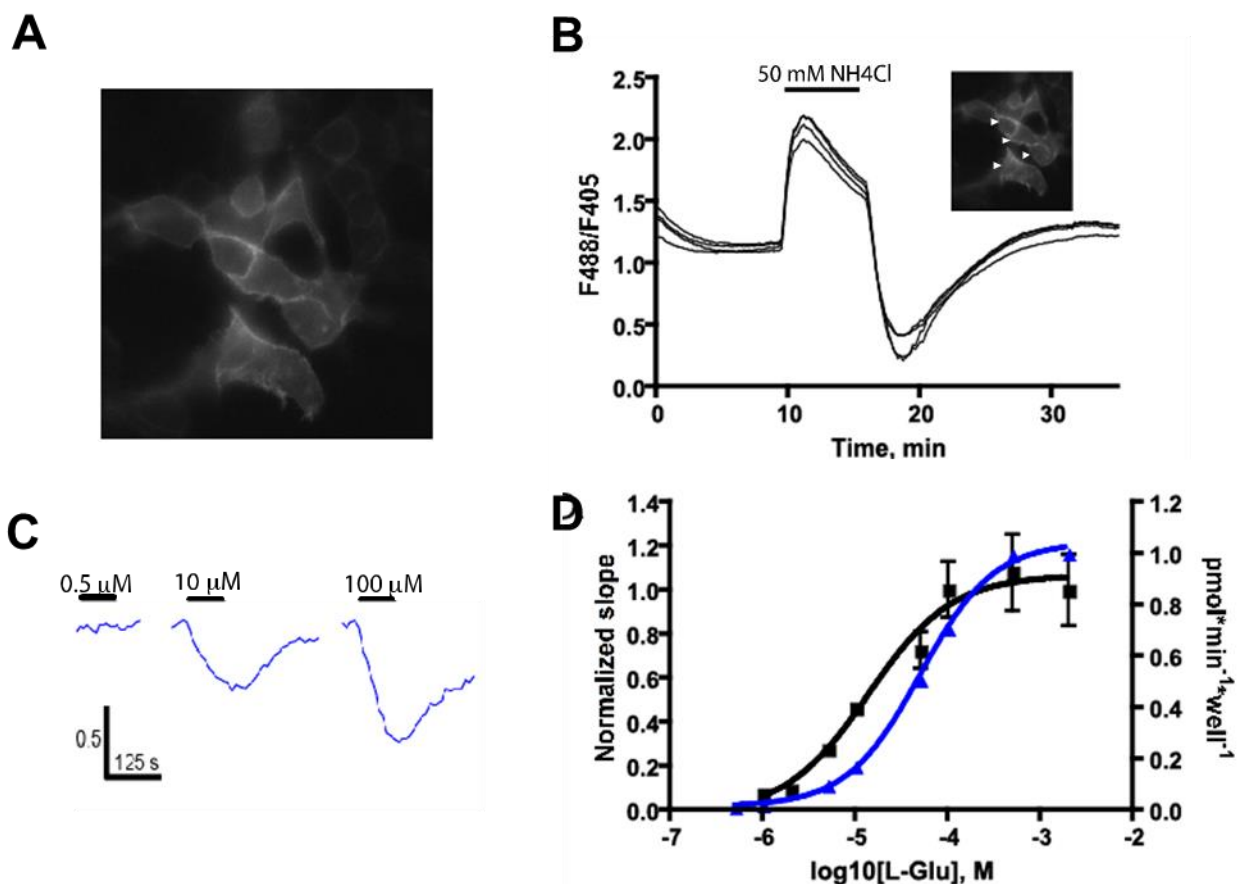


Figure C3. mEGFPpH detects intracellular pH changes induced by glutamate transport.

A) Representative fluorescent image of HEK293 cells transiently expressing the membrane bound (myristolated) EGFPpH sensor. **B)** Representative fluorescence traces of mEGFPpH transfected HEK293 cells (inset) perfused with 50 mM NH₄Cl. Left axis indicates the ratio of fluorescence from excitation at 488 nm to fluorescence of excitation 410 nm (F_{488}/F_{410}). Arrows in inset indicate cells from which traces were recorded. **C)** Perfusion of increasing concentrations of L-Glu results in increased rate and amplitude of mEGFPpH fluorescence decrease in HEK293 cells co-transfected with hEAAT3 and mEGFPpH. **D)** Comparison plot of the magnitude of the slope of EGFPpH F_{488}/F_{410} decrease (left y-axis) as a function of the applied L-glutamate concentration and that obtained for [³H]-L-glutamate transport activity (right y-axis) in similarly transfected cells. L-glutamate induced a concentration dependent and

saturatable increase in the rate of mEGFPpH F_{488}/F_{410} decrease that was similar to the rate of [^3H]-L-Glu transport over the same range.

reliable sensor for monitoring pH dependent transport processes (Figure C3B). As predicted, perfusion of increasing concentrations of the substrate glu caused a concentration-dependent decrease in 488/405 fluorescent ratio in HEK293 cells transfected with both EAAT3 and the mEGFPpH sensor indicative of a net acidic transport process. These data support the use of this sensor as readout for proton coupled transport.

C.4.4. Cysteine is Transported as a Thiolate Anion Through EAAT3

If cys is transported in the neutral zwitterionic form, then the carrier would need to bind a proton from the extracellular milieu to complete the coupling normal for transport of a substrate. This would create a net acidic transport cycle as demonstrated for the transport of glu (Figure C3C). Alternatively, if EAAT3 is mediating a deprotonation mechanism for bound cysteine, then at physiological pH, the negatively charged cysteine would rebind a proton once released to the intracellular space (assuming a normal pK_a for cys of 8.3). Therefore, our mEGFPpH sensor should delineate between these two processes. With HEK293 cells transiently expressing either EAAT2 or EAAT3 and the mEGFPpH sensor, application of 100 μ M caused a decrease in the fluorescent ratio indicative of a net intracellular accumulation of protons, as previously described for glu transport (Figure C4A and C4B, left) (6). Likewise, application of 200 μ M Secys also caused the net influx of protons in a mechanism indistinguishable from glu transport (Figure C4A and C4B, right). In contrast, application of 1 mM cys did not elicit any transport response in EAAT2, but elicited a small increase in the fluorescent ratio, consistent with a transport cycle which did not mediate the net influx of protons. These data indicate that cys is transported as the negatively charged thiolate which presumably rebinds intracellular protons after deocclusion from the EAATs. With the elimination of alternative hypotheses, it is most likely that EAAT3 mediates the deprotonation of bound cysteine, completing the stoichiometric coupling of the transport cycle

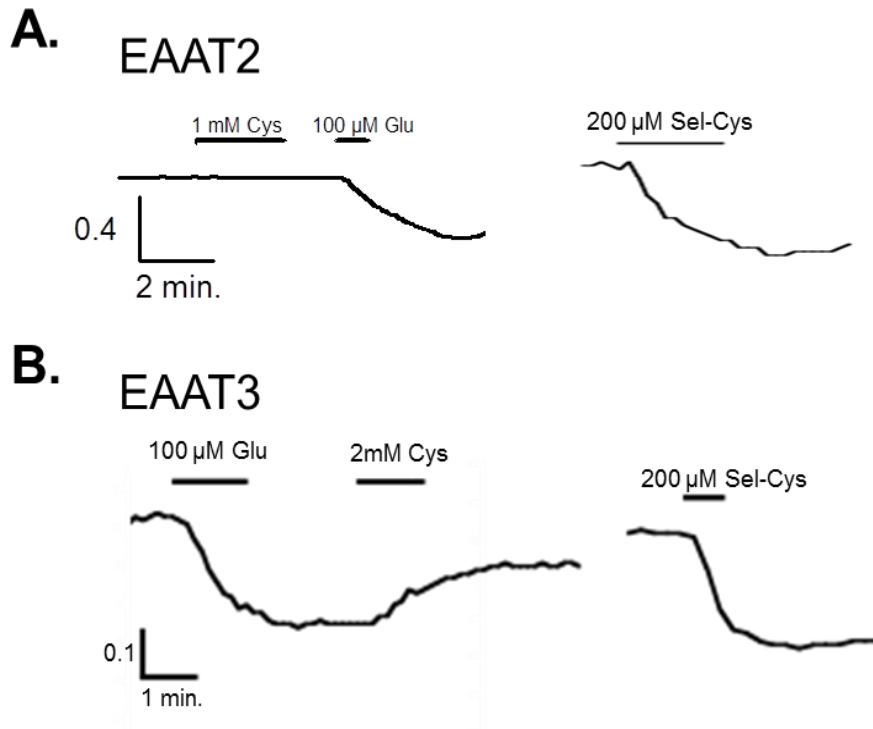


Figure C4 Transport of substrates in cells expressing hEAAT2 and hEAAT3 differentially affects intracellular pH. A) In cells co-expressing hEAAT2, 1 mM L-Cys induces no change in mEGFPpH fluorescence while 100 μ M L-Glu and 100 μ M L-Selenocysteine induce intracellular acidification (decreasing fluorescence). B) In cells co-expressing hEAAT3, 1 mM L-Cys induces intracellular alkalinization (increasing fluorescence) while 100 μ M L-Glu and 100 μ M L-Selenocysteine both induce intracellular acidification (decreasing fluorescence).

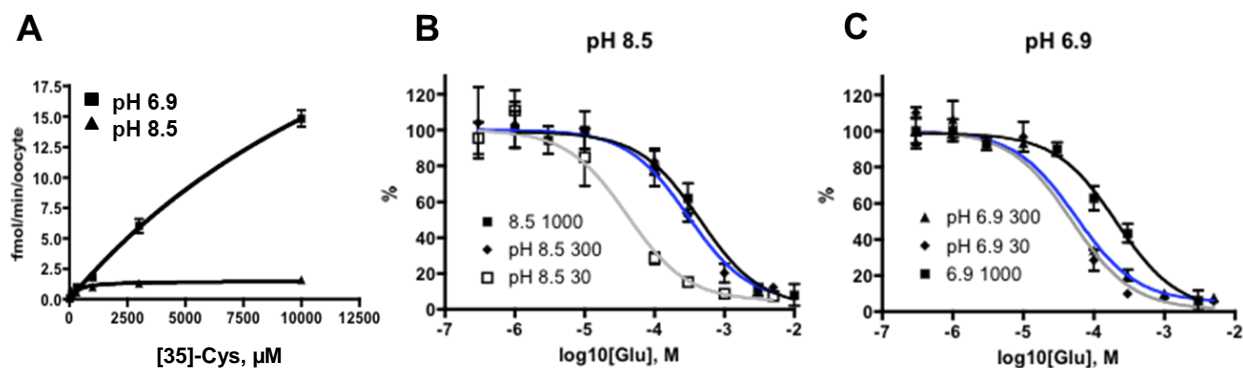


Figure C5. Effect of pH on L-cysteine transport properties of hEAAT3. **A)** Concentration dependent [35 S]-L-Cys transport in hEAAT3 expressing oocytes at pH 6.9 and pH 8.5 with Michaelis-Menten curve fit, with calculated K_m of $> 2 \text{ mM}$ and $660 \mu\text{M}$ for pH 6.9 and pH 8.5 respectively. **B)** and **C)** Inhibition of [35 S]-L-cysteine transport (30 μM , 300 μM , or 1000 μM L-cys) at varying concentrations of L-glutamate in hEAAT3 expressing oocytes measured at pH 6.9 (B) and pH 8.5 (C).

either with the proton gained from the cys substrate itself, or by shuffling the cys side chain proton to the extracellular milieu if a proton is already bound to the carrier (27).

C.4.5. pH Dependence of Cysteine Interactions in EAAT3

Our hypothesis is that EAAT3 is capable of a cys deprotonation scheme as part of the cys binding mechanism. If true, one would expect to see a pH dependence to cysteine interactions. We measured the transport kinetics of ^{35}S -cys through EAAT3 expressed in *Xenopus* oocytes and, as predicted, transport velocity was drastically increased at pH 6.9 as compared to transport at pH 8.5. Additionally, the competitive binding of glu and cys to EAAT3 displayed interesting pH dependences. The IC_{50} for glu inhibition of cys at high pH (8.5), where > 50% of the cys present is in its deprotonated form, was dependent on the concentration of cys present. With 30 μM cys, IC_{50} of glu was $31.5 \pm 7.13 \mu\text{M}$ (Figure C5B). At higher concentrations of cys, the IC_{50} was shifted to $267.1 \pm 12.1 \mu\text{M}$ and $455.5 \pm 157.8 \mu\text{M}$ for 300 μM and 1 mM cys, respectively. When these experiments were replicated with a pH of 6.9, where the cys present is in its protonated form, the IC_{50} of glu inhibition of cys was $42.8 \pm 9.8 \mu\text{M}$ and 42.5 ± 12.1 for 30 μM and 300 μM cys, but only at the highest concentration of 1 mM was the IC_{50} right shifted to $210.3 \pm 58.8 \mu\text{M}$. We interpret this data to signify that cys behaves as two different substrates in its competition to glu, depending on the protonation of its side chain thiol group. These complex kinetic behaviors support that EAAT3 has a different relative affinity and therefore molecular interaction with cys when deprotonated. After the induced fit of binding, likely satisfaction of the R477 (EAAT3) side chain, does the thiolate form of cys translocate across the membrane.

C.5. DISCUSSION

Here we investigated the mechanism of cys transport by the SLC1 family of glutamate transporters. The EAAC1 (EAAT3) knockout animal model displayed a distinct phenotype where glutathione production was severely hindered and there was a significant increase in reactive oxygen species and loss of neurons in these mice (15). Several other lines of evidence support

the role of EAAT3 mediated cys transport in the central nervous system (22,23,28,29). Therefore, if EAAT3 is the sole source of cys for neurons in the nervous system, it would be of great importance for future investigations.

The role of EAAT3 in cys transport is hard to resolve since there are several known transport machinery that are capable of cys translocation across the membrane. For example, the alanine/serine/cysteine transporters (ASCTs) are neutral amino acid exchangers which can readily mediate the flux of cysteine and are strongly expressed in the CNS.(30-33). These carriers are members of the SLC1 family of transporter and share ~35 % homology to the EAATs. The role of ASCTs have not been confirmed with knockout studies yet it has been proposed that ASCT2 plays a role in glutamine translocation and is involved in the glutamate-glutamine pathway (34,35). In contrast, ASCT1 does not transport gln and, thus, may play a role in the exchange of cys in neurons (30). There are two other transport systems which may play a role in the translocation of cys *in vivo*. System N and A transporters of sodium coupled neutral amino acid transporters (SNATs) can mediate the transport of cysteine but their roles have been limited to regulating glutamine transport in the glutamate-glutamine cycle similar to ASCT2 (36). Additionally cysteine-glutamate exchangers (XCTs) are also present and may be another candidate for cysteine accumulation in neurons. Indeed, it has been proposed that XCTs and EAATs 3 and 4 may work together to drive GSH production (37). Thus with so many different transporters co-localized in the same systems, it is challenging to resolve the individual roles of each carrier or how they coordinate to mediate cysteine metabolism in the CNS.

Zerangue and Kavanaugh (1996) originally proposed that cysteine transport occurred through EAAT3 as the neutral zwitterionic form of cysteine due to a lack of alteration to the EC₅₀ at pH higher than 7.5. This is not surprising because our data suggest that the transporter can readily mediate the deprotonation of cys and so shifting the equilibrium toward the thiolate species in solution would not necessarily reveal any insight into the mechanism of transport. Our data supports the transport of cys as a negatively charged species for multiple reasons.

First, a recent series of crystal structures from an archeal homolog of the EAATs, Glt_{Ph}, depicts several substrate and inhibitor interactions (38,39). In these structures, substrates are demonstrated to be coordinated by several residues which have been previously substantiated to have a role in substrate interactions. For example, mutation of R447 (EAAC1) drastically alters the substrate specificity of EAATs from a preference for acidic substrates to neutral substrates. The Glt_{Ph} crystal structure also depicts the coordination of the side chain carboxylic group by R397 (the equivalent residue to R447). Thus, it is highly likely that EAATs can only mediate the interaction with anionic species due to the necessary interaction with the positively charged R447 residue. The only manner in which cys could satisfy the charge of this coordinating residue is if cys is transported as the negatively charged thiolate form. Second, Secys is an excellent congener for cys and is readily transported by all EAAT isoforms with an apparent affinity and velocity similar to glu. The structure of cys and Secys are near identical and the only major difference between these two substrates is the pK_a of the side chain. Secys, with a pK_a ~5.3, would be predominately deprotonated and negatively charged at physiological pH. This charged species can readily interact with the EAAT binding sites of any isoform. However, only EAAT3 can readily mediate transport of cys, suggesting that there is a particular mechanism in place for the deprotonation of glu by EAAT3 alone. Additional evidence which supports this mechanism is the lack of net acidic transport with the translocation of cys by EAAT3. Both glu and Secys mediate the net influx of a proton during the transport cycle yet cys does not demonstrate this property. The only mechanism which explains this phenomenon is that cys is transported as a thiolate which then rebinds a proton once it is released to the intracellular milieu.

It is unclear exactly how the deprotonation of cys is mediated by EAAT3. Work done by Watzke et al. (2000) resolved the lingering question at the time of whether the pH altering species in the EAAT transport cycle was a proton or a hydroxyl ion (27,40,41). Additionally, the authors demonstrated that the ordered binding of substrates to the outward-open conformation

of EAAC1 would occur with glu (or cys) binding after the proton (42). Furthermore, investigations in the residue E373 (EAAC1) revealed its involvement with the protonation mechanism in some manner, due to the loss of pH dependent transport with mutations at this position. The role of E373, however, is not entirely clear as it also forces the transporter into the obligate exchange mode of glu translocation and this phenomena is replicated with Y374 (EAAC1) mutations which show a loss of K^+ interaction (43). It is possible that the sites of K^+ and H^+ interaction are the same but clearly more research will be needed to unravel these interactions further. Our data does not dispute the ordered binding of substrates as we cannot distinguish the order in our experimental models, nonetheless, our data do support a mechanism that is dependent on pH. In order to resolve our data with those previously published, our model involves a proton shuffle mechanism with the transfer of the cys side chain proton, releasing a previously bound proton to the extracellular space, allowing for the induced fit or lower energy interaction of the cysteine thiolate side chain with R447. Although this mechanism is speculative currently, it does fit with all available data. To further resolve the exact binding mechanism and downstream steps, additional experiments would be necessary which employ higher resolution techniques.

Here we resolved the mechanism of substrate interactions in the family of EAATs. Cys is a rate limiting precursor for GSH synthesis and the mechanism of cys regulation and transport remains unclear. Although there are a number of carriers which have been demonstrated to be capable of cys transport *in vitro*, EAAT3 has been demonstrated to modulate GSH levels and neuronal viability *in vivo*. One remaining question is how EAAT3 mediates cys transport *in vivo*, especially considering the exposure of EAAT3 to glu during excitatory neurotransmission. It is possible that while EAAT2 mediates the majority of glu transport during neurotransmission, EAAT3 is responsible for a basal level of cys transport which can mediate the necessary synthesis of GSH, protecting neurons from oxidative stress. Our data here clarify the role of

EAAT3 in cysteine transport and resolve disparate data in the field concerning this substrate-carrier interaction.

C.6. REFERENCES

1. Tzingounis, A. V., and Wadiche, J. I. (2007) Glutamate transporters: confining runaway excitation by shaping synaptic transmission. *Nat Rev Neurosci* **8**, 935-947
2. Arriza, J. L., Fairman, W. A., Wadiche, J. I., Murdoch, G. H., Kavanaugh, M. P., and Amara, S. G. (1994) Functional comparisons of three glutamate transporter subtypes cloned from human motor cortex. *J Neurosci* **14**, 5559-5569
3. Grunewald, M., and Kanner, B. I. (2000) The accessibility of a novel reentrant loop of the glutamate transporter GLT-1 is restricted by its substrate. *J Biol Chem* **275**, 9684-9689
4. Slotboom, D. J., Sobczak, I., Konings, W. N., and Lolkema, J. S. (1999) A conserved serine-rich stretch in the glutamate transporter family forms a substrate-sensitive reentrant loop. *Proc Natl Acad Sci U S A* **96**, 14282-14287
5. Seal, R. P., Leighton, B. H., and Amara, S. G. (2000) A model for the topology of excitatory amino acid transporters determined by the extracellular accessibility of substituted cysteines. *Neuron* **25**, 695-706
6. Zerangue, N., and Kavanaugh, M. P. (1996) Flux coupling in a neuronal glutamate transporter. *Nature* **383**, 634-637
7. Fairman, W. A., Vandenberg, R. J., Arriza, J. L., Kavanaugh, M. P., and Amara, S. G. (1995) An excitatory amino-acid transporter with properties of a ligand-gated chloride channel *Nature* **375**, 599-603
8. Torres-Salazar, D., and Fahlke, C. (2006) Intersubunit interactions in EAAT4 glutamate transporters *J Neurosci* **26**, 7513-7522
9. Watzke, N., Bamberg, E., and Grewer, C. (2001) Early intermediates in the transport cycle of the neuronal excitatory amino acid carrier EAAC1 *J Gen Physiol* **117**, 547-562

10. Torres-Salazar, D., and Fahlke, C. (2007) Neuronal Glutamate Transporters Vary in Substrate Transport Rate but Not in Unitary Anion Channel Conductance in *The Journal of Biological Chemistry*
11. Melzer, N., Biela, A., and Fahlke, C. (2003) Glutamate modifies ion conduction and voltage-dependent gating of excitatory amino acid transporter-associated anion channels *J Biol Chem* **278**, 50112-50119
12. Bergles, D. E., Tzingounis, A. V., and Jahr, C. E. (2002) Comparison of coupled and uncoupled currents during glutamate uptake by GLT-1 transporters. *J Neurosci* **22**, 10153-10162
13. Kanai, Y., and Hediger, M. A. (1992) Primary structure and functional characterization of a high-affinity glutamate transporter. *Nature* **360**, 467-471
14. Zerangue, N., and Kavanaugh, M. P. (1996) Interaction of L-cysteine with a human excitatory amino acid transporter. *J Physiol* **493 (Pt 2)**, 419-423
15. Aoyama, K., Suh, S. W., Hamby, A. M., Liu, J., Chan, W. Y., Chen, Y., and Swanson, R. A. (2006) Neuronal glutathione deficiency and age-dependent neurodegeneration in the EAAC1 deficient mouse. *Nat Neurosci* **9**, 119-126
16. Dringen, R. (2000) Glutathione metabolism and oxidative stress in neurodegeneration. *Eur J Biochem* **267**, 4903
17. Diamond, J. S., and Jahr, C. E. (1997) Transporters buffer synaptically released glutamate on a submillisecond time scale. *J Neurosci* **17**, 4672-4687
18. Grewer, C., Watzke, N., Wiessner, M., and Rauen, T. (2000) Glutamate translocation of the neuronal glutamate transporter EAAC1 occurs within milliseconds. *Proc Natl Acad Sci U S A* **97**, 9706-9711
19. Lehre, K. P., and Danbolt, N. C. (1998) The number of glutamate transporter subtype molecules at glutamatergic synapses: chemical and stereological quantification in young adult rat brain. *J Neurosci* **18**, 8751-8757

20. Holmseth, S., Dehnes, Y., Huang, Y. H., Follin-Arbelet, V. V., Grutle, N. J., Mylonakou, M. N., Plachez, C., Zhou, Y., Furness, D. N., Bergles, D. E., Lehre, K. P., and Danbolt, N. C. (2012) The Density of EAAC1 (EAAT3) Glutamate Transporters Expressed by Neurons in the Mammalian CNS. *The Journal of neuroscience : the official journal of the Society for Neuroscience* **32**, 6000-6013
21. Mathews, G. C., and Diamond, J. S. (2003) Neuronal glutamate uptake Contributes to GABA synthesis and inhibitory synaptic strength. *The Journal of neuroscience : the official journal of the Society for Neuroscience* **23**, 2040-2048
22. Aoyama, K., Watabe, M., and Nakaki, T. (2012) Modulation of neuronal glutathione synthesis by EAAC1 and its interacting protein GTRAP3-18. *Amino acids* **42**, 163-169
23. Watabe, M., Aoyama, K., and Nakaki, T. (2007) Regulation of glutathione synthesis via interaction between glutamate transport-associated protein 3-18 (GTRAP3-18) and excitatory amino acid carrier-1 (EAAC1) at plasma membrane. *Mol Pharmacol* **72**, 1103-1110
24. Berman, A. E., Chan, W. Y., Brennan, A. M., Reyes, R. C., Adler, B. L., Suh, S. W., Kauppinen, T. M., Edling, Y., and Swanson, R. A. (2011) N-acetylcysteine prevents loss of dopaminergic neurons in the EAAC1^{-/-} mouse. *Ann Neurol* **69**, 509-520
25. Elsliger, M. A., Wachter, R. M., Hanson, G. T., Kallio, K., and Remington, S. J. (1999) Structural and spectral response of green fluorescent protein variants to changes in pH. *Biochemistry* **38**, 5296-5301
26. Watts, S. D., Suchland, K. L., Amara, S. G., and Ingram, S. L. (2012) A sensitive membrane-targeted biosensor for monitoring changes in intracellular chloride in neuronal processes. *PloS one* **7**, e35373
27. Watzke, N., Rauen, T., Bamberg, E., and Grewer, C. (2000) On the mechanism of proton transport by the neuronal excitatory amino acid carrier 1. *J Gen Physiol* **116**, 609-622

28. Aoyama, K., Matsumura, N., Watabe, M., and Nakaki, T. (2008) Oxidative stress on EAAC1 is involved in MPTP-induced glutathione depletion and motor dysfunction. *Eur J Neurosci* **27**, 20-30
29. Aoyama, K., and Nakaki, T. (2013) Neuroprotective properties of the excitatory amino acid carrier 1 (EAAC1). *Amino acids* **45**, 133-142
30. Arriza, J. L., Kavanaugh, M. P., Fairman, W. A., Wu, Y. N., Murdoch, G. H., North, R. A., and Amara, S. G. (1993) Cloning and expression of a human neutral amino acid transporter with structural similarity to the glutamate transporter gene family. *J Biol Chem* **268**, 15329-15332
31. Zerangue, N., and Kavanaugh, M. P. (1996) ASCT-1 is a neutral amino acid exchanger with chloride channel activity *J Biol Chem* **271**, 27991-27994
32. Utsunomiya-Tate, N., Endou, H., and Kanai, Y. (1996) Cloning and functional characterization of a system ASC-like Na⁺-dependent neutral amino acid transporter. *J Biol Chem* **271**, 14883-14890
33. Broer, A., Wagner, C., Lang, F., and Broer, S. (2000) Neutral amino acid transporter ASCT2 displays substrate-induced Na⁺ exchange and a substrate-gated anion conductance. *Biochem J* **346 Pt 3**, 705-710
34. Uwechue, N. M., Marx, M. C., Chevy, Q., and Billups, B. (2012) Activation of glutamate transport evokes rapid glutamine release from perisynaptic astrocytes. *The Journal of physiology* **590**, 2317-2331
35. Rusakov, D. A. (2012) Astroglial glutamate transporters trigger glutaminergic gliotransmission. *J Physiol* **590**, 2187-2188
36. Chaudhry, F. A., Reimer, R. J., and Edwards, R. H. (2002) The glutamine commute: take the N line and transfer to the A. *J Cell Biol* **157**, 349-355

37. Lim, J., Lam, Y. C., Kistler, J., and Donaldson, P. J. (2005) Molecular characterization of the cystine/glutamate exchanger and the excitatory amino acid transporters in the rat lens. *Invest Ophthalmol Vis Sci* **46**, 2869-2877
38. Yernool, D., Boudker, O., Jin, Y., and Gouaux, E. (2004) Structure of a glutamate transporter homologue from *Pyrococcus horikoshii*. *Nature* **431**, 811-818
39. Boudker, O., Ryan, R. M., Yernool, D., Shimamoto, K., and Gouaux, E. (2007) Coupling substrate and ion binding to extracellular gate of a sodium-dependent aspartate transporter. *Nature* **445**, 387-393
40. Amato, A., Ballerini, L., and Attwell, D. (1994) Intracellular pH changes produced by glutamate uptake in rat hippocampal slices. *J Neurophysiol* **72**, 1686-1696
41. Bouvier, M., Szatkowski, M., Amato, A., and Attwell, D. (1992) The glial cell glutamate uptake carrier countertransports pH-changing anions. *Nature* **360**, 471-474
42. Grewer, C., Watzke, N., Rauen, T., and Bicho, A. (2003) Is the glutamate residue Glu-373 the proton acceptor of the excitatory amino acid carrier 1? *J Biol Chem* **278**, 2585-2592
43. Zhang, Y., Bendahan, A., Zerbiv, R., Kavanaugh, M. P., and Kanner, B. I. (1998) Molecular determinant of ion selectivity of a (Na⁺ + K⁺)-coupled rat brain glutamate transporter. *Proc Natl Acad Sci U S A* **95**, 751-755

APPENDIX D: COUPLING BETWEEN SUBSTRATE TRANSPORT AND ANION CHANNEL GATING IN EXCITATORY AMINO ACID TRANSPORTERS

D.1. SUMMARY OF CONTRIBUTIONS

My contribution to the document below warrant both inclusion as a co-author as well as inclusion in my thesis document. Since the inception of the study I have provided significant input in both the development of experiments, interpretation of results, writing of the document, as well as addressing outside readers concerns. Specifically, I significantly helped in interpretation of R388 transport activity, L376C mediated structural changes, TBOA mediated stabilization of outward facing states, and many aspects of the project that were not included in the manuscript as written here. For example, I designed and executed several experiments aimed at how R388C could be used to further our understanding of the role of this residue in mediating substrate transport and channel gating mechanism although these data was not included in the final drafts of the manuscript for issues of clarity.

D.2. ABSTRACT

In the mammalian central nervous system, excitatory amino acid transporters (EAATs) are responsible for the binding and reuptake of glutamate after release into the synapse. This activity is crucial for precise neuronal communication and for maintaining extracellular glutamate concentrations below neurotoxic levels. In addition to their ability to transport glutamate from the extracellular space, EAATs also have a thermodynamically-uncoupled anion conductance. Using site directed mutagenesis and electrophysiological recordings in *Xenopus* oocytes, we have identified a highly conserved, positively charged residue in transmembrane domain 7

(TM7) that when substituted for a negative charged amino acid eliminates both substrate gated anion conductance and substrate transport current. Our data suggest that this mutation locks the chloride channel in the Na-bound conducting state and therefore no increase in the anion current is observed upon application of saturating concentrations of glutamate. This is the first evidence of a residue that directly modulates both substrate transport and substrate-dependent gating of the anion conductance. The data presented here suggest that arginine 388 (EAAT1) may be playing a crucial role in the coupling of substrate transport and substrate-dependent anion channel gating. We believe this mutant can be used as a tool to better understand the structural basis of anion permeation through EAATs, as well as the conformational changes involved in substrate-dependent anion channel opening.

D.3. INTRODUCTION

The major excitatory neurotransmitter glutamate is efficiently cleared from the extracellular space into surrounding neuronal and glial cells through a transport mechanism mediated by excitatory amino acid transporters (EAATs). This mechanism prevents sustained glutamate receptors activation which can cause neuronal death by excitotoxic mechanisms (1). EAATs couple the influx of one glutamate molecule to the inward movement of three sodium ions, one proton, and to the counter transport of one potassium ion (2,3). In addition, they mediate a thermodynamically-uncoupled anion conductance that is either a leak conductance or is gated by Na^+ and substrate interactions (4-6). The EAAT-associated anion conductance has been suggested to support electrogenic glu uptake by holding the membrane potential to negative values (5,7) as well as dampening cell excitability and preventing additional glutamate release (8-10).

EAATs quaternary structure are homotrimeric complexes of three identical subunits (11-14) with 8 transmembrane (TM) domains and two reentrant hairpin loops (HP1 and HP2) (11,15-17). Although many studies have contributed to our understanding of the transport

mechanism in the EAATs, less is known about the structural-function relationship of the uncoupled anion conductance mediated by this class of proteins. Residues located on TM2 have been reported to affect anion permeation and even anion selectivity (18), suggesting that the permeation pore may be formed by the residues from this region. Interpretation of data from experiments designed to elucidate the gating mechanism of the anion channel in the EAATs has proven challenging. Conserved residues in TM2 (19), TM5, TM7 (20), and HP2 (6) have been mutated and observed to impact anion permeation and/or gating. Interestingly, none of those mutant transporters showed a major effect on substrate transport (6,19-21). Therefore, it is likely that the pore domain is located in a region of the transporter that is distinct from the regions of substrate interactions. However, the substrate dependence of the gating mechanism would suggest that residues which couple these two processes would exist and mutations of such residues would impact the relationship between substrate binding, transport, and channel activity.

In the present study, we identified a highly conserved basic residue in the N-terminal segment of TM7 (R388 in EAAT1) that affected both substrate transport and gating of the anion channel. The EAAT-associated anion conductance is a pore mediated anion permeation that has been demonstrated to have multiple conducting states. The leak conductance is activated by Na⁺ ions in the absence of glu (22-24) in neuronal isoforms and the substrate gated conductance state is reached upon application of glu or aspartate (asp) in the presence of Na⁺ (4,5,22). When the conserved residue R388 (EAAT1) is mutated to an acidic amino acid, the leak conductance is observed, but neither the EAAT-associated substrate gated anion current (Figure 2) nor the electrogenic transport current remains (Figure 1C and D). The physiological relevance of the EAAT-associated chloride conductance has been resolved only for the EAAT5 isoform. Identification of regions involved in anion channel gating as well as the regions lining the aqueous permeation pore will provide strong tools for future exploration of the role of channel functionality in the EAATs.

D.4. EXPERIMENTAL PROCEDURE

D.4.1. Heterologous Expression of hEAAT1

Point mutations were introduced into the wild type (WT) hEAAT1, cysteineless hEAAT1 (hEAAT1Cs) and WT rEAAT4 cDNAs using the QuikChange mutagenesis kit (Stratagene). EAAT1 and EAAT4 capped cRNA was synthesized from SmaI-linearized pOTV constructs through use of MESSAGE machine kits (Ambion, Austin, TX). Subsequently, cRNA was resuspended in 10 μ l of water, and stored in 2- μ l aliquots at -80°C until use. 50 nl of cRNA were injected using a nanoliter injector (Nanoliter 2000, World Precision Instruments, Sarasota, FL, USA), and oocytes were kept at 18°C in ND-96 solution supplemented with 2.5 mM sodium pyruvate and 100 $\mu\text{g/ml}$ gentamycin sulfate until recording. Oocytes expressing hEAAT1 and rEAAT4 were measured 2 to 3 days after injection. Since we performed cysteine substitutions for cysteine modification experiments on hEAAT1, all the hEAAT1 mutant transporters were constructed on a cysteine-null transporter (hEAAT1Cs).

D.4.2. Electrophysiology

Glutamate transporter-associated currents were recorded in oocytes by two-electrode voltage clamp using a GeneClamp500B (Axon Instruments, Union City, CA, USA) amplifier. Recording solution contain (in mM): 96 NaCl, 4 KCl, 0.3 CaCl_2 , 1 MgCl_2 , 5 HEPES, pH 7.4. Oocytes were held at 0 mV, and currents elicited by 200 ms voltage steps between -100 mV and $+60$ mV were filtered at 2kHz (-3dB) and digitalized with a sampling rate of 10 kHz using a Digidata 1332 AD/DA converter (Axon Instruments, Union City, CA, USA). Glutamate transport currents were measured by subtracting current amplitudes in a NaCl-based glutamate-free solution from current amplitudes in an external solution supplemented with 1 mM L-glutamate. Anion currents were determined after exchanging the external solution to (in mM): 96 NaNO_3 , 4 KCl, 0.3 CaCl_2 , 1 MgCl_2 , 5 HEPES, pH 7.4 in the absence or in the presence of 1 mM external glutamate without any current subtraction procedure.

D.4.3. Radiolabeled Transport Assays

Radiolabeled transport assays were performed in *Xenopus* oocytes 2-3 days after injection with EAAT cRNA. Oocytes were washed 3 times by transferring to wells containing ND96 buffers and with gentle agitation. Oocytes were then transferred to wells containing 200 nM 3,4,-³H-L-glutamate (Perkin Elmer) for 10 min before transferring to wash wells to remove residual glutamate with ice cold ND96. Oocytes were lysed with 0.1 N NaOH and 1% SDS and the accumulated radiolabeled substrate was counted in the individual oocytes by liquid scintillation counting.

D.4.4. Data Analysis

Data were analyzed with pClamp9 (Axon Instruments) and SigmaPlot (Jandel Scientific, San Rafael, CA, USA) programs. Current-voltage relationships at various substrate concentrations were constructed by plotting isochronal current amplitudes 5 ms after the voltage step versus the membrane potential.

D.5. RESULTS

D.5.1. Mutating Arginine 388 Affects Substrate Transport

In order to investigate both anion channel activity as well as substrate transport properties of EAAT1, we mutated arginine 388 (R388 hEAAT1), a highly conserved residue located at the tip of TM7 (Figure 1A and B). When R388 is substituted by a small non-polar amino acid, both transport current and substrate gated anion permeation are reduced by about 80%. Nevertheless in these mutant transporters glu is still able to gate the substrate-gated anion conductance and its transport remains electrogenic (Supplementary Figure 1). On the other hand, when this positively charged residue is substituted by an acidic amino acid, the

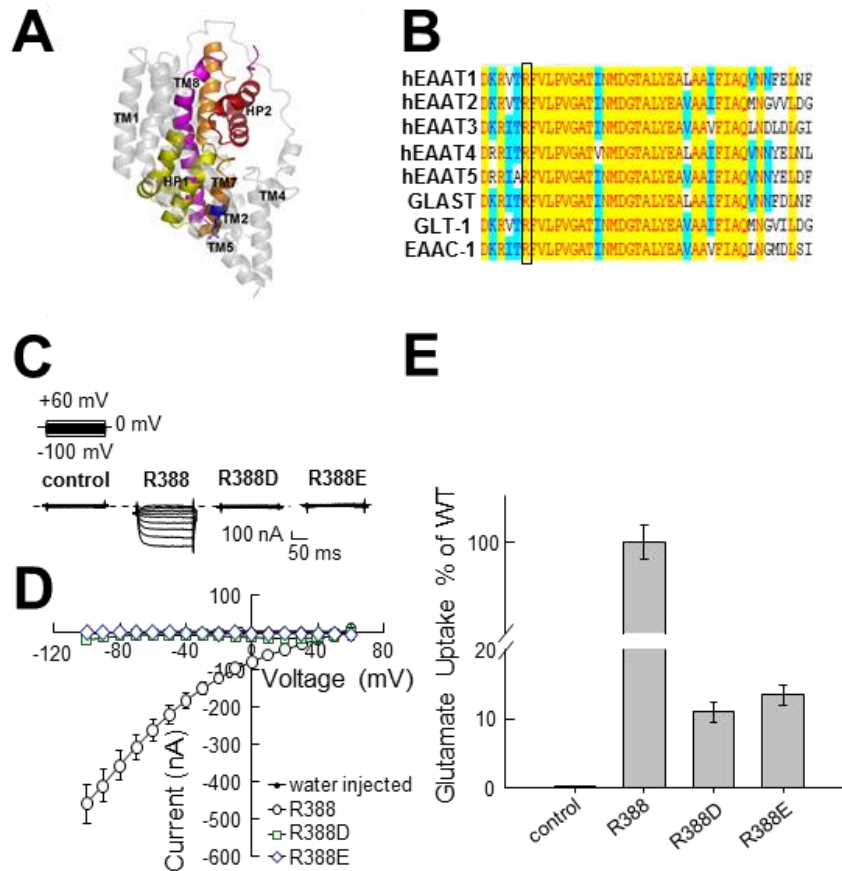


Figure D1. R388 has a significant role in substrate transport. **(A)** Localization of residue R388 (highlighted in blue) in the ribbon representation of a monomeric subunit of EAATs. Highlighted in colors are HP1 (yellow), TM7 (orange), HP2 (red) and TM8 (magenta). **(B)** Alignment of the region of the primary amino acid sequence containing R388 (boxed) in several EAAT isoforms. Totally conserved residues (yellow) and partially conserved residues (blue) are displayed in the alignment. **(C)** Representative current traces from oocytes expressing EAAT1 R388, R388D, and R388E, as well as water-injected oocytes in response to a series of voltage pulses from -100 to +60 mV. **(D)** Current-voltage relationship obtained from oocytes expressing EAAT1 R388 (open circles, n=7), EAAT1 R388D (open squares, n=7) and EAAT1 R388E (open diamonds, n=8), as well as from water-injected oocytes (n=6). Na^+ gated currents were subtracted from glu induced current amplitudes for clarity. **(E)** Radioactive glu uptake from the

same oocytes in B). Controls represent water injected oocytes. Error bars represent standard deviation of the mean. For statistical evaluation, Student's t-Test was used.

mutant transporters are no longer able to elicit substrate transport currents nor glutamate gated anion permeation (Figure 1 and 2).

Figure 1C and 1D show representative recordings and averaged current-voltage (I-V) relationships from oocytes expressing either hEAAT1 cysteine-less wild type (hEAAT1Cs) (black open circles), hEAAT1Cs R388D (green open squares) or hEAAT1Cs R388E (blue open diamonds) in a NaCl based extracellular solution. EAAT currents in the presence of glu at negative potentials are comprised of the glu transport currents and to a lesser degree the anion channel mediated currents. In physiological conditions, transport currents show a strong voltage dependent inward rectification while the glu gated anion conductance is predominant at positive potentials (4,5). After subtraction of the currents recorded in the absence of glutamate, no R388 mutants displayed no significant currents which indicates that R388E/D mutants do not mediate an electrophysiological response to application of glu as compared to R388 (Figure 1C and 1D; n=5). No differences from background currents were observed in oocytes expressing hEAAT1Cs R388D or hEAAT1Cs R388E. The lack of transport currents in oocytes expressing the mutant transporters could be due to a failure of the mutant proteins to be synthesized, erroneous trafficking, a decreased expression in the plasma membrane, their incapacity to bind glutamate, or a disruption of the transport mechanism. To discriminate between these possibilities, we performed radiolabeled glu transport assays on the same oocytes after current measurements. Figure 1E demonstrates that although both mutants exhibit a reduced uptake activity compared with hEAAT1Cs WT, they do significantly accumulate glutamate more than tenfold above background (water injected oocytes), demonstrating that the mutant transporters are expressed and that glutamate not only can bind to these mutants but also can be translocated to the cytoplasm. The loss of transport currents in R388D and R388E while still exhibiting transport capacity for glu could be indicative of an exchange mechanism of transport. Without net glutamate translocation due to full cycle transport, EAAT do not generate transport currents (25-27). These results demonstrate that an acidic amino acid substitution in position

388 allows glutamate binding, but it causes a dramatic change in the transport mechanism, presumably preventing completion of the full transport cycle.

D.5.2. Arginine 388 Plays a Crucial Role in Anion Channel Gating

After measuring the transport currents in a NaCl-based solution (Figure 1), we perfused the same oocytes with a NaNO₃-based solution to study the effects of these mutations on the substrate gated anion conductance. Figure 2 shows I-V relationships in response to a series of voltage pulses from -100 to +60 mV in the absence (closed black circles) and the presence (open red circles) of 1 mM L-glu from oocytes expressing hEAAT1Cs WT (A, n=10), hEAAT1Cs R388D (B, n=7) or hEAAT1Cs R388E (C, n=8). We observed that the current in the presence of glutamate (red open circles) was not significantly different from the current in the absence of glu (closed black circles; corresponding data points superimpose). No substrate induced current was observed using either SCN⁻ as the main permeant anion in the presence of 1 mM glu or in the presence of 1 mM D-aspartate (Supplementary Figure 3). The currents recorded from hEAAT1Cs R388D and hEAAT1Cs R388E expressing oocytes are much larger than the currents obtained from water injected oocytes (Figure 2 B and C) and they are blocked by the competitive antagonist DL-threo-β-benzoyloxyaspartate (DL-TBOA) nearly to the background levels (Supplementary Figure 1), demonstrating that they are currents mediated by hEAAT1 transporters. These data suggest that R388 plays an important role in the mechanism coupling substrate interactions to anion channel gating.

D.5.3. Mutating Arginine 388 to an Acidic Amino acid, Shifts the Conformational Equilibrium of the Channel to the Leak Conducting States

The lack of glutamate induced currents in oocytes expressing either acidic amino acid substitution in the R388 position could be due to the channel being locked or constrained in its maximal open probability state in the absence of substrate. Another possibility is that these mutant transporters cannot undergo the conformational changes subsequent to glutamate

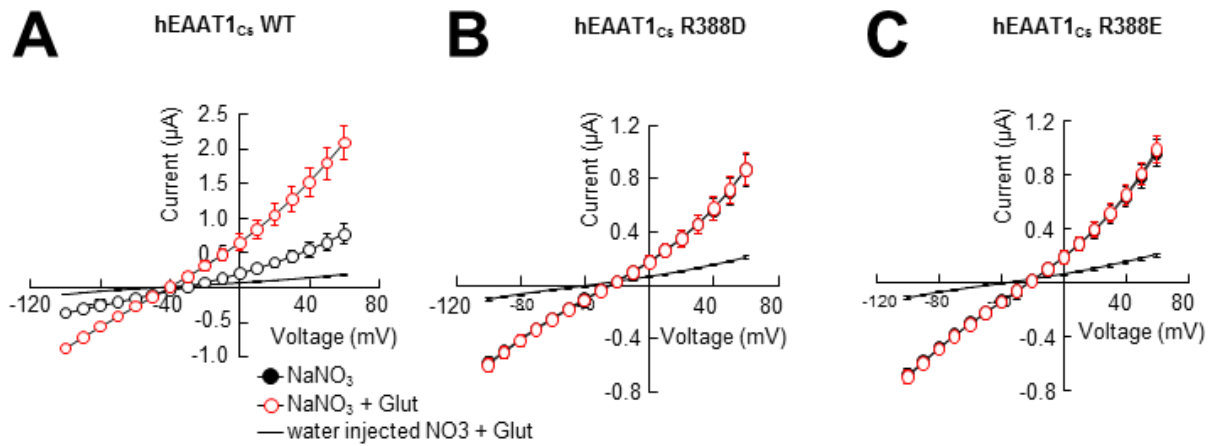


Figure D2. R388 has a crucial role in activating the substrate gated anion conductance.

(A-C) Current-Voltage relationship from oocytes expressing hEAAT1Cs WT (A, n=10), or R388D (B, n=7) or R388E (C, n=8) mutants perfused with a NO₃-based solution in the absence (closed black circles) and in the presence (open red circles) of 1 mM glutamate. Solid lines represent currents recorded in a NO₃-based solution in the presence of 1mM Glutamate from water-injected oocytes (n=6).

binding required to enter the substrate gated conducting state. In order to investigate the second of these two possibilities, we measured the relative anion conductance (which can be estimated by the ratio of the macroscopic current at a certain potential in the presence of one anion with respect to a different anion) of the wild type and mutant EAATs. As shown in Figure 3E and 3F (white bars, $n = 8$), application of 500 μM glutamate in oocytes expressing hEAAT1Cs WT increases both the $\text{NO}_3^-/\text{Cl}^-$ and the SCN^-/Cl^- relative conductances by approximately 3 fold as compared to Na^+ alone. Since glutamate did not increase the macroscopic current amplitude in any of the buffer conditions applied to oocytes expressing hEAAT1Cs R338D or hEAAT1Cs R388E mutants (Figure 3C and 3D, $n=6$) compared with hEAAT1Cs WT (Figure 3A and 3B, $n=8$), we expected the relative conductance for the mutants to be similar to either the Na^+ or $\text{Na}^+ + 500 \mu\text{M glu}$ conditions seen in hEAAT1Cs WT. As shown in Figure 3E and 3F (grey bars, $N = 6$) in Figure 3E and 3F (grey bars, $n=6$), the relative conductances measured from oocytes expressing R388D were identical to those corresponding to the Na^+ only condition in WT transporters, suggesting that the asp or glu substitution in this position prevents the channel from transitioning into the glutamate gated conducting state.

To further support our conclusion, we estimated and compared the relative permeability ratios between NO_3^- and Cl^- , as well as SNC^- and Cl^- . Since the relative permeability was previously demonstrated to be increased by glutamate application in the EAATs, we estimated the relative permeability ratios by measuring the reversal potential under different anion containing buffers in the presence of Na^+ alone or with Na^+ and 500 $\mu\text{M glu}$. Using the Goldman-Hodging-Katz equation and assuming the intracellular Cl^- concentration in the oocytes to be approximately 40 mM (20) one can calculate the relative permeability ratios for each of the conducting states. Unfortunately, due to the large transport current mediated by hEAAT1 transporters and its contribution to the total macroscopic current, the reversal potential of the anion conductance in the presence of glutamate cannot be accurately measured in oocytes expressing this isoform. Therefore, we expressed rEAAT4 WT and mutant transporters in

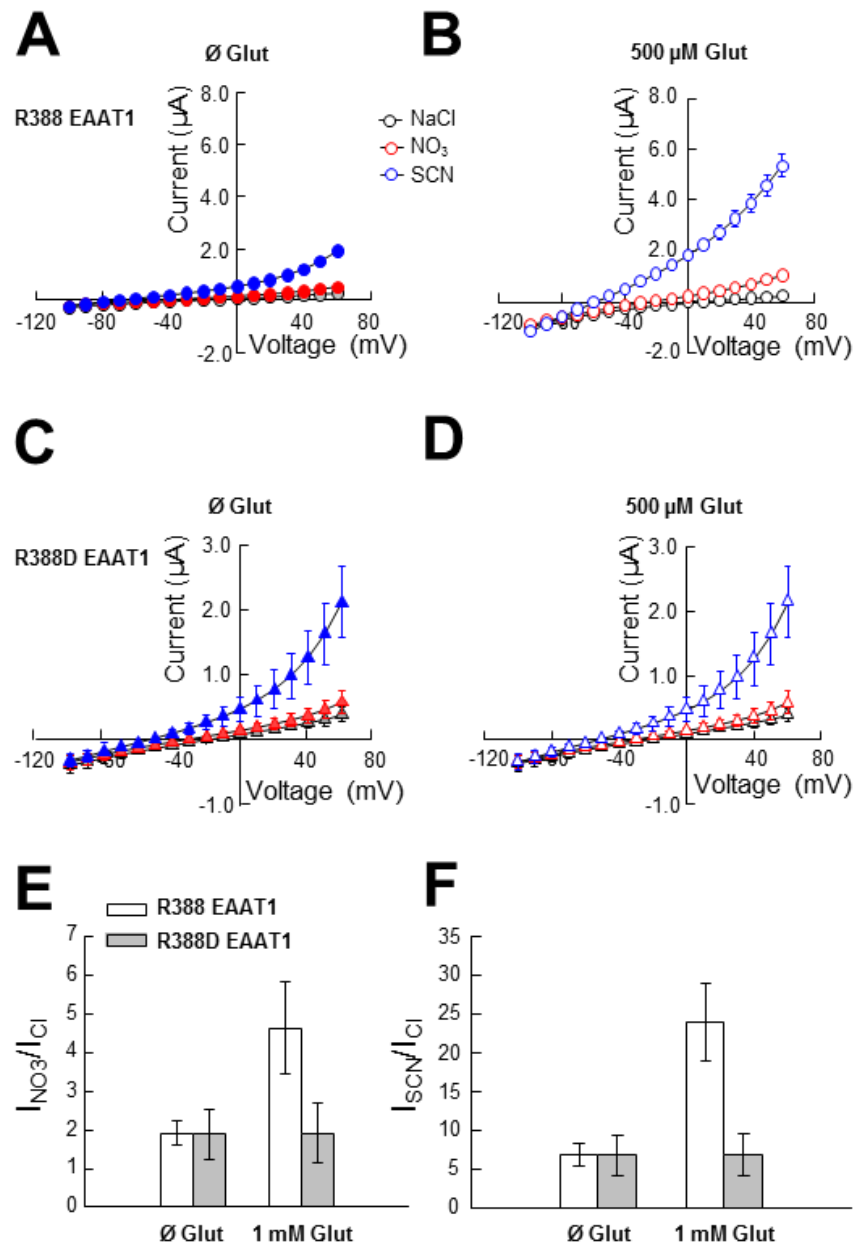


Figure D3. Relative anion conductance in R388D EAAT1 is not affected by glutamate. (A-D) Current-Voltage relationship from oocytes expressing R388 EAAT1 (A and B, n=7), or mutant R388D (C and D, n=8) in response to different anions (Cl, grey symbols, NO₃ red symbols and SCN, blue symbols) in the absence (A and C, closed symbols) and in the presence

(B and D, open symbols) of 1 mM Glutamate. (*E* and *F*) Relative conductances obtained from A-D.

Xenopus oocytes to look at the relative permeability ratios since EAAT4 has been demonstrated to have a dramatically lower rate of transport (4,28). First we determined whether the same phenotype was observed in the R388 homolog mutation on rEAAT4, R410E. As observed in oocytes expressing hEAAT1 R388E, no additional macroscopic current was observed upon glutamate application in oocytes expressing rEAAT4 R410E (Figure 4B, n=7) as compared to rEAAT4 WT (Figure 4A, n=7). These data are consistent with results seen in EAAT1. We next measured the relative anion permeability ($P_{\text{NO}_3^-}/P_{\text{Cl}^-}$) of EAAT4-associated anion channels. $P_{\text{NO}_3^-}/P_{\text{Cl}^-}$ was increased after application of 1 mM glu, as previously described (6,24) (Figure 4C, white bar, n=9). In contrast, application of glu did not affect the $\text{NO}_3^-/\text{Cl}^-$ nor the SCN^-/Cl^- permeability ratio in oocytes expressing rEAAT4 R410E and its value was similar to WT transporters in the absence of glu (Figure 4C, grey bar, n=7). As observed with hEAAT1, glu also increases the relative anion conductance of rEAAT4 WT transporters while leaving rEAAT4 R410E values similar to the one in the absence of substrate (Figure 4D). Taken together, these data support that in both isoforms (hEAAT1 and rEAAT4), mutating this positively charged residue to an acidic amino acid prevents the channel from transitioning from the leak or Na^+ gated conducting states into the glu gated conducting state and therefore glu binding and/or translocation is no longer able to increase anion permeation.

D.5.4. R388E/D Alters Accessibility of HP1 Residues in the Outward-facing Conformations

EAATs can exist in at least two structurally distinct conformations, outward- and inward-facing. A recent crystal structure solved has allowed for a proposed transport mechanism between these two states (29). A large segment of the protein (TM6, HP1, TM7, HP2, and TM8) classified as the transport domain, performs a significant movement between these two proposed conformations (11,29). The conformational changes that induces the substrate dependent anion conducting state may share overlap with conformational changes necessary for the transport process. Since our data suggest that the substitution of R388(R410 in EAAT4)

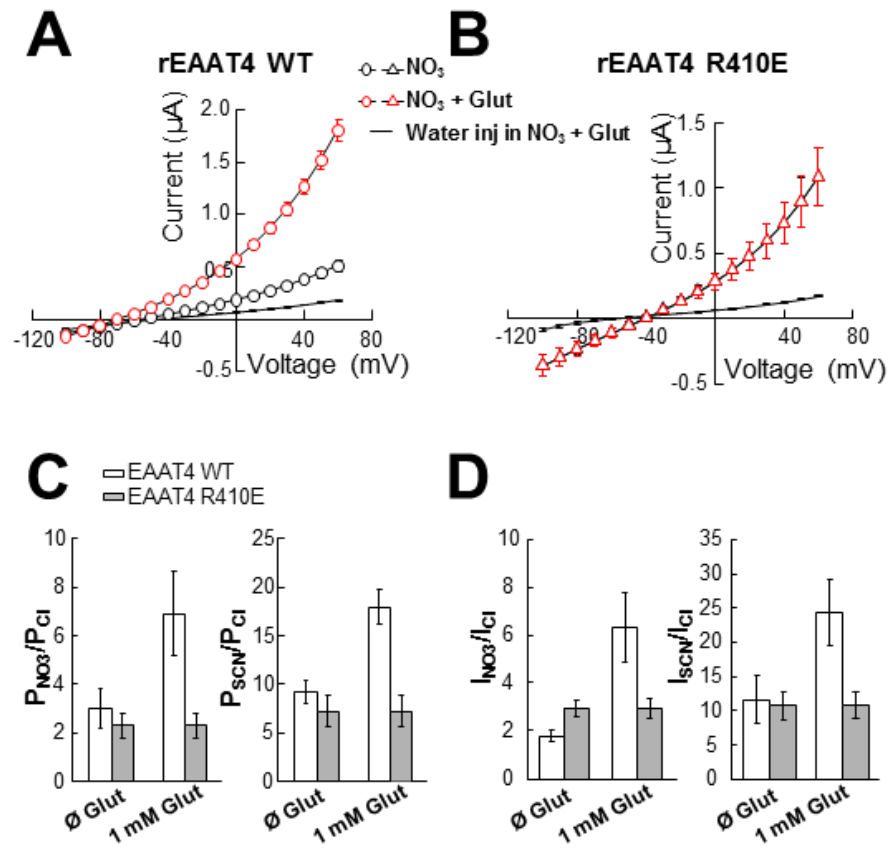


Figure D4 Relative anion permeability and relative anion conductance in R410E EAAT4 mimic the leak conducting state of WT transporters. (**A** and **B**) Current-Voltage relationship from oocytes expressing WT EAAT4 (**A**, $n=9$), or mutant R410E (**B**, $n=8$) in the absence (black symbols) and the presence (red symbols) of 1 mM Glutamate. Solid lines represent currents recorded in a NO_3 -based solution in the presence of 1mM Glutamate from water-injected oocytes ($n=8$). (**C** and **D**) Permeability ratios (**C**) and relative conductances (**D**) obtained from **A** and **B**.

by an acidic amino acid, prevents the channel from transitioning to the glutamate gated conducting state, we propose that the phenotype that results from this mutation may be due to some impairment of such a movement. To test our hypothesis, we used the accessibility of residues in HP1, which when substituted to cysteine, can only be modified when the transporter is in the inward facing state (30). The point mutation L376C was created on the hEAAT1Cs WT and hEAAT1Cs R388D and assayed channel activity. The single cysteine mutant hEAAT1Cs L376C showed a similar channel phenotype compared to WT (Figure 5A), while oocytes expressing the double mutant hEAAT1Cs L376C-R388D displayed the same impaired gating function of R388E/D alone (Figure 5B). Interestingly, incubation of oocytes expressing the double mutant transporters hEAAT1Cs L376C-R388D for 5 minutes with 100 μ M NEM under physiological conditions (96 mM Na-based solution), was sufficient to cause a 50% reduction of the transport activity of the double mutant proteins (Figure 5D), but not in the L376C mutant alone (Figure 5C). These results suggest that when a negative charge is located at position 388, the L376 residue is more exposed to the intracellular milieu. Oocytes expressing L376C alone are exposed to a high extracellular K^+ solution, L376C is accessible to modification from the cytoplasm by 100 μ M of the permeable maleimide reagent NEM, causing a reduction of the uptake by 70% in oocytes expressing this mutant transporter (data not shown). One could claim that the modification at position 376 was caused by extracellular accessibility as a result of an aberrant structure caused by the mutations themselves. If the R388D mutation shifts the carrier equilibrium to an intermediate outward state, thus allowing L376C to become exposed to modification even in external Na^+ conditions, then forcing the transporter into a fully outward conformation should preclude any modifications on the double mutant. In order to support our hypothesis we tested the effect of NEM in oocytes previously incubated with TBOA, which would trap the transporter in an outward, HP2-open conformation. Compared with vehicle treated controls, pre-treatment of the R388D-L376C double mutant with DL-TBOA blocked the

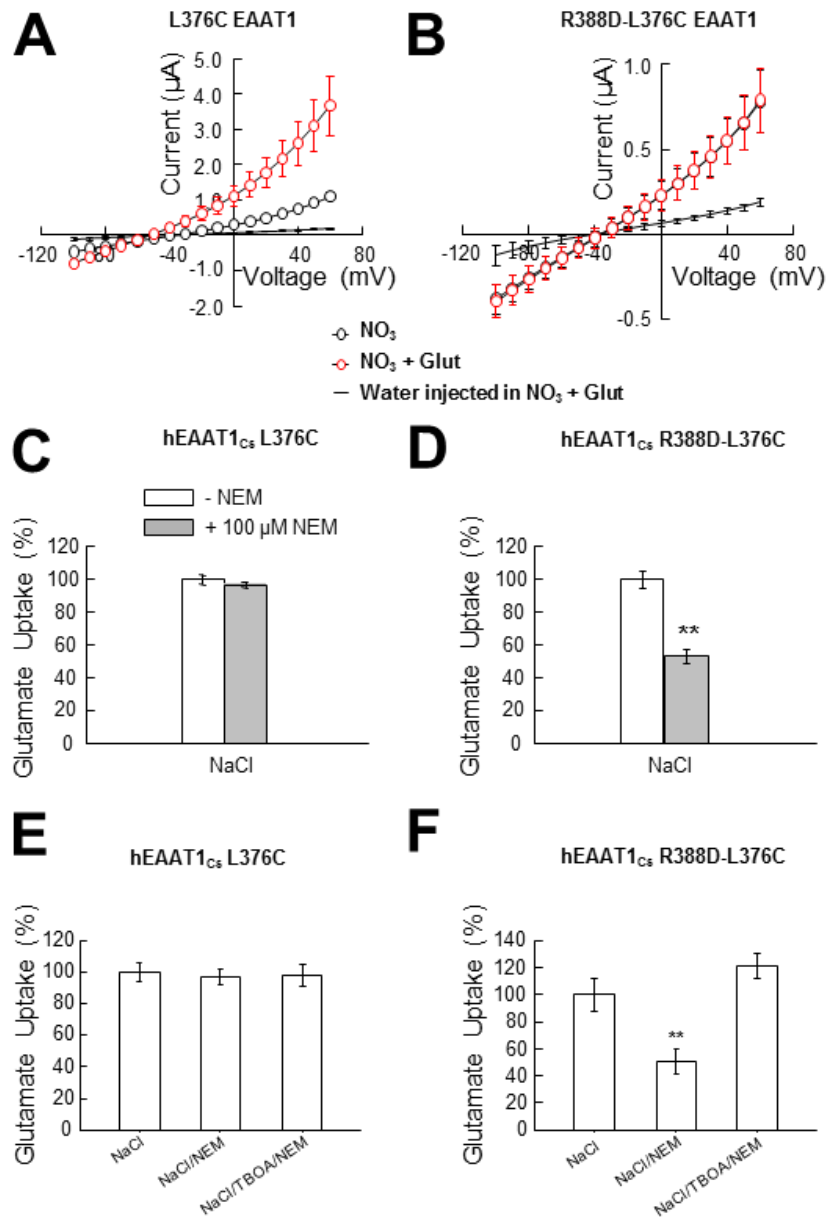


Figure D5. R388D mediates an altered accessibility of HP1 residues to modifying reagents. (**A** and **B**) Current-Voltage relationships from oocytes expressing L376C EAAT1 (**A**, n=6) and R388D-L376C (**B**, n=10) EAAT1 in the absence (black symbols) and the presence (red symbols) of 1mM Glutamate. Solid lines represent currents recorded in a NO₃-based solution in the presence of 1mM Glutamate from water-injected oocytes (n=8). (**C-H**) Radioactive glutamate uptake from oocytes expressing L376C EAAT1 (**C**, **E** and **G**) or R388D-

L376C EAAT1 (D, F and H). (**C** and **D**) Glutamate uptake from oocytes that were treated for 5 minutes (white bars) or not (grey bars) with 0.25 mM NEM. The treatment was done in normal Na-based solution (96 mM NaCl) or in a K-based solution (96 mM KCl) (n>9 for each condition). (**E** and **F**) TBOA effect on glutamate uptake in oocytes that were or not previously incubated with 0.25 mM NEM in a Na-based solution (n>8 for each condition). (**G** and **H**) NEM modification effect on glutamate uptake on oocytes that were or not previously incubated with TBOA (n>10 for each condition). For comparison uptake was normalized by the uptake in normal conditions (96 mM NaCl and no incubation with NEM and/or TBOA). Error bars represent standard error of the mean and ** indicates a $p < 0.01$ with an ANOVA.

reduction in uptake observed with NEM modification in the L376C-R388D double mutant. These data suggest that the alteration of R388 to an acidic residue alters both the mechanism of anion channel gating as well as shifts the transporter equilibrium into an intermediate-outward state, displaying increased intracellular accessibility of HP1 residues.

Our results demonstrate that when an acidic amino acid occupies position R388 in EAATs, the transport cycle cannot be completed and the substrate gated anion conductance is no longer activated. This is the first time that a residue has been demonstrated to play a role in both transport and gating processes and therefore is likely involved in their mechanistic coupling. In addition, our results indicates that this mutation may shift the transport domain lower into the membrane field, increasing HP1 accessibility to the intracellular milieu, a movement that might resemble the normal, physiological gating process for the anion conductance.

D.6. DISCUSSION

Here we investigate the functional consequences of mutating a highly conserved arginine residue in TM7 in both EAAT1 and EAAT4. R388 is a positive charged amino acid conserved among the whole EAAT family (Figure 1B), located at the tip of TM7, a region in close proximity to residues participating in substrate binding and translocation (31), as well as to regions proposed to play a role in anion permeation (20,32). During the last 10 years, major progress has been achieved in our understanding of the mechanism of substrate transport. Yet, the molecular determinants underlying anion channel gating and permeation remain poorly understood. These two different processes have been proven to be thermodynamically uncoupled (4,5) and modification of HP2 abolishes substrate transport while not reducing anion channel activity, highlighting their independent processes (33-35). However, the interaction of substrates such as Na^+ and glu at the binding site influences channel activity, supporting a coupling mechanism between the two processes. Initially, a detailed noise analysis study of the

EAAT-mediated currents proposed a structural coupling between substrate transport and anion channel gating, suggesting that EAAT-associated anion conductance may be gated by conformational changes involved in substrate translocation (36). Analyses using pre-steady state kinetics have further supported that initial conformational changes associated with transport and anion channel gating are related (22,37,38). Additionally, data derived from a combination of electrophysiology and voltage clamp fluorometry also supports such a mechanism (39). Here, we reveal a conserved basic residue located in the tip of TM7, which plays a crucial role in the coupling mechanism of substrate interaction and anion channel gating.

R388 is located adjacent to other basic residues, K384 and R385, which have been previously demonstrated to effect the glu mediated anion channel gating and ion permeation properties of EAATs (Figure 1B)(20). K384 and R385 mutations effect the substrate induced current amplitudes but not substrate transport, therefore it was hypothesized that these residues are involved in substrate induced channel gating. It was also proposed that these residues interact with other residues in TM2-TM3 loop and TM7 (19,20). However, because these residues which influence anion flux do not exhibit a significant effect on substrate transport, it is unlikely that they comprise part of the gating mechanism.

In oocytes expressing the R388E/D mutants, no transport current could be readily measured (Figure 1C and D). In contrast, radiolabeled glu is still able to accumulate in those cells, demonstrating that glu can bind to the mutant transporters and the transport mechanism is still active although operates in an electroneutral fashion (Figure 1E). Recently crystallographic data was obtained using TM2 and HP2 crosslinking with double cysteine mutants in Glt_{Ph} (29). The authors proposed that this structure depicts an inward oriented conformational state, which lead them to propose that the core domain (TM 7, TM 8, HP1, and HP2) undergoes a large movement of approximately 15 Å toward the cytoplasm during substrate transport. In 2012, a smaller inward movement of the core domain of about 3.5 Å, referred to as an intermediate outward facing conformation (iOFS) was observed in Glt_{Ph} (32). Such a movement altered the

conformation of the N-terminal tip of TM7, near where R388 is located. These data suggests that this small amplitude conformational change results in the formation of a cavity lined by conserved hydrophobic residues in TM2 and TM5, regions previously propose to participate in anion permeation (19,20). Our data suggests that the inability of glutamate to gate the substrate induced anion conductance in the R388D and R388E mutant transporters may be a result of stabilization of the mutant transporters in such an intermediate conformation. If accurate, then it is likely that the significantly reduced transport capacity and lack of full cycle transport are due to this structural perturbation.

EAAT-associated anion channels are multi-state channels (40,41), with two predominant open states mediated by several conformations accessed during the transport cycle; a leak or Na^+ bound open state and the Na^+ and glutamate bound open state. Both these open states exhibit different anion permeabilities (6,24) and open probabilities (24,40,42). Several stationary and non-stationary noise analysis studies in different EAAT isoforms, using different ionic conditions, agree that they share a maximum absolute open probability of ~ 0.6 at saturating Na^+ and glutamate concentrations (24,40,42,43). The lack of substrate activated current in oocytes expressing the hEAAT1cs R388D, hEAAT1cs R388E, or rEAAT4 R410E mutants could be the result of the mutant channels having reached their maximum open probability state. Alternatively they might be trapped in the leak state and cannot undergo the transition to the glu induced open states. We measured the relative anion conductance and anion permeability ratios in oocytes expressing WT and mutant EAAT transporters from two different species and isoforms. Our results suggest that the mutant channels, although still able to bind Na^+ and glu (Figure 2C), are not able to undergo the transition to the glutamate-gated state. Although these results do not necessarily rule out an altered single channel conductance or increased open probability for the leak or Na^+ gated state, the data are indicative of channel characteristics disparate from the glu induced open states and identical to the leak channel state.

It is clear from the data presented here that the initial binding of glu is not sufficient to gate the substrate-gated anion conductance because R388E/D mutants display glutamate interaction without substrate induced gating of the channel. Although this loss of gating could be an unnatural by-product of mutation of R388, our interpretation is supported by data from pre-steady-state kinetic experiments indicating multiple events occur in order to active the anion conductance (22,37).

In an attempt to better understand the nature of the carrier with a R388D mutation, we assayed for markers indicative of an altered structural conformation. Our modification experiments using cysteine substitution mutants strongly suggest that when the R388D mutation is present, under physiological conditions where the carrier would be stabilized in the outward-open conformation, an intermediate conformation is favored with HP1 residues accessible to the intracellular space. It is interesting to note that due to the ability of R388 mutants to still bind glu and TBOA, as well as complete at least partial transport cycles, indicates that these mutant carriers can still visit a range of conformational states (32). Indeed, inhibitor binding can re-stabilize the outward-open conformation similar to a WT transporter as indicated by the loss of NEM labeling of L376C-R388D in the presence of TBOA. Likely, R388 mutants alter the energy profiles of conformational states, possibly mimicking the recent intermediate outward facing structure (iOFs), and have serendipitously revealed an intermediate open channel state. We believe our findings open new avenues toward the complete understanding of the complex interaction of substrate transport and anion channel activity possessed by the EAATs.

D.7. REFERENCES

1. Danbolt, N. C. (2001) Glutamate uptake. *Prog Neurobiol* **65**, 1-105
2. Zerangue, N., and Kavanaugh, M. P. (1996) Flux coupling in a neuronal glutamate transporter. *Nature* **383**, 634-637

3. Levy, L. M., Warr, O., and Attwell, D. (1998) Stoichiometry of the glial glutamate transporter GLT-1 expressed inducibly in a Chinese hamster ovary cell line selected for low endogenous Na⁺-dependent glutamate uptake. *J Neurosci* **18**, 9620-9628
4. Fairman, W. A., Vandenberg, R. J., Arriza, J. L., Kavanaugh, M. P., and Amara, S. G. (1995) An excitatory amino-acid transporter with properties of a ligand-gated chloride channel *Nature* **375**, 599-603
5. Wadiche, J. I., Amara, S. G., and Kavanaugh, M. P. (1995) Ion fluxes associated with excitatory amino acid transport *Neuron* **15**, 721-728
6. Torres-Salazar, D., and Fahlke, C. (2006) Intersubunit interactions in EAAT4 glutamate transporters *J Neurosci* **26**, 7513-7522
7. Eliasof, S., and Jahr, C. E. (1996) Retinal glial cell glutamate transporter is coupled to an anionic conductance. *Proc Natl Acad Sci U S A* **93**, 4153-4158
8. Veruki, M. L., Morkve, S. H., and Hartveit, E. (2006) Activation of a presynaptic glutamate transporter regulates synaptic transmission through electrical signaling. *Nature neuroscience* **9**, 1388-1396
9. Melzer, N., Torres-Salazar, D., and Fahlke, C. (2005) A dynamic switch between inhibitory and excitatory currents in a neuronal glutamate transporter *Proc Natl Acad Sci U S A* **102**, 19214-19218
10. Wersinger, E., Schwab, Y., Sahel, J. A., Rendon, A., Pow, D. V., Picaud, S., and Roux, M. J. (2006) The glutamate transporter EAAT5 works as a presynaptic receptor in mouse rod bipolar cells. *The Journal of physiology* **577**, 221-234
11. Yernool, D., Boudker, O., Jin, Y., and Gouaux, E. (2004) Structure of a glutamate transporter homologue from *Pyrococcus horikoshii*. *Nature* **431**, 811-818
12. Haugeto, O., Ullensvang, K., Levy, L. M., Chaudhry, F. A., Honore, T., Nielsen, M., Lehre, K. P., and Danbolt, N. C. (1996) Brain glutamate transporter proteins form homomultimers. *J Biol Chem* **271**, 27715-27722

13. Gendreau, S., Voswinkel, S., Torres-Salazar, D., Lang, N., Heidtmann, H., Detro-Dassen, S., Schmalzing, G., Hidalgo, P., and Fahlke, C. (2004) A trimeric quaternary structure is conserved in bacterial and human glutamate transporters. *J Biol Chem* **279**, 39505-39512
14. Yernool, D., Boudker, O., Folta-Stogniew, E., and Gouaux, E. (2003) Trimeric subunit stoichiometry of the glutamate transporters from *Bacillus caldotenax* and *Bacillus stearothermophilus*. *Biochemistry* **42**, 12981-12988
15. Seal, R. P., and Amara, S. G. (1998) A reentrant loop domain in the glutamate carrier EAAT1 participates in substrate binding and translocation. *Neuron* **21**, 1487-1498
16. Grunewald, M., Menaker, D., and Kanner, B. I. (2002) Cysteine-scanning mutagenesis reveals a conformationally sensitive reentrant pore-loop in the glutamate transporter GLT-1. *J Biol Chem* **277**, 26074-26080
17. Brocke, L., Bendahan, A., Grunewald, M., and Kanner, B. I. (2002) Proximity of two oppositely oriented reentrant loops in the glutamate transporter GLT-1 identified by paired cysteine mutagenesis. *J Biol Chem* **277**, 3985-3992
18. Leighton, B. H., Seal, R. P., Watts, S. D., Skyba, M. O., and Amara, S. G. (2006) Structural rearrangements at the translocation pore of the human glutamate transporter, EAAT1. *J Biol Chem* **281**, 29788-29796
19. Ryan, R. M., Mitrovic, A. D., and Vandenberg, R. J. (2004) The chloride permeation pathway of a glutamate transporter and its proximity to the glutamate translocation pathway *J Biol Chem* **279**, 20742-20751
20. Huang, S., and Vandenberg, R. J. (2007) Mutations in transmembrane domains 5 and 7 of the human excitatory amino acid transporter 1 affect the substrate-activated anion channel *Biochemistry* **46**, 9685-9692

21. Vandenberg, R. J., Mitrovic, A. D., Chebib, M., Balcar, V. J., and Johnston, G. A. (1997) Contrasting modes of action of methylglutamate derivatives on the excitatory amino acid transporters, EAAT1 and EAAT2. *Mol Pharmacol* **51**, 809-815
22. Watzke, N., Bamberg, E., and Grewer, C. (2001) Early intermediates in the transport cycle of the neuronal excitatory amino acid carrier EAAC1 *J Gen Physiol* **117**, 547-562
23. Schwartz, E. A., and Tachibana, M. (1990) Electrophysiology of glutamate and sodium co-transport in a glial cell of the salamander retina. *J Physiol* **426**, 43-80
24. Melzer, N., Biela, A., and Fahlke, C. (2003) Glutamate modifies ion conduction and voltage-dependent gating of excitatory amino acid transporter-associated anion channels *J Biol Chem* **278**, 50112-50119
25. Bendahan, A., Armon, A., Madani, N., Kavanaugh, M. P., and Kanner, B. I. (2000) Arginine 447 Plays a Pivotal Role in Substrate Interactions in a Neuronal Glutamate Transporter. *The Journal of Biological Chemistry* **275**, 37436-37442
26. Kavanaugh, M. P., Bendahan, A., Zerangue, N., Zhang, Y., and Kanner, B. I. (1997) Mutation of an amino acid residue influencing potassium coupling in the glutamate transporter GLT-1 induces obligate exchange. *J Biol Chem* **272**, 1703-1708
27. Otis, T. S., and Kavanaugh, M. P. (2000) Isolation of current components and partial reaction cycles in the glial glutamate transporter EAAT2 *J Neurosci* **20**, 2749-2757
28. Mim, C., Balani, P., Rauen, T., and Grewer, C. (2005) The glutamate transporter subtypes EAAT4 and EAATs 1-3 transport glutamate with dramatically different kinetics and voltage dependence but share a common uptake mechanism *J Gen Physiol* **126**, 571-589
29. Reyes, N., Ginter, C., and Boudker, O. (2009) Transport mechanism of a bacterial homologue of glutamate transporters. *Nature* **462**, 880-885

30. Shlaifer, I., and Kanner, B. I. (2007) Conformationally Sensitive Reactivity to Permeant Sulfhydryl Reagents of Cysteine Residues Engineered into Helical Hairpin 1 of the Glutamate Transporter GLT-1. *Molecular Pharmacology* **71**, 1341-1348
31. Jiang, J., and Amara, S. G. (2010) New views of glutamate transporter structure and function: Advances and challenges *Neuropharmacology*
32. Verdon, G., and Boudker, O. (2012) Crystal structure of an asymmetric trimer of a bacterial glutamate transporter homolog. *Nat Struct Mol Biol* **19**, 355-357
33. Seal, R. P., Shigeri, Y., Eliasof, S., Leighton, B. H., and Amara, S. G. (2001) Sulfhydryl modification of V449C in the glutamate transporter EAAT1 abolishes substrate transport but not the substrate-gated anion conductance *Proc Natl Acad Sci U S A* **98**, 15324-15329
34. Borre, L., Kavanaugh, M. P., and Kanner, B. I. (2002) Dynamic equilibrium between coupled and uncoupled modes of a neuronal glutamate transporter. *J Biol Chem* **277**, 13501-13507
35. Ryan, R. M., and Vandenberg, R. J. (2002) Distinct conformational states mediate the transport and anion channel properties of the glutamate transporter EAAT-1 *J Biol Chem* **277**, 13494-13500
36. Picaud, S. A., Larsson, H. P., Grant, G. B., Lecar, H., and Werblin, F. S. (1995) Glutamate-gated chloride channel with glutamate-transporter-like properties in cone photoreceptors of the tiger salamander. *Journal of neurophysiology* **74**, 1760-1771
37. Grewer, C., Watzke, N., Wiessner, M., and Rauen, T. (2000) Glutamate translocation of the neuronal glutamate transporter EAAC1 occurs within milliseconds. *Proc Natl Acad Sci U S A* **97**, 9706-9711
38. Mim, C., Tao, Z., and Grewer, C. (2007) Two Conformational Changes Are Associated with Glutamate Translocation by the Glutamate Transporter EAAC1 *Biochemistry* **46**, 9007-9018

39. Hotzy, J., Machtens, J. P., and Fahlke, C. (2012) Neutralizing aspartate 83 modifies substrate translocation of excitatory amino acid transporter 3 (EAAT3) glutamate transporters. *J Biol Chem* **287**, 20016-20026
40. Larsson, H. P., Picaud, S. A., Werblin, F. S., and Lecar, H. (1996) Noise analysis of the glutamate-activated current in photoreceptors. *Biophys J* **70**, 733-742
41. Kovermann, P., Machtens, J. P., Ewers, D., and Fahlke, C. (2010) A conserved aspartate determines pore properties of anion channels associated with excitatory amino acid transporter 4 (EAAT4). *The Journal of biological chemistry* **285**, 23676-23686
42. Torres-Salazar, D., and Fahlke, C. (2007) Neuronal Glutamate Transporters Vary in Substrate Transport Rate but Not in Unitary Anion Channel Conductance in *The Journal of Biological Chemistry*
43. Machtens, J. P., Kovermann, P., and Fahlke, C. (2011) Substrate-dependent Gating of Anion Channels Associated with Excitatory Amino Acid Transporter 4. *The Journal of biological chemistry* **286**, 23780-23788

APPENDIX E: STRUCTURE OF THE PENTAMERIC LIGAND-GATED ION CHANNEL GLIC BOUND WITH ANESTHETIC KETAMINE

E.1. SUMMARY OF CONTRIBUTIONS

I contributed to this article by designing all the electrophysiological experiments. I also collected much of the electrophysiological data such as the ketamine IC_{50} curve and gap free recordings demonstrated in Figure 1. As one of the co-authors, I revised the manuscript as well.

Structure of the Pentameric Ligand-Gated Ion Channel GLIC Bound with Anesthetic Ketamine

Jianjun Pan,^{1,8} Qiang Chen,^{1,8} Dan Willenbring,¹ David Mowrey,^{1,2} Xiang-Peng Kong,⁶ Aina Cohen,⁷ Christopher B. Divito,³ Yan Xu,^{1,4,5,*} and Pei Tang^{1,2,5,*}

¹Department of Anesthesiology

²Department of Computational and System Biology

³Department of Neurobiology

⁴Department of Structural Biology

⁵Department of Pharmacology and Chemical Biology

Biomedical Science Tower 3, 3501 Fifth Avenue, University of Pittsburgh School of Medicine, Pittsburgh, PA 15260, USA

⁶Department of Biochemistry, 550 First Avenue, MSB 329, New York University School of Medicine, New York, NY 10016, USA

⁷Stanford Synchrotron Radiation Lightsource, 2575 Sand Hill Road, MS: 99, Menlo Park, CA 94025, USA

⁸These authors contributed equally to this work

*Correspondence: xu2@pitt.edu (Y.X.), tangp@anes.upmc.edu (P.T.)

<http://dx.doi.org/10.1016/j.str.2012.08.009>

SUMMARY

Pentameric ligand-gated ion channels (pLGICs) are targets of general anesthetics, but a structural understanding of anesthetic action on pLGICs remains elusive. GLIC, a prokaryotic pLGIC, can be inhibited by anesthetics, including ketamine. The ketamine concentration leading to half-maximal inhibition of GLIC (58 μ M) is comparable to that on neuronal nicotinic acetylcholine receptors. A 2.99 Å resolution X-ray structure of GLIC bound with ketamine revealed ketamine binding to an intersubunit cavity that partially overlaps with the homologous antagonist-binding site in pLGICs. The functional relevance of the identified ketamine site was highlighted by profound changes in GLIC activation upon cysteine substitution of the cavity-lining residue N152. The relevance is also evidenced by changes in ketamine inhibition upon the subsequent chemical labeling of N152C. The results provide structural insight into the molecular recognition of ketamine and are valuable for understanding the actions of anesthetics and other allosteric modulators on pLGICs.

INTRODUCTION

Clinical application of general anesthetics is indispensable in modern medicine, but the molecular mechanisms of general anesthesia remain unclear. The complexity of plausible anesthetic targets and the lack of accurate structural information of these targets have hindered progress toward a mechanistic understanding. Among all the receptors involved in neuronal signal transduction, a family of pentameric ligand-gated ion channels (pLGICs) has been identified as a target for general anesthetics. Anesthetics often inhibit the agonist-activated current in the excitatory nicotinic acetylcholine receptors (nAChRs) or serotonin 5-HT₃ receptors, but potentiate the inhibitory glycine

and GABA_A receptors (Franks and Lieb, 1994; Hemmings et al., 2005). Although our understanding of general anesthetic modulation on these receptors has progressed dramatically in the last decade (Forman and Miller, 2011), it remains a formative challenge to resolve high-resolution structures of these pLGICs, and to pinpoint where and how anesthetics act on these channels to modulate their functions.

The structure of a bacterial homolog of pLGICs from *Gloeobacter violaceus* (GLIC) has been solved by X-ray crystallography (Bocquet et al., 2009; Hilf and Dutzler, 2009), showing a similar architecture of extracellular (EC) and transmembrane domains (TM) to that of the *Torpedo marmorata* nAChR solved by electron microscopy (Unwin, 2005). The EC domain of GLIC resembles the X-ray structures of the acetylcholine-binding proteins (AChBPs) (Brejc et al., 2001; Celie et al., 2004; Hansen et al., 2005) and the EC domain of α 1-nAChR (Dellisanti et al., 2007), presenting similar intersubunit cavities for agonist or antagonist binding (Hansen et al., 2005). Despite the fact that GLIC opens upon lowering pH (Bocquet et al., 2007) and does not require agonist binding to the conventional site as for pLGICs, its responses to general anesthetics resemble those of nAChRs. A proton-activated Na⁺ current in GLIC can be inhibited by anesthetics, as demonstrated previously (Nury et al., 2011; Weng et al., 2010) and in this study. Anesthetic binding sites in GLIC have been investigated by steady-state fluorescence quenching experiments (Chen et al., 2010) and X-ray crystallography (Nury et al., 2011). Whereas the crystal structures of anesthetic desflurane- and propofol-bound GLIC revealed an intrasubunit binding site in the TM domain, the fluorescence experiments with halothane and thiopental suggested additional sites in the EC and TM domains of GLIC. The sensitivity to anesthetics and amenability to crystal structure determination make GLIC ideally suited for revealing where and how general anesthetics act on pLGICs.

Ketamine has been widely used for the induction and maintenance of general anesthesia. Although ketamine is commonly known as a dissociative anesthetic acting as a noncompetitive antagonist on the N-methyl-D-aspartate (NMDA) receptor (Harrison and Simmonds, 1985), it is also a potent inhibitor of neuronal

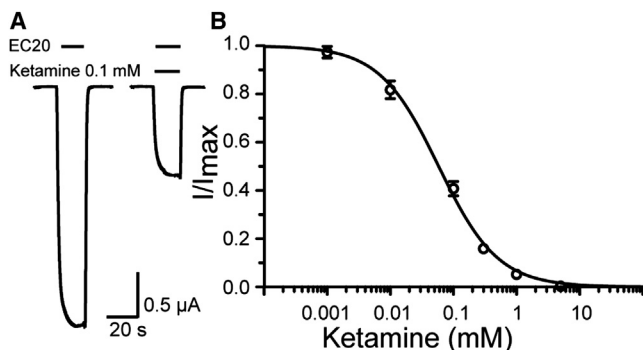


Figure 1. Ketamine Inhibition of GLIC at EC20

(A) Representative current traces of GLIC expressed in *Xenopus oocytes* in the absence and presence of 100 μ M ketamine.

(B) Inhibition of the GLIC current by ketamine. Response to inhibition is expressed as a fraction of current induced at EC20 in the presence of an indicated concentration of ketamine relative to that in the absence of ketamine. The data are reported as the mean \pm SEM from $n \geq 8$ oocytes and fit to the Hill equation. Error bars less than the symbol size are not visible.

nAChRs (Coates and Flood, 2001; Yamakura et al., 2000). The action sites of ketamine in these receptors have not been identified previously. Here, we show the crystal structure of ketamine-bound GLIC. A preexisting cavity in the EC domain of GLIC is found to be the site for ketamine binding. Functional relevance of the site is evidenced by electrophysiology measurements in combination with site-directed mutations and subsequent chemical labeling to mimic anesthetic binding. Combined with the previous knowledge of anesthetic binding to the TM domain of GLIC (Nury et al., 2011), the anesthetic binding site discovered in the EC domain provides an additional structural template for the future design and evaluation of novel general anesthetics and therapeutic allosteric modulators of pLGICs.

RESULTS

Ketamine Inhibition on GLIC

We found that the anesthetic ketamine inhibited currents of the *Xenopus oocytes* expressing GLIC in a concentration-dependent manner (Figure 1). At the proton concentration near EC20 (pH 5.5) for GLIC activation, inhibition concentration with half-maximal response (IC₅₀) for ketamine on GLIC is 58 μ M, which is comparable to the ketamine IC₅₀ values on the $\alpha 7$ nAChR (20 μ M) and the $\alpha 4\beta 2$ nAChR (50–72 μ M) (Coates and Flood, 2001; Yamakura et al., 2000).

The Crystal Structure of Ketamine-Bound GLIC

To identify ketamine binding site(s) in GLIC, we co-crystallized ketamine with GLIC and solved the structure to a resolution of 2.99 Å. Crystallographic and refinement parameters are summarized in Table 1. Strong electron densities for ketamine were found in all five equivalent pockets in the F_o-F_c omit electron density map (see Figure S1 available online). Figure 2 shows the refined structure and a stereo view of the 2F_o-F_c electron density map for the ketamine binding site, revealing ketamine in a pre-existing cavity between adjacent subunits in the EC domain of GLIC. The ketamine site in GLIC is near the homolo-

Table 1. Data Collection and Refinement Statistics

Data Collection and Process	
Beamline	SSRL BL 12-2
Wavelength (Å)	0.9795
Space group	C2
Unit cell (Å)	184.1, 132.7, 162.1
β (°)	103.6
Resolution (Å)	25–2.99
R _{merge} (%) ^a	8.3 (59.8)
Completeness (%) ^a	97.6 (92.3)
$\langle I/\sigma \rangle$ ^a	12.6 (2.2)
Unique reflections ^a	74,604 (1,0257)
Redundancy ^a	3.9 (3.9)
Refinement statistics	
Resolution (Å)	24.8–2.99
No. Reflections (test set)	68,525 (3,452)
R _{work} /R _{free}	0.187/0.219
Non-H protein (ligand) atoms	13,358 (675)
B-factors (Å ²)	
Protein	70.6
Detergents	125.0
Lipids	119.1
Solvent	51.7
Ketamine	122.3
Rms deviations	
Bond lengths (Å)	0.008
Bond angles (degrees)	1.22
Rotamer outliers (%)	8.3
Ramachandran outliers (%)	0.97
Ramachandran favored (%)	93.3
PDB code	4F8H

^aValues in the parentheses are for highest resolution shell.

gous orthosteric agonist site in Cys-loop receptors, but it is 9–10 Å closer to the TM domain (Figure S2). It partially overlaps with the binding interface of large antagonists in Cys-loop receptors (Bourne et al., 2010; Hansen et al., 2005).

Interactions Stabilizing Ketamine in the Binding Pocket

Positively charged at a low pH, ketamine is stabilized in an amphipathic pocket, where it contacts mostly hydrophilic residues to form electrostatic interactions with these residues, in addition to van der Waals interactions with some hydrophobic residues. As depicted in Figure 3, on one side of the pocket, the chloro group of ketamine points to the positively charged amine of K183 of $\beta 10$ and the phenyl ring faces F174 and L176 of loop C. On a different side of the pocket, the aminium of ketamine makes electrostatic interactions with side chains of N152, D153, and D154 of the $\beta 8$ – $\beta 9$ loop (loop F). The carbonyl group of ketamine can potentially form a hydrogen bond with the hydroxyl group of Y23 on $\beta 1$. The amide carbonyl oxygen of N152 is 3 Å away from the aminium of ketamine. GLIC is activated at low pH and the protonation states of titratable residues are responsible for channel activities. K183 of the

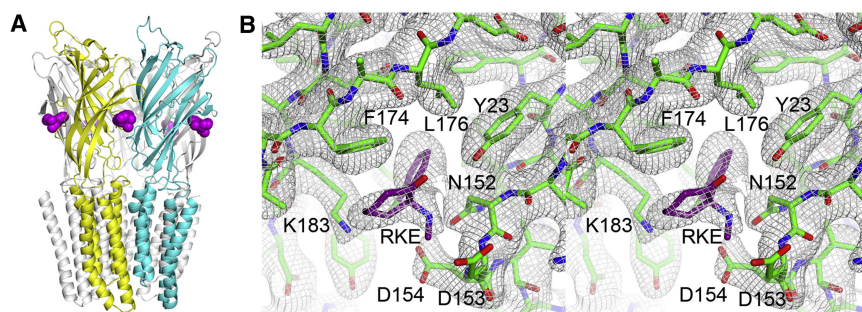


Figure 2. The Crystal Structure of GLIC Bound with Five Ketamine Molecules

(A) A side view of the structure with ketamine molecules in purple color. A pair of principal and complementary subunits for ketamine binding is depicted in yellow and cyan, respectively. Note that ketamine is a few Å below loop C. (B) A stereo view of the 2Fo-Fc electron density map, contoured at 1.0 σ level, for the ketamine binding site. See also Figures S1 and S2.

principal side carries a positive charge on its side chain, whereas the side chains of D153 and D154 of the complementary side are likely negatively charged. Thus, electrostatic interactions have contributed significantly to stabilizing ketamine binding (Figure S3).

Functional Relevance of the Ketamine-Binding Pocket

The functional relevance of the identified ketamine site was validated by site-directed mutations and subsequent chemical labeling of a pocket residue to mimic anesthetic binding. As shown in Figure 4, the ketamine-binding pocket is involved in the GLIC activation. A single mutation in the pocket, N152C, shifted EC₅₀ from pH 5.0 in the wild-type (WT) GLIC to pH 5.4 in the N152C mutant (Figure 4A). Ketamine binding to the pocket is evidenced by a higher IC₅₀ value for the N152C mutant (110 μ M) in comparison to IC₅₀ of the WT GLIC (58 μ M) (Figure 4B). Removal of a favorable electrostatic interaction between the aminium of ketamine and the amide carbonyl oxygen of N152 in the mutant may account for the reduced ketamine inhibition. The functional relevance of the ketamine binding site is further substantiated by the results of labeling 8-(chloromercuri)-2-dibenzofuransulfonic acid (CBFS) to N152C after mutating the only native cysteine residue in GLIC (C27A). Covalent labeling of the introduced cysteines with reagents like CBFS has been used previously to mimic alcohol binding to specific residues in pLGICs (Howard et al., 2011). The CBFS bonding to N152C mimicked the ketamine effect and resulted in inhibition to the mutant current (Figure 4C). The residual current from the CBFS bonding could be completely inhibited by ketamine, but with a higher IC₅₀ of 180 μ M (Figure S4). The weakening of ketamine's inhibition is somewhat expected, considering the interruption of CBFS to the pocket and to potential interactions between ketamine and its surrounding residues. The channel resumed a normal function once CBFS was removed from N152C after treatment with 10 mM DTT. Collectively, these data indisputably demonstrate functional significance of the ketamine-binding pocket revealed in the crystal structure.

DISCUSSION

The functional importance of the EC domain in pLGICs has been well established based on the data that agonist or antagonist binding to the orthosteric site regulates channel activities allosterically (Changeux and Edelstein, 2005; Sine and Engel, 2006). Our structure reveals a drug-binding pocket in the EC domain, showing that ketamine is not in, but 9–10 Å below, the orthosteric agonist-binding site. In the superimposed crystal structures of

the ketamine-bound GLIC and the agonist- or antagonist-bound AChBP (Bourne et al., 2010; Celie et al., 2004; Hansen et al., 2005; Hibbs et al., 2009; Ihara et al., 2008; Talley et al., 2008), one can see clearly that ketamine is outside the binding loci for agonists (Figure S2). However, the ketamine binding site overlaps partially with the extended interaction surface of bulky antagonists bound to AChBP (Figure S2), suggesting that ketamine may inhibit GLIC in a way similar to how competitive antagonists inhibit the functions of nAChRs. No agonist other than protons has been found for GLIC so far. It is unclear if the EC domain, especially the region for agonist or antagonist binding, plays any functional role in GLIC as in other pLGICs. Our data highlight the functional importance of the EC domain of GLIC. The functional relevance of the identified ketamine site has been established by compelling data of mutations and the CBFS labeling in combination with electrophysiology measurements. Several residues lining the ketamine pocket in GLIC are from the β 8– β 9 loop and β 10. Their interplay with the TM2–TM3 loop from the channel domain is thought to be essential for communication between agonist binding and channel activation in pLGICs (Sine and Engel, 2006). Both our structural and functional results suggest that the pre-existing cavity in the EC domain, other than the conventional agonist-binding site, can accommodate a drug molecule and modulate the functions of the GLIC channel.

Despite a profound inhibition effect on GLIC upon ketamine binding, our crystal structure shows little difference from the apo GLIC structure (Bocquet et al., 2009; Hilf and Dutzler, 2009). For residues within 4 Å from the bound ketamine, their root-mean-square deviation (rmsd) relative to the apo structure is only 0.4 Å. The structural resilience to anesthetic binding was also observed in the desflurane- and propofol-bound GLIC structures (Nury et al., 2011). Whether a structural response to ligand binding can be observed under crystallization may depend on binding sites, ligands, crystallization conditions, or other factors. The crystal structure of ELIC, the pentameric ligand-gated ion channel from *Erwinia chrysanthemi*, shows significant conformational changes near and beyond the binding site of acetylcholine (Pan et al., 2012), while agonist binding to the homologous site of the pentameric *Caenorhabditis elegans* glutamate-gated chloride channel α (GluCl) results in little conformational changes in the crystal structures (Hibbs and Gouaux, 2011). It remains a challenge to capture different conformations crystallographically for a given pLGIC (Gonzalez-Gutierrez et al., 2012).

The structural and functional results of ketamine binding to GLIC present a compelling case for the allosteric action of

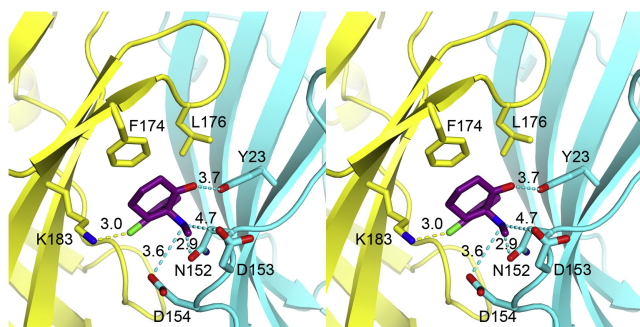


Figure 3. Stereo View of Atomic Details of the Ketamine Binding Pocket

Dashed lines indicate distances in Å between the ketamine atoms and the relating residues for electrostatic interactions. Residues on the principal and complementary sites of the pocket are colored in yellow and cyan, respectively. Note the position of ketamine relative to N152, in which the mutation affected GLIC activation and ketamine inhibition. See also Figures S3 and S5 and Table S1.

anesthetics. The ketamine pocket is nearly 30 Å away from the channel gate. The previously identified site for propofol or desflurane is in the upper part of the TM domain within a subunit of GLIC (Nury et al., 2011), distinct from the ketamine binding site. Two factors may have contributed to different sites of allosteric action for these drugs. First, ketamine is more soluble in the aqueous phase than propofol and desflurane. It is more attractive to the solvent-exposed pocket offering electrostatic, hydrogen bonding, and van de Waals interactions (Figure S3). Second, ketamine has a larger molecular size than either propofol or desflurane. The ketamine pocket in GLIC is comprised of flexible loops and has a volume of ~248 Å³, compatible with a ketamine volume of 219 Å³ (Table S1). Crystal structures of anesthetic bound GLIC reported here and previously (Nury et al., 2011) reveal at least two sets of sites for anesthetic binding. Existence of multiple anesthetic binding sites in GLIC has been suggested by several studies. Tryptophan fluorescence quenching experiments showed halothane and thiopental binding in the EC domain, TM domain, and the EC-TM interface of GLIC (Chen et al., 2010). Molecular dynamic simulations suggested that in addition to EC and TM domains, isoflurane could also migrate into the GLIC channel (Brannigan et al., 2010; Willenbring et al., 2011). Multiple anesthetic sites were also identified in other pLGICs. In *Torpedo* nAChR, azetomidate photolabeled not only some pore-lining residues, but also the agonist-binding site in the EC domain (Ziebell et al., 2004). The volatile anesthetic halothane was also found to photolabel both the TM and EC domains (Chiara et al., 2003). Some halothane-labeled residues in the EC domain of nAChR were from the β9 and β10 strands (Chiara et al., 2003), suggesting that the ketamine site in our structure represents a homologous site for anesthetic binding in other pLGICs.

Ketamine has been traditionally classified as an NMDA receptor antagonist (Harrison and Simmonds, 1985). Our structural and functional data reported here, along with previous functional studies of ketamine on nAChRs, may aid in a paradigm shift and call for a comprehensive examination of ketamine action on pLGICs. Ketamine inhibited the recombinant neuronal

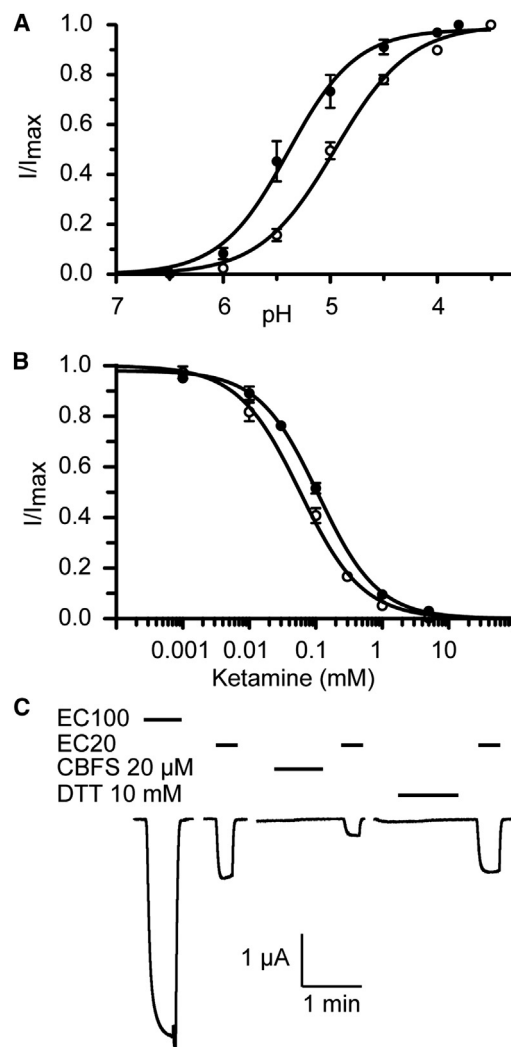


Figure 4. Functional Relevance of the Ketamine-Binding Site

(A) A single mutation of N152C in the binding pocket altered pH activation of the channel. Currents of the N152C mutant (solid circle) and the wild-type GLIC (open circle) expressed in *Xenopus* oocytes were normalized to the maximum current at pH 3.8 or 3.5, respectively.

(B) The N152C mutation weakened the ketamine inhibition. Responses of the N152C mutant (solid circle) and the wild-type GLIC (open circle) are expressed as the fraction of current induced at EC20 in the presence of the indicated concentrations of ketamine relative to that in the absence of ketamine.

(C) Representative current traces of the N152C_C27A mutant at different pH values, before and after labeling of 8-(chloromercuri)-2-dibenzofuransulfonic acid (CBFS) at a concentration of 20 μM, and after the treatment of 10 mM dithiothreitol (DTT). The application of CBFS or DTT to *Xenopus* oocytes lasted for ~2 min and was followed by the subsequent application of pH 7.4 buffer before a new measurement. The data in (A) and (B) are reported as the mean ± SEM from n ≥ 8 oocytes and fit to the Hill equation. Error bars less than the symbol size are not visible. See also Figure S4.

nAChRs in a subunit-dependent manner (Coates and Flood, 2001; Yamakura et al., 2000). IC₅₀ values of ketamine measured from *Xenopus* oocyte expressing human α7 and α4β2 nAChRs (Coates and Flood, 2001; Yamakura et al., 2000) were close to our measured value with GLIC in this study. From the modeled structures of the α7 and α4β2 nAChRs (Haddadian et al., 2008;

Mowrey et al., 2010), it is notable that both proteins have a pocket similar to the ketamine pocket in GLIC, where several acidic residues are on one side of the pocket (Figure S5). These negatively charged residues could attract ketamine and stabilize the ketamine binding. A greater number of negatively charged residues in the pocket of $\alpha 7$ than $\alpha 4\beta 2$ nAChRs seem to be consistent with the observation that the $\alpha 7$ nAChR is more sensitive to ketamine inhibition than the $\alpha 4\beta 2$ nAChR (Coates and Flood, 2001).

The discovery of the ketamine-binding pocket expands the scope of the drug-binding mode and is particularly valuable for the understanding of functional data related to drug action in the EC domain of pLGICs. There may also be other sites for ligand binding in the EC domain of heteromeric nAChRs and GABA_A receptors (Hansen and Taylor, 2007). For a long time, the search for targets of soluble drugs, such as benzodiazepine and its derivatives, was focused on sites equivalent to but not the orthosteric ligand site in GABA_A receptors (Boileau et al., 1998; Morlock and Czajkowski, 2011; Sigel and Buhr, 1997). Residue selection for mutagenesis and subsequent functional studies have relied heavily on structures of ligand-bound AChBPs (Celie et al., 2004; Hansen et al., 2005) because of the limited number of high-resolution structures with ligand binding to pLGICs (Dellisanti et al., 2007; Li et al., 2011; Pan et al., 2012) and the lack of experimental structures for GABA_A receptors. The atomic binding mode of ketamine in GLIC provides an additional structural template, which is invaluable for the design of novel modulators or the search for optimal binding modes of benzodiazepine derivatives at the interfaces of various subtype subunits (Richter et al., 2012).

EXPERIMENTAL PROCEDURES

Protein Expression and Purification

GLIC was expressed as a fusion of Maltose-binding protein (MBP) using a plasmid generously provided by Professor Raimund Dutzler's group. The protocol for GLIC expression and purification was modified from the published protocols (Bocquet et al., 2009; Hilf and Dutzler, 2009) and detailed in the Supplemental Experimental Procedures. The purified GLIC was concentrated to ~10 mg/ml and used for crystallization.

Crystallization

Crystallization was performed using the sitting-drop method at 4°C. GLIC was pre-equilibrated with 0.5 mg/ml *E. coli* polar lipids (Avanti Polar Lipids) and 1 mM ketamine (Fort Dodge) for at least 1 hr at 4°C before being mixed in a 1:1 ratio with the reservoir solution containing 10%–12% PEG 4000, 225 mM ammonium sulfate, and 50 mM sodium acetate buffer (pH 3.9–4.1). Crystals of GLIC containing ketamine usually appeared within 1 week. For cryoprotection, the crystals were flash frozen in liquid nitrogen after soaking for 30 min in the reservoir solution supplemented with 20% glycerol and 10 mM ketamine.

Structural Data Collection and Analysis

The X-ray diffraction data were acquired on beamline 12-2 at the Stanford Synchrotron Radiation Lightsource and processed using the XDS program (Kabsch, 2010). The structure was determined by molecular replacement using the apo-GLIC structure (PDB code 3EAM) without detergent, lipid, and water molecules, as the starting model. Phenix (version: 1.6.4-486) (Adams et al., 2010) and Coot (Emsley et al., 2010) were used for structure refinement and model building. After several cycles of refinement, six detergent and ten lipid molecules were built into well-defined extra electron densities using Coot (Emsley et al., 2010). Noncrystallographic symmetry (NCS) restraints were applied for five subunits in each unit cell. Automatic solvent detection,

update, and refinement were used for the placement of water molecules. Manual inspection and adjustment were performed at a later stage. Finally, ketamine binding sites were determined based on the $F_o - F_c$ difference map and ketamine molecules were built into five equivalent sites showing significant electron densities. Initial ketamine geometry was obtained using Gaussian 03 at the HF/6-31G level of theory (Frisch et al., 2003). Both R- and S-ketamine enantiomers were used in structural refinements. R-ketamine showed interactions with surrounding residues more energetically favorable and was used in the final structure. The final structure was obtained after additional refinement cycles. Crystal structure analysis was performed using Phenix and CCP4 (Winn et al., 2011). PyMOL (Schrodinger, 2010) and VMD (Humphrey et al., 1996) programs were used for structural analysis and figure preparation.

Molecular Biology and GLIC Expression in *Xenopus laevis* Oocytes

Plasmids encoding GLIC in the pTLN vector for GLIC expression in *Xenopus laevis* oocytes was a generous gift from Professor Raimund Dutzler of University of Zürich, Zürich, Switzerland. Site-directed mutagenesis was introduced with the QuikChange Lightning Kit (Stratagene) and confirmed by sequencing. The plasmid DNA was linearized with MluI enzyme (New England BioLabs). Capped complementary RNA was transcribed with the mMessage mMachine SP6 kit (Ambion) and purified with the RNeasy kit (QIAGEN). The defolliculated stage V-VI oocytes were injected with cRNA (10–25 ng each) and maintained at 18°C in modified Barth's solution (MBS) containing 88 mM NaCl, 1 mM KCl, 2.4 mM NaHCO₃, 15 mM HEPES, 0.3 mM Ca(NO₃)₂, 0.41 mM CaCl₂, 0.82 mM MgSO₄, 10 µg/ml sodium penicillin, 10 µg/ml streptomycin sulfate, 100 µg/ml gentamycin sulfate (pH 6.7). Functional measurements were performed on oocytes 16–40 hr after the injection.

Oocyte Electrophysiology

Two-electrode voltage clamp experiments were performed at room temperature with a model OC-725C amplifier (Warner Instruments) and a 20 µl oocyte recording chamber (Automate Scientific). Oocytes were perfused with ND96 buffer (96 mM NaCl, 2 mM KCl, 1.8 mM CaCl₂, 1 mM MgCl₂, 5 mM HEPES [pH 7.4]) and clamped to a holding potential of –40 to –60 mV. Data were collected and processed using Clampex 10 (Molecular Devices). Nonlinear regressions were performed using Prism software (Graphpad). Ketamine (Sigma-Aldrich) was prepared as a 100 mM stock at a specific pH and diluted with freshly prepared ND96 to a desired concentration. 8-(chloromercuri)-2-dibenzofuransulfonic acid (CBFS) was purchased as sodium salt (Sigma-Aldrich). The stock solution of CBFS (200 µM) was prepared with ND96 and diluted to a desired concentration before application. To measure CBFS labeling effects, data were collected at various pH or various ketamine concentrations at pEC20, followed by ~2 min washout using ND96 (pH 7.4), 1–2 min treatment with 20 µl CBFS, ~2 min to washout free CBFS, and data collection at various pH or various ketamine concentrations at a new pEC20. Covalent bonding of CBFS to GLIC mutants was confirmed by comparing currents at pEC20 before and after applying the reducing reagent, 10 mM dithiothreitol (DTT), to the CBFS-treated oocytes.

ACCESSION NUMBERS

Atomic coordinates and structure factors for the ketamine bound GLIC have been deposited in the Protein Data Bank (<http://www.pdb.org>) with the accession code 4F8H.

SUPPLEMENTAL INFORMATION

Supplemental Information includes five figures, one table, and Supplemental Experimental Procedures and can be found with this article online at <http://dx.doi.org/10.1016/j.str.2012.08.009>.

ACKNOWLEDGMENTS

We thank Prof. Raimund Dutzler's lab for the GLIC plasmid and the discussion about GLIC expression; Prof. Thomas R. Kleyman's lab for providing *Xenopus laevis* oocytes for the electrophysiology experiments; Prof. Ossama

B. Kashlan and Dr. Tommy Tillman for their help in functional measurements; Profs. Ken Yoshida, Susan Amara, Guillermo Calero, and Mr. Jared Sampson for their assistance in the early stage of the project; Ms. Sandra C. Hirsch for her editorial assistance. Portions of this research were carried out at the Stanford Synchrotron Radiation Lightsource, a Directorate of SLAC National Accelerator Laboratory and an Office of Science User Facility operated for the US Department of Energy Office of Science by Stanford University. The SSRL Structural Molecular Biology Program is supported by the DOE Office of Biological and Environmental Research and by the National Institutes of Health, National Institute of General Medical Sciences (including P41GM103393) and the National Center for Research Resources (P41RR001209). The research was supported by NIH gGrants R01GM066358, R01GM056257, R37GM049202, and T32GM075770.

Received: June 7, 2012

Revised: August 10, 2012

Accepted: August 10, 2012

Published: September 4, 2012

REFERENCES

- Adams, P.D., Afonine, P.V., Bunkóczi, G., Chen, V.B., Davis, I.W., Echols, N., Headd, J.J., Hung, L.W., Kapral, G.J., Grosse-Kunstleve, R.W., et al. (2010). PHENIX: a comprehensive Python-based system for macromolecular structure solution. *Acta Crystallogr. D Biol. Crystallogr.* 66, 213–221.
- Bocquet, N., Prado de Carvalho, L., Cartaud, J., Neyton, J., Le Poupon, C., Taly, A., Grutter, T., Changeux, J.P., and Corringer, P.J. (2007). A prokaryotic proton-gated ion channel from the nicotinic acetylcholine receptor family. *Nature* 445, 116–119.
- Bocquet, N., Nury, H., Baaden, M., Le Poupon, C., Changeux, J.P., Delarue, M., and Corringer, P.J. (2009). X-ray structure of a pentameric ligand-gated ion channel in an apparently open conformation. *Nature* 457, 111–114.
- Boileau, A.J., Kucken, A.M., Evers, A.R., and Czajkowski, C. (1998). Molecular dissection of benzodiazepine binding and allosteric coupling using chimeric gamma-aminobutyric acidA receptor subunits. *Mol. Pharmacol.* 53, 295–303.
- Bourne, Y., Radic, Z., Aróz, R., Talley, T.T., Benoit, E., Servent, D., Taylor, P., Molgó, J., and Marchot, P. (2010). Structural determinants in phycotoxins and AChBP conferring high affinity binding and nicotinic AChR antagonism. *Proc. Natl. Acad. Sci. USA* 107, 6076–6081.
- Brannigan, G., LeBard, D.N., Hénin, J., Eckenhoff, R.G., and Klein, M.L. (2010). Multiple binding sites for the general anesthetic isoflurane identified in the nicotinic acetylcholine receptor transmembrane domain. *Proc. Natl. Acad. Sci. USA* 107, 14122–14127.
- Brejč, K., van Dijk, W.J., Klaassen, R.V., Schuurmans, M., van Der Oost, J., Smit, A.B., and Sixma, T.K. (2001). Crystal structure of an ACh-binding protein reveals the ligand-binding domain of nicotinic receptors. *Nature* 411, 269–276.
- Celie, P.H., van Rossum-Fikkert, S.E., van Dijk, W.J., Brejč, K., Smit, A.B., and Sixma, T.K. (2004). Nicotine and carbamylcholine binding to nicotinic acetylcholine receptors as studied in AChBP crystal structures. *Neuron* 41, 907–914.
- Changeux, J.P., and Edelstein, S.J. (2005). Allosteric mechanisms of signal transduction. *Science* 308, 1424–1428.
- Chen, Q., Cheng, M.H., Xu, Y., and Tang, P. (2010). Anesthetic binding in a pentameric ligand-gated ion channel: GLIC. *Biophys. J.* 99, 1801–1809.
- Chiara, D.C., Dangott, L.J., Eckenhoff, R.G., and Cohen, J.B. (2003). Identification of nicotinic acetylcholine receptor amino acids photolabeled by the volatile anesthetic halothane. *Biochemistry* 42, 13457–13467.
- Coates, K.M., and Flood, P. (2001). Ketamine and its preservative, benzethonium chloride, both inhibit human recombinant alpha7 and alpha4beta2 neuronal nicotinic acetylcholine receptors in *Xenopus* oocytes. *Br. J. Pharmacol.* 134, 871–879.
- Dellisanti, C.D., Yao, Y., Stroud, J.C., Wang, Z.Z., and Chen, L. (2007). Crystal structure of the extracellular domain of nAChR alpha1 bound to alpha-bungarotoxin at 1.94 Å resolution. *Nat. Neurosci.* 10, 953–962.
- Emsley, P., Lohkamp, B., Scott, W.G., and Cowtan, K. (2010). Features and development of Coot. *Acta Crystallogr. D Biol. Crystallogr.* 66, 486–501.
- Forman, S.A., and Miller, K.W. (2011). Anesthetic sites and allosteric mechanisms of action on Cys-loop ligand-gated ion channels. *Can. J. Anaesth.* 58, 191–205.
- Franks, N.P., and Lieb, W.R. (1994). Molecular and cellular mechanisms of general anaesthesia. *Nature* 367, 607–614.
- Frisch, M.J., Trucks, G.W., Schlegel, H.B., Scuseria, G.E., Robb, M.A., Cheeseman, J.R., Montgomery, J.A., Vreven, T., Kudin, K.N., Burant, J.C., et al. (2003). Gaussian 03, Revision C.02. Gaussian, Inc.
- Gonzalez-Gutierrez, G., Lukk, T., Agarwal, V., Papke, D., Nair, S.K., and Grosman, C. (2012). Mutations that stabilize the open state of the *Erwinia chrysanthemi* ligand-gated ion channel fail to change the conformation of the pore domain in crystals. *Proc. Natl. Acad. Sci. USA* 109, 6331–6336.
- Haddadian, E.J., Cheng, M.H., Coalson, R.D., Xu, Y., and Tang, P. (2008). In silico models for the human alpha4beta2 nicotinic acetylcholine receptor. *J. Phys. Chem. B* 112, 13981–13990.
- Hansen, S.B., Sulzenbacher, G., Huxford, T., Marchot, P., Taylor, P., and Bourne, Y. (2005). Structures of *Aplysia* AChBP complexes with nicotinic agonists and antagonists reveal distinctive binding interfaces and conformations. *EMBO J.* 24, 3635–3646.
- Hansen, S.B., and Taylor, P. (2007). Galanthamine and non-competitive inhibitor binding to ACh-binding protein: evidence for a binding site on non-alpha-subunit interfaces of heteromeric neuronal nicotinic receptors. *J. Mol. Biol.* 369, 895–901.
- Harrison, N.L., and Simmonds, M.A. (1985). Quantitative studies on some antagonists of N-methyl D-aspartate in slices of rat cerebral cortex. *Br. J. Pharmacol.* 84, 381–391.
- Hemmings, H.C., Jr., Akabas, M.H., Goldstein, P.A., Trudell, J.R., Orser, B.A., and Harrison, N.L. (2005). Emerging molecular mechanisms of general anesthetic action. *Trends Pharmacol. Sci.* 26, 503–510.
- Hibbs, R.E., and Gouaux, E. (2011). Principles of activation and permeation in an anion-selective Cys-loop receptor. *Nature* 474, 54–60.
- Hibbs, R.E., Sulzenbacher, G., Shi, J., Talley, T.T., Conrod, S., Kem, W.R., Taylor, P., Marchot, P., and Bourne, Y. (2009). Structural determinants for interaction of partial agonists with acetylcholine binding protein and neuronal alpha7 nicotinic acetylcholine receptor. *EMBO J.* 28, 3040–3051.
- Hilf, R.J., and Dutzler, R. (2009). Structure of a potentially open state of a proton-activated pentameric ligand-gated ion channel. *Nature* 457, 115–118.
- Howard, R.J., Murail, S., Ondricek, K.E., Corringer, P.J., Lindahl, E., Trudell, J.R., and Harris, R.A. (2011). Structural basis for alcohol modulation of a pentameric ligand-gated ion channel. *Proc. Natl. Acad. Sci. USA* 108, 12149–12154.
- Humphrey, W., Dalke, A., and Schulten, K. (1996). VMD: visual molecular dynamics. *J. Mol. Graph.* 14, 33–38.
- Ihara, M., Okajima, T., Yamashita, A., Oda, T., Hirata, K., Nishiwaki, H., Morimoto, T., Akamatsu, M., Ashikawa, Y., Kuroda, S., et al. (2008). Crystal structures of *Lymanaea stagnalis* AChBP in complex with neonicotinoid insecticides imidacloprid and clothianidin. *Invert. Neurosci.* 8, 71–81.
- Kabsch, W. (2010). Integration, scaling, space-group assignment and post-refinement. *Acta Crystallogr. D Biol. Crystallogr.* 66, 133–144.
- Li, S.X., Huang, S., Bren, N., Noridomi, K., Dellisanti, C.D., Sine, S.M., and Chen, L. (2011). Ligand-binding domain of an alpha7-nicotinic receptor chimera and its complex with agonist. *Nat. Neurosci.* 14, 1253–1259.
- Morlock, E.V., and Czajkowski, C. (2011). Different residues in the GABAA receptor benzodiazepine binding pocket mediate benzodiazepine efficacy and binding. *Mol. Pharmacol.* 80, 14–22.
- Mowrey, D., Haddadian, E.J., Liu, L.T., Willenbring, D., Xu, Y., and Tang, P. (2010). Unresponsive correlated motion in alpha7 nAChR to halothane binding explains its functional insensitivity to volatile anesthetics. *J. Phys. Chem. B* 114, 7649–7655.
- Nury, H., Van Renterghem, C., Weng, Y., Tran, A., Baaden, M., Dufresne, V., Changeux, J.P., Sonner, J.M., Delarue, M., and Corringer, P.J. (2011). X-ray

structures of general anaesthetics bound to a pentameric ligand-gated ion channel. *Nature* 469, 428–431.

Pan, J., Chen, Q., Willenbring, D., Yoshida, K., Tillman, T., Kashlan, O.B., Cohen, A., Kong, X.P., Xu, Y., and Tang, P. (2012). Structure of the pentameric ligand-gated ion channel ELIC cocrystallized with its competitive antagonist acetylcholine. *Nat. Commun.* 3, 714.

Richter, L., de Graaf, C., Sieghart, W., Varagic, Z., Mörzinger, M., de Esch, I.J., Ecker, G.F., and Ernst, M. (2012). Diazepam-bound GABAA receptor models identify new benzodiazepine binding-site ligands. *Nat. Chem. Biol.* 8, 455–464.

Schrodinger, L. (2010). The PyMOL Molecular Graphics System, Version 1.3r1 (Portland, OR: Schrödinger, LLC).

Sigel, E., and Buhr, A. (1997). The benzodiazepine binding site of GABAA receptors. *Trends Pharmacol. Sci.* 18, 425–429.

Sine, S.M., and Engel, A.G. (2006). Recent advances in Cys-loop receptor structure and function. *Nature* 440, 448–455.

Talley, T.T., Harel, M., Hibbs, R.E., Radic, Z., Tomizawa, M., Casida, J.E., and Taylor, P. (2008). Atomic interactions of neonicotinoid agonists with AChBP: molecular recognition of the distinctive electronegative pharmacophore. *Proc. Natl. Acad. Sci. USA* 105, 7606–7611.

Unwin, N. (2005). Refined structure of the nicotinic acetylcholine receptor at 4Å resolution. *J. Mol. Biol.* 346, 967–989.

Weng, Y., Yang, L., Corringer, P.J., and Sonner, J.M. (2010). Anesthetic sensitivity of the *Gloeobacter violaceus* proton-gated ion channel. *Anesth. Analg.* 110, 59–63.

Willenbring, D., Tian Liu, L., Xu, Y., and Tang, P. (2011). Binding of Isoflurane to Glic Alters the Structure and Dynamics of the Protein. *Biophys. J.* 100, 273a.

Winn, M.D., Ballard, C.C., Cowtan, K.D., Dodson, E.J., Emsley, P., Evans, P.R., Keegan, R.M., Krissinel, E.B., Leslie, A.G., McCoy, A., et al. (2011). Overview of the CCP4 suite and current developments. *Acta Crystallogr. D Biol. Crystallogr.* 67, 235–242.

Yamakura, T., Chavez-Noriega, L.E., and Harris, R.A. (2000). Subunit-dependent inhibition of human neuronal nicotinic acetylcholine receptors and other ligand-gated ion channels by dissociative anesthetics ketamine and dizocilpine. *Anesthesiology* 92, 1144–1153.

Ziebell, M.R., Nirthanan, S., Husain, S.S., Miller, K.W., and Cohen, J.B. (2004). Identification of binding sites in the nicotinic acetylcholine receptor for [3H] azetomidate, a photoactivatable general anesthetic. *J. Biol. Chem.* 279, 17640–17649.